# Using Surface Methods to Understand the Ohaaki Hydrothermal Field, New Zealand

*A thesis submitted in partial fulfillment of the requirements for the degree of*

**Doctor of Philosophy in Geology**

*at the*

Department of Geological Sciences
University of Canterbury

*By*

**Clinton F.W. Rissmann**


**University of Canterbury**

**2010**

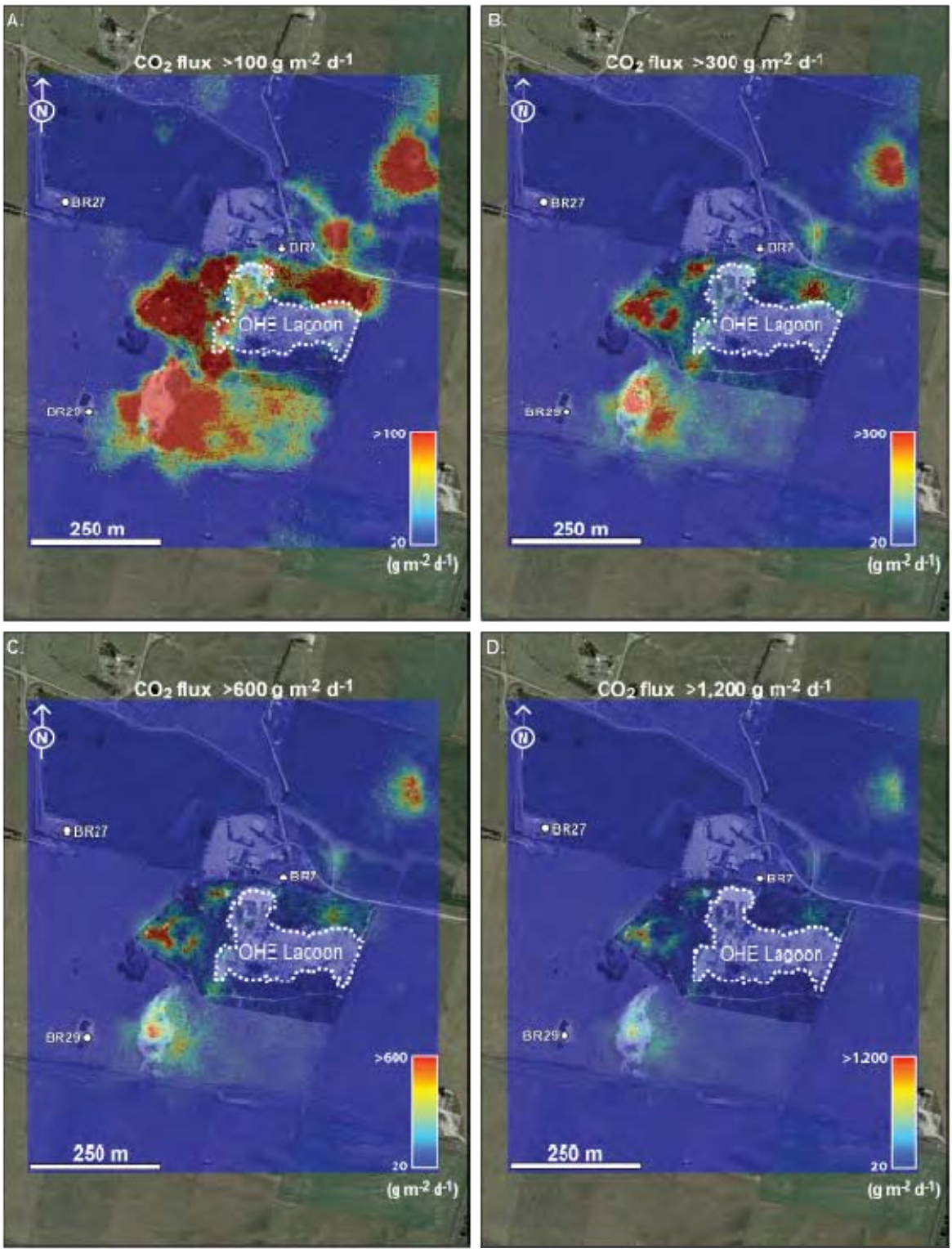


**Pixel plot models of $CO_2$ flux at the surface of the Ohaaki East thermal area**

# Abstract

After water vapour, $CO_2$ is the most abundant gas associated with magmatic hydrothermal systems. The detection of anomalous soil temperature gradients, and/or a significant flux of magmatic volatiles, is commonly the only surface signature of an underlying high temperature reservoir. For both heat (as water vapour) and gas to ascend to the surface, structural permeability must exist, as the unmodified bulk permeability of reservoir rock is too low to generate the focussed fluid flow typical of magmatic hydrothermal systems. This thesis reports the investigation into the surface heat and mass flow of the Ohaaki hydrothermal field using detailed surface measurements of $CO_2$ flux and heat flow. Detailed surface measurements form the basis of geostatistical models that quantify and depict the spatial variability of surface heat and mass flow, across the surface of both major thermal areas, as high resolution pixel plots. These maps, in conjunction with earlier heat and mass flow studies, enable: (i) estimates of the pre-production and current $CO_2$ emissions and heat flow for the Ohaaki Field; (ii) interpretation of the shallow permeability structures governing fluid flow, and; (iii) the spatial relationships between pressure-induced ground subsidence and permeability.

Heat flow and $CO_2$ flux surveys indicate that at Ohaaki the soil zone is the dominant ($\geq$ 70% and up to 99%) pathway of heat and mass release to the atmosphere from the underlying hydrothermal reservoir. Modelling indicates that although the total surface heat and mass flow at Ohaaki is small, it is highly focused (i.e., high volume per unit area) relative to other fields within the Taupo Volcanic Zone (TVZ). Normalised $CO_2$ emissions are comparable to other volcanic and hydrothermal fields both regionally and globally. Despite 20 years of production, there is little difference between pre-production and current $CO_2$ emission rates. However, the similarity of $CO_2$ emission rates masks a 40% increase in $CO_2$ emissions from new areas of intense steaming ground that have developed in response to production of the field for electrical energy production. This increase in thermal ground emissions is offset by emission losses associated with the drying up of all steam heated pools and alkali-Cl outflows from the Ohaaki West (OHW) thermal area, in response to production-induced pressure decline. The location of surface thermal areas is governed by the occurrence of buried or partially emergent lava domes, whereas the magnitude of $CO_2$ flux, mass flow, and heat flow occurring within each thermal area is determined by the proximity of each dome (thermal areas) to major upflow zones.

Buried or partially emergent silicic lava domes act as cross-stratal pathways for fluid flow, connecting the underlying reservoir to the surface, and bypassing several hundred metres of the poorly permeable Huka Falls Formation (HFF) caprock. For each dome complex the permeable structures governing fluid flow are varied. At Ohaaki West, thermal activity is controlled by a deep-rooted concentric fracture zone, developed during eruption of the Ohaaki Rhyolite dome. Within the steam-heated Ohaaki East (OHE) thermal area, flow is controlled by a high permeability fault damage zone (Broadlands Fault) developed within the apex of the Broadlands Dacite dome. Structures controlling alkali-Cl fluid flow at OHW also

appear to control the occurrence and shape of major subsidence bowls (e.g., the Main Ohaaki Subsidence Bowl), the propagation of pressure decline to surface, and the development and localization of pore fluid drainage. Across the remainder of the Ohaaki field low amplitude ground subsidence is controlled by the extent of aquifer and aquitard units that underlie the HFF, and proximity to the margins of the hot water reservoir. The correlation between the extent of low amplitude ground subsidence and the margins of the field reflects the coupled relationship between the hot water reservoir and reservoir pressure. Only where thick vapour-phase zones buffer the vertical propagation of deep-seated pressure decline to the surface (i.e., OHE thermal area), is ground subsidence not correlated with subvertical structural permeability developed within the HFF.

This thesis makes contributions to regional and global research on geothermal and hydrothermal systems by: (i) quantifying the origin, mass, and upward transport of magmatic carbon from geothermal reservoirs; (ii) assessing the changes to the natural surface heat and mass flow of the Ohaaki Field following 20 years of production; (iii) establishing the utility of surface $CO_2$ flux and heat flow surveys to identify major upflow zones, estimate minimum mass flow, and determine the enthalpy of reservoirs; (iv) providing insight into the hydrothermal, structural and lithological controls over hydrothermal fluid flow; (v) demonstrating the influence of extinct silicic lava domes as important structural elements in the localisation of hydrothermal fluid flow; (vi) identifying the hydrostructural controls governing the spatial variability in the magnitude of pressure-induced ground subsidence, from which predictive models of subsidence risk may be defined, and; (vii) developing new technologies and characterising methods used for detailed assessment of surface heat and mass flow.

# Acknowledgements

I would firstly like to thank my supervisors. From the inception to completion of this PhD, Professor Jim Cole has encouraged and guided me as a true professional and mentor. His passion for the advancement of others and the success of scientific endeavour is truly inspirational! Thanks for being so patient as I balanced a life as a school teacher and student. To Dr. Bruce Christenson, your depth of knowledge and ability to see the 'big picture' has set the benchmark for me as a scientist. In addition to your intellect, your humility and generosity has been hugely significant to my own growth, both as a scientist and as a person. Thank you for your time and friendship. Dr. Cindy Werner provided the initial impetus for this work and took time to instruct me in $CO_2$ flux surveys and geostatistical analysis. As a 'remote' supervisor she always responded to my numerous enquires(!!) with her own research, providing me with insight into the implementation and potential of $CO_2$ flux surveys. Dr. Matthew Leybourne has been an unofficial supervisor (and an official one once before!), and a huge source of support, intellect, friendship, and rapid editorial review! Matt's effort to encourage a truly global context to my study has furthered my own evolving conceptual understanding of earth systems.

In addition to my supervisors, several people have been significant sources of support throughout my doctoral studies. In particular, Associate Professor Jerry Fairley has been a voice of encouragement, direction and support. Thank you for responding to my emails and for investing your valuable time in my studies – cheers! Dr. Andrew Nicol and Mr. Hannu Seebeck gave selflessly of their time by joining me in the field, and providing some much needed structural-geological rigour to my work! Thanks to Dr. Ben Kennedy and Dr. Uwe Ring, here at Canterbury, for providing important insights and reviews of my work. The staff of GNS Wairakei and the geothermal group of Contact Energy gave selflessly of their time, equipment and expertise – thank you all very much.

Thank you to Pat Roberts at the University of Canterbury for your forbearance and organisational expertise. John Southward provided invaluable assistance with all things computer-related. Stefan Lendnal, your genius with all things electronic, and your incredible generosity of time has been instrumental (excuse the pun) in the development and success of various pieces of field equipment required for heat flow and geochemical sampling. Financial support from: (i) a Canterbury Doctoral Scholarship; (ii) a Contact Energy Ltd research grant; (iii) a Mighty River Power e-grant, and; (iv) the Mason Trust of the University of Canterbury, is gratefully acknowledged.

To my erstwhile and often lacerated, dehydrated and sunburnt field assistants, Dr. Matthew Hughes, Paul Chisholm of the Taupo Chisholm's, Megan Fookes (a.k.a. Moggs), and Moritz Ohnacker, thank you for your company, hard work and humour! I'll never forget Matt Hughes disappearing down an extinct tomo, skewering Moggs with a temperature probe, Moritz's keen interest and quick grasp of things hydrothermal, Paul being accosted by cattle, cooking lunches in the ground, and burning my backside whilst making heat flow measurements! A huge thank you to Denise, Gary and Paul Chisholm for a place

to stay, incredible meals, and insightful conversation, especially from Gary, on the imminent threat of Global Warming. Seriously, the generosity of the Taupo Chisholm's has been one of the most rewarding aspects of my numerous field trips – thank you so much!

Thank you to the students of Adams House Boys High Hostel for the laughs, exasperation and the privilege of being part of your lives. To PhD companions and close friends, Phil Rose and Matt Hughes, thanks for many wonderful conversations and laughs over the last few years on topics academic, philosophical, and most importantly, those that lacked any merit whatsoever! Thanks to Anekant Wandres and Peter Griffiths for the laughs and a place to stop and chew the fat. To fellow students Kate Pedley, Rose Turnball, Chad Deering, Jeremy O'Brien, Sam Hampton and Tom Wilson, thank you for your welcoming faces during my often irregular trips to the department.

To my Mother and Father, thank you for encouraging and supporting my interest in the natural world. Without your help along the way I would never have made it this far. I am very proud to call you my folks! To my sisters, brother-in-laws, nephews and nieces, you have all been part of this journey, keeping me sane, and providing me with a place to call home.

Lastly, and most importantly, thank you my beloved Carmen for your belief, support and encouragement. I dedicate this work to you and to our beautiful wee daughter to be.

# Table of Contents

## LIST OF FIGURES

## LIST OF TABLES

# Chapter 1

# Introduction

This thesis presents the results of detailed sampling of surface mass and heat flow within the Ohaaki hydrothermal field, New Zealand (Fig. 1.1). Although the content of each chapter differs, each is based on the different types of information that can be extracted from detailed surveys of surface heat and mass flow. Therefore, these studies demonstrate the use of direct, high resolution surveys of surface $CO_2$ flux and heat flow to accurately quantify heat and mass flow from hydrothermal reservoirs, define and better understand the spatial distribution of permeability structures governing fluid flow, provide high resolution images of the behaviour of hydrothermal fluids at the surface and subsurface, and provide a spatio-structural context to the pattern of pressure induced ground subsidence.

## 1.1 Thesis objectives and implementation

The objectives of this thesis are to provide a better understanding of the chemical and structural controls of the magnitude, nature and location of surface fluid flow within the Ohaaki hydrothermal field, and to apply these findings at a regional and global level. These objectives are realised by:

1. Quantification of the total surface heat and mass flow for the field, both prior to production of the field for electrical energy generation and following ~ 20 years of generation (Chapter 2).
2. Comparison of this heat and mass flow with the chemistry and structure of the Ohaaki Field (Chapter 2).
3. Placing the heat and mass flow of the Ohaaki Field within a regional and global context (Chapter 2).
4. The generation of detailed maps of surface heat and mass flow from which permeability structures are determined, and integrated structural models of fluid flow from source to surface developed (Chapters 2 and 3).
5. Placing the structural controls over fluid flow within the Ohaaki Field into a regional and global perspective (Chapter 3).
6. Application of fluid flow models, developed in Chapters 2 and 3, to understanding the spatio-structural and hydrothermal controls over production-induced ground subsidence occurring at Ohaaki (Chapter 4).

## 1.2 Exploration potential, heat and mass flow, and carbon emissions

The guidance of $CO_2$ flux surveys by statistical sampling methodologies and the application of stochastic simulation models constitute the state-of-the-art in mass flow assessment and spatial representation of surface characteristics (Goovaerts, 1997; Boomer et al., 2000; Goovaerts, 2001; Welles et al., 2001; Cardellini et al., 2003; Emerson and Rajagopal, 2004). The advent of infrared $CO_2$ gas analysers (IRGA) allows instantaneous flux measurement and is a more sensitive technology than equivalent chemical detectors for determining flux rates (Evans et al., 2001; LI-COR, 2007; Alavoine et al., 2008; Venterea et al., 2009). Relative to traditional soil volatile surveys (i.e., soil Hg) which measure concentration, flux surveys provide a means of estimating the mass flow from a reservoir, and therefore the potential to identify major upflow zones, along with regions of enhanced permeability (Chiodini et al., 1998; Brombach et al., 2001; Chiodini et al., 2005; Werner and Cardellini, 2006). However, the application of $CO_2$ flux surveys to the exploration of undeveloped or 'blind' hydrothermal systems requires calibration against well understood systems (Klusman et al., 2000; Werner and Cardellini, 2006). Therefore, the application of a $CO_2$ flux survey to one of the most intensively studied hydrothermal reservoirs of the world was considered an important benchmark in the calibration of this method.

Further to the exploration potential of $CO_2$ flux surveys, the employment of $CO_2$ flux and heat flow methodologies sought to better constrain the natural heat and mass flow of the Ohaaki Field. This is driven by the poor constraint and large reported range of natural heat flow values for the Ohaaki Field (i.e., 76 – 240 MW) (Dickinson, 1967; MacDonald, 1975), along with recent findings that $CO_2$ flux surveys produce more realistic estimates of the total mass and heat flow released from hydrothermal reservoirs (Chiodini et al., 2005; Fridriksson et al., 2006). These claims are based on the relatively conservative nature of $CO_2$ when contrast with water vapour (Henley and Ellis, 1983; Bischoff and Rosenbauer, 1996; Lowenstern, 2001; Chiodini et al., 2005). The condensation of ascending water vapour within meteoric waters beneath the vadose zone is commonly reflected at the land surface by the decoupling of surface heat flow from $CO_2$ flux (Chiodini et al., 2005; Fridriksson et al., 2006; Werner and Cardellini, 2006). These findings suggest that $CO_2$ flux is proportionately more representative of heat and mass flow than estimates based on surface heat flow measurements alone. Such observations may have significant implications for regional heat and mass flow budgets calculated for volcanic hydrothermal systems, and therefore warranted further investigation.

Another objective of this thesis is to contribute data on the amount of $CO_2$ that is discharged from individual geothermal systems, both within the Taupo Volcanic Zone (TVZ) and globally. The debate over climate change and the rise of atmospheric $CO_2$ has spurred a global effort to better characterise the natural sources and sinks of carbon. In particular, a call has been made for more direct measurement of greenhouse gas emissions so that global cycling models are more representative of actual fluxes (IPCC, 1996; Werner et al., 2000; GCP, 2003; GHGIS, 2009). Despite the central TVZ being the most active rhyolitic centre on earth, producing on average 0.3 $m^3\ s^{-1}$ of magma for the past 340 ka, 4200 ± 500 MW of surface heat flow and discharging $10^8$ $m^3$ of high temperature (≥ 250ºC) fluid per year (Cole, 1990;

Hochstein, 1995; Wilson et al., 1995; Sibson and Rowland, 2003), there have previously only been two studies that directly measure $CO_2$ emissions at individual fields (Wardell et al., 2001; Werner and Cardellini, 2006). Therefore, the lack of direct $CO_2$ surveys for the TVZ constitutes a significant gap in global carbon inventories, which this study seeks to address by providing accurate emissions data for the Ohaaki Field.

## 1.3 Structural and volcanological controls over fluid flow

A primary objective of this study was to better define the geochemical, structural and hydrogeological relationships between the deep reservoir and the surface of the Ohaaki Field, in order to address fundamental questions as to how structural and geological elements, in conjunction with rock properties, interact with fluids at different levels (depths) within hydrothermal regimes (Koide and Bhattacharji, 1975; Wohletz and Heiken, 1992; Curewitz and Karson, 1997; Rowland and Sibson, 2004; Anderson and Fairley, 2008). Of particular relevance is how these elements influence fluid pathways and whether such pathways are to some extent predictable. The answers to these questions have important implications for exploration and extraction of hydrothermal and epithermal mineral resources both within the TVZ and further afield.

The value of any surface survey is dependant on the scale at which it is applied and the sample density (Goovaerts, 1999; Boomer et al., 2000; Goovaerts, 2001; Emerson and Rajagopal, 2004). In general however, observations of fluid flow about faults and lava domes are limited to an assessment based on a small number of observations within the area of interest (e.g., Stewart et al., 1992; Barton et al., 1995; Curewitz and Karson, 1997; Rowland and Sibson, 2004). Another objective of this study therefore was to provide one of the highest sample density $CO_2$ flux and heat flow surveys, undertaken both within the TVZ and globally, so as to best resolve spatial trends in surface permeability, and reduce the uncertainty in emissions and heat flow model estimates. The particular value of such high resolution surveys is the ability to provide images of fluid circulation about structural (faults and fractures) and geological elements (e.g., lava domes) (Fairley and Hinds, 2004; Heffner and Fairley, 2006). Such images enable conceptual models of fluid flow to be tested by comparing predicted behaviours against observations of active systems (Rowland and Sibson, 2004; Heffner and Fairley, 2006).

Although the nature and role of deep-seated basement faults in (pre-330 ka) in governing fluid flow at Ohaaki are well understood (Wood et al., 2001; Christenson et al., 2002; Rae et al., 2007), the shallow (post-330 ka) controls over fluid flow are not (Wood et al., 2001; Rowland and Sibson, 2004). Therefore, an additional objective of this thesis was to develop integrated models of fluid flow that define the linkage between the deep reservoir and the surface.

## 1.4 A spatio-structural model of pressure-induced ground subsidence

The absence of high resolution maps of surface permeability structures, both structural and geological, has hindered efforts to predict pressure-induced ground subsidence occurring within the exploited geothermal fields of the TVZ (Allis, 2000; Allis and Zhan, 2000; Grant, 2000; White et al., 2005). This

uncertainty persists for the TVZ, despite demonstrations from global studies of the relationship between structural elements and ground subsidence (Amelung et al., 1999; Hoffmann et al., 2001; Burbey, 2002; Anderssohn et al., 2008). Therefore, in this thesis I sought to present the first spatio-structural model for a TVZ hydrothermal field by which the spatial pattern and controls over the magnitude and occurrence of pressure-induced ground subsidence could be explained. An important objective of this study was to provide a means by which the risk of subsidence may be predicted for undeveloped and underdeveloped fields, wherever a poro-elastic rock unit occurs at or near the surface, both regionally and globally.

## 1.5 Thesis structure

An understanding of the chemical and structural controls over the magnitude, nature and location of surface fluid flow within the Ohaaki hydrothermal is approached by quantifying the magnitude and nature of the heat and mass flow within surface thermal areas (Chapter 2), placing quantified values within the hydrothermal, geochemical and structural framework of the Ohaaki Field (Chapter 2 and 3), and providing a regional and global context to these findings (Chapter 2 and 3). Chapter 3 utilises detailed maps of surface heat and mass flow gradients, some of which were developed in Chapter 2, to infer the permeability structures governing fluid flow at the surface of the field, and from which conceptual models of fluid flow from source to surface are presented. The models developed in Chapters 2 and 3 are then applied to a case study of the spatial relationships between structural permeability and pressure-induced ground subsidence occurring within the Ohaaki Field.

The body of the thesis is comprised of three chapters (Chapters 2-4), each containing scientific manuscripts which will be submitted to international peer-reviewed journals within the next few months. Chapters 2 – 4 are preceded by an outline of the intended journal for publication, publication status of the manuscript at the time of thesis submission, and the main purpose of the manuscript in fulfilling the thesis objectives. The methodologies, applications and results described in the chapters are direct outcomes of the author's own research; however, contributions from co-authors have been invaluable and their input is also detailed at the start of each chapter.

A significant component of this thesis was the development and implementation of various pieces of equipment for: (i) the measurement of surface heat flow, (ii) sampling of subsoil gases and, (iii) quantifying the $CO_2$ concentration of the steam phase supplying both major areas of surface thermal activity. The design, implementation, and where applicable, calibration, of this equipment is presented in Appendix 1 and 2. The appendices provide evidence of additional research content especially with respects to surface heat flow by ground-based calorimetry. While most of this work has been done by Mr. Rissmann, contributions from co-authors have been invaluable and their input is also detailed at the start of each appendix.

## 1.6 References


Alavoine, G., Houlbert, J.-C. and Nicolardot, B., 2008. Comparison of three methods to determine C decomposition of organic materials in soils under controlled conditions. Pedobiologia, 52(1): 61-68.

Allis, R.G., 2000. Review of subsidence at Wairakei Field, New Zealand. Geothermics, 29(4-5): 455-478.

Allis, R.G. and Zhan, X., 2000. Predicting subsidence at Wairakei and Ohaaki geothermal fields, New Zealand. Geothermics, 29(4-5): 479-497.

Amelung, F., Galloway, D.L., Bell, J.W., Zebker, H.A. and Laczniak, R.J., 1999. Sensing the ups and downs of Las Vegas; InSAR reveals structural control of land subsidence and aquifer-system deformation. Geology, 27(6): 483-486.

Anderson, T.R. and Fairley, J.P., 2008. Relating permeability to the structural setting of a fault-controlled hydrothermal system in southeast Oregon, USA. Journal of Geophysical Research, vol. 113, no. B5, Citation B05402.

Anderssohn, J., Wetzel, H.-U., Walter, T.R., Motagh, M., Djamour, Y. and Kaufmann, H., 2008. Land subsidence pattern controlled by old alpine basement faults in the Kashmar Valley, northeast Iran; results from InSAR and levelling. Geophysical Journal International, 174(1): 287-294.

Barton, C.A., Zoback, M.D. and Moos, D., 1995. Fluid flow along potentially active faults in crystalline rock. Geology 23 (8): 683–686.

Bischoff, J.L. and Rosenbauer, R.J., 1996. The alteration of rhyolite in $CO_2$ charged water at 200 and 350 degrees C; the unreactivity of $CO_2$ at higher temperature. Geochimica et Cosmochimica Acta, 60(20): 3859-3867.

Boomer, K., Werner, C. and Brantley, S.L., 2000. $CO_2$ emissions related to the Yellowstone volcanic system; 1, Developing a stratified adaptive cluster sampling plan. Journal of Geophysical Research, 105(B5): 10817-10830.

Brombach, T., Hunziker, J.C., Chiodini, G., Cardellini, C. and Marini, L., 2001. Soil diffuse degassing and thermal energy fluxes from the southern Lakki Plain, Nisyros (Greece). Geophysical Research Letters, 28(1): 69-72.

Burbey, T.J., 2002. The influence of faults in basin-fill deposits on land subsidence, Las Vegas Valley, Nevada. Hydrogeology Journal, 10(525-538).

Cardellini, C., Chiodini, G. and Frondini, F., 2003. Application of stochastic simulation to $CO_2$ flux from soil; mapping and quantification of gas release. Journal of Geophysical Research, 108: no.B9, 13.

Chiodini, G., Cioni, R., Guidi, M., Raco, B. and Marini, L., 1998. Soil $CO_2$ flux measurements in volcanic and geothermal areas. Applied Geochemistry, 13(5): 543-552.

Chiodini, G., Granieri, D., Avino, R., Caliro, S., Costa, A. and Werner, C., 2005. Carbon dioxide diffuse degassing and estimation of heat release from volcanic and hydrothermal systems. Journal of Geophysical Research, 110: no.B8, 17.

Christenson, B.W., Mroczek, E.K., Kennedy, B.M., van Soest, M.C., Stewart, M.K. and Lyon, G., 2002. Ohaaki reservoir chemistry; characteristics of an arc-type hydrothermal system in the Taupo volcanic zone, New Zealand. Journal of Volcanology and Geothermal Research, 115(1-2): 53-82.

Cole, J.W., 1990. Structural control and origin of volcanism in the Taupo volcanic zone, New Zealand. Bulletin of Volcanology, 52(6): 445-459.

Curewitz, D. and Karson, J.A., 1997. Structural settings of hydrothermal outflow; fracture permeability maintained by fault propagation and interaction. Journal of Volcanology and Geothermal Research, 79(3-4): 149-168.

Dickinson, D.J., 1967. The natural heat output of the Broadlands geothermal area, 1967. Report, Department of Scientific and Industrial Research - Geophysics Division, Wellington.

Emerson, C.W. and Rajagopal, R., 2004. Measuring toxic emissions from landfills using sequential screening. Computers, Environment and Urban Systems, 28(3): 265-284.

Evans, W.C., Sorey, M.L., Kennedy, B.M., Stonestrom, D.A., Rogie, J.D. and Shuster, D.L., 2001. High $CO_2$ emissions through porous media; transport mechanisms and implications for flux measurement and fractionation. Chemical Geology, 177: 15-29.

Fairley, J.P. and Hinds, J.J., 2004. Field observation of fluid circulation patterns in a normal fault system. Geophysical Research Letters, 31.

Fridriksson, T., Kristjansson, B.R., Armannsson, H., Margretardottir, E., Olafsdottir, S. and Chiodini, G., 2006. $CO_2$ emissions and heat flow through soil, fumaroles, and steam-heated mud pools at the Reykjanes geothermal area, SW Iceland. Applied Geochemistry, 21(9): 1551-1569.

GCP, 2003. Global Carbon Project Report No. 1: Science Framework and Implementation. Report No. 1, Earth System Science Partnership (IGBP, IHDP, WCRP, DIVERSITAS), Canberra.
GHGIS, 2009. Global Greenhouse Gas Information System Interagency Workshop on Needs and Capabilities. In: Riley Duren et al. (Editors), Global Greenhouse Gas Information System Interagency Workshop on Needs and Capabilities, Albuquerque, New Mexico.
Goovaerts, P., 1997. Kriging vs. stochastic simulation for risk analysis in soil contamination. In: A. Soares, J. Gomez-Hernandez and R. Froidevaux (Editors), Quantitative Geology and Geostatistics, vol. 9, pp. 247-258.
Goovaerts, P., 1999. Geostatistics in soil science; state-of-the-art and perspectives. In: J. de Gruijter (Editor), Geoderma. Elsevier, Amsterdam, pp. 1-45.
Goovaerts, P., 2001. Geostatistical modelling of uncertainty in soil science. In: I.O.A. Odeh and A.B. McBratney (Editors), Geoderma. Elsevier, Amsterdam, pp. 3-26.
Grant, M.A., 2000. Projected subsidence at Tauhara. 22nd New Zealand Geothermal Workshop, University of Auckland Geothermal Institute, pp. 247-250.
Heffner, J. and Fairley, J., 2006. Using surface characteristics to infer the permeability structure of an active fault zone. Sedimentary Geology, 184: 255-265.
Henley, R.W. and Ellis, A.J., 1983. Geothermal systems ancient and modern; a geochemical review. Earth-Science Reviews, 19(1): 1-50.
Hochstein, M.P., 1995. Crustal heat transfer in the Taupo volcanic zone (New Zealand): comparison with other volcanic arcs and explanatory heat source models. Journal of Volcanology and Geothermal Research, 68(1-3): 117-151.
Hoffmann, J., Zebker, H.A., Galloway, D.L. and Amelung, F., 2001. Seasonal subsidence and rebound in Las Vegas Valley, Nevada, observed by synthetic aperture radar interferometry. Water Resources Research, 37(6): 1551-1566.
IPCC, 1996. IPCC Guidelines for national greenhouse gas inventories. Accessed May 2008, http://www.ipcc.ch.
Klusman, R.W., Moore, J.N. and LeRoy, M.P., 2000. Potential for surface gas flux measurements in exploration and surface evaluation of geothermal resources. Geothermics, 29(6): 637-670.
Koide, H. and Bhattacharji, S., 1975. Formation of fractures around magmatic intrusions and their role in ore localization. Economic Geology and the Bulletin of the Society of Economic Geologists, 70(4): 781-799
LI-COR, 2007. QA/QC of Large Datasets of Soil Surface $CO_2$ Efflux Measurements LI-COR Environmental. http://www.licor.com/env/webinars/webinars.jsp.
Lowenstern, J.B., 2001. Carbon dioxide in magmas and implications for hydrothermal systems. Mineralium Deposita, 36(6): 490-502.
MacDonald, W.J.P., 1975. The useful heat contained in the Broadlands geothermal field. Second United Nations symposium on the development and use of geothermal resources, San Francisco, Calif., United States, pp. 1113-1119.
Rae, A.J., Rosenberg, M.D., Bignall, G., Kilgour, G.N. and Milicich, S.D., 2007. Geological results of production well drilling in the western steamfield, Ohaaki geothermal system: 2005-2007. 29th New Zealand Geothermal Workshop, University of Auckland Geothermal Institute, pp. 7.
Rowland, J.V. and Sibson, R.H., 2004. Structural controls on hydrothermal flow in a segmented rift system, Taupo volcanic zone, New Zealand. Geofluids, 4(4): 259-283.
Sibson, R.H. and Rowland, J.V., 2003. Stress, fluid pressure and structural permeability in seismogenic crust, North Island, New Zealand. Geophysical Journal International, 154(2): 584-594.
Stewart, M.K., Lyon, G.L., Robinson, B.W. and Glover, R.B., 1992. Fluid flow in the Rotorua geothermal field derived from isotopic and chemical data. Geothermics, 21(1-2): 141-163.
Venterea, R., Spokas, K.A. and Baker, J.M., 2009. Accuracy and Precision Analysis of Chamber-Based Nitrous Oxide 1 Gas Flux Estimates. Soil Science Society of America Journal, 73:1087-1093.
Welles, J.M., Demetriades-Shah, T.H. and McDermitt, D.K., 2001. Considerations for measuring ground $CO_2$ effluxes with chambers. Chemical Geology, 177(1-2): 3-13.
Werner, C., Brantley, S.L. and Boomer, K., 2000. $CO_2$ emissions related to the Yellowstone volcanic system; 2, Statistical sampling, total degassing, and transport mechanisms. Journal of Geophysical Research, 105(B5): 10831-10846.
Werner, C. and Cardellini, C., 2006. Comparison of carbon dioxide emissions with fluid upflow, chemistry, and geologic structures at the Rotorua geothermal system, New Zealand. Geothermics, 35(3): 221-238.

White, P.J., Lawless, J.V., Terzaghi, S. and Okada, W., 2005. Advances in Subsidence Modelling of Exploited Geothermal Fields. Proceedings of the World Geothermal Conference, Antalya, Turkey.
Wilson, C.J.N., Houghton, B.F., McWilliams, M.O., Lanphere, M.A., Weaver, S.D. and Briggs, R.M., 1995. Volcanic and structural evolution of Taupo volcanic zone, New Zealand; a review. Journal of Volcanology and Geothermal Research, 68(1-3): 1-28.
Wohletz, K. and Heiken, G., 1992. Volcanology and Geothermal Energy. University of California Press, Berkeley.
Wood, C.P., Brathwaite, R.L. and Rosenberg, M.D., 2001. Basement structure, lithology and permeability at Kawerau and Ohaaki geothermal fields, New Zealand. Geothermics, 30(4): 461-481.

## 1.7 Figures

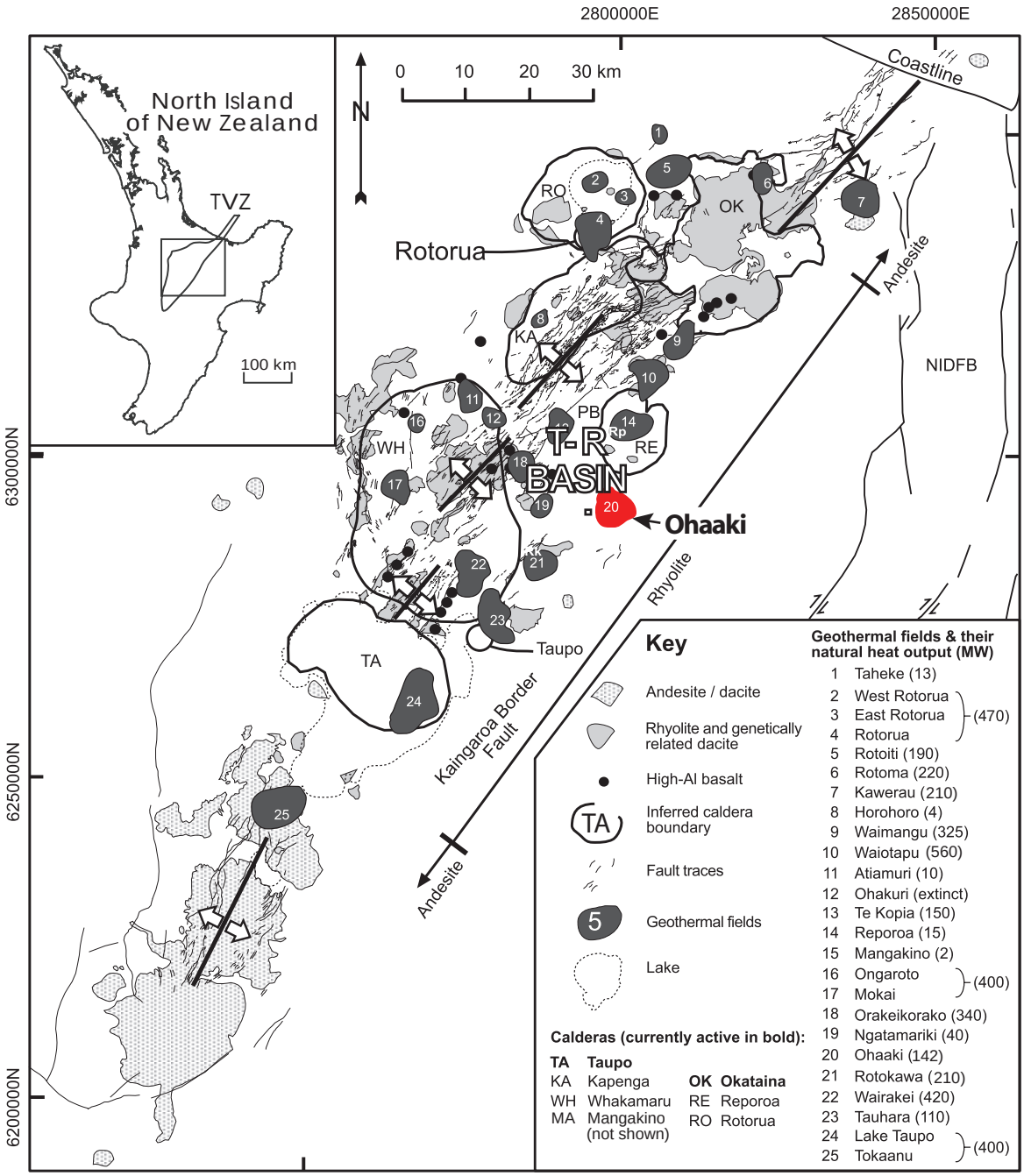


Figure 1.1. Map of the Taupo Volcanic Zone showing the distribution of geothermal systems, defined by the presence of low-resistivity zones (<30 Ωm) in relation to rift architecture, major volcanic rock types and caldera boundaries (modified from Rowland & Sibson 2004). Where T-R basin denotes the location of the Taupo Reporoa Basin and the Ohaaki hydrothermal field is in red. NIDFB, North Island Dextral Fault Belt. Major towns, Taupo and Rotorua, are labelled.

# Chapter 2

# Surface heat flow and $CO_2$ emissions within the Ohaaki hydrothermal field, Taupo Volcanic Zone, New Zealand – structural and geochemical controls

**Clinton Rissmann[a], Cynthia Werner[b], Bruce Christenson[c], Jim Cole[a]**

*[a]Department of Geological Sciences, University of Canterbury, Private Bag 4800, Christchurch, New Zealand*

*[b]USGS, Cascades Volcano Observatory, Vancouver, Washington, U.S.A.*

*[c]GNS Science, P.O. Box 30368, Lower Hutt, New Zealand*

*To be submitted to:* **Journal of Volcanology and Geothermal Research**

## Contributions

Mr. Rissmann conducted the literature review, undertook the fieldwork, geospatial mapping, and wrote the manuscript. Dr. Werner (Volcanic Fluid Geochemist and $CO_2$ flux specialist) trained Mr. Rissmann in $CO_2$ flux methodologies and geostatistical analysis. Dr. Christenson (Volcanic Fluid Geochemist) guided and assisted Mr. Rissmann with subsoil gas sampling for isotopic analyses. Prof. Cole and Dr. Werner reviewed this paper prior to a pre-submission review by Dr. Peter Kelly and Dr. Steven Ingebritsen of the Cascades Volcano Observatory, United States Geological Survey (USGS). Comments from USGS reviewers were favourable, however, some technical issues were raised, namely: (i) the applicability of empirical heat flow equations developed for the Wairakei Field to Ohaaki, and; (ii) the reliability of the vapour-phase $CO_2$ concentration, provided by an earlier study (Mahon and Finlayson, 1972), for the calculations used in the following study. Both technical issues are the focus of ongoing research by Mr. Rissmann and will be rectified before submission to an International Peer Review Journal (for details please see Appendices 1 and 2). Editorial and minor technical issues raised by USGS reviewers were rectified and incorporated into the following manuscript.

## 2.1 Abstract

Current and pre-production $CO_2$ emissions and heat flow from areas of surface thermal activity were determined for the Ohaaki hydrothermal field, New Zealand. Soil diffuse degassing and thermal ground heat flow was quantified by an intensive soil flux and soil temperature survey within and surrounding each thermal area. Detailed soil temperature measurements were used to determine surface heat flow, with both diffuse $CO_2$ fluxes and heat flow modelled geostatistically by sequential Gaussian simulation. The heat loss from the geothermal reservoir was also determined from $CO_2$ emissions by multiplying the molar $H_2O/CO_2$ ratio of the vapour phase supplying areas of surface thermal activity. Current diffuse $CO_2$ emissions equate to 111 ± 6.7 t $d^{-1}$ with an associated observed heat flow (i.e., derived from soil temperature measurements) of 70 ± 6.4 MW. This observed heat flow contrasts with 127 ± 7.6 MW of heat loss from the geothermal reservoir, as determined from diffuse $CO_2$ emissions. This large discrepancy is attributed to the condensation of >40% of the ascending steam phase within the subsurface, due to interactions with cold groundwater, and suggests that soil $CO_2$ flux measurement can be a more reliable means of quantifying the energy release from a geothermal reservoir. From the quantification of heat loss, and pre-production heat flow data, a pre-production (i.e., prior to development for electrical energy generation) $CO_2$ emission rate of 97 t $d^{-1}$ and 122 MW of surface heat flow was determined for the Ohaaki Field. These figures indicate a decline of 52 MW in surface heat flow and a minor increase of 14 t $d^{-1}$ in net $CO_2$ emissions, following 20 years of production for electrical energy generation. The similarity of $CO_2$ emission rates masks a 40% increase in $CO_2$ emissions from new areas of intense steaming ground, which is offset by $CO_2$ emission losses associated with the drying up of all steam heated pools and alkali-Cl outflows from the OHW thermal area. The increase in thermal ground at OHW reflects the enhancement of shallow permeability by ground fracturing and a possible increase in shallow vapour phase pressures, both as a result of production of the field. Analysis of the structural controls over surface emissions indicate that all three thermal areas occur above the apex of buried or partially emergent volcanic dome complexes, which act as ‘cross-stratal’ pathways for fluid flow, by effectively bypassing several hundred metres of poorly permeable cap rock. Whereas the location of each thermal area is determined by the occurrence of dome complexes, the magnitude of surface emissions and heat flow is determined by the proximity of each thermal area to major upflow zones. Carbon isotopic analysis of soil gas verifies the connection between the magmatic $CO_2$ source and both major areas of surface thermal activity. Normalising $CO_2$ emissions and heat flow by the area ($km^2$) of the high temperature reservoir, and that of thermal ground, indicates that although the total surface mass flow at Ohaaki is small, it is highly focused (i.e., high volume per unit area) relative to other fields within the TVZ. Normalised $CO_2$ emissions for Ohaaki are comparable to those reported for volcanic and hydrothermal fields worldwide. From these results a picture emerges of a gas-dominated hydrothermal reservoir sealed by a very effective cap rock, within which volcanic dome complexes function as pathways of preferential vertical permeability, focusing fluid flow, and acting as pressure release valves for the underlying high temperature reservoir.

## 2.2 Introduction

### 2.2.1 Background

A large number of studies over the last 15 years have shown that diffuse degassing of $CO_2$ through the soils of active volcanic and volcanic-hydrothermal systems, constitutes a major, if not *the* major, pathway of gaseous discharge to the atmosphere (Chiodini et al., 1998; Mörner and Etiope, 2002). Diffuse degassing of $CO_2$ through soils has also provided a means to better estimate the energy release from volcanic and volcanic-hydrothermal systems relative to conventional heat flow surveys (Brombach et al., 2001; Chiodini et al., 2005; Fridriksson et al., 2006). Water vapour is more prone to scrubbing by shallow groundwaters than $CO_2$, which behaves relatively conservatively under the T-P conditions of steam-heated hydrothermal surface features (Chiodini et al., 2005). As a result a significant portion of the thermal energy (as high enthalpy water vapour) may be removed laterally from the system, within the subsurface, by groundwater flow, without any visible or sensible signature at the land surface (Macdonald, 1975; Chiodini et al., 2005; Fridriksson et al., 2006).

The Ohaaki hydrothermal field, New Zealand, is the site of a 116 $MW_e$ installation that has been producing electrical energy for municipal supply for over 20 years. There is little complete and/or detailed data on the pre-production (i.e., pre-1988) heat flow associated with the areas of surface thermal activity; estimates range from 73 – 204 MW (Dickinson, 1967; Dawson and Dickinson, 1970; Macdonald, 1975). Production of the field over the last 20 years has resulted in some major changes in the natural surface thermal activity (Hunt and Graham, 1997; Glover et al., 2000; Hunt and Bromley, 2000). As a result considerable uncertainty surrounds both the pre-production and current status of surface thermal activity.

In this work we present a detailed survey of the current soil diffuse $CO_2$ flux and heat flow occurring at the surface of the Ohaaki Field. Comparison of estimates of heat flow from diffuse $CO_2$ degassing and soil temperature flow enables an estimation of the magnitude of water vapour condensation occurring within shallow meteoric groundwaters that overly the high temperature reservoir. From this estimation and partial pre-production heat flow data, we reconstruct the pre-production heat flow and $CO_2$ emissions for the field, and then provide the first assessment of the impact of production on total heat flow and $CO_2$ emissions.

Measured heat flow and $CO_2$ emissions are placed within a regional and international context by normalising by the area of the high temperature reservoir and the extent of thermal ground. We then compare $CO_2$ flux and total mass flow with current models of hydrothermal fluid flow, and assess the broad structural controls governing surface thermal activity. Finally, isotopic analysis of $CO_2$ within soil gases is used to assess the origin of $CO_2$, the physical processes occurring during transport from depth to the surface, and the mode of gas transport within the areas of surface thermal activity.

### 2.2.2 Geological and hydrothermal background

The Ohaaki Field is a liquid dominated hydrothermal system which occurs along the eastern boundary, or volcanic arc, of the Taupo Volcanic Zone (Fig. 2.1). The hot water reservoir, as defined by the area of low resistivity (i.e., < 10 mΩ), extends across an area of 12.7 $km^2$, with high non-condensable gas concentrations causing boiling at depths >1,500 m, and a maximum reservoir temperature of 310ºC (Grant, 1977; Hedenquist, 1990; Giggenbach, 1995; Christenson et al., 2002). Two major high temperature plumes enter the reservoir through permeable pathways in the Ohaaki Fault (West Bank upflow) and Broadlands Fault (East Bank upflow) in the NW and SE sectors of the field, respectively (Fig. 2.2; Christenson et al., 2002; Rae et al., 2007).

Relative to the West Bank upflow, the East Bank is more magmatic, with significantly greater non-condensable gas concentrations, and higher B, but lower Cl (Giggenbach, 1989; Hedenquist, 1990; Christenson et al., 2002). Compositional differences are attributed to two, shallowly emplaced (≥ 4.5 km), intrusive bodies - the East Bank intrusive is younger and correspondingly more magmatic than its West Bank counterpart, and is thought to be emplaced at a shallower level (Christenson et al., 2002). Although distinct from one another, the fluid chemistry of each upwelling is characteristically volcanic-magmatic or 'arc-type', consistent with high non-condensable gas concentrations and large $N_2$/Ar ratios (Fig. 2.2; Giggenbach, 1989; Giggenbach, 1995; Christenson et al., 2002).

The stratigraphy of the Ohaaki reservoir is here divided into: (1) the Mesozoic greywacke basement that underlies the field; (2) the pre-330 ka volcanic-sedimentary strata of the Waikora and Tahorakuri Formations that directly overly the basement; (3) the 330 ka Rangitaiki Ignimbrite that overlies these, and; (4) the post-330 ka volcanic-sedimentary infill (Fig. 2.3). The greywacke basement is block-faulted over four major NE-trending (arc parallel) and steeply dipping normal faults and falls from -700 mRSL (relative sea level) in the SE corner to -2,100 mRSL in the NW over a lateral distance of ~2.8 km (Wood et al., 2001; Rae et al., 2007). The majority of this relief (1,400 m) is accommodated by the major fault scarps of the Ohaaki Fault Zone and Broadlands Fault Zone, which occur within the NW and SE corners of the field, respectively (Figs. 2.2 and 2.3)

The reservoir overlying the greywacke basement is a complex assemblage of pre-330 ka volcaniclastics and post-330 ka volcanic domes, intercalated with pyroclastic deposits from large caldera forming eruptions to the west (Fig. 2.3). With the exception of the fractured and brecciated apex of each dome, volcanic lavas tend to inhibit vertical fluid movement (Henrys and Hochstein, 1990; Hedenquist, 1990). Pyroclastic flow deposits and porous volcaniclastic units (i.e., the Rangitaiki Ignimbrite, Rautawiri Breccia and the shallow Waiora Formation) act as permeable aquifers through which ascending alkali-Cl hot waters outflow laterally (Hedenquist, 1990; Wood, 1994). The Waiora Formation forms an important shallow alkali-Cl aquifer, which, in places, directly underlies the Huka Falls Formation (HFF) (Wood, 1994). The reservoir is capped by the poorly permeable mudstones of the HFF, which at Ohaaki are

especially thick (mean of ~ 220 m and a maximum thickness of 440 m; Contact Energy, 2006).

Several authors have noted that the surface heat flow at Ohaaki is small relative to the size of the high temperature reservoir (70 – 204 MW and 12.7 $km^2$, respectively; Grindley, 1970; Mahon and Finlayson, 1972; MacDonald, 1975; Hedenquist, 1990). Anomalous heat flow is confined to three areas of surface thermal activity that are referred to here as the Ohaaki West (OHW), Ohaaki East (OHE) and BR6 thermal areas (Fig. 2.2). The OHW thermal area is situated in the NW on the West Bank of the field, the OHE thermal area in the SE sector of the field on the East Bank, and the BR6 thermal area along the western central margin of the field.

Prior to development of the field for electricity generation in 1988, the OHW thermal area contained the greatest range of geothermal features, including the large volume (mean discharge rate of ~10 L $s^{-1}$) alkali-Cl outflow of the Ohaaki Pool (or Ngawha), ~ 5,000 $m^2$ of steam-heated pools, and ~ 77,000 $m^2$ of thermal ground with temperatures ≥ 50ºC at 1.0 m depth (Dickinson, 1967; Allis et al., 1983; Dawson, 1988). The smaller OHE thermal area was dominated by thermal ground (~23,000 $m^2$), interspersed with a few moderately sized steam-heated pools of acid-sulfate composition, and numerous small boiling mud pots (< 1,000 $m^2$), with no evidence for alkali-Cl outflows (Dickinson, 1967; Mahon and Finlayson, 1972; Allis and Webber 1984; Dawson, 1988). Relative to these two major areas, the pre-production thermal activity of the BR6 thermal area was negligible, with only one small area (< 400 $m^2$) of soil temperatures in excess of 50ºC at 1.0 m depth, and no steam-heated pools or alkali-Cl outflows (Allis and Webber, 1984; Dawson, 1988).

Since initial production of the field in 1988, the OHW thermal area has seen a major decline, with the drying up of all steam-heated pools and the large alkali-Cl outflow of the Ohaaki Pool (Glover et al., 2000; Hunt and Bromley, 2000). Despite the decline in these features, several large tracts of active thermal ground occur within the OHW thermal area, some of which show signs of increased activity (Hunt and Bromley, 2000). Conversely, Hunt and Bromley (2000) reported that the thermal activity of the OHE thermal area appeared unaffected by ten years of production.

## 2.3. Methods

### 2.3.1 Field measurement of $CO_2$ flux and soil temperature

Soil diffuse $CO_2$ fluxes and shallow soil temperatures (0.15 m) were measured at 2,663 and 2,563 locations, respectively, across areas of thermal and non-thermal ground on the West- and East Bank of the Ohaaki Field (Fig. 2.4). All flux and soil temperature measurements were made at least 3 days after light rainfall, and 5 days following heavy rain, during the summer months of 2006 - 2008. Surface $CO_2$ fluxes were measured using a West Systems accumulation chamber (Welles et al., 2001; Carapezza and Granieri, 2004) and a LICOR LI-820 infrared gas analyzer.

At all flux sites the soil temperature was measured at a depth of 0.15 m, typically within 0.2 m of the

accumulation chamber footprint, using a Yokogawa TX-10 digital thermometer and a K-type thermocouple (the measured accuracy is ± 0.3ºC). For sites where soil temperature exceeded boiling point at 0.15 m, detailed incremental temperature-depth measurements were made until boiling point depth was reached. Within the OHE thermal area a total of 53, 1.0-m-depth, temperature readings were made so as to assess any changes in the distribution and/or magnitude of soil temperatures mapped in earlier surveys (i.e., Allis and Webber, 1984; Hunt and Graham, 1997).

At each site, the easting and northing were logged by GPS, and $CO_2$ flux and soil temperature recorded. Barometric pressure and ambient air temperature were recorded at the start of each day and after each set of 25 consecutive measurements. Initially, the survey focused on areas of active thermal ground within the OHW and OHE thermal areas, and was then extended to cover all areas of historically documented thermal ground (subsoil temperatures $\geq$ 25ºC above ambient at 1.0 m depth), concluding with a survey of the peripheral non-thermal ground surrounding each thermal area. Within the minor BR6 thermal area, flux and temperature measurements were made at 15 m intervals along 12 transects (Fig. 2.4). Only three small areas (< 16 $m^2$ at $\leq$ 200 g $m^{-2}$ $d^{-1}$) of moderately elevated flux were detected for this area, so therefore a more detailed survey was not undertaken. On the East Bank, flux and temperature measurements were made at 15 – 25 m intervals along 26 transects over areas for which no surface thermal activity was evident (i.e., no subsoil temperature anomaly or surface thermal features), yet for which geochemical data indicates the upwelling of high temperature plumes at depth (Figs. 2.2 and 2.4; Christenson et al., 2002).

Poor access within the OHW thermal area (due to drilling platforms, tree felling, and inaccessible terrain) resulted in data gaps of up to 150 m. Complete coverage was possible across the OHE thermal area. However, in both thermal areas minor paving (roads, well and pipeline footings and drilling platforms) associated with well-field infrastructure impeded natural vapour phase flow. Paving is most significant within the OHW thermal area where it accounts for ~5% of the total surface area.

The sampling design within the OHW and OHE thermal areas was based on a simple random sampling pattern with an adaptive sampling component, whereby adjustments to the sampling pattern and sampling density were determined by magnitude of measured $CO_2$ flux rate, and/or soil temperature. Whenever, an elevated $CO_2$ flux or soil temperature was encountered the sampling pattern was adapted to characterise the extent of the anomaly by sampling directly above, below, to the right, and to the left of the initial sample location. Sample density was also increased to a maximum of 15 m (minimum of 5 m) within areas of anomalous flux and/or soil temperature, resulting in a higher sampling density, or clustering of sampling points within and about the anomaly. A return to background $CO_2$ flux values, and/or soil temperatures, governed the return to 'normal' sampling densities (i.e., every ~25 m) and the simple random sampling pattern. Adaptive sampling was triggered whenever $CO_2$ flux values exceeded 3 ppm $s^{-1}$, and/or soil temperatures, at 0.15 m, exceeded ambient air temperature at the time of sampling.

Adaptive sampling was implemented to improve the chances of accurately representing the spatial variability of surface $CO_2$ flux and soil temperature across the land surface, in addition to providing a representative data set for estimating the total emissions and heat flow for each thermal area. Due to greater sample densities within areas of anomalous flux and/or soil temperature, adaptive sampling results in higher sample density (i.e., clustering) within areas of anomalous flux and/or soil temperature, relative to background areas, causing bias in the population statistics if left untreated (Journel, 1994; Goovaerts, 1997; Deutsch and Journel, 1998). Debiasing or declustering of the data is achieved by weighting each datum according to its closeness to surrounding data (Journel, 1994; Deutsch and Journel, 1998). Closely spaced, or clustered, data points are less heavily weighted than those that are further apart. Declustering does not change the value of the sampled variable, only the influence of each sample (Journel, 1994; Goovaerts, 1997). Once weighted the representative or true summary statistics for the entire surveyed area may be calculated.

### 2.3.2 Data treatment and $CO_2$ emissions

Upon completion of the surveys, the $CO_2$ flux and soil temperature data sets for the OHW and OHE thermal areas were declustered using the cell declustering algorithm, DECLUS, within the software toolbox WinGslib (Deutsch and Journel, 1998). Each declustered data set was modelled geostatistically using the sequential Gaussian simulation (sGs) algorithm (*sgsim*), also within WinGislib. The main steps in the analyses of each data set, for each thermal area, include: (1) n-score normalisation of the declustered data; (2) computation of the experimental variogram of n-score values; (3) the definition of the variogram model for each data set; (4) 500 sequential simulations (or realisations) of the normal score of data, and; (5) the back-transformation of the simulated normal values into simulated values for the original variable (Cardellini et al., 2003; Chiodini et al., 2004).

Post-processing of the 500 realisations of the flux grid included: (i) computation of the mean flux and the probability of high and low fluxes at each location, and; (ii) the generation of 2D pixel plots of $CO_2$ flux across the surface of the field. Emission rates (t $d^{-1}$) for each realization were calculated by summing the simulated flux across the grid and multiplying by the grid area. The average and standard deviations of the emission rates were then calculated from the 500 flux realizations made for each grid area.

### 2.3.3 Heat flow through soil

At the time of the survey a water-filled calorimeter was not available for a direct assessment of the relationship between surface heat flow and soil temperature. Shallow soil temperatures were therefore transformed to equivalent heat flow values using the empirical equations of Dawson (1964) and Hochstein and Bromley (2005). These authors measured shallow soil temperatures, boiling point depth, and surface heat flow, from areas of thermal ground within the Wairakei Field. In both instances surface heat flow, in $Wm^{-2}$, was measured using a specially designed, water-filled calorimeter (see Hochstein and Bromley, 2005). From the relationship between surface heat flow and soil temperature, empirical power-

law functions were derived by which shallow soil temperatures may be transformed to equivalent heat flow values (Eqs. 1 and 2).

For areas where soils did not reach boiling point within 0.15 m of the surface, heat flow was calculated using Dawson's (1964) equation:

$$H_s = 5.2 \times 10^{-6} t_{15}^4 \quad (1)$$

where $H_s$ is the heat flow (in $Wm^{-2}$) at the soil surface and $T_{15}$ is the soil temperature at 0.15 m in ºC. For high temperature sites where the boiling point was reached within 0.15 m of the surface, Hochstein and Bromley's (2005) equation was applied:

$$H_s = a\left(\frac{z_{BP}}{z_0}\right)^{-b} \quad (2)$$

where $a$ = 185 W $m^{-2}$, $b$ = 0.757, $z_{BP}$ is the depth at which boiling point was reached in metres, and $z_0$ denotes unit depth (1 m). Particular care was taken to accurately measure the depth at which boiling point was reached, as major gains in heat flow occur for only slight increases in soil temperature once boiling point has been reached (Dawson, 1964; Hochstein and Bromley, 2005). Equation (1) was applied to 2,241 measurements, and equation (2) to 322. The total heat flow (MW) of both thermal areas was then modelled through 500 sGs realisations after the method described above for soil $CO_2$ flux.

The empirical power-law functions developed for the Wairakei Field have been used by many authors to transform shallow soil temperatures to equivalent heat flow values in areas of surface thermal activity, both in New Zealand and globally (Sorey and Colvard, 1994; Allis et al., 1999; Mongillo and Graham, 1999; Fridriksson et al., 2006). However, some uncertainty surrounds the application of the Wairakei power-law function to soil temperatures at different hydrothermal fields (Hochstein and Bromley, 2005). This uncertainty arises as each field, and possibly each patch of thermal ground, may exhibit a unique relationship between surface heat flow and soil temperature.

### 2.3.4 Steam flow through soil

By assuming that the heat flow of each thermal area is a manifestation of water vapour (hereafter referred to as steam) transported from the underlying reservoir to the surface, the mass flow of steam through the soil, $F_{stm,HF}$ in kg $s^{-1}$, can be computed, applying the methodology of Fridriksson et al. (2006):

$$F_{stm,HF} = \frac{H_s}{\left(h_{s,98.7°C} - h_{w,tr}\right)} \quad (3)$$

where $H_s$ is the measured thermal ground heat flow (in W), $h_{s,98.7^oC}$ is the enthalpy of steam at 98.7ºC (boiling point at Ohaaki) and $h_{w,tr}$ is the enthalpy of water at 20ºC, which was the mean air temperature during the survey periods (2,673.7 kJ $kg^{-1}$ and 83.9 kJ $kg^{-1}$, respectively).

### 2.3.5 Steam mass flow from $CO_2$ flux

Mahon and Finlayson (1972) reported concentrations of 0.6 molal or 26.4 g $kg^{-1}$ of $CO_2$ for the steam phase issuing from areas of vigorously steaming ground within the OHW thermal area. Using the documented $H_2O/CO_2$ ratio of the vapour phase supplying the OHW thermal area (i.e., 1000 g $kg^{-1}$/26.4 g $kg^{-1}$ = 37.90) the mass flow of steam accompanying the surface $CO_2$ flux was computed by:

$$Fstm,CO_2 = F_{CO_2} \times \frac{[H_2O]}{[CO_2]} \quad (4)$$

where $Fstm,CO_2$ is the steam mass flow, in kg $s^{-1}$, and $FCO_2$ is the mass flow rate of $CO_2$ in kg $s^{-1}$.

### 2.3.6 Reconstruction of pre-production $CO_2$ emissions

Since development of the Ohaaki Field for energy production in 1988, all steam-heated pools and the large alkali-Cl outflow of the Ohaaki Pool have dried up in response to the propagation of production induced-pressure decline from the underlying reservoir to the surface (Bromley et al., 1993; Allis et al., 1997; Glover et al., 2000). The status of the large alkali-Cl seepage from the OHW thermal area to the Waikato River is unknown, with pre-production outflow sites along the left bank lying below river level due to ground subsidence. However, given the sensitivity of the Ohaaki Pool to reservoir pressure decline (see Glover et al., 2000) it is likely that the alkali-Cl seepages from the OHW thermal area have also ceased. The cessation of alkali-Cl outflows (seepages and the Ohaaki Pool) is consistent with the far greater sensitivity of liquid-dominated outflows to perturbations in reservoir pressure relative to steam-heated features (Sorey et al., 1980; Grant et al., 1982). In addition to the disappearance of surface pools, a significant area of historically active thermal ground adjacent to the Ohaaki Pool has disappeared (Hunt and Graham, 1997; Hunt and Bromley, 2000). However, other areas of historically active thermal ground have expanded in size, with a significant, albeit unquantified, increase in surface heat flow evident in repeat Thermal Infrared (TIR) surveys, flown in 1988, and again in 1998 (Hunt and Bromley, 2000).

Due to these significant changes it was necessary to rely on pre-production or ‘historical’ estimates of surface heat flow for the OHW thermal area (Dickinson, 1967). Dickinson (1967) assessed thermal ground heat flow from measurement of shallow (0.15 m) soil temperatures, using a method similar to that described in section 2.3.3. The heat flow associated with surface pools (both steam-heated and alkali-Cl), surface water outflows, and seepage to the Waikato River, were also assessed using a variety of methodologies as described in detail by Dickinson (1964, 1967). From these measurements the total pre-

production heat flow of the OHW thermal area was divided into the contribution from: (i) thermal ground; (ii) steam-heated pools; (iii) alkali-Cl hot springs and; (iv) dilute alkali-Cl seepage to the Waikato River.

The pre-production $CO_2$ emissions associated with the steam-heated activity of the area were then computed by deriving the equivalent mass flow of steam from pre-production heat flow data, as per Eq. (3), and then multiplying by the representative $CO_2$ concentration of the steam phase. Reports of vigorous gaseous ebullition of steam-heated pools within the OHW thermal area confirms that pool waters were saturated with respect to $CO_2$, and therefore, all $CO_2$ entering steam-heated pools was released to the atmosphere (Dickinson, 1967; Mahon and Finlayson, 1972).

The $CO_2$ emissions associated with pre-production liquid outflows of alkali-Cl hot water were computed by determining the mass flow of alkali-Cl hot waters supplying the area, and then multiplying by the dissolved $CO_2$ concentration of the surface outflows (see Seward and Kerrick, 1996). The pre-production mass flow was determined from the pre-production heat flow data by:

$$F_{res} = \frac{H_{alk}}{H_{DF}} \tag{5}$$

where $F_{res}$ is the mass flow of deep alkali-Cl hot waters in kg $s^{-1}$, $H_{alk}$ is the pre-production surface heat flow associated with alkali-Cl outflows (Ohaaki Pool and seepages to Waikato River, ~ 62 MW; Dickinson, 1967) in J $s^{-1}$ (W), and $H_{DF}$ is the enthalpy, in J $kg^{-1}$, of the deep reservoir fluid at reservoir temperatures (Dickinson, 1967; Hedenquist, 1972). Due to the dilute nature of Ohaaki reservoir fluids (Cl = 1,000 mg $kg^{-1}$ at 310°C), $H_{DF}$ is taken as that of pure water (1,395 J $g^{-1}$ at 310ºC) at the equilibrium saturated vapour pressure.

From a comparison of the $CO_2$ concentration of surface and deep-reservoir alkali-Cl hot waters for the OHW thermal area, it is evident that the majority (> 95%) of dissolved $CO_2$ within deep parent waters is lost through decompressive boiling (Mahon and Finlayson, 1972; Hedenquist, 1990). Therefore, a mean surface-water $CO_2$ concentration of 0.01 molal (or 0.4 g $kg^{-1}$) was determined for the alkali-Cl outflows of the OHW thermal area on the basis of pre-production chemical data for the Ohaaki Pool, and seepages occurring along the left bank of the Waikato River (Mahon and Finlayson, 1972). This value was then multiplied by the mass flow derived from Eq. (5) in order to determine the net $CO_2$ emission rate associated with alkali-Cl outflows.

### 2.3.7 Carbon isotopes of soil $CO_2$ flux

A total of 40 subsoil gas samples were collected at 0.5 m depth from within the OHW and OHE thermal areas for determination of $\delta^{13}CO_2$. Surface flux and soil temperature (0.15 m) were measured at each site,

and subsoil gases were drawn under vacuum into Tedlar bags. Bags were purged three times before the final sample was taken. An attempt was made to sample throughout the range of flux and soil temperature values, in order to characterise any end-member signatures. Carbon-stable-isotope ratios of $CO_2$ were analysed by Iso-Trace Ltd., Dunedin, New Zealand, and the National Isotope Centre, GNS Science, Lower Hutt, New Zealand. Results are presented using δ notation as permil (‰) deviations from the VPDB standard. Subsoil $\delta^{13}CO_2$ compositions are compared with those reported for deep production well and bleed-line gas discharges at Ohaaki (Christenson et al., 2002).

## 2.4 Results

### 2.4.1 Diffuse fluxes and soil temperature

Measured $CO_2$ fluxes range from undetectable (< 3 g $m^2$ $d^{-1}$) to 27,518 g $m^{-2}$ $d^{-1}$. On five occasions within the OHW thermal area the detection limit (i.e., 20,000 ppm $s^{-1}$) of the infrared $CO_2$ detector was overwhelmed, indicating localised fluxes in excess of 32,000 g $m^{-2}$ $d^{-1}$. The arithmetic and declustered means of surface $CO_2$ flux for the OHW and OHE data sets are 157 and 122 g $m^{-2}$ $d^{-1}$ and 86 and 77 g $m^{-2}$ $d^{-1}$, respectively. The OHW and OHE flux populations return coefficients of variation (CV; the standard deviation divided by the mean) of 6.1 and 5.7, respectively, where a CV > 1 is consistent with a non-normal (positively skewed) approximately log-normal population distribution, as is evident in the histograms of measured $CO_2$ flux (Fig. 2.5).

Cumulative probability plots of flux data sets indicate: (i) no significant overlap between background (soil respired $CO_2$ fluxes) and hydrothermal flux populations; (ii) a negligible contribution, < 1%, from background fluxes to the net total emissions, and; (iii) a threshold value of 15 g $m^{-2}$ $d^{-1}$ by which the two flux populations may be differentiated.

Within the OHW thermal area, 16% percent of the fluxes exceeded 100 g $m^{-2}$ $d^{-1}$, compared with 25% within the OHE thermal area. However, 40 measurements exceeded 1,000 g $m^{-2}$ $d^{-1}$ at OHW, compared to only 11 measurements > 1,000 g $m^{-2}$ $d^{-1}$ within the OHE thermal area. Surface $CO_2$ emissions along transects over the BR6 thermal area were negligible, with only three small areas (≤ 4 $m^2$) where $CO_2$ emissions (max = 200 g $m^{-2}$ $d^{-1}$) exceed the background value of 15 g $m^{-2}$ $d^{-1}$ for biogenic soil fluxes. On the East Bank, surface $CO_2$ fluxes and shallow soil temperatures along transects over the areas of deep upwelling, as outlined by elevated $N_2$/Ar isopleths, were all at or below background.

Shallow (0.15 m) soil temperatures across the Ohaaki field ranged from 10°C to boiling point (98.7ºC). The correlation of the 0.15 m soil temperature data set with the natural log of fluxes displayed no relationship ($R^2$ = 0.08). Similarly, for high temperature sites ($T$>50ºC) no significant spatial relationship (i.e., $R^2$ = 0.45 and 0.39, for the OHW and OHE thermal areas, respectively) was evident between $CO_2$ flux and soil temperature, indicating that differing processes control temperature and $CO_2$ flux distributions.

A good fit between the experimental variograms and model variograms was obtained for each flux population with nugget values of 0.56 and 0.46, both sills equal to 1, and effective ranges of 120 m and 200 m, respectively (Fig. 2.5). Similarly, model variograms for heat flow data sets were fitted by superposition of exponential and Gaussian models with nugget values of 0.20 and 0.21, sills of 1.0, and effective ranges of approximately 110 m and 130 m, for the OHW and OHE thermal areas, respectively.

The results of the 500 simulations are depicted in Figures 2.6 and 2.7 for the OHW and OHE thermal areas. These models illustrate that diffuse degassing and anomalous heat flow extend over hundreds of metres in both the OHW and OHE thermal areas. For the most part, areas of anomalous degassing and heat flow are consistent with previously mapped thermal areas, and overlap with mapped geothermal features (hot pools, springs and steam vents) and thermally tolerant plant species. Within both major thermal areas several large patches of anomalous $CO_2$ flux coincide with regions of cold, unaltered ground, indicating the decoupling or stripping of the steam phase below the land surface (Fig. 2.6).

### 2.4.2 Heat flow through soil

Heat flow through the soils of the OHW and OHE thermal areas, estimated using Eq. (1) and Eq. (2), ranged from 0.2 to 2,460 W $m^{-2}$, with mean heat flow values of 44 W $m^{-2}$ and 38 W $m^{-2}$, respectively. The average soil-based heat flow from 500 simulations, equates to 43 ± 5 MW and 27 ± 4 MW for the OHW and OHE thermal areas respectively, with a combined total of 70 ± 6.4 MW (Table 2.1). Assuming that condensation of steam within the soil is the dominant heat transfer mechanism, the mass flow of steam supplying the thermal soils of each area equates to 1,430 ± 155 t $d^{-1}$ and 880 ± 115 t $d^{-1}$, respectively (Eq. 3).

### 2.4.3 Diffuse $CO_2$ emissions through soil

The mean emission rates from 500 simulations equate to 72 ± 6 t $d^{-1}$ and 39 ± 3 t $d^{-1}$ for the OHW and OHE thermal areas, respectively (Table 2.1). Multiplying by the representative $H_2O/CO_2$ ratio for the steam phase at Ohaaki gives steam mass flow values of approximately 2,700 ± 240 t $d^{-1}$ and 1,480 ± 95 t $d^{-1}$ (Eq. 4). By rearranging Eq. (3) these steam mass flow rates equate to approximately 82 ± 7 MW and 45 ± 3 MW of thermal energy, respectively. These heat flow values are > 40% larger than the observed heat flow values determined by direct measurement of soil temperatures (section 2.4.2.).

### 2.4.4 Historical $CO_2$ emissions and heat flow

By applying Eq. (3) to pre-production heat flow values of 25 MW and 8.6 MW, steam mass flow rates of 9.5 kg $s^{-1}$ (~820 t $d^{-1}$) and 3.3 kg $s^{-1}$ (~285 t $d^{-1}$) are computed for the thermal ground and steam-heated pools of the OHW thermal area, respectively (Table 2.1). On the basis of these steam mass flow rates and the representative $CO_2$ concentration in steam supplying the OHW thermal area, pre-production $CO_2$ emission rates equate to 0.25 kg $s^{-1}$ (22 t $d^{-1}$) for thermal ground and 0.09 kg $s^{-1}$ (7.5 t $d^{-1}$) for steam-heated pools (Eq. 3; Table 2.1). Applying the same methodology to the minor heat flow (~ 0.2 MW)

associated with the small steam-heated pools of the OHE thermal area yields a steam mass flow of 0.08 kg $s^{-1}$ or 6.9 t $d^{-1}$. The latter equates to a $CO_2$ mass flow of 0.002 kg $s^{-1}$ or an emission rate of approximately 0.18 t $d^{-1}$. Using the same methodology, the low total heat flow (i.e., < 0.1 MW) of the BR6 thermal area equates to a steam mass flow of < 0.04 kg $s^{-1}$ and a corresponding $CO_2$ mass flow of 0.09 t $d^{-1}$.

From a combined pre-production heat flow of 61.5 MW and by applying Eq. (5), a deep upflow of approximately 44 kg $s^{-1}$ of alkali-Cl hot waters is determined for the OHW thermal area. Using the mean dissolved $CO_2$ concentration of surface alkali-Cl outflows, the corresponding mass flow of $CO_2$ equates to approximately 0.02 kg $s^{-1}$ or 1.7 t $d^{-1}$ (Table 2.1).

### 2.4.5 Carbon isotopes of soil $CO_2$ flux

Carbon isotope values for subsoil $CO_2$ ranged from -16.7‰ to -2.4‰ within the OHW and OHE thermal areas (Table 2.2). For high temperature (≥ 45ºC @ 0.15 m), high flux (≥ 300 g $m^{-2}$ $d^{-1}$) sites, however, $\delta^{13}CO_2$ values varied only slightly around mean values of -7.4 ± 0.3‰ and -6.5 ± 0.6‰ for the OHW and OHE thermal areas, respectively. Both of these mean subsoil $\delta^{13}CO_2$ values are similar to the mean bleed-line $\delta^{13}CO_2$ compositions of the West- (-7.5 ± 1.1‰) and East Bank (-6.8 ± 0.7‰) reservoirs, respectively (Christenson et al., 2002). (Bleed-line samples refer to gas samples taken from the wellhead of closed or non-producing wells.)

Subsoil $\delta^{13}CO_2$ variability is greater for low temperature (< 45ºC), low flux (< 300 g $m^{-2}$ $d^{-1}$) sites, with ranges of -6.7 to -10.9‰ and -2.4 to -16.7‰ and means of -9.0 ± 2.3‰ and -5.2 ± 1.8‰ for the OHW and OHE thermal areas, respectively. Within the OHE thermal area, all low temperature (≥ 17 ≤ 40ºC), low to moderate flux (≥ 15 ≤ 300 g $m^{-2}$ $d^{-1}$) sites exhibited heavy $\delta^{13}CO_2$ values of -6.2 to -2.4‰. No enrichment in subsoil $\delta^{13}CO_2$ was observed for low or moderate flux sites within the OHW thermal area. However, no subsoil gas samples were taken over the range 100 – 300 g $m^{-2}$ $d^{-1}$ for OHW, resulting in an unintended bias in the sampling to towards either high- or low-flux sites. Within the OHW thermal area several isotopically depleted signatures (i.e., -9.0‰ to -12.51‰) were measured at sites of low flux and ambient soil temperature, all of which supported dense stands of non-thermal plant species. In pastoral soils, just outside the margins of the OHE thermal area, a depleted signature of -16.7‰ was measured.

## 2.5 Discussion

### 2.5.1 Pre-production, current and composite heat flow and $CO_2$ emissions

From Table 2.3 it is evident that heat-flow values computed from $CO_2$ emissions are 47% and 40% larger than observed heat flow computed from shallow soil temperatures within the OHW and OHE thermal areas, respectively. As $CO_2$ is noncondensable under the T-P conditions of surface steam-heated features (Chiodini et al., 2005) this suggests that approximately 1,300 t $d^{-1}$ (39 MW) and 600 t $d^{-1}$ (18 MW) of the ascending steam phase has been lost within the subsurface of the OHW and OHE thermal areas,

respectively, likely as a result of condensation within shallow meteoric groundwaters. The > 40% loss of the steam phase is consistent with: (i) the observed decoupling of heat flow from $CO_2$ flux anomalies at the surface of both major thermal areas, where $CO_2$ anomalies are by far the most extensive (Figs. 2.6 and 2.7); (ii) evidence for the entrainment of hydrothermal fluids by inflows of shallow meteoric groundwaters, occurring at the base of the HFF, and the removal of these fluids from the field by the Waikato River (MacDonald, 1975; Hedenquist, 1990) and; (iii) recent studies of combined heat flow and $CO_2$ flux from hydrothermal areas in Iceland and Italy, where similar results were explained in terms of condensation of steam within shallow ground waters (Chiodini et al., 2004; Fridriksson et al., 2006).

Carbon dioxide emissions computed from pre-production heat flow data are therefore likely to be underestimated. Increasing the $CO_2$ emissions associated with the thermal ground and steam-heated pools of the OHW thermal area by 47% returns values of 42 t $d^{-1}$ (~ 15,300 t $yr^{-1}$) and 14 t $d^{-1}$ (~ 5,200 t $yr^{-1}$), respectively (Table 2.1). $CO_2$ emissions associated with the steam-heated pools of the OHE thermal area equate to 0.3 t $d^{-1}$ (or ~ 110 t $yr^{-1}$) when increased by 40%. Applying an increase of 40% to the small BR6 thermal area yields values of 0.15 t $d^{-1}$ (or ~ 55 t $yr^{-1}$).

The $CO_2$ emissions associated with the pre-production alkali-Cl outflows from the OHW thermal area equate to < 1.7 t $d^{-1}$ or ~ 620 t $yr^{-1}$. This small emission rate, relative to the large alkali-Cl mass flow (3,800 t $d^{-1}$) for the OHW thermal area, is considered a maximum as >95% of the $CO_2$ dissolved within these waters was lost during decompressive boiling, prior to discharge at the surface (chemical data from Mahon and Finlayson, 1972; Hedenquist, 1990). Under the T-P conditions of the surface, degassing of residual dissolved $CO_2$ from alkali-Cl hot waters is not favoured (Werner and Cardellini, 2006).

The combined pre-production emissions associated with the OHW thermal area equate to ~ 58 t $d^{-1}$ or 21,000 t $yr^{-1}$ and were associated with pre-production heat flow of ~ 95 MW (Table 2.1; Dickinson, 1967). These values contrast with a current total emission rate for the OHW thermal area of 72 ± 6 t $d^{-1}$ or 26,250 ± 2,190 t $yr^{-1}$ and an observed heat flow of 43 ± 5 MW. These figures indicate an increase of approximately 40% in the thermal ground emissions and heat flow for the OHW thermal area since initial production of the field in 1988. An increase of 40% in thermal ground emissions are based on the assumption that Dickinson's (1967) estimate of the pre-production thermal-ground heat flow is accurate, and on evidence for temporal stability in the extent and temperature of thermal ground prior to production (see Thompson, 1967; Allis and Webber, 1984; Hunt and Graham, 1997).

An increase in thermal ground heat flow is consistent with repeat Thermal Infrared (TIR) surveys flown in 1988, and again in 1998, which display a marked increase in the extent of thermal ground, and the magnitude of surface heat flow (Hunt and Bromley, 2000). Hunt and Bromley (2000) noted that this visible increase was associated with the proliferation of tension fractures due to production-induced ground subsidence within the OHW thermal area. Unfortunately, vegetative screening precluded attempts

to accurately quantify the heat-flow increases evident in TIR images (Hunt and Bromley, 2000).

Since 1998, tension fractures have continued to proliferate in response to ongoing ground subsidence. This is especially notable within the large area of thermal ground adjacent to well BR9 where numerous linear fractures, developed along the shoulder of a major subsidence bowl (i.e., within a zone of maximum tensional strain), appear to control the extent and spatial orientation of thermal ground and $CO_2$ emissions (Fig. 2.8). This large tract of thermal ground appears to have developed since the detailed soil temperature survey of Allis and Webber in 1984, and now accounts for ~74% (or 53.3 ± 4.4 t $d^{-1}$) of the total $CO_2$ emissions of the OHW thermal area. Ground subsidence due to production-induced pressure decline has increased the permeability of surface units through the proliferation of tension fractures, thereby enabling a greater portion of steam and hydrothermal gases to ascend from the underlying reservoir to the surface. Similarly, pre-production thermal ground southeast of well BR4 is likely to have been enhanced by subsidence-induced tensional fracturing, with surface fractures of up 0.2 m in width, from which steam was seen to be escaping, and where boiling point temperatures were measured. An increase in the vapour pressure of the steam phase overlying the West Bank upflow, due to exploitation of the West Bank reservoir, may also contribute to an increase in diffuse emissions, as observed at the Karapiti thermal area within the nearby Wairakei Field (Mongillo et al., 1988; Glover et al., 1999; Bromley and Hochstein, 2000; Bromley and Hochstein, 2005).

Comparisons of 1.0 m depth soil temperature surveys conducted during this study and pre-production surveys indicate no significant changes in the temperature range, or the extent of thermal ground associated with the OHE thermal area (Thompson, 1967; Allis and Webber, 1984). Because thermal activity within the OHE thermal area has been stable for the last 20 years of production, current values of diffuse heat flow and $CO_2$ emissions may be used as proxy for pre-production values. Likewise, the temporal stability of this area enables pre-production heat-flow and $CO_2$ emissions for the small steam-heated pools of the area to be used to provide a composite estimate of the total emission rate and heat flow of approximately 40 ± 3 t $d^{-1}$ (~14,600 ± 1100 t $yr^{-1}$) and 27 ± 3 MW (Table 2.1). The overwhelming majority (99%) of emissions and surface heat flow are associated with the soils of the OHE thermal area, whereas emissions from thermal ground equate to ~ 72% (or 42 t $d^{-1}$) of the total pre-production emissions for the OHW thermal area (Table 2.1).

The combined or ‘composite’ pre-production emissions and heat flow values for the Ohaaki Field equate to 97 t $d^{-1}$ (or ~35,400 t $yr^{-1}$) and 122 MW, respectively (Table 2.1). By comparison, current total emissions and heat flow equate to 111 ± 6.7 t $d^{-1}$ (or ~40,515 ± 2,450 t $yr^{-1}$) and 70 ± 6 MW, respectively. Due to the absence of statistical information on the pre-production heat flow population (e.g., sample number, range, mean, or standard deviation) it not possible to provide a statistical assessment of the difference between the pre-production and current $CO_2$ emissions rate. The pre-production emission rate does however fall within the range of current emissions (87 $td^{-1}$ and 145 $td^{-1}$), and is close to the lower

bounds of the uncertainty associated with the mean current emission rate. The small mass difference between pre-production and current $CO_2$ emissions masks a 42% increase in $CO_2$ emissions from thermal ground within the OHW thermal area. Here, the expansion of thermal ground compensates for the losses associated with the disappearance of steam-heated pools and alkali-Cl outflows within the same area.

Currently, the movement of steam and $CO_2$ through the soils of the Ohaaki Field constitutes the major (>99%) pathway of heat and mass transfer from the underlying geothermal reservoir to the atmosphere (Table 2.1). Prior to production, when steam-heated pools and alkali-Cl outflows contributed to the total heat and mass flow budget of the Ohaaki Field, $CO_2$ discharge through the soil zone accounted for 80% of the total $CO_2$ emissions. In contrast, only 43% of the pre-production heat flow was associated with thermal soils, the remainder (57%) was associated with the large volume alkali-Cl outflows of the OHW thermal area, and a smaller contribution from steam-heated pools. Numerous studies over the last 15 years that show the soil zone typically constitutes a major, if not *the* major, pathway for mass and heat transfer from the underlying hydrothermal reservoir to the atmosphere (Chiodini et al., 1988; Werner et al., 2000; Favara et al., 2001; Mörner and Etiope, 2002; Fridriksson et al., 2006).

A net decline in post-production surface heat flow by 52 MW for the Ohaaki Field reflects a decrease of 70 MW due to the loss of standing pools (both steam-heated and alkali-Cl, ~19 MW), and the large alkali-Cl seepage along the Waikato River (51.5 MW; Dickinson, 1967). The above decline has been offset by a post-production increase of 20 MW in thermal ground heat flow within the highly perturbed OHW thermal area. Further work is required to confirm the current status of the seepage and to improve the general reliability of the current heat flow estimate. However, given the reported sensitivity of the Ohaaki Pool, and liquid dominated outflows in general, to production-induced pressure decline (see Sorey et al., 1980 and Glover et al., 2000), it is reasonable to assume that the dilute alkali-Cl component of the seepages have declined. Even if seepages still occur they are unlikely to contribute more that 1.0% to the total $CO_2$ emission rate, and therefore, can be excluded from the current emissions estimate.

The pre-production and current $CO_2$ emissions presented above are similar, albeit slightly larger, than an earlier emissions estimate of 31,240 t $yr^{-1}$ (7.1 x $10^8$ mol $yr^{-1}$) published by Seward and Kerrick (1996) for the Ohaaki Field. That estimate was based on a total natural heat flow of 100 MW, which does not appear to have included the heat flow associated with areas of thermal ground, and a low deep reservoir $CO_2$ concentration of 13.2 g $kg^{-1}$. Estimates of $CO_2$ emissions based on deep reservoir concentrations are subject to considerable error due to the likelihood that significant amounts of deep $CO_2$ are scrubbed from the gas stream through water-rock interaction (Werner and Cardellini, 2006). For these reasons the similarity of emission rates are considered fortuitous.

### 2.5.2 Normalised heat flow and $CO_2$ emissions

It has long been recognised that, relative to the size of the deep hot-water reservoir, the area of surface

thermal activity at Ohaaki is small (Studt and Thompson, 1969; Dawson and Dickinson, 1971; Mahon and Finlayson, 1972; Macdonald, 1975; Bibby et al., 1995). Valid comparisons of the normalised emissions and heat flow levels depend on how the area of a given field is defined, as well as the accuracy of published emission rates and heat flow. For the TVZ, thermal-ground and resistivity data are relativity well constrained (see Dawson and Dickinson, 1970; Bibby et al., 1995). However, for international studies of diffuse emissions, uncertainty is introduced by the range of methods by which the extent of thermal ground is defined (Mörner and Etiope, 2002).

Comparison of the resistivity-normalised diffuse emission rates for the Ohaaki Field (~2,300 t $yr^{-1}$ $km^{-2}$) with the nearby Rotorua Field (~14,600 t $yr^{-1}$ $km^{-2}$; Werner and Cardellini, 2006) confirm that, relative to the size of the high-temperature reservoir, the volume of surface fluid discharge at Ohaaki is indeed small. However, if the pre-production diffuse emissions from both fields are normalised by the area of thermal ground, the emission rate for the Ohaaki Field increases markedly, approaching that of Rotorua (i.e., 24,500 t $yr^{-1}$ $km^{-2}$ and 25,500 t $yr^{-1}$ $km^{-2}$, respectively). Further, the thermal-ground-normalised emission rate for Ohaaki is approximately 4 times greater than that of Karapiti geothermal area in New Zealand (Werner et al., 2004), and is comparable to other volcanic degassing areas globally (Fig 2.9; Mörner and Etiope, 2002).

Figure 2.9 presents the thermal-ground and resistivity-normalised heat flow for a number of TVZ hydrothermal fields, including the pre-production heat flow for the Ohaaki Field. As with $CO_2$ emissions, the resistivity normalised heat flow for Ohaaki is small, < 10 MW $km^{-2}$, relative to other TVZ fields. However, when normalised by the area of thermal-ground heat flow increases to 102 MW $km^{-2}$, or more than twice the normalised heat flow of any other field within the TVZ.

Normalised emissions and heat flow levels illustrate that, although the total volume of fluid discharge at Ohaaki is relatively small, it is highly concentrated or focused relative to other fields throughout the TVZ. Focused fluid discharge within both major thermal areas is also supported by $CO_2$ flux rates ≥ 21,000 g $m^{-2}$ $d^{-1}$, which are the highest values reported for volcanic systems within the TVZ (Wardell et al., 2001; Werner et al., 2004; Werner and Cardellini, 2006), and are comparable to values reported for active volcanoes and volcanic hydrothermal systems worldwide (Chiodini et al., 1998; Hernandez et al., 2000; Hernandez et al., 2001; Aiuppa et al., 2004; Bergfeld et al., 2006; Fridriksson et al., 2006; Giammanco et al., 2007).

### 2.5.3 Relationship of $CO_2$ flux to reservoir chemistry and upflow zones

The highest fluxes measured (> 32,000 g $m^{-2}$ $d^{-1}$) and the greatest numbers of high fluxes were recorded within the OHW thermal area. The OHW thermal area is directly above the West Bank upflow, where the highest permeabilities exist for rapid transport between the $CO_2$ source, and the surface and deep fluids release the greatest proportion of $CO_2$ as they ascend, due to depressurization and boiling at depth. The

spatial overlap between the OHW thermal area and the West Bank upflow is displayed diagrammatically in Figures 2.2 and 2.10, within which key reservoir metrics of hot fluid upflow (reservoir Cl concentration, reservoir temperature, and $N_2$/Ar ratios) are contoured from production well data (Hedenquist, 1990; Christenson et al., 2002).

A maximum rate of 21,236 g $m^{-2}$ $d^{-1}$ and a lower number of high fluxes were recorded for the OHE thermal area. The high flux rate and high emission rate of the OHE thermal area is nevertheless consistent with a direct connection to the East Bank upflow. A direct connection is consistent with: (i) the spatial correlation between the OHE thermal area and maximum Cl concentrations and temperatures for the deep reservoir (Figs. 2.2 and 2.10); (ii) elevated $N_2$/Ar ratios from wells within the area that coincide with elevated $N_2$/Ar ratios (≥300 – air corrected) measured by the authors from steam-heated mud pots, and; (iii) anomalous subsoil Hg(v) concentrations (Koga et al., 1982; Murray, 1997).

The $CO_2$ flux from the BR6 thermal area is negligible (mean 24 g $m^{-2}$ $d^{-1}$), with a few small areas of moderately high values (max = 220 g $m^{-2}$ $d^{-1}$) detected during transect surveys. Here, at the margins of the field, the underlying aquifers are steam-heated meteoric waters of very high bicarbonate concentration (max = 2,284 mg $L^{-1}$), moderate temperature (~160ºC) and low-Cl (28 mg $kg^{-1}$) concentration, which exist within the fractured apex of the East Broadlands Rhyolite. The composition of these waters and the absence of a significant $CO_2$ flux indicate the condensation of a minor mass flux of steam and $CO_2$, boiled off the deep reservoir, within the cold meteoric groundwaters of the East Broadlands Rhyolite (Hedenquist, 1990; Christenson et al., 2002). A marginal fluid flow regime beneath the BR6 thermal area is consistent with the low surface $CO_2$ flux and heat flow detected during the surface survey, and is also supported by the lack of any significant sorbed Hg or free Hg vapour anomaly within the soils of the area (Koga et al., 1982; Murray, 1997).

Collectively, the above relationships demonstrate that surface $CO_2$ fluxes can be used to identify major upflow zones within the underlying reservoir, and therefore, that flux surveys have significant implications for the exploration of undeveloped fields. Within the OHW thermal area however, the current anomalous heat flow and $CO_2$ flux rates in part reflect the production-induced perturbations as discussed in section 2.5.1.

### 2.5.4 Structural controls governing surface fluid discharge

Whereas the magnitude of fluid discharge is determined by the proximity to a major upflow the physical occurrence of surface thermal activity is governed by the location of dome complexes. Indeed, all three thermal areas are located near the apexes of extinct volcanic dome complexes. Surface $CO_2$ flux and heat flow decline rapidly and then cease altogether with distance from the apex of each dome (Figs. 2.2 and 2.11).

Extinct dome complexes act as ‘cross-stratal pathways’ for fluid flow, by bypassing several hundred metres of poorly permeable HFF cap rock and connecting the underlying reservoir to the surface. The structural factors governing this relationship include: (i) the greater topographic relief of dome complexes which causes the poorly permeable HFF cap rock to thin above the apex of each dome, and; (ii) the localisation of enhanced vertical permeability about or within the apex of each dome (Grindley, 1970; Henrys and van Dijck, 1987; Henrys and Hochstein, 1990). The attenuation of thermal activity with distance from each dome apex reflects: (i) the rapid decline in fracture density with distance from the apex of each dome, which causes the dome lavas to transition from aquifer-like units to aquitards (Grindley, 1970; Hedenquist, 1990), and; (ii) a concomitant and rapid increase in the thickness of the HFF cap rock with distance from the topographically elevated apex of each dome (Figs. 2.3 and 2.11).

However, the extent of thermal ground at Ohaaki accounts for less than 10% of the total surface area of the underlying high temperature reservoir (thermal ground area defined by soil temperatures ≥25ºC at 1.0 m depth). Away from dome apexes, across > 90% of the field, surveys of surface variables (i.e., soil temperature, $CO_2$ flux, subsoil $CO_2$ and Hg concentrations) show no evidence for surface discharge of geothermal fluids, despite high temperature aquifers at depth (in particular the Waiora Formation).

In addition to the capping effect of the HFF, borehole temperatures indicate large temperature inversions at the base of the HFF, associated with inflows of meteoric groundwaters towards the Waikato River (Macdonald, 1975; Hedenquist, 1990). These cold groundwaters appear to enter the field predominantly through the shallow or emergent dome complexes that flank the field, and then flow beneath the HFF, entraining shallow hydrothermal fluids as they flow towards the Waikato River (MacDonald, 1975; Hedenquist, 1990). The loss of a large volume of hydrothermal fluids at the base of the HFF is supported by shallow resistivity data which depicts tongues of low resistivity water (< 50 Ωm) that follow the course of the Waikato River, both upstream and downstream of the field margins (MacDonald, 1975).

The high degree of structural control at Ohaaki has been commented on by several authors whom attribute the small surface mass flow of the Ohaaki reservoir to three main factors: (i) the especially thick sequence of poorly permeable HFF, with a mean thickness of ~ 220 m (MacDonald, 1975; Koga et al., 1982; Contact Energy, 2006); (ii) the occurrence of the HFF as the uppermost unit of the reservoir, and; (iii) inflows of shallow meteoric groundwaters which entrain the majority of the deep upflows and carry them as subterranean flows towards the Waikato River (MacDonald, 1975; Hedenquist, 1990).

For hydrothermal fields occurring outside of the Reporoa Basin the HFF is thinner, and/or does not form the uppermost layer of the underlying reservoir (Bibby et al., 1984; Grindley, 1986; Wood 1992). A gross approximation of the effectiveness of the HFF as a cap to fluid flow is evident in a contour map of the HFF (Fig. 2.11). Here it is apparent that wherever the thickness of the HFF is less than approximately 180 m, and there are hot fluids at depth, surface thermal features occur. Conversely, where the HFF ≥ 180 m,

fluids are unable to ascend to the surface and no surface thermal activity - either as elevated soil temperatures or anomalous $CO_2$ - is evident, despite the presence of high temperature fluids just beneath the formation.

From the above, a picture arises of a gas-dominated reservoir sealed by a very effective cap rock that is punctuated by isolated regions of enhanced vertical permeability, in the form of volcanic dome complexes, which appear to act as pressure release valves for the underlying reservoir. The focusing of fluid flow by dome complexes is consistent with thermal-ground-normalised heat flow levels that are at least twice that of other fields within the TVZ. Thermal-ground-normalised emissions are also comparable to those reported for volcanic and hydrothermal fields worldwide.

### 2.5.5. Dome controlled fluid flow

The role of dome complexes in governing surface fluid discharge at Ohaaki departs from the more typical fault-controlled discharge documented for the majority of hydrothermal fields, both within the TVZ and internationally (Nairn et al., 1994; Curewitz and Karson, 1997; Chiodini et al., 2004; Rowland and Sibson, 2004; Fridriksson et al., 2006 and others). Recently however, in a diffuse-degassing survey of the nearby Rotorua system, Werner and Cardellini (2006) noted the role of dome apexes as preferential pathways for fluid flow. As at Ohaaki, rhyolite dome complexes within the Rotorua Field are partially or wholly buried by thick lacustrine deposits which thin above the apex of each dome, and enable high temperature fluids to ascend to the surface from the underlying reservoir (Wood, 1992; Werner and Cardellini, 2006). The similarity between these fields, and the prevalence of young volcanic dome complexes and thick lacustrine deposits throughout the TVZ, raises the possibility that dome complexes play an important role in the localisation of surface thermal activity within other hydrothermal fields of the TVZ.

Aside from the gross control of dome complexes over fluid flow, the specific architecture of the fractures governing the spatial distribution of thermal activity is poorly understood. The possibility that normal faults transect the Ohaaki Rhyolite (OHW) and the Broadlands Dacite (OHE) is consistent with the proximity of major normal faults, and the understanding that high competency and low porosity of dome lavas favour fault propagation within the TVZ (see Rowland and Sibson, 2004). However, as raised by Werner and Cardellini (2006) for the Rotorua Field, the brittle structures governing fluid flow may actually reflect surficial structures related to dome growth and cooling. This point however, may not explain the nature of the permeability developed within the poorly permeable lacustrine units which mantle the dome complexes at Rotorua and Ohaaki. The bulk permeability of the HFF is too low (0.01 - 0.3 mD) to account for the focused fluid flow documented for the OHW and OHE thermal areas, which suggests that macro scale permeability features, such as integrated faults or fractures, govern the fluid flow. Additional work is underway to better assess the architecture and origin of brittle structures governing the thermal activity, and the focusing of fluid flow at Ohaaki.

### 2.5.6 Origins of degassed $CO_2$

From Figure 2.12, it can be seen that for high flux sites (i.e. ≥300 g $m^{-2}$ $d^{-1}$), the $\delta^{13}CO_2$ composition of subsoil $CO_2$ is very uniform, varying only slightly around mean values of -7.4 ± 0.3‰ and -6.5 ±0.6‰ for the OHW and OHE thermal areas, respectively. These signatures are very similar to the mean $\delta^{13}CO_2$ composition of West Bank and East Bank bleed-line gas samples (-7.4 ± 1.1‰ and -6.5 ± 0.3‰, respectively), but enriched relative to deep production-well fluids, which display little observable distinction between the West- and East Bank reservoirs (mean $\delta^{13}CO_2$ = -8.3 ± 0.5‰; Christenson et al., 2002). The $\delta^{13}CO_2$ signature of deep production fluids coincide with the isotopically lighter end of the range of typical mantle values (-6.5 ± 2.5‰; e.g. Nishio et al., 1998), which in conjunction with $\delta^{13}CH_4$ values indicates a predominantly magmatic origin for the carbon, with perhaps a small contribution from organic (kerogen) sources (see Christenson et al., 2002).

Christenson et al. (2002) attributed the enrichment of bleed-line $\delta^{13}CO_2$ gas samples over the deep reservoir fluids to boiling induced fractionation and/or associated calcite deposition in the respective wellbores. Likewise, we attribute the enrichment of mean $\delta^{13}CO_2$ of high flux sites to boiling induced fractionation during the ascent of the magmatic $CO_2$ source towards the surface. Boiling induced fractionation can also explain the enrichment of East Bank $\delta^{13}CO_2$ values for bleed-line and high-flux subsoil $CO_2$, relative to the West Bank. The higher noncondensable gas contents of the East Bank reservoir are thought to result in more vigorous, or longer boiling, and therefore, a greater component of isotopic enrichment (Fig. 2.12).

Preservation of the boiled $\delta^{13}CO_2$ signature of reservoir fluids for high-flux sites is consistent with advective gas transport through the soil zone, and is a common feature of hydrothermal and volcanic areas (Natale et al., 2000; Camarda et al., 2007). During advective gas transport under a pressure gradient, the soil zone is saturated with $CO_2$ and diffusive fractionation of the isotopologues of $CO_2$ ($M^{12}CO_2$ = 44 and $M^{13}CO_2$= 45) does not occur, preserving the isotopic signature of the $CO_2$ source as it ascends from the underlying reservoir (Capasso, 2001; Camarda et al., 2007).

The $\delta^{13}CO_2$ composition of low to moderate $CO_2$ flux sites (15 to < 300 g $m^{-2}$ $d^{-1}$) exhibits a far wider range (-2.4 to -8.6‰), as well as being significantly enriched (-5.2 ± 1.7‰) relative to the mean values reported for high flux sites (Fig. 2.12). This isotopic enrichment is explained in terms of diffusive fractionation of the isotopologues of $CO_2$ ($M^{12}CO_2$ = 44 and $M^{13}CO_2$= 45) as they diffuse along a concentration gradient between the subsoil (porous media) and the atmosphere (Amundson et al., 1998; Camarda et al., 2007). Specifically, the slightly different atomic masses of the isotopologues of $CO_2$ result in accumulation of the heavier $^{13}CO_2$ molecule within the soil, relative to its lighter $^{12}CO_2$ counterpart, which diffuses at a faster rate along the concentration gradient (Cerling, 1984; Amundson et al., 1998). This mass bias, or fractionation effect, imparts a characteristic enrichment in subsoil $^{13}CO_2$ of up to +4.4‰, relative to the isotopic signature of the $CO_2$ source, for any purely diffusive system under steady

state conditions (Cerling, 1984; Amundson et al., 1998).

Diffusive and advective transport processes may occur simultaneously, as is evident in Figure 2.12, where for the same range of surface flux (between 15 - 300 g $m^{-2}$ $d^{-1}$), isotopic values reflect either dominantly diffusive enrichment, mixed diffusive-advective or purely advective (no-fractionation) conditions. The most enriched subsoil value from the OHE thermal area equates to an enrichment over the mean for high flux sites of ~ +4.1‰, indicating nearly pure diffusive gas transport (93% of the maximum diffusive enrichment value of +4.4‰) (Fig. 2.12). Interestingly, $\delta^{13}CO_2$ values for moderate to low flux sites within the OHW thermal area display no significant diffusive isotopic enrichment. This may reflect the lack of data over the 100 to 1,000 g $m^{-2}$ $d^{-1}$ flux range, or more direct flow paths related to macro scale fractures associated with ground subsidence in this area.

The exact surface-flux threshold at which gas transport moves from purely diffusive to mixed diffusive-advective, and then on to purely advective, is poorly constrained by the data and dependant on the permeability of the soil (air-filled porosity and tortuosity), which will change from site to site due to the innate heterogeneities of soil texture and the role of steam condensation in reducing permeability. Nonetheless, on the basis of Figure 2.12, we propose approximate flux thresholds of < 30 g $m^{-2}$ $d^{-1}$ for purely diffusive gas transport, between 30 and 300 g $m^{-2}$ $d^{-1}$ for combined diffusive-advective transport, and ≥ 300 g $m^{-2}$ $d^{-1}$ for purely advective gas transport.

Although a magmatic $CO_2$ component was evident at all sites, the contribution from an isotopically depleted $CO_2$ source is evident for low temperature ($T \leq$ ambient air temperature at the time of sampling), low flux sites (<30 g $m^{-2}$ $d^{-1}$), all of which supported dense stands of non-thermal vegetation. This isotopically depleted source is most likely soil respired (biogenic) $CO_2$ (-23‰ for C3 plants; Amundson et al., 1998), which mixes with and dilutes the isotopically heavier magmatic component (Fig. 2.12). Those sites with the most depleted isotopic signatures (-12.5 to -16.7‰) have soil profiles with well developed A and B horizons, and decreasing soil temperatures with depth (measured to 1.3 m). Accordingly, the threshold at which biogenic soil $CO_2$ flux constitutes a significant portion of the overall $CO_2$ flux is estimated at ≤ 30 g $m^{-2}$ $d^{-1}$. The biogenic $CO_2$ signature is likely to decline in concert with increasing soil temperatures (>35ºC), and/or $CO_2$ flux, due to the negative effects of these parameters on vegetation density, and hence biomass accumulation (Gerlach et al., 2001). This observation is supported by cumulative probability plots that depict two distinct (non-overlapping) flux populations that correspond to a low-flux, biogenic soil-respired endmember, and a high-flux, magmatic hydrothermal endmember.

The initial isotopic results suggest a two-stage fractionation process for low-flux sites, characterized by boiling during fluid ascent within the underlying reservoir, and then isotopic enrichment as $CO_2$ diffuses through the porous media of the soil zone. For high-flux sites the $\delta^{13}CO_2$ signature is unaffected by near surface (soil zone) fractionation processes, and reflects the composition of the boiled magmatic $CO_2$

source.

## 2.6 Conclusion

Pre-production and current $CO_2$-emission and heat-flow data for the Ohaaki Field indicate a 40% increase in diffuse soil degassing, and a net decrease of ~ 50 MW (42%) in surface heat flow, following 20 years of production. The increase in soil diffuse degassing reflects the influence of production of the field on shallow permeability within the OHW thermal area (ground subsidence) and a likely increase in the pressure of the shallow vapour phase. The decline in heat flow reflects the disappearance of alkali-Cl springs and seeps due to the sensitivity of liquid outflows to declining reservoir pressures. Despite these, changes post-production $CO_2$ emissions are only slightly larger than pre-production emissions.

The predominance of diffuse degassing as the major pathway for gaseous exchange at Ohaaki supports numerous recent publications that point to the release of globally significant amounts of $CO_2$, by diffuse degassing through the soils of volcanic hydrothermal systems (Mörner and Etiope, 2002; Werner and Cardellini, 2006). Use of diffuse $CO_2$ flux measurement to assess the energy release from the Ohaaki reservoir indicates that a significant portion ($\geq$ 40%) of the ascending steam phase is lost before reaching the soil zone. This observation is consistent with recent findings that $CO_2$ flux surveys may provide a more accurate measure of heat released from volcanic and volcanic-hydrothermal reservoirs than conventional heat flow surveys (Chiodini et al., 2005; Fridriksson et al., 2006), and underlines the value of $CO_2$ flux surveys for resource estimation.

Normalised $CO_2$ emissions and heat flow support earlier observations that surface mass flow at Ohaaki is small relative to the size of the high-temperature reservoir, but also indicate that surface fluid discharge is highly focused (high volume per unit area) relative to other TVZ hydrothermal systems. This is consistent with a high degree of structural control at Ohaaki. Buried or emergent dome complexes govern the location of each area of surface thermal activity by effectively bypassing several hundred metres of the poorly permeable cap rock, which masks the existence of the high-temperature reservoir. Dome complexes act as pathways of preferential vertical permeability, focusing fluid flow and functioning as pressure release valves for the underlying reservoir. Whereas the location of surface thermal activity is governed by the occurrence of buried dome complexes, the magnitude of surface flux depends upon the proximity of each dome complex to major upflow zones. Indeed, variability in the location, spatial extent, and magnitude of $CO_2$ flux, is consistent with established geochemical and geophysical models of the Ohaaki Field. Significantly, these results demonstrate that $CO_2$ flux surveys may be used to identify main upflow zones, and areas of structural permeability in undeveloped hydrothermal systems.

Finally, the estimated amount of $CO_2$ released by the Ohaaki system, and the chemical and isotopic signature of discharged fluids and gases, support the presence of a predominantly magmatic origin for the carbon, and verifies the connection between both major thermal areas and the underlying high-

temperature reservoir. On the basis of the relationship between the magnitude of flux and the isotopic composition of soil $CO_2$, gas transport transitions from purely diffuse (< 30 g $m^{-2}$ $d^{-1}$) through to mixed advective-diffusive (30 – 300 g $m^{-2}$ $d^{-1}$) before becoming purely advective at flux rates > 300 g $m^{-2}$ $d^{-1}$.

## 2.7 Acknowledgements

We thank the staff of the geothermal group at Contact Energy for access to the Ohaaki Field, logistical and field support and for critical review. Likewise we thank the staff of Wairakei GNS who donated generously of their time and experience and also aided in the maintenance and lease of field equipment, provided access to detailed cross-sections, and historical reports. Valuable field assistance was provided by C. Rigg, M. Hughes, M. Ohnacker, and M. Fookes. The majority of funding for this project was provided by Contact Energy, with additional support from the Mason Trust Fund of the University of Canterbury.

## 2.8 References

Aiuppa, A., Caleca, A., Federico, C., Gurrieri, S. and Valenza, M., 2004. Diffuse degassing of carbon dioxide at Somma-Vesuvius volcanic complex (Southern Italy) and its relation with regional tectonics. Journal of Volcanology and Geothermal Research, 133(1-4): 55-79.

Allis, R.G. and Webber, S., 1984. Shallow temperature measurements at Wairakei and Broadlands fields. Geophysics Division Report, 197: 27.

Allis, R.G., Nash, G.D., Johnson, S.D., Thomasson, R.L., Hanson, J., Capuano, L.E., Jr., Schochet, D., Livesay, B., Page, T., Lovekin, J.W. and Johnson, S.E., 1999. Conversion of thermal infrared surveys to heat flow; comparison from Dixie Valley, Nevada, and Wairakei, New Zealand, Transactions - Geothermal Resources Council, vol. 23. GRC - Geothermal Resources Council, Davis, pp. 499-504.

Amundson, R., Stern, L., Baisden, T. and Wang, Y., 1998. The isotopic composition of soil and soil-respired $CO_2$. Geoderma, 82(1-3): 83-114.

Bergfeld, D., Evans, W.C., Howle, J.F. and Farrar, C.D., 2006. Carbon dioxide emissions from vegetation-kill zones around the resurgent dome of Long Valley Caldera, eastern California, USA. Journal of Volcanology and Geothermal Research, 152(1-2): 140-156.

Bibby, H.M., Dawson, G.B., Rayner, H.H., Stagpoole, V.M. and Graham, D.J., 1984. The structure of the Mokai geothermal field based on geophysical observations. Journal of Volcanology and Geothermal Research, 20(1-2): 1-20.

Bibby, H.M., Caldwell, T.G., Davey, F.J. and Webb, T.H., 1995. Geophysical evidence on the structure of the Taupo volcanic zone and its hydrothermal circulation. Journal of Volcanology and Geothermal Research, 68(1-3): 29-58.

Brombach, T., Hunziker, J.C., Chiodini, G., Cardellini, C. and Marini, L., 2001. Soil diffuse degassing and thermal energy fluxes from the southern Lakki Plain, Nisyros (Greece). Geophysical Research Letters, 28(1): 69-72.

Bromley, C., Hunt, T.M. and Morris, C., 1993. Cold Downflows of Groundwater at Ohaaki Geothermal Field: Preliminary Results. 15th New Zealand, Geothermal Workshop, University of Auckland Geothermal Institute, pp. 181-186.

Bromley, C.J. and Hochstein, M.P., 2000. Heat transfer of the Karapiti fumarole (1946-2000). 22nd New Zealand Geothermal Workshop, University of Auckland Geothermal Institute, pp 87-92.

Camarda, M., De Gregorio, S., Favara, R. and Gurrieri, S., 2007. Evaluation of carbon isotope fractionation of soil $CO_2$ under an advective-diffusive regime: A tool for computing the isotopic composition of unfractionated deep source. Geochimica et Cosmochimica Acta, 71(12): 3016-3027.

Capasso, G., D'Alessandro. W., Favara, R., Inguaggiato, S. and Parello, F., 2001. Kinetic isotope fractionation of $CO_2$ carbon due to diffusion processes through the soil. Water-Rock Interaction, 10: 1497-1499.

Carapezza, M.L. and Granieri, D., 2004. $CO_2$ soil flux at Vulcano (Italy); comparison between active and passive methods. Applied Geochemistry, 19(1): 73-88.

Cardellini, C., Chiodini, G. and Frondini, F., 2003. Application of stochastic simulation to $CO_2$ flux from soil; mapping and quantification of gas release. Journal of Geophysical Research, 108: no.B9, 13.
Cerling, T.E., 1984. The stable isotopic composition of modern soil carbonate and its relationship to climate. Earth and Planetary Science Letters, 71(2): 229-240.
Chiodini, G., Cioni, R., Guidi, M., Raco, B. and Marini, L., 1998. Soil $CO_2$ flux measurements in volcanic and geothermal areas. Applied Geochemistry, 13(5): 543-552.
Chiodini, G., Avino, R., Brombach, T., Caliro, S., Cardellini, C., De Vita, S., Frondini, F., Granirei, D., Marotta, E. and Ventura, G., 2004. Fumarolic and diffuse soil degassing west of Mount Epomeo, Ischia, Italy. Journal of Volcanology and Geothermal Research, 133(1-4): 291-309.
Chiodini, G., Granieri, D., Avino, R., Caliro, S., Costa, A. and Werner, C., 2005. Carbon dioxide diffuse degassing and estimation of heat release from volcanic and hydrothermal systems. Journal of Geophysical Research, 110: no.B8, 17.
Christenson, B.W., Mroczek, E.K., Kennedy, B.M., van Soest, M.C., Stewart, M.K. and Lyon, G., 2002. Ohaaki reservoir chemistry; characteristics of an arc-type hydrothermal system in the Taupo volcanic zone, New Zealand. Journal of Volcanology and Geothermal Research, 115(1-2): 53-82.
Contact Energy, 2006. Ohaaki well and feed zone stratigraphic database.
Curewitz, D. and Karson, J.A., 1997. Structural settings of hydrothermal outflow; fracture permeability maintained by fault propagation and interaction. Journal of Volcanology and Geothermal Research, 79(3-4): 149-168.
Dawson, G.B., 1964. The nature and assessment of heat flow from hydrothermal areas. New Zealand Journal of Geology and Geophysics, 7(1): 155-171.
Dawson, G.B. and Dickinson, D.J., 1970. Heat flow studies in thermal areas of the North Island of New Zealand. Geothermics, 2(Part 1): 466-473.
Dawson, G.B., 1988. Broadlands Geothermal Field Environmental Monitoring (Ground Temperature and Geothermal Feature Survey). Report No. 91, Department of Scientific and Industrial Research (D.S.I.R.). Wellington.
Deutsch, C.V. and Journel, A.G., 1998. GSLIB: Geostatistical Software Library and User's Guide. Applied Geostatistics Series. Oxford University Press, New York, Oxford.
Dickinson, D.J., 1967. The natural heat output of the Broadlands geothermal area, 1967. Report, Department of Scientific and Industrial Research - Geophysics Division, Wellington.
Favara, R., Giammanco, S., Inguaggiato, S. and Pecoraino, G., 2001. Preliminary estimate of $CO_2$ output from Pantelleria Island volcano (Sicily, Italy): evidence of active mantle degassing. Applied Geochemistry, 16(7-8): 883-894.
Fridriksson, T., Kristjansson, B.R., Armannsson, H., Margretardottir, E., Olafsdottir, S. and Chiodini, G., 2006. $CO_2$ emissions and heat flow through soil, fumaroles, and steam-heated mud pools at the Reykjanes geothermal area, SW Iceland. Applied Geochemistry, 21(9): 1551-1569.
Gerlach, T.M., Doukas, M.P., McGee, K.A. and Kessler, R., 2001. Soil efflux and total emission rates of magmatic $CO_2$ at the Horseshoe Lake tree kill, Mammoth Mountain, California, 1995-1999. In: D. Bergfeld, F. Goff and P. Allard (Editors), Chemical Geology. Elsevier, Amsterdam, pp. 101-116.
Giammanco, S., Parello, F., Gambardella, B., Schifano, R., Pizzullo, S. and Galante, G., 2007. Focused and diffuse effluxes of $CO_2$ from mud volcanoes and mofettes south of Mt. Etna (Italy). Journal of Volcanology and Geothermal Research, 165(1-2): 46-63.
Giggenbach, W.F., 1989. The chemical and isotopic position of the Ohaaki Field within the Taupo volcanic zone. 11th New Zealand Geothermal Workshop, University of Auckland Geothermal Institute, pp. 81-88.
Giggenbach, W.F., 1995. Variations in the chemical and isotopic composition of fluids discharged from the Taupo Volcanic Zone, New Zealand. Journal of Volcanology and Geothermal Research, 68(1-3): 89-116.
Glover, R.B., Mroczek, E.K., Finlayson, J.B., Simmons, S.F., Morgan, O.E. and Dunstall, M.G., 1999. Changes in major gas concentrations in the Karapiti thermal area in response to development at Wairakei. 21st New Zealand Geothermal Workshop, University of Auckland Geothermal Institute, pp. 7-13.
Glover, R.B., Hunt, T.M. and Severne, C.M., 2000. Impacts of development on a natural thermal feature and their mitigation; Ohaaki Pool, New Zealand. Geothermics, 29(4-5): 509-523.
Goovaerts, P., 1997. Kriging vs. stochastic simulation for risk analysis in soil contamination. Quantitative Geology and Geostatistics, vol. 9, pp. 247-258.
Grant, M.A., Donaldson, I.G. and Bixley, P.F., 1982. Geothermal reservoir engineering Academic Press,

New York.
Grindley, G.W., 1970. Subsurface structures and relation to steam production in the Broadlands geothermal field, New Zealand. Geothermics, 2(Part 1): 248-261.
Grindley, G.W., 1986. Subsurface geology and structure of the Kawerau geothermal field. Report 10, Department of Scientific and Industrial Research, Wellington.
Hedenquist, J.W., 1990. The thermal and geochemical structure of the Broadlands-Ohaaki geothermal system, New Zealand. Geothermics, 19(2): 151-185.
Henrys, S.A. and van Dijck, M.F., 1987. Structure of concealed rhyolites and dacites in the Broadlands-Ohaaki geothermal field. 9th New Zealand Geothermal Workshop, University of Auckland Geothermal Institute, pp. 43-48.
Henrys, S.A. and Hochstein, M.P., 1990. Geophysical structure of the Broadlands-Ohaaki geothermal field (New Zealand). Geothermics, 19(2): 129-150.
Hernandez, P.A., Natale, G., Tsunomori, F., Sugiyama, K., Ito, T., Notsu, K., Okada, H., Salazar, J.M., Perez, N.M., 2000. Diffuse emissions of carbon dioxide from Tarumae Volcano, Japan. Transactions, American Geophysical Union, vol.81, no.48, Suppl., pp.1319, 28 Nov 2000
Hernández, P.A., Salazar, J.M., Shimoike, Y., Mori, T., Notsu, K. and Pérez, N., 2001. Diffuse emission of $CO_2$ from Miyakejima volcano, Japan. Chemical Geology, 177(1-2): 175-185.
Hochstein, M.P. and Bromley, C.J., 2005. Measurement of heat flux from steaming ground. Geothermics, 34(2): 131-158.
Hunt, T.M. and Graham, D.J., 1997. Shallow ground temperature and groundwater temperature monitoring at Ohaaki (Broadlands) Geothermal Field. Institute of Geological and Nuclear Sciences, Taupo.
Hunt, T.M. and Bromley, C.J., 2000. Some environmental changes resulting from development of Ohaaki geothermal field, New Zealand. World Geothermal Conference, Kyushu, Japan, pp. 621-626.
Journel, A.G., 1994. Resampling from stochastic simulations. Environmental and Ecological Statistics 1: 63-91.
Koga, A., Taguchi, S. and Mahon, W.A.J., 1982. The use of volatile constituents in geothermal fluids for assessing the type, potential and near surface permeability of a geothermal system; the Broadlands geothermal area, N.Z, Proceedings of Pacific Geothermal Conference, vol.4. University of Auckland Geothermal Institute, Auckland, pp. 135-138.
MacDonald, W.J.P., 1975. The useful heat contained in the Broadlands geothermal field. Second United Nations symposium on the development and use of geothermal resources, San Francisco, Calif., United States, pp. 1113-1119.
Mahon, W.A.J. and Finlayson, J.B., 1972. The chemistry of the Broadlands geothermal area, New Zealand. American Journal of Science, 272(1): 48-68.
Milicich, S.D., 2010. A 3D computer model of the Ohaaki Reservoir. GNS Science, Wairakei.
Mongillo, M.A., Allis, R.G. and Freeston, D.H., 1988. Continuing changes in surface activity at Craters of the Moon thermal area, Wairakei. 10th New Zealand Geothermal Workshop, University of Auckland Geothermal Institute, pp. 345-349.
Mongillo, M.A. and Graham, D.J., 1999. Quantitative evaluation of airborne video TIR survey imagery. 21st NZ Geothermal Workshop, University of Auckland, pp. 151-156.
Mörner, N.-A. and Etiope, G., 2002. Carbon degassing from the lithosphere. Global and Planetary Change, 33(1-2): 185-203.
Murray, K.S., 1997. The use of soil Hg to delineate zones of upwelling in low-to-moderate temperature geothermal systems. Geothermics, 26(2): 193-202.
Nairn, I.A., Wood, C.P. and Bailey, R.A., 1994. The Reporoa Caldera, Taupo volcanic zone; source of the Kaingaroa Ignimbrites. Bulletin of Volcanology, 56(6-7): 529-537.
Nishio, Y., Sasaki, S., Gamo, T., Hiyagon, H. and Sano, Y., 1998. Carbon and helium isotope systematics of North Fiji Basin basalt glasses: carbon geochemical cycle in the subduction zone. Earth and Planetary Science Letters, 62: 239 - 257.
Rae, A.J., Rosenberg, M.D., Bignall, G., Kilgour, G.N. and Milicich, S.D., 2007. Geological results of production well drilling in the western steamfield, Ohaaki geothermal system: 2005-2007. 29th New Zealand Geothermal Workshop, University of Auckland Geothermal Institute, pp. 7.
Rowland, J.V. and Sibson, R.H., 2004. Structural controls on hydrothermal flow in a segmented rift system, Taupo volcanic zone, New Zealand. Geofluids, 4(4): 259-283.
Seward, T.M. and Kerrick, D.M., 1996. Hydrothermal $CO_2$ emission from the Taupo Volcanic Zone, New Zealand. Earth and Planetary Science Letters, 139(1-2): 105-113.

Sorey, M.L., Grant, M.L. and Bradford, E., 1980. Nonlinear effects in two-phase flow to wells in geothermal reservoirs. Water Resources Research, vol. 16, pp. 767–777.
Sorey, M.L. and Colvard, E.M., 1994. Measurements of heat and mass flow from thermal areas in Lassen Volcanic National Park, California, 1984–93. US Geological Survey, Water Resources Investigations Report 94-4180-A: 35 p.
Studt, F.E. and Thompson, G.E.K., 1969. Geothermal heat flow in the North Island of New Zealand. New Zealand Journal of Geology and Geophysics, 12(4): 673-683.
Thompson, G.E.K., 1967. Ground temperatures at a depth of one metre. Report, Department of Scientific and Industrial Research - Geophysics Division, Wellington.
Wardell, L.J., Kyle, P.R., Dunbar, N. and Christenson, B., 2001. White Island volcano, New Zealand: carbon dioxide and sulfur dioxide emission rates and melt inclusion studies. Chemical Geology, 177(1-2): 187-200.
Welles, J.M., Demetriades-Shah, T.H. and McDermitt, D.K., 2001. Considerations for measuring ground $CO_2$ effluxes with chambers. Chemical Geology, 177(1-2): 3-13.
Werner, C., Brantley, S.L. and Boomer, K., 2000. $CO_2$ emissions related to the Yellowstone volcanic system; 2, Statistical sampling, total degassing, and transport mechanisms. Journal of Geophysical Research, 105(B5): 10831-10846.
Werner, C., Hochstein, M.P., Bromley, C.J., Manville, V.R. and Tilyard, D., 2004. $CO_2$-flux of steaming ground at Karapiti (Wairakei, NZ). Geological Society of New Zealand 117A: 115-116.
Werner, C. and Cardellini, C., 2006. Comparison of carbon dioxide emissions with fluid upflow, chemistry, and geologic structures at the Rotorua geothermal system, New Zealand. Geothermics, 35(3): 221-238.
Wood, C.P., 1992. Geology of the Rotorua geothermal system. Geothermics, 21(1-2): 25-41.
Wood, C.P., 1994. The Waiora Formation geothermal aquifer, Taupo volcanic zone, New Zealand. 16th New Zealand Geothermal Workshop, University of Auckland Geothermal Institute, pp. 121-126.
Wood, C.P., Brathwaite, R.L. and Rosenberg, M.D., 2001. Basement structure, lithology and permeability at Kawerau and Ohaaki geothermal fields, New Zealand. Geothermics, 30(4): 461-481.

## 1.7 Figures

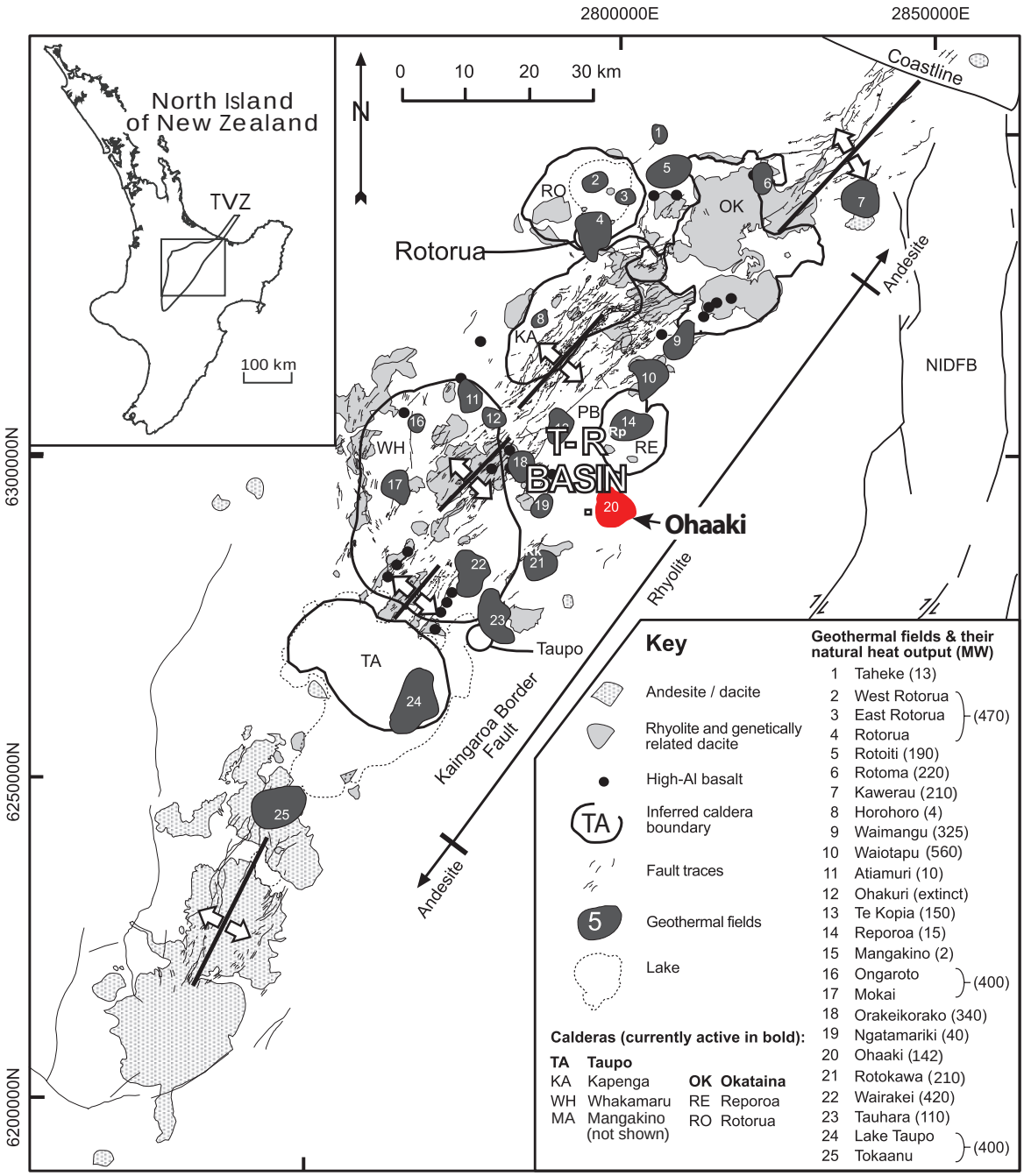


Figure 2.1. Map of the Taupo Volcanic Zone showing the distribution of geothermal systems, defined by the presence of low-resistivity zones (<30 Ωm) in relation to rift architecture, major volcanic rock types and caldera boundaries (modified from Rowland & Sibson 2004). Where T-R basin denotes the location of the Taupo Reporoa Basin and the Ohaaki hydrothermal field is in red. NIDFB, North Island Dextral Fault Belt. Major towns, Taupo and Rotorua, are labelled.

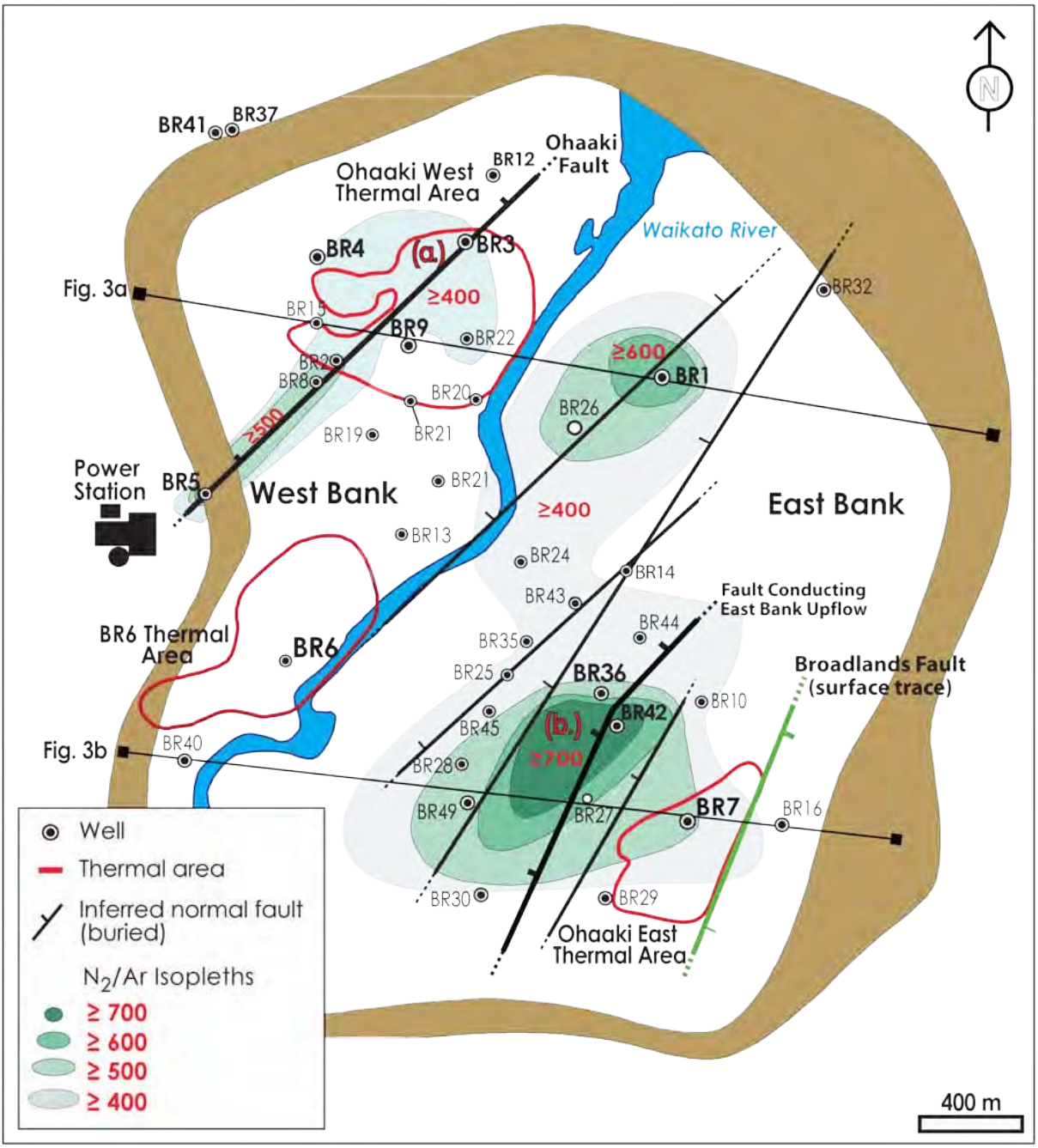


Figure 2.2. Plan view of the Ohaaki Field including resistivity boundary, inferred deep-seated normal faults, $N_2$/Ar isopleths and location of major thermal areas (from Christenson et al., 2002; Wood et al., 2001). $N_2$/Ar isopleths denote the major hydrothermal upflows of the field. The Ohaaki Fault occurs in the upper left of the field and conducts the West Bank upflow. The East Bank upflow occurs through another major normal fault in the SE. The surface trace of the Broadlands Fault is shown in green (this study). The location of major thermal areas, Ohaaki West (OHW) and Ohaaki East (OHE), and low temperature BR6 thermal area are shown. Thermal areas are delineated by 1.0 m depth temperatures ≥ 25ºC after Allis and Webber, (1984) and this study. The line of cross-section for Figures 3a and 3b are also displayed.

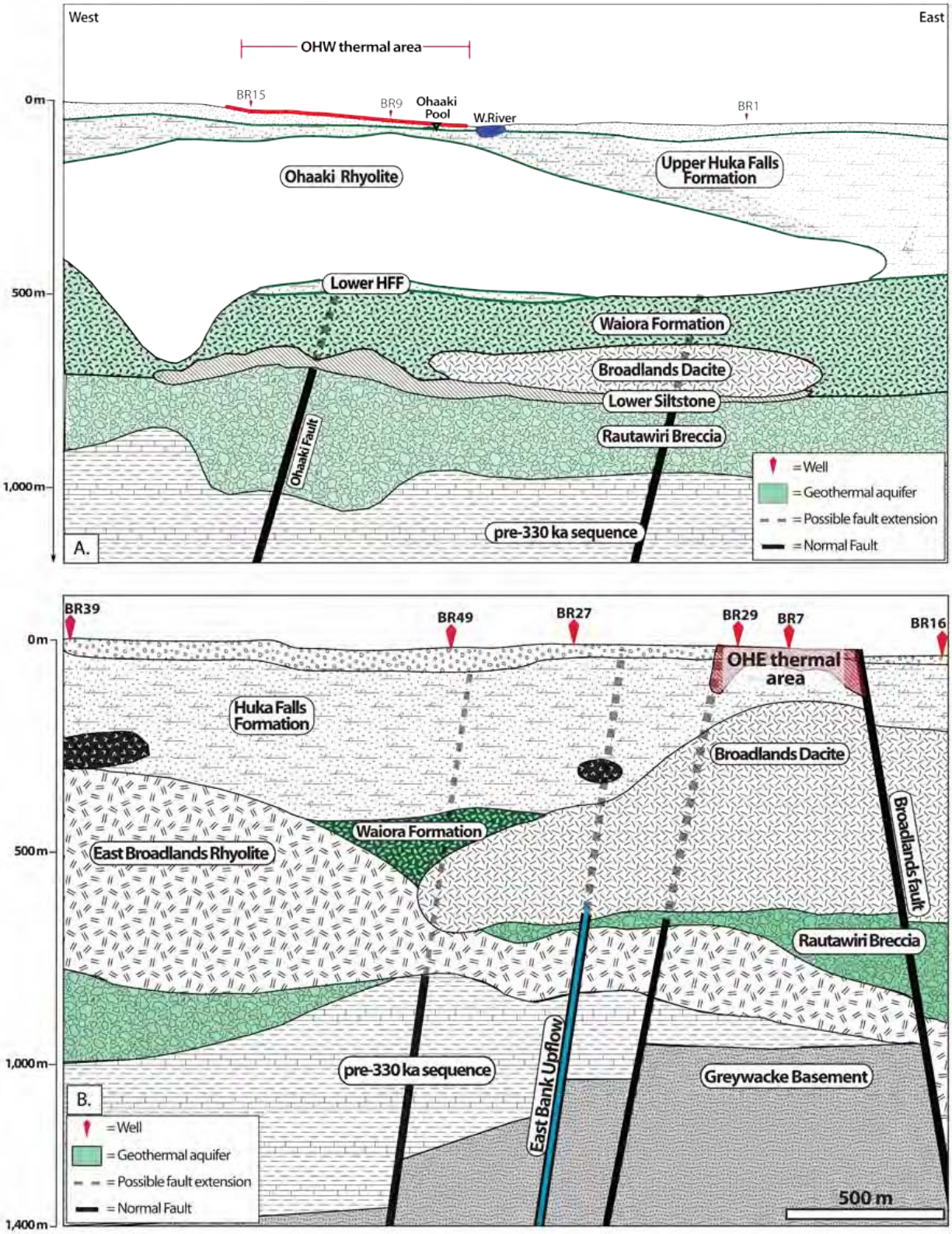


Figure 2.3. East – west cross sections through the Ohaaki reservoir (modified from Milicich, 2010). (a) Cross section through the NW sector of the field and the OHW thermal area. (b) Cross section through the SE sector of the field and the OHE thermal area. Fault locations are idealised and not to scale. The black blobs occurring within the HFF, (b), are distal flow lobes of the Ohaaki Rhyolite.

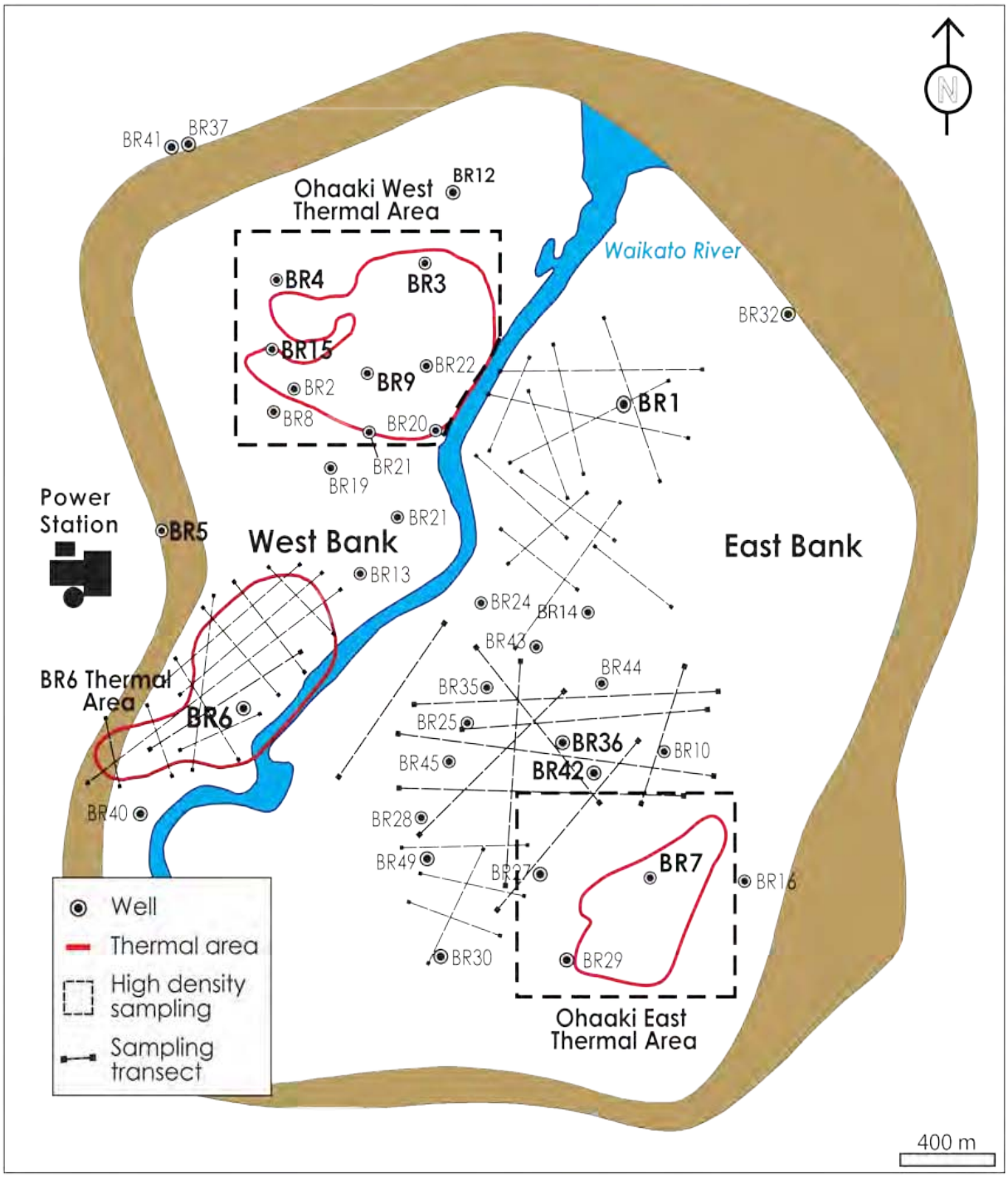


Figure 2.4. Map of sampling locations within the Ohaaki Field. Boxed and dashed areas delimit the extent of the intensive $CO_2$ flux and soil temperature survey. $CO_2$ flux and soil transects across the East Bank reservoir occur above a region of deep upwelling as defined by reservoir chemistry.

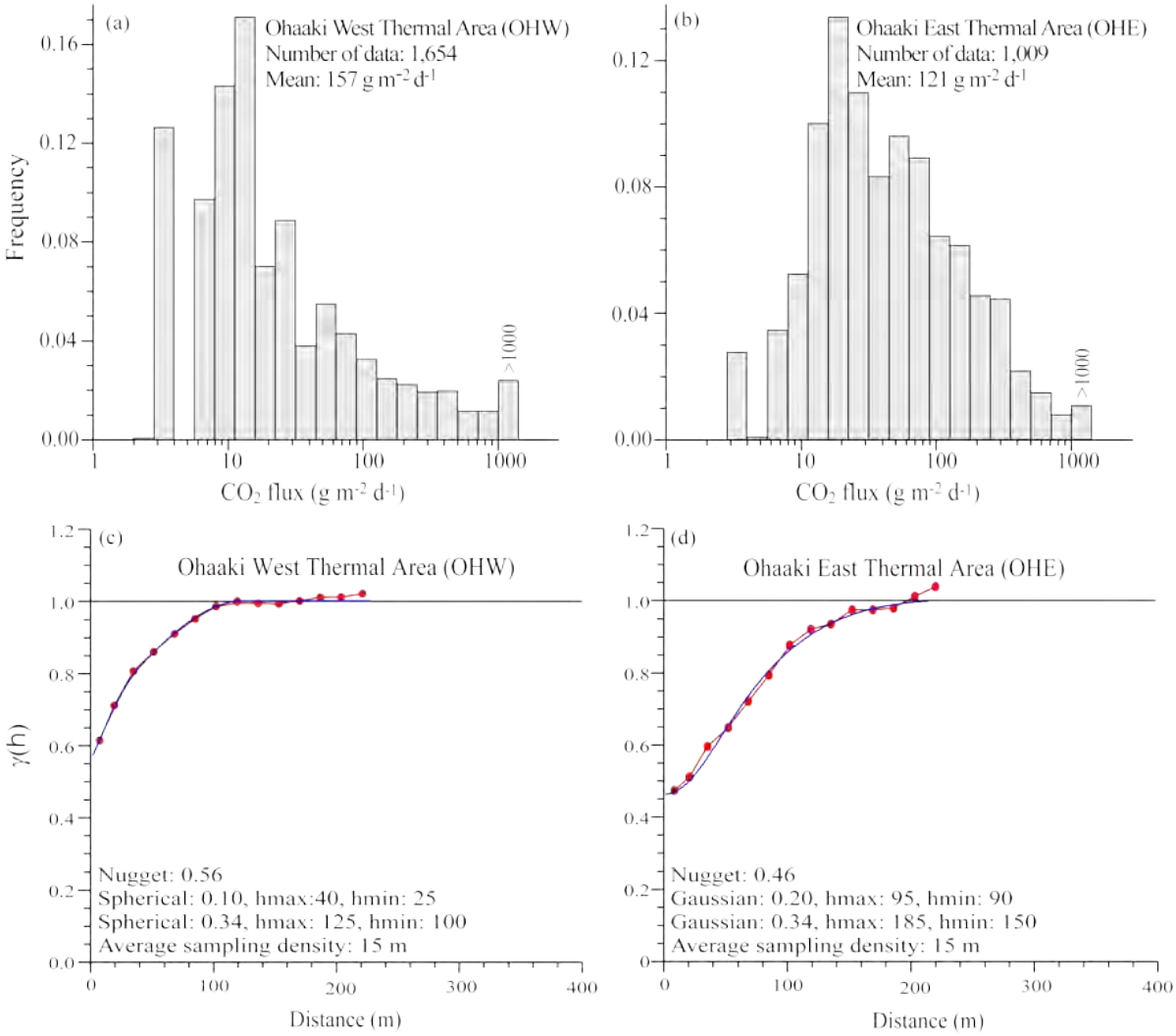


Figure 2.5. (a – b) Frequency histograms showing $CO_2$ flux populations and statistics for the OHW and OHE thermal areas. (c – d) Experimental semivariogram for $CO_2$ measurements within the OHW and OHE thermal areas.

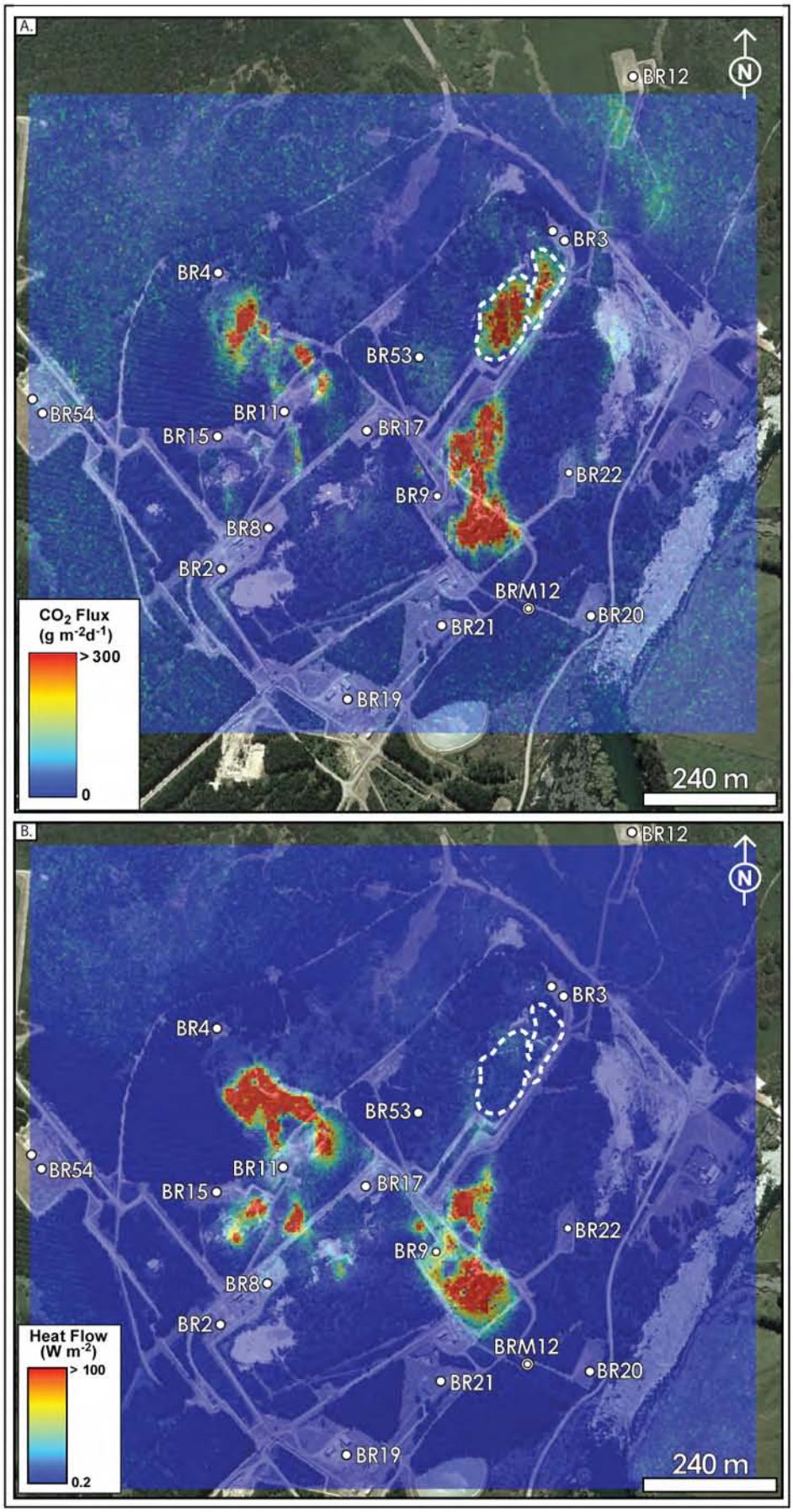


Figure 2.6. (a) Pixel plot of sequential Gaussian simulations of diffuse $CO_2$ flux through the soil of the OHW thermal area. (b) Pixel plot of sequential Gaussian simulations of thermal ground heat flow within the OHW thermal area. Note: (i) absence of heat flow anomaly despite elevated $CO_2$ flux SW of well BR3, and; (ii) the anomalous $CO_2$ flux and heat flow associated with the large tract of thermal ground adjacent to well BR9.

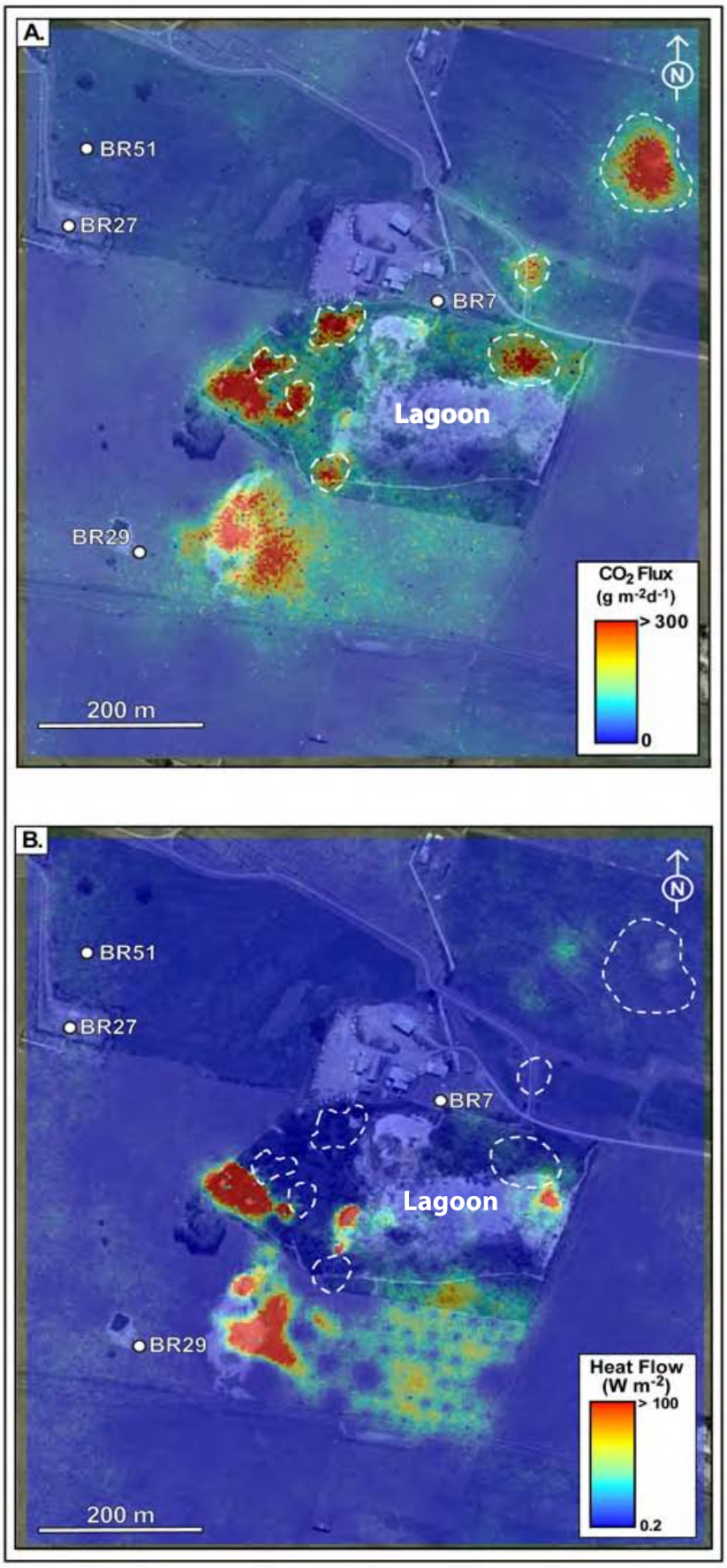


Figure 2.7. (a) Pixel plot of sequential Gaussian simulations of diffuse $CO_2$ flux through the soil of the OHE thermal area. (b) Pixel plot of sequential Gaussian simulations of thermal ground heat flow within the OHE thermal area. Note: (i) decoupling of heat flow from $CO_2$ flux within the NE corner of thermal area and; (ii) minor heat flow and low $CO_2$ flux across the lagoon area, within which several steam-heated pools and numerous small boiling mud pots occur.

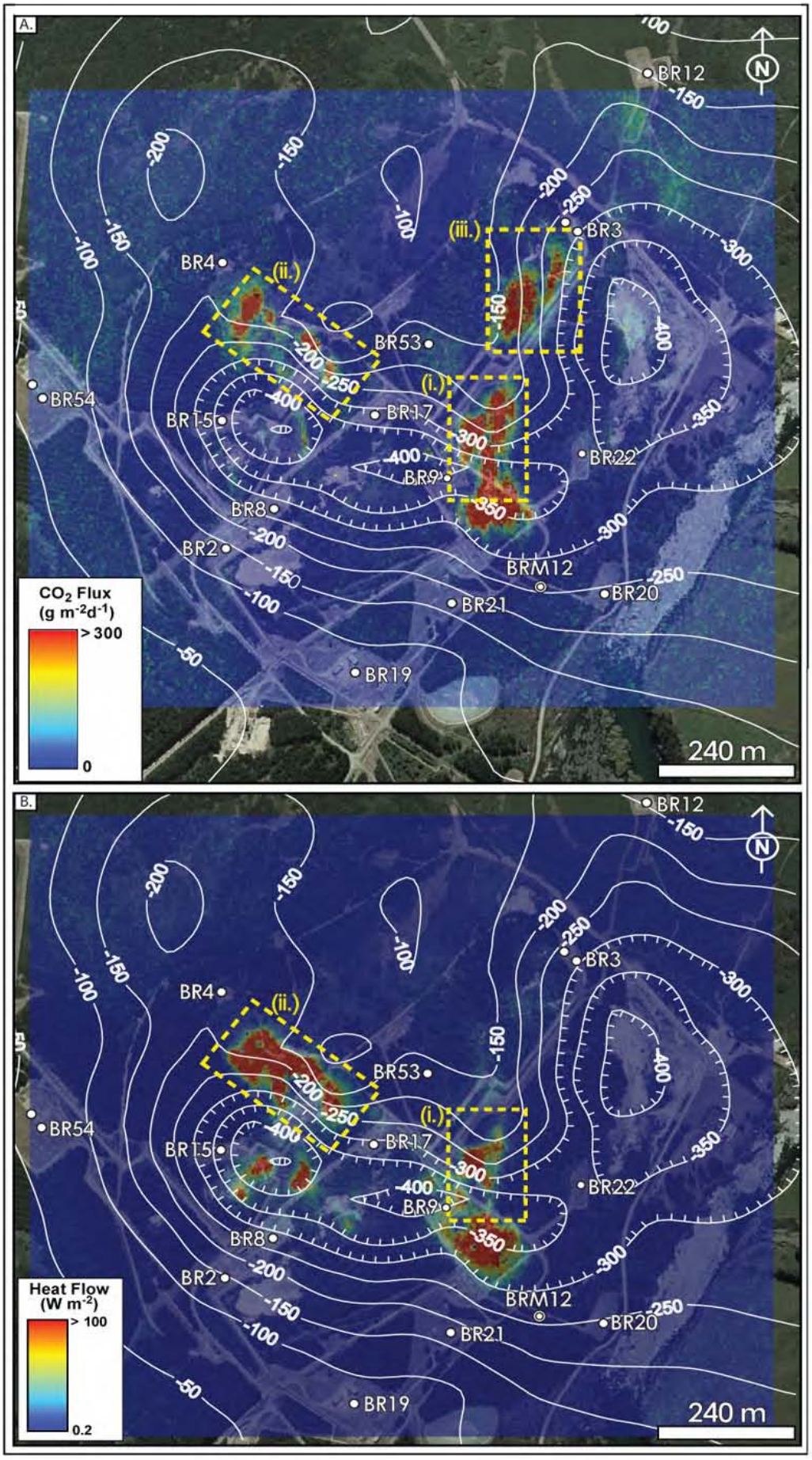


Figure 2.8. Overlay of subsidence contours for the Ohaaki West thermal area onto: (a) $CO_2$ flux, and; (b) heat flux. Note the predominance of $CO_2$ flux anomalies along zones of maximum tensional strain (where contours are closest) as a result of production-induced tensional fracturing due to ground subsidence.

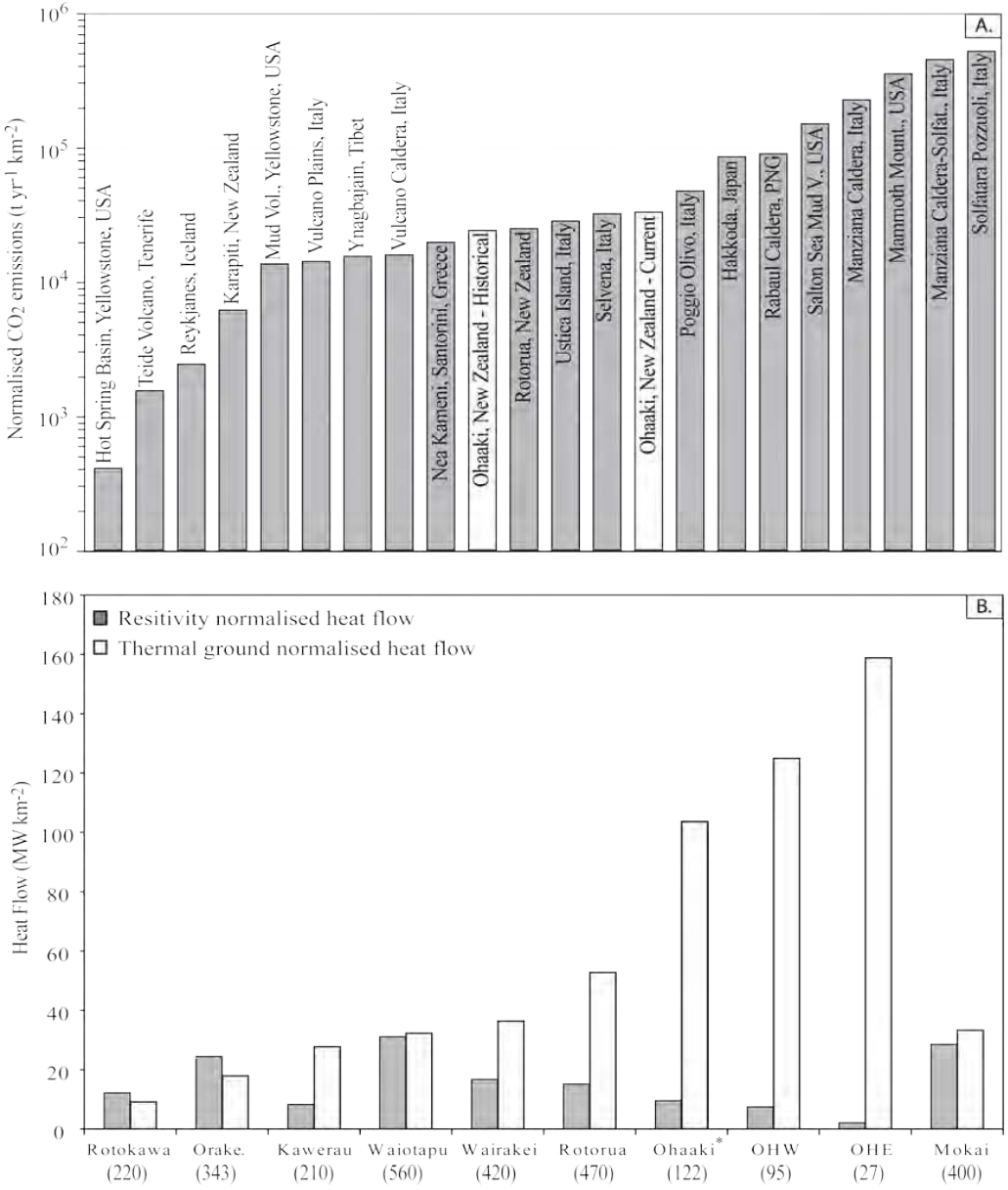


Figure 2.9. (a) Plot of thermal-ground normalised $CO_2$ emissions for the Ohaaki hydrothermal system and other volcanic and hydrothermal systems worldwide (Morner and Etiope, 2002; Werner et al., 2004; Werner and Cardellini, 2006; Fridriksson et al., 2006). (b) Plot of resistivity- and thermal-ground-normalised heat flow for the Ohaaki hydrothermal system and other hydrothermal systems within the TVZ (Dawson and Dickinson, 1970; Bibby et al., 2005; this study). Bracketed values denote the total heat flow for individual fields. Pre-production heat flow has been plotted for the Ohaaki Field. Heat flow and emissions are normalised by the area (km$^2$) of thermal ground with temperatures >25ºC above ambient (see Dawson and Dickinson, 1970) or to the area of low resitivity (< 10 Ωm, after Bibby et al., (1995)), that delineates the surface area of the underlying high temperature reservoir. Where Orake. = Orakeikorako geothermal field.

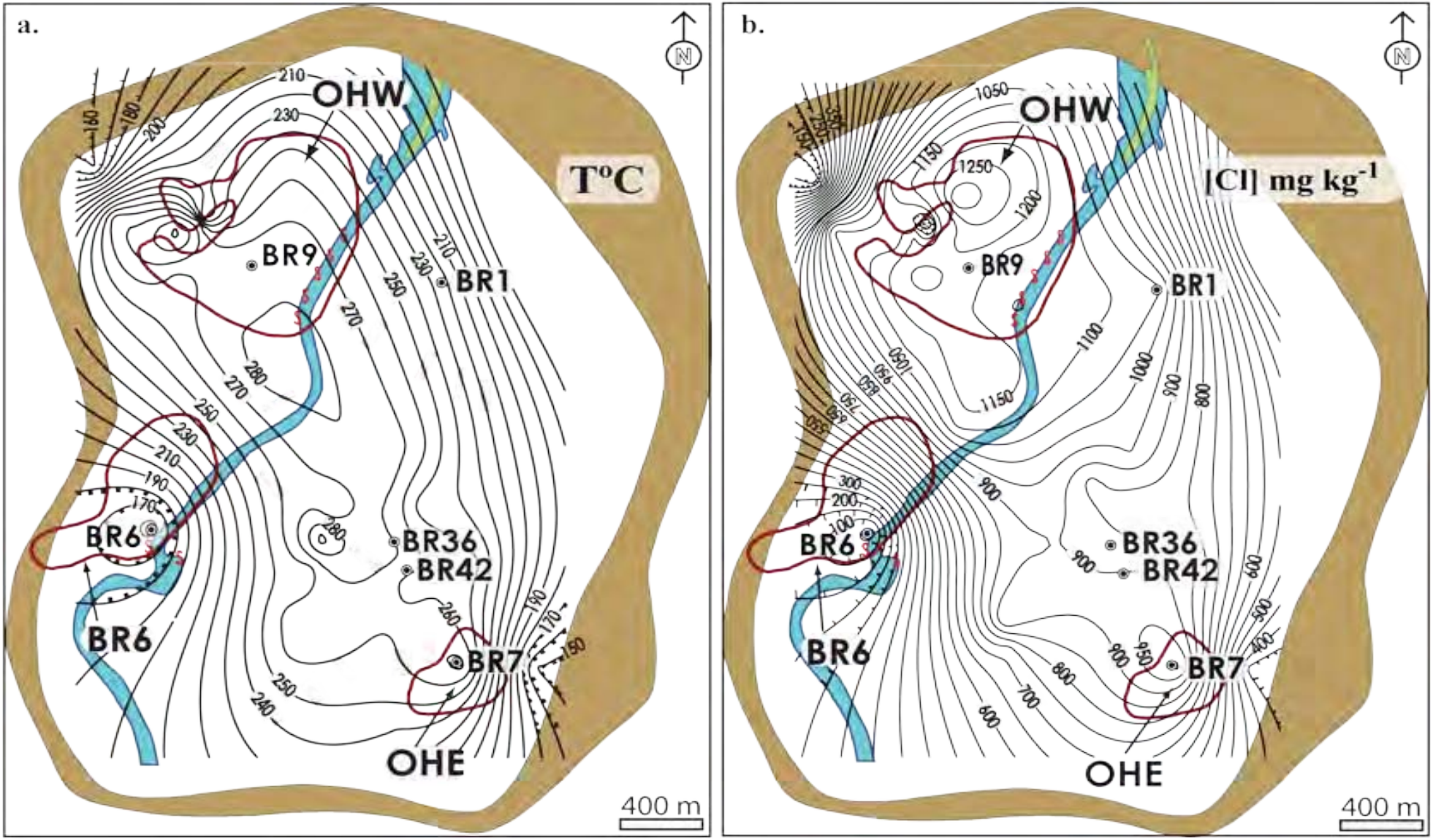


Figure 2.10. (a) Contour plot of deep reservoir temperature (ºC) based on quartz geothermometry, measured enthalpies and measured temperatures for Ohaaki wells (from Hedenquist, 1990). (b) Contour plot of reservoir Cl concentration (mg kg-1) corrected for steam loss and excess enthalpy for Ohaaki wells (Hedenquist, 1990).

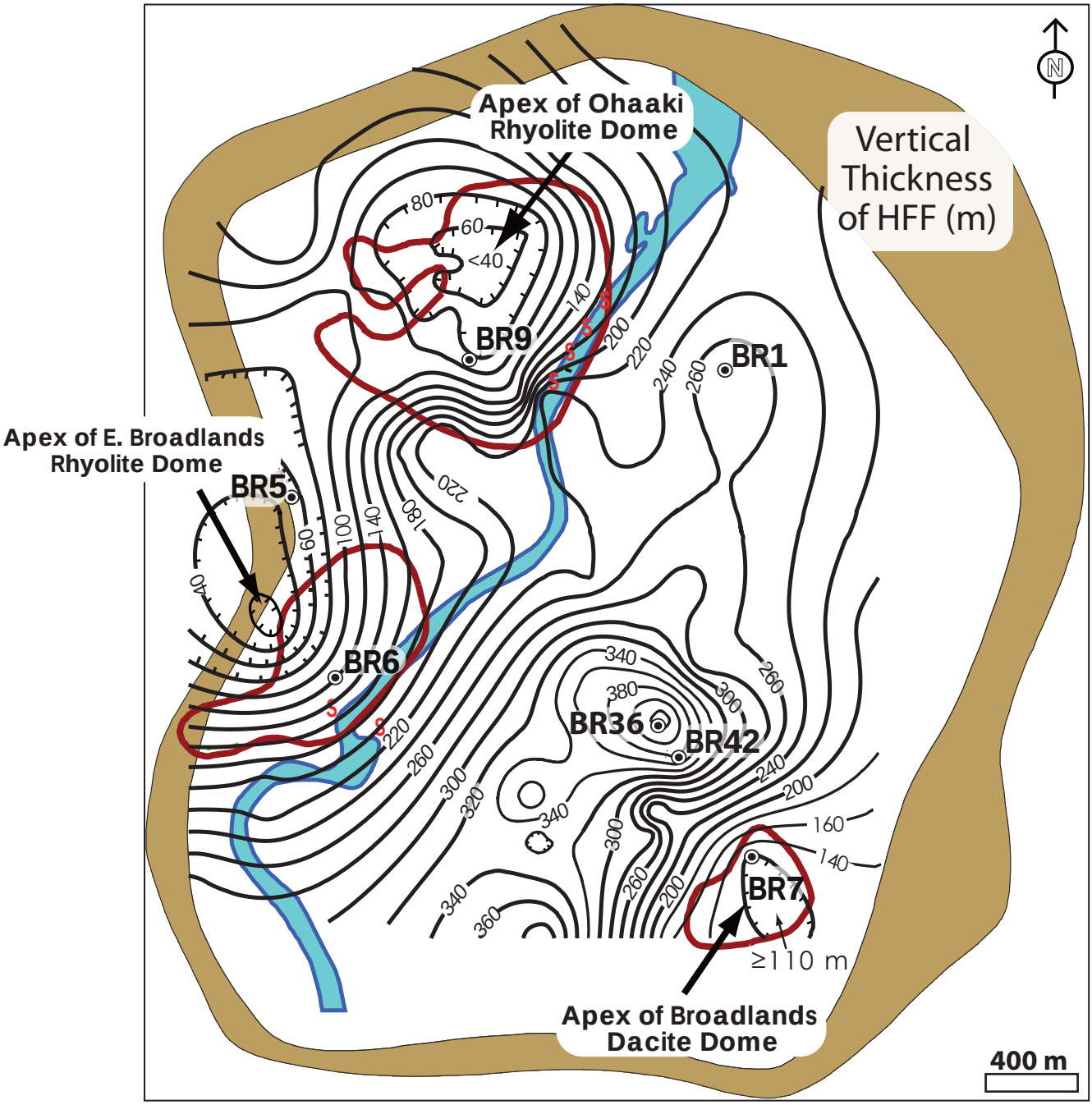


Figure 2.11. Contour plot of the combined vertical thickness of the HFF; shown in m. Note the thinning of the HFF and the occurrence of thermal areas (red outlines) above the apices of the Ohaaki Rhyolite dome in the NW, the Broadlands Dacite dome in the SE and the East Broadlands Rhyolite in the SW.

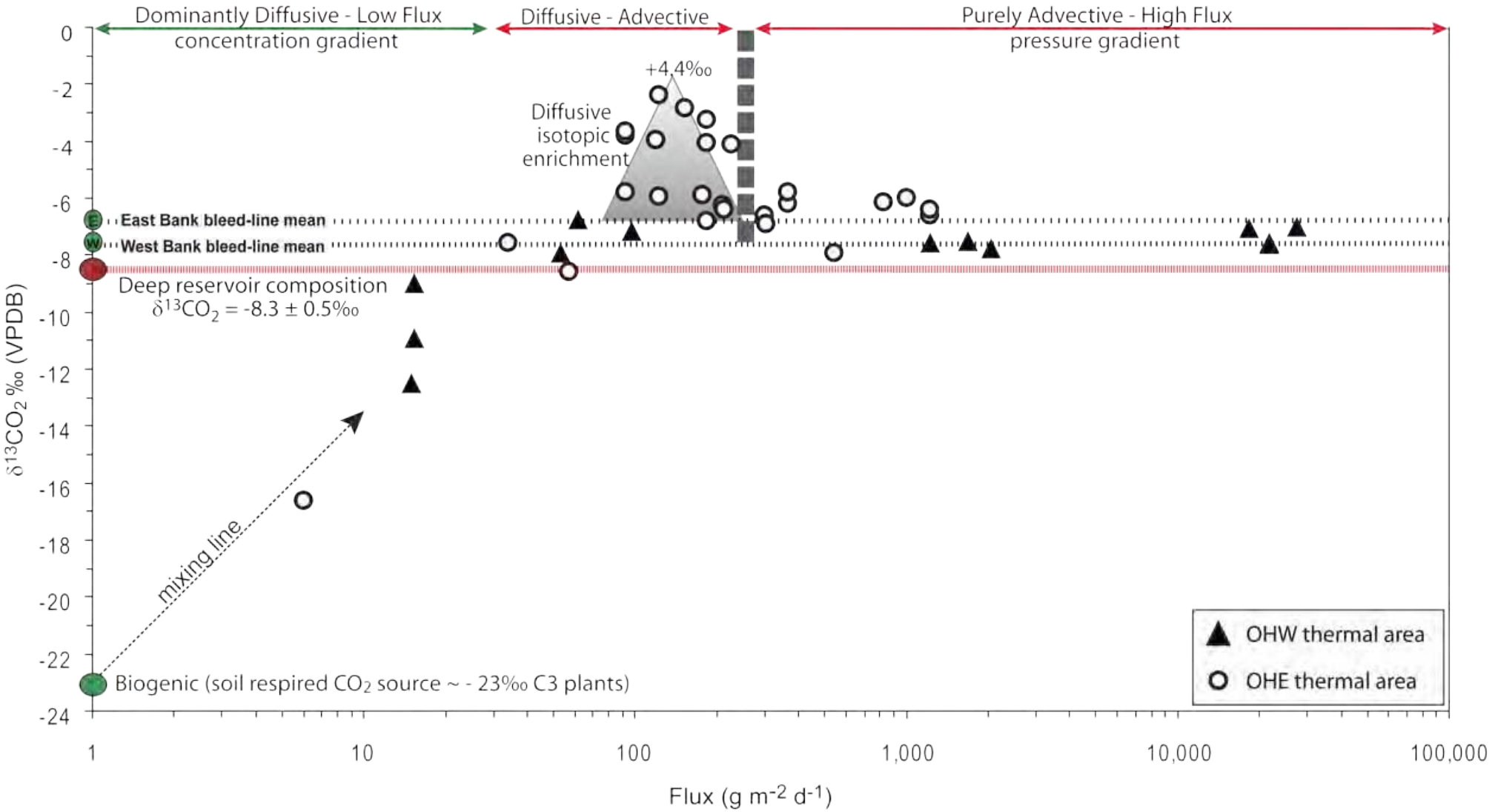


Figure 2.12. Plot of subsoil (0.5 m) $\delta^{13}CO_2$ composition versus $CO_2$ flux for the OHW and OHE thermal areas. For high flux sites in both thermal areas the $\delta^{13}CO_2$ composition is similar to that of mean bleed-line gas samples for the West and East Bank reservoirs, representing the boiled magmatic $CO_2$ source.

Table 2.1a. Pre-production, current and composite heat flow for the Ohaaki Field

| | | Pre-production Heat Flow (MW) | | | |
|---|---|---|---|---|---|
| Source | Location | Steam-heated Pools | Thermal Ground | Alkali-Cl outflows | Total |
| Dickinson (1967) | OHW | 8.6 | 25 | 61.5 | 95.1 |
| | OHE | < 0.2 | N/M | NN | <0.2 |
| | BR6 | <0.01 | < 0.1 | NN | <0.1 |
| | | | | | 95.4 |
| | | Current Heat Flow (MW) | | | |
| This study (2010) | OHW | D | 43.3 ± 5 | D | 43.3 ± 5.0 |
| | OHE | N/M | 26.7 ± 3 | NN | 26.7 ± 3.0 |
| | BR6 | D | N/M | NN | N/M |
| | | | | | 70 ± 6.0 |
| | | Composite (pre- and current) Heat Flow (MW) | | | |
| Combined | OHW | 8.6 | 25 | 61.5 | 95.1 |
| Dickinson (1967) | OHE | <0.2 | 26.7 ± 3.0 | NN | 26.9 |
| This Study (2010) | BR6 | <0.01 | <0.1 | NN | 0.1 |
| | | | | | 122.1 |

Table 2.1b. Pre-production, current and composite $CO_2$ emissions for the Ohaaki Field

| | | Pre-production $CO_2$ emissions (t $d^{-1}$) | | | |
|---|---|---|---|---|---|
| Source | Location | Steam-heated Pools | Thermal Ground | Alkali-Cl outflows | Total |
| Dickinson (1967) | OHW | 14.15 (7.5) | 41.5 (22) | 1.7 | 57.35 |
| | OHE | 0.3 (0.18) | N/M | NN | 0.3 |
| | BR6 | N/A | 0.15 (0.09) | NN | 0.15 |
| | | | | | 57.8 |
| | | Current $CO_2$ emissions (t $d^{-1}$) | | | |
| This study (2009) | OHW | D | 72 ± 6 | D | 43.3 ± 5.0 |
| | OHE | N/M | 39 ± 3 | NN | 26.7 ± 3.0 |
| | BR6 | D | N/M | NN | N/M |
| | | | | | 70 ± 6.0 |
| | | Composite (pre- and current) $CO_2$ emissions (t $d^{-1}$) | | | |
| Combined | OHW | 14.15 | 41.5 | 1.7 | 57.35 |
| Dickinson (1967) | OHE | 0.3 | 39 ± 3 | NN | 39.3 |
| This Study (2010) | BR6 | <0.01 | 0.15 | NN | 0.15 |
| | | | | | 96.8 |

Where OHW = Ohaaki West thermal area; OHE = Ohaaki East thermal area; BR6 = BR6 thermal area. Note observed heat flow values in table 2.1a are those calculated from shallow soil temperatures. For pre-production $CO_2$ emissions in Table 2.1b., bracketed values denote the uncorrected emissions from historical heat flow data. Composite values are combined values from pre-production and current measurements. Unbracketed values are the emission values corrected for subsurface condensation of steam. Where NN = not naturallyoccuring; N/M = not measured and; D = disappeared after production (currently absent).

Table 2.2. Subsoil (0.5 m) $\delta^{13}CO_2$ compostion, sampling temperature, and flux

| Thermal area | Soil Temp (°C) | $CO_2$ flux (g m $^{-2}$ d$^{-1}$) | $\delta^{13}CO_2$ (VPDB , ‰) |
|---|---|---|---|
| BR6 | 14 | 15 | -12.5 |
| OHE | 24 | 34 | -7.6 |
| | 15 | 38 | -16.6 |
| | 98 | 57 | -8.6 |
| | 24 | 92 | -5.8 |
| | 18 | 92 | -3.8 |
| | 40 | 92 | -3.7 |
| | 22 | 120 | -4.0 |
| | 19 | 122 | -5.9 |
| | 34 | 122 | -2.4 |
| | 17 | 153 | -2.8 |
| | 18 | 178 | -5.9 |
| | 20 | 184 | -4.1 |
| | 27 | 184 | -3.3 |
| | 45 | 184 | -6.8 |
| | 45 | 210 | -6.3 |
| | 45 | 210 | -6.2 |
| | 46 | 214 | -6.4 |
| | 25 | 226 | -4.1 |
| | 45 | 301 | -6.6 |
| | 75 | 306 | -6.9 |
| | 17 | 367 | -6.2 |
| | 47 | 367 | -5.8 |
| | 98 | 543 | -7.9 |
| | 70 | 827 | -6.2 |
| | 88 | 1,010 | -6.0 |
| | 95 | 1,225 | -6.6 |
| | 95 | 1,225 | -6.4 |
| OHW | 20 | 15 | -10.9 |
| | 16 | 15 | -9.0 |
| | 99 | 53 | -7.9 |
| | 26 | 61 | -6.7 |
| | 16 | 97 | -7.2 |
| | 56 | 1,227 | -7.6 |
| | 45 | 1,687 | -7.5 |
| | 48 | 2,055 | -7.8 |
| | 86 | 18,401 | -7.1 |
| | 91 | 21,774 | -7.6 |
| | 91 | 21,774 | -7.6 |
| | 99 | 27,518 | -7.0 |

BR6 = BR6 thermal area; OHE = Ohaaki East thermal area; OHW = Ohaaki West thermal area.

Table 2.3. Comparison of observed and $CO_2$ derived heat flow

| | Heat Flow (MW) | | | $t\ d^{-1}$ |
|---|---|---|---|---|
| | Observed | $CO_2$ derived | Condensed | Condensed steam mass flow |
| OHW | 43 ± 5 | 82 ± 7 | 39 ± 4.8 | 1,284 |
| OHE | 27 ± 4 | 45 ± 3 | 18 ± 2.6 | 592 |

Where, condensed heat flow refers to the MW of heat energy lost within the subsurface due to the condensation of a portion of the ascending steam phase (water vapour) within shallow meteoric groundwaters; and condensed steam mass flow refers to the equivalent mass of steam condensed within these shallow groundwaters.

# Chapter 3

# A comparison of permeability distributions arising from different structural settings, Ohaaki hydrothermal field, New Zealand

---

**Clinton Rissmann[a], Andrew Nicol[b], Jim Cole[a], Bruce Christenson[b], Jerry Fairley[c], Sarah Milicich[d], Matthew Leybourne[b], Ben Kennedy[a]**

*[a]Department of Geological Sciences, University of Canterbury, Private Bag 4800, Christchurch, New Zealand*

*[b]GNS Science, P.O. Box 30368, Lower Hutt, New Zealand*

*[c]Department of Geological Sciences, University of Idaho, Moscow, Idaho, USA*

*[d]GNS Science, Wairakei Research Centre, Taupo, New Zealand*

*To be submitted to:* **Geofluids**

## Contributions

Mr. Rissmann developed this study in response to considerable uncertainty surrounding the shallow structural controls over fluid flow at Ohaaki, and after reading several papers on the application of surface surveys to questions of structural permeability. Mr. Rissmann conducted the literature review, undertook the fieldwork, geospatial mapping, and wrote the manuscript. Technical and editorial reviews by Drs. Nicol (structural geology), Kennedy (lava dome structure and permeability), Werner (application of heat and mass flow studies to structural interpretation), and Fairley (fluid flow models and hydrology) were incorporated into the manuscript. Additional editorial input was provided by Prof. Cole and Dr. Leybourne. The data collected by Mr. Rissmann and used in this study was reviewed and supported by the efforts of Dr. Christenson. Miss Sarah Milicich of GNS Science developed and provided cross-sectional models of the Ohaaki Reservoir, and provided important insights into reservoir permeability through her work on reservoir isotherm models.

## 3.1 Abstract

Studies have shown that sufficient permeability for hydrothermal fluid flow is dependant upon the nature of the structural elements (faults or volcanic products) occurring within a given field, and upon the material properties of the reservoir rock (density, intrinsic porosity, permeability, and tensile strength). Here we present fluid flow models for the distribution and origins of permeability within the two major thermal areas (Ohaaki West and Ohaaki East) of the Ohaaki hydrothermal field, Taupo Volcanic Zone, New Zealand. Fluid flow models are based on detailed mapping of surface heat and mass flow gradients (e.g., soil temperature, $CO_2$ flux, sorbed and vapour phase soil Hg, soil alteration intensity, vegetative composition, location temperature and type of surface geothermal features), together with structural and volcanic/stratigraphic information on the field. The Ohaaki East and West thermal areas are above silicic domes which are located above normal faults and below low permeability (~0.1 mD) clay-rich lake sediments up to 120 m thick across the dome apices. High heat and mass flow (95 MW and 90 kg $s^{-1}$, respectively) within the Ohaaki West thermal area occurs in a horseshoe-shaped belt about the apex of the Ohaaki Rhyolite dome. This concentric pattern of high heat and mass flow is inferred to arise from concentric fractures formed during the eruption of the dome, which are charged by vertical fluid flow up along the Ohaaki Fault. In the Ohaaki East thermal area high $CO_2$ flux and soil temperature ($CO_2$ flux up to 21,000 g $m^{-2}$ $d^{-1}$ and boiling point temperatures i.e., 98.7ºC equivalent to 39 ± 3 $td^{-1}$ of $CO_2$ and 27 ± 4 MW across an area of ~0.7 $km^2$) decrease dramatically across the projected surface location of the Broadlands Fault, from which it is suggested that the fault acts as a localised conduit-barrier fluid flow system to the surface. Fluid flow up along the fault, from basement into the dacite dome and through the Huka Falls Formation cap rock, occurs via fractures in the fault zone. Conversely, low permeability fault rock within the Broadlands Fault may prevent eastward migration of hydrothermal fluids across the fault. Fluid flow through the Huka Falls Formation cap rock, above dome apices in both thermal areas, may have been facilitated by brittle failure in response to cementation by hydrothermal silica and/or calcite, and induced by either overpressure or tectonic faulting. Away from the apices of each lava dome (and the Ohaaki West and East thermal areas), across >95% of the field, fluid flow is impeded by the material properties of the Huka Falls Formation cap rock. These findings demonstrate the role of silicic lava domes in: (i) localising fluid flow through eruptive structures and stratigraphy, and; (ii) the provision of islands of locally competent and low porosity rock which favour the development of highly permeable fault zones. The influence of sharp spatial changes in the rock properties (density, intrinsic porosity, permeability, and tensile strength) of a hydrothermal reservoir on the permeability and delineation of normal faults is also demonstrated. These findings may have widespread application in the Taupo Volcanic Zone, and other regions globally where large magmatic hydrothermal systems underlie silicic lava domes, or more generally for geothermal (magmatic or otherwise) environments where rock properties (density, intrinsic porosity, permeability, and tensile strength) vary sharply in three-dimensions.

## 3.2 Introduction

Bulk rock-mass permeability of unfractured rock is generally too low to satisfy the conditions of focused, large volume fluid flow typical of hydrothermal systems (Norton and Knapp, 1977; Knapp and Norton, 1978; Lowell et al., 1993; Curewitz and Karson, 1997; Sibson, 2000; Rowland and Sibson, 2004). Permeability for hydrothermal fluid flow may arise through a number of processes operating at different temporal and spatial scales. These include: (a) magma intrusion, (b) magma degassing, (c) hydrovolcanic processes, (d) self-structural permeability creation and destruction related to hydrothermal fluid circulation and mineral deposition, (e) regional-scale faulting, and, (f) remnant high permeability zones produced by volcanic products including extinct lava domes, dykes and permeable pyroclastic units (Koide and Bhattacharji, 1975; Norton and Knapp, 1977; Knapp and Norton, 1978; Wohletz and Heiken, 1992; Lowell et al., 1993; Curewitz and Karson, 1997; Sibson, 2000; Rawling et al., 2001; Rowland and Sibson, 2004). Which of these different types of permeability are most important for hydrothermal fluid flow at a given site is dependant on the tectonomagmatic setting, the characteristics of the reservoir (e.g., rock material and heat source properties), and the temporal scale of observation.

Since the first investigations into the potential of the Ohaaki Geothermal Field for electrical energy production, debate has surrounded the origin of the permeability governing its location and spatial distribution (Healy, 1968; Grindley, 1970). Healy (1968) attributed the location and spatial distribution of thermal activity of the Ohaaki West (OHW) thermal area to superficial fractures related to eruption of the Ohaaki Rhyolite dome. Healy's model contrasts with that of Grindley (1970) who argued that the NNE alignment of hot springs at the ground surface was likely associated with fluid flow along the deep-seated Ohaaki Fault which transects the dome. Drilling programmes during the 1980's and 1990's suggest that vertical displacement of the Ohaaki Reservoir on the Ohaaki Fault is likely to be low (e.g., < 30m), with most (> 200 m) fault throw occurring before ~330 ka (Wood, 1996). An apparent lack of vertical displacement post ~330 ka on many of the faults in the Ohaaki Field, coupled with the absence of unequivocal fault traces at the ground surface, have lead to a general reluctance to attribute the upward flow of fluid to relatively high permeabilities in fault zones (Healy, 1968; IGNS, 1998; Wood et al., 2001). This reluctance persists despite abundant indirect evidence for integrated vertical permeability along 'projected' fault surfaces of the two major upflow zones, which occur within the field, including: (i) geophsyical models that depict the near vertical ascent of high temperature plumes from depths > 2.5 km before being deflected at the base of the poorly permeable Huka Falls Formation (HFF) cap rock (MacDonald, 1975; Bibby et al., 1995); (ii) the spiking of isotherms along projected fault surfaces from depth towards the surface of the field (Hedenquist, 1990; Christenson et al., 2002); (iii) elongate silicification envelopes that extend up into the post-330 ka cover sequence along projected faults (Hochstein and Henrys, 1989) and; (iv) the occurrence of $CO_2$ fluxes and mass flow rates consistent with a deep-seated connection (Chapter 2).

Differing opinions as to the geometry of the Ohaaki Rhyolite (i.e., dome or flow lobe) also have important implications for the origin of the permeability governing surface thermal activity within the OHW. Henrys and others (1987, 1990) questioned a locally eruptive origin for the Ohaaki Rhyolite on the basis of the thickening of the flow to the NW, suggesting it was a flow lobe derived from an eruptive centre to the west or NW of the field margins. Although the interpretations of Henrys et al. have not been favoured by many, they raise the possibility that geothermal fluids do not reach the surface via a magmatic dome.

To address the controversy over what processes control the near surface (e.g., <2 km) flow paths of geothermal fluids at the Ohaaki Field, we have collected, compiled and re-examined fluid flow data from the two major thermal areas (Ohaaki East and Ohaaki West) of the Ohaaki hydrothermal field. This has been accomplished by detailed mapping of surface thermal activity (e.g., steam-heated pools, alkali-Cl hot springs and seeps, silica sinter aprons from alkali-Cl outflows, thermal ground, and, altered soils and distinctive vegetative compositions at the land surface), and the magnitude of surface heat and mass flow gradients associated with thermal activity. From each map of surface heat and mass flow, interpretative models of the permeability variations governing fluid flow, are presented in conjunction with geological data for the Ohaaki Field, and relevant models of volcanic dome structure and fluid flow associated with normal faulting. Ancillary data supporting the existence of large (>100 m throw) normal faults at the surface of the Ohaaki Field are also presented from an earlier, and little known soil gas survey of the field (see Koga et al., 1982). The data suggest that high permeability zones formed within rhyolitic domes and faults zones have been exploited by geothermal fluids which flow to the surface. Our conclusions may have implications for other geothermal fields, particularly in the Taupo Volcanic Zone (TVZ).

## 3.3 Geological and hydrothermal setting

The Ohaaki Field is located within the large (~720 $km^2$) Reporoa Basin, along the eastern boundary of the TVZ (Fig. 3.1). The TVZ is a 250 km northeast trending zone of mainly andesitic to rhyolitic arc/back arc volcanism, within continental crust of the central North Island, New Zealand (Cole, 1990). TVZ volcanism formed over the past 1.6 Myr and is spatially coincident with a narrow (15-40 km wide) zone of active crustal extension known as the Taupo Rift (Wilson et al., 1995). Volcanism and rifting in the TVZ, which formed in association with subduction of the Pacific Plate beneath the North Island, produced crustal thinning and high average geothermal heat flow (~700 $mW/m^2$) (Bibby et al., 1995; Stratford and Stern, 2006; Nicol et al., 2007). Heat flow in the TVZ is highly variable and is focused within 23 main geothermal fields, one of which is the Ohaaki Field.

The Ohaaki Field is a liquid dominated hydrothermal system with an areal extent of ~12.7 $km^2$ and a maximum recorded reservoir temperature of 310ºC (Hedenquist, 1990; Christenson et al., 2002). Two major high temperature (>290ºC) plumes feed the reservoir (Fig. 3.2), both of which exhibit a characteristically

volcanic-magmatic or 'arc-type' fluid composition (Giggenbach, 1989; Christenson et al., 2002). The Ohaaki Field supplies a geothermal power plant with an installed capacity of 116 MWe, which has been supplying the national electricity grid since being commissioned in 1989.

The stratigraphy of the Ohaaki reservoir is here divided into: (1) the Mesozoic greywacke basement that underlies the field; (2) the pre-330 ka volcanic-sedimentary strata of the Waikora and Tahorakuri Formations that directly overlie the basement; (3) the 330 ka Rangitaiki Ignimbrite, and; (4) the post-330 ka volcanic-sedimentary fill (Fig. 3.3). The greywacke basement is faulted by four or more major NE-striking (arc parallel) normal faults. As these faults cannot be traced to the surface little is known about the dip range, although a value of 55º - 75º is assumed for the deeper segments within the greywacke basement (Wood et al., 2001). These faults are largely responsible for a fall in the altitude of the top basement from -700 m RSL (relative to sea level) in the SE to -2,100 m RSL in the NW over a lateral distance of ~2.8 km (Fig. 3.2; Wood et al., 2001; Christenson et al., 2002; Rae et al., 2007). The role of large NE-trending normal faults, as conduits for high temperature fluids to enter the Ohaaki reservoir, is well established with a strong spatial correlation between basement faults and geochemical markers of major upflow zones (i.e., $N_2$/Ar isopleths, Cl concentration and temperature; Fig. 3.2; Christenson et al., 2002; Rae et al., 2007).

The reservoir overlying the greywacke basement is a complex assemblage of pre-330 ka volcaniclastics and post-330 ka volcanic domes, intercalated with pyroclastic deposits from large caldera forming eruptions to the west (Fig. 3.3). With the exception of the fractured and brecciated apex of each dome, dome lavas are thought to act as aquitards to vertical fluid flow (Hedenquist, 1990; Henrys and Hochstein, 1990). Conversely, pyroclastic flow deposits and porous volcaniclastic units (i.e., the Rangitaiki Ignimbrite, Rautawiri Breccia and the shallow Waiora Formation) act as permeable aquifers through which ascending hot alkali-Cl waters flow laterally (Hedenquist, 1990; Wood, 1994).

The Waiora Formation forms an important shallow alkali-Cl hosting aquifer, which in places directly underlies the HFF (Wood, 1994). The Ohaaki Reservoir is sealed by the low permeability (0.1 mD) lacustrine mudstone of the HFF, which is of low competence (unconfined compressive strength of 1.2 to 2.7 MPa), high clay content (up to 85%), high porosity ($\phi$ mean = 56%), and has a mean vertical thickness of ~ 220 m, with a maximum thickness of 440 m (Rosenberg et al., 1999; Allis and Zhan, 2000; Read et al., 2003; Contact Energy, 2006). The HFF at Ohaaki is a very effective cap rock (sealing layer) to the underlying high temperature reservoir (MacDonald, 1975; Koga et al., 1982; Chapter 2). Across most of the field the HFF is covered by unconsolidated Late Quaternary alluvium (5 – 45 m) from the Waikato River, and by mixed pyroclastic air fall deposits.

### 3.3.1 Thermal areas and structural permeability

All three areas of surface thermal activity at Ohaaki occur above buried or partially emergent volcanic dome complexes (Fig. 3.4). With lateral distance from each dome apex, surface thermal activity, including elevated soil temperatures, volatile flux (magmatic gases), hot springs, thermally tolerant vegetation and altered ground, decline and then cease altogether (Chapter 2). Distal from dome apices and over 95 % of the area field no surface manifestations of geothermal activity (e.g., elevated temperature or anomalous $CO_2$ flux) occur, despite the presence of high temperature fluids at the base of the voluminous HFF cap rock (Koga et al., 1982; Chapter 2).

The OHW thermal area occurs in the NW sector of the field, directly above a high (246 m RSL) on the top of the Ohaaki Rhyolite. This high is most commonly considered to be the apex of an eruptive lava dome that intruded along the Ohaaki Fault (Fig. 3.2; Healy, 1968; Grindley, 1970; Risk, 1976; IGNS, 1998). At the apex of the dome the Ohaaki Rhyolite has a drilled thickness of ~ 450 m (Contact Energy, 2006). A contour map of the upper surface (top) of the Ohaaki Rhyolite, constructed from drill core, show an approximately circular dome, with steep southern, southeastern, and northeastern flanks, and a radius of ~ 600 m from the apex of the dome to the 80 m RSL contour of the northeastern flank. Above the apex, the low permeability HFF thins and the rhyolite is partially emergent above the HFF (Fig. 3.4). Directly beneath the dome, the West Bank upflow enters the reservoir via vertical flow along the Ohaaki Fault (Fig. 3.2; Hedenquist, 1990; Christenson et al., 2002; Rae et al., 2007).

Prior to development of the field for electricity generation, the OHW thermal area (~1.0 $km^2$) contained the greatest range of types of geothermal activity within the Ohaaki Field, including the large volume (mean discharge rate of ~10 L $s^{-1}$) alkali-Cl outflow of the Ohaaki Pool, ~ 5,000 $m^2$ of steam-heated pools, ~ 77,000 $m^2$ of thermal ground (with temperatures $\geq$ 50ºC at 1.0 m depth), and large tracts of intensely altered but thermally inert (or cold) ground (Dickinson, 1967; Mahon and Finlayson, 1972; Allis and Webber, 1984; Dawson, 1988). The pre-production heat and mass flow for the OHW thermal area was calculated at 95 MW and 90 kg $s^{-1}$, respectively, of which 70% was associated with seepage of dilute alkali-Cl fluids from the area into the Waikato River (Chapter 2).

Above the apex of the Ohaaki Rhyolite dome, Grindley (1970) argued that several small NE-striking fault traces, intersected by NW “cross faults,” controlled the locations of surface thermal activity, including the alignment of hot springs. Although Grindley (1970) favoured the view that these small fault traces formed in association with the Ohaaki Fault, he acknowledged that there was insufficient data to rule out the possibility that thermal activity at the surface was influenced by the geometry and location of the Ohaaki Rhyolite.

The smaller (~0.7 $km^2$) Ohaaki East (OHE) thermal area occurs in the SE corner of the field directly above the apex of the Broadlands Dacite dome, which is thought to have erupted along NE-trending basement faults that underlie the area (Figs. 3.2 and 3.3; Henrys and van Dijck, 1987; Henrys and Hochstein, 1990). Here, the low permeability HFF thins from > 400 m thick to ~110 m above the dome apex, and surface thermal activity is dominated by a vapour phase, including ~23,000 $m^2$ of 'steaming ground' interspersed with a few moderately sized steam-heated pools of acid-sulfate composition, and numerous small boiling mud pots (< 1,000 $m^2$) (Dickinson, 1967; Mahon and Finlayson, 1972; Allis and Webber, 1984; Dawson, 1988; Hunt and Graham, 1997; IGNS, 1998; Chapter 2). Repeat studies of soil temperature and thermal features indicate no significant change in surface activity at OHE despite 20 years of energy production (Hunt and Graham, 1997; Hunt and Bromley, 2000; Chapter 2). The recent $CO_2$ flux and heat flow models presented in this paper indicate a $CO_2$ emission rate of $39 \pm 3$ t $d^{-1}$ and a surface heat flow of $27 \pm 3$ MW for this small thermal area (Chapter 2).

Although Healy (1968) made no mention of the structural controls governing surface thermal activity within the OHE thermal area, Grindley (1970) argued that two intersecting lineaments, trending NE and ENE, control the spatial pattern of surface activity. These he assigned as normal (i.e., the NE-trending Broadlands Fault) and normal-dextral (ENE) faults associated with the underlying East Bank horst (Fig. 3b).

### 3.3.2 Lava Dome Structure in the TVZ and Mayor Island

Observational data for the internal structure of lava domes within the TVZ is limited. However, some inferences as to the internal structure have been made from field studies of TVZ lava domes (Brothers, 1957; Lewis, 1968; Cole, 1970; Buck et al., 1981). Lewis (1968) described the geology and structure of five dacite cumulo-domes that coalesce to form Mt Tauhara and concluded that eruptive activity had migrated from place to place within the vent and in the circular core of both the 'Main' and 'Breached' domes. The generally concentric shape of these domes were attributed to the circular nature of the 'central orifice' (dome core) from which lavas were extruded and emplaced as block and ash flows about the flanks. Buck et al. (1981) described a similar eruptive style for the final phase of the Mayor Island volcanics, defining a rhyolite dome erupted from a central vent with block and ash flows emplaced on the steep flanks of the dome. Both descriptions confirm dome growth occurred exogenously in response to the extrusion of a concentric dome core (lava plug or flow lobe) from the central crater.

Cole (1970) described a different growth mode for the for the Tarawera, Wahanga, and Crater Domes on the basis of 'onion-skin' joint patterns, concentric with the spherodial banding, towards the centre of each dome. These distinctive features led Cole to argue for predominantly endogenous dome growth caused by inflation of the dome core from within. It is common for dome growth to transition from exogenous to endogenous,

and *vice versa*, over the life time of a dome in response to changes in the dynamics of lava supply (Hale and Wadge, 2005). The relevance for the work that follows is that each mode of dome growth results in differing permeability distributions that may be important for the hydrology of a hydrothermal system post-eruption.

## 3.4 Methods

### 3.4.1 Ohaaki West thermal area

Since initiation of power production from the Ohaaki Field, the extent and spatial distribution of surface thermal activity occurring within the OHW thermal area has changed markedly (Glover et al., 2000; Hunt and Bromley, 2000; Chapter 2). These changes reflect localised increases in permeability due to ground fracturing associated with production-induced ground subsidence, the cessation of liquid dominated outflows due to reservoir pressure decline, and a possible increase in the pressure of the steam envelope beneath the area, again due to production of the field (Allis and Zhan, 2000; Glover et al., 2000; Hunt and Bromley, 2000; Chapter 2). Due to these artificially induced changes it was necessary to reconstruct the spatial extent and magnitude of pre-production thermal activity within the OHW thermal area.

Reconstruction was accomplished by integrating data from direct and indirect measurements of surface heat and mass flow provided by pre-production surveys of: (i) soil temperature (i.e., 0.15 m and 1.0 m depth measurements) and heat flow (Dickinson, 1967; Thompson, 1967; Allis and Webber, 1984; Hunt and Graham, 1997); (ii) free Hg vapour and sorbed Hg within the soils of the area (Koga et al., 1982); (iii) the location, form and extent of surface thermal features (i.e., alkali-Cl hot springs and associated silica sinter, steam-heated pools, boiling mud pots, steaming ground, steam vents and sulphur mounds), as well as their respective temperature and composition (Thompson, 1967; Mahon and Finlayson, 1972; Dawson, 1988; Glover et al., 2000); (iv) pre-production and post-production aerial photography of thermal features and the composition and spatial distribution of thermal and non-thermal vegetation, and; (v) field-based assessment of soil temperature, vegetative composition, and soil alteration intensity.

The detailed soil temperature survey of Allis and Webber (1984) provided significant constraints on the extent of pre-production thermal ground with temperatures $\geq 25^{o}C$ and $\geq 50^{o}C$ at 1.0 m depth. Our spatial mapping of the type and temperature of pre-production surface thermal areas (i.e., hot springs through to mud volcanoes and silica sinter), as well as the location of extinct thermal activity, has been guided by Dawson (1988). Dickinson (1967) provided a measure of the natural heat flow at the surface of the OHW thermal area associated with the tracts of thermal ground, steaming-pools, the alkali-Cl Ohaaki hot spring, and seepage of dilute alkali-Cl hot water. The spatial extent and intensity of thermal activity defined by these surveys has been checked against the groundcover and vegetative composition evident in pre-production aerial photographs.

The distribution of pre-production thermal activity was mapped at four levels (i.e., $TL_1 - TL_4$), which were defined according to pre-production values of soil temperature (at both 0.15 m and 1.0 m depth), surface volatile concentration, and the location and temperature of thermal features (Dawson, 1967; Thompson, 1967; Koga et al., 1982; Allis and Webber, 1984; Dawson, 1988). Each thermal intensity level corresponds to a specified temperature range and coincides with a distinct vegetative composition (Table 3.1).

Within an active thermal area vegetative composition (i.e., species richness) and plant stature are determined firstly by the soil temperature gradient, and secondly by the alteration intensity of the soil (Given, 1980; Burns, 1997; Bromley and Hochstein, 2005). However, in areas of extinct thermal activity it is the alteration intensity of the soil that determines the composition and stature of plant species due to the low pH, low nutrient status, and phytotoxic Al-concentrations of these soils (Given, 1980; Burns, 1997; Martin et al., 2000). The influence of soil alteration intensity on species composition is an important characteristic of thermal areas and has long been recognised as a useful tool for identifying areas of extinct (former) thermal activity (Dawson and Dickinson, 1970). Plants capable of surviving in chemically limited soils are restricted to colonising species, such as the epacrid shrubs of the genus *leptospermum* (Manuka and Kanuka), and recently introduced species such as blackberry (*Rubus fruticosus*). Both species are known colonisers of bare and nutrient limited ground (Burns, 1997), and at Ohaaki rarely exceed heights of 2.0 m. With declining alteration intensity, both species richness and plant stature increases, until, at the margins of a thermally affected area, the dominant regional vegetation (i.e., mixed broadleaf forest) is obtained (Given, 1980; Burns, 1997).

Within the OHW thermal area extinct thermal ground was identified by comparing the extent of pre-production thermal activity with the composition and stature of vegetative cover evident in pre-production aerial photographs. Soil temperatures (to 1.4 m) and soil core (2.0 m) were also taken at each site so as to confirm the presence of altered ground and determine the ambient temperature. With distance from inferred outflow sites a general decline in soil alteration intensity was observed along with a marked increase in species richness and plant stature. The increase in both species composition and plant stature was easily identified in pre-production aerial photographs as series of steps radiating out from the locus of former outflows.

For each extinct thermal area, thermal intensity levels ($TL_1 - TL_4$) were assigned according to: (i) vegetative composition and plant stature; (ii) soil alteration intensity; (iii) proximity to extinct or pre-production thermal features, and; (iv) a compensation for the fact that former hot bare ground is quickly colonised by adapted plant species as temperatures decline. The latter is well illustrated by several sites of pre-production thermal ground within the area which became extinct soon after production (Allis and Webber, 1984; Chapter 2). These former high temperatures sites (80ºC – 98.7ºC at 0.15 m depth) were once characterised by bare altered

ground (clay crust), audible steam vents, and isolated patches of moss and lichen. Following > 15 years of ambient ground temperature the same sites are characterised by dense thickets of *Leptospermum sp.* (<1.2 m) and rare blackberry (*Rubus fruticosus*), with no sign of higher order plant species.

### 3.4.2 Ohaaki East thermal area

Since initiation of production of the field there has been no resolvable change in the spatial distribution or the intensity of surface thermal activity occurring within the OHE thermal area, which is smaller than OHW (Hunt and Graham, 1997; Hunt and Bromley, 2000; Chapter 2). Due to the stability of this area a recent high density (mean sample spacing of 15 m) $CO_2$ flux and soil temperature survey was used to define the mass flow gradients occurring across the surface of the OHE thermal area (see Chapter 2).

Soil temperature and $CO_2$ flux anomalies develop in response to the passage of water vapour (steam) and $CO_2$ to the surface from the underlying high temperature reservoir. Whereas it is common for steam to be stripped from the ascending vapour phase, $CO_2$ behaves relatively conservatively (i.e., less prone to condensation) under the T-P conditions of steam-heated thermal ground (Chiodini et al., 2005; Fridriksson et al., 2006; Chapter 2). For this reason $CO_2$ is routinely used to define permeability structures in areas of volcanic activity for which large subaerial inputs of magmatic $CO_2$ are the norm (Giammanco et al., 1997; Etiope et al., 1999; Werner and Cardellini, 2006; Carapezza et al., 2009).

Using the magnitude of surface $CO_2$ flux as a proxy for permeability the following four levels of mass flow were delineated across the surface of the OHE thermal area: $TL_1 \geq 1{,}200$ g $m^{-2}$ $d^{-1}$; $TL_2 \geq 600$ g $m^{-2}$ $d^{-1}$; $TL_3 \geq 300$ g $m^{-2}$ $d^{-1}$ and; $TL_4 \geq 100$ g $m^{-2}$ $d^{-1}$. These values were chosen on the basis of significant differences in the spatial extent of surface flux occurring at each value. For fluxes $\geq 300$ g $m^{-2}$ $d^{-1}$ gas transport is dominated by advection, whereas for lower fluxes (< 300 g $m^{-2}$ $d^{-1}$) the diffusive gas transport component becomes increasingly important (Chapter 2). The prevalence of advective mass transport (> 300 g $m^{-2}$ $d^{-1}$) within the OHE thermal area substantiates the existence of a pressure gradient between the $CO_2$ of the vapour phase, within the reservoir, and that of the surface of the OHE thermal area. Such pressure gradients are common feature of geothermal and volcanic settings (Natale et al., 2000; Camarda et al., 2007) and validate the use of mass flow measurements ($CO_2$ flux) as a proxy for shallow permeability both at OHE and in other geothermal settings.

Although condensation of steam within the soil zone and development of shallow (<0.5 m) lateral outflows tends to mask the finer detail of structural permeability, repeat measurement of shallow soil temperature can provide useful insight into both flow direction and the existence of impermeable barriers to fluid flow (Fairley and Hinds, 2004; Heffner and Fairley, 2006). For this reason the spatial extent of shallow (0.15 m) soil temperature anomalies were mapped at 35ºC, 50ºC, 75ºC and 98.7ºC (i.e., boiling point for the Ohaaki

Field). These soil temperature values were selected as they best define the maximum and minimum extent of the hydrothermal soil temperature anomaly, and the variation in the pattern(s) of the anomaly, with increasing or decreasing temperature.

## 3.5 Results

### 3.5.1 Ohaaki West thermal area

The general pattern of thermal ground within the OHW thermal area is defined by radial transitions from $TL_1$ to $TL_4$ ground, with increasing distance from the sites of maximum heat and mass flow (i.e., $TL_1$ ground) (Fig. 3.5). The distance over which the transition occurs from $TL_1$ to $TL_4$ ground appears to scale with the size and/or historical discharge rate ($Ls^{-1}$) and temperature of the thermal outflow. Where outflows occur in close proximity to each other, thermal ground may only transition through one or two steps of the thermal ground intensity levels (i.e., from $TL_1$ to $TL_2$ ground).

The resolution of the boundaries of $TL_3$ and $TL_4$ ground is limited by the shallow and spatially restricted extent of pre-production (0.15 m to 1.0 m) soil temperature surveys, the lower resolution afforded by vegetative methods to delineate mass and heat flow gradients, the disturbance of natural vegetative patterns due to development of the field, and recent fluvial activity (Fig. 3.5). However, $TL_1$ and $TL_2$ ground is well-defined and describes a distinctly arcuate or crescent-shaped zone of thermal activity, which is approximately 145 to 280 m wide. This activity partially encircles the apex of the Ohaaki Rhyolite, between the 180 mRSL and 240 mRSL contours on the top of the rhyolite, above which the HFF ranges between 60 m - 160 m in thickness (Fig. 3.6). This broad, approximately crescent-shaped zone of thermal activity is hereafter referred to as the OHW thermal crescent (OWTC) and encompasses all documented thermal activity associated with the OHW thermal area (Dickinson, 1967; Thompson et al., 1967; Mahon and Finlayson, 1972; Koga et al., 1982; Allis and Webber, 1984; Dawson, 1988; Hunt and Graham, 1997). Also evident is the conspicuous absence of thermal activity, both ancient and pre-production, across the apex of the Ohaaki Rhyolite, where the HFF is at its thinnest and in a wide corridor NNW along the long axis of the dome (Fig. 3.6).

Running through the centre of the OWTC, and forming an arc through the historical steaming ground SW of well BR3, the alkali-Cl Ohaaki Pool, wells BR22, BR9 and BR15 is a thin belt of thermal activity, which constitutes the historical locus of the most vigorous and sustained outflows (highest mass flow) of the OHW thermal area (Fig. 3.6; Dickinson, 1967; Thompson et al., 1967; Grindley, 1970 Mahon and Finlayson, 1972; Allis and Webber, 1984; Dawson, 1988; Hunt and Graham, 1997; Glover et al., 2000). This concentric or annular belt of thermal activity, hereafter named the Ohaaki West Thermal Belt (OWTB, Fig. 3.6), appears to partially encircle the apex of the Ohaaki Rhyolite, continuing from well BR33 through a patch of pre-production thermal ground to the site of extinct hydrothermal outflow, NNW of well BR4 (Fig. 3.7).

### 3.5.2 Ohaaki East thermal area

The spatial gradients in $CO_2$ flux and soil temperature reveal the occurrence of anomalous permeability across a large portion of the surveyed area, with a distinctive NNE orientation, and a crisp, seemingly linear eastern boundary to the anomaly (Figs. 3.8 and 3.9). Within metres of the eastern boundary both soil temperature and $CO_2$ flux change from being anomalously high (1,200 g $m^{-2}$ $d^{-1}$ of $CO_2$ and 50ºC) to background values (15 g $m^{-2}$ $d^{-1}$ $CO_2$ and 20ºC). Conversely, the western bounds of the anomaly are more diffuse and irregular and show some correlation with the topographic relief of the area. The absence of anomalous $CO_2$ flux across the OHE lagoon masks a minor transfer of $CO_2$ and heat through the steam-heated pools and numerous boiling mud pots of the OHE lagoon (Chapter 2). An area of paved ground NNW of well BR7 may mask some of the natural permeability of this area.

With increasing $CO_2$ flux the areas of greatest permeability are resolved as quasi-circular flux anomalies or blebs (Fig. 3.8). Conversely, at lower flux rates, circular flux anomalies coalesce to form broader and more complex patterns. Soil temperature anomalies are more complex and less defined, likely as a result of condensation of ascending steam within the near surface of the soil zone and the merging of shallow lateral outflows (Fig. 3.9). Aside from the gross control of the Broadlands Dacite dome over the thinning of the HFF, the distribution of permeability at the surface of the OHE thermal area shows no strong spatial correlation with the shape of the Broadlands Dacite dome (Fig. 3.10).

## 3.6 Discussion

### 3.6.1 OHW thermal area fluid flow model

From the results of our intensive mapping of heat and mass flow gradients within the OHW thermal area it is evident that the major permeability structures associated with hydrothermal fluid flow are concentrically distributed about the apex of the Ohaaki Rhyolite, and are not linear as proposed by Grindley (1970). This concentric distribution, when taken in conjunction with the conspicuous absence of thermal activity across the apex of the Ohaaki Rhyolite, as well as the general shape and dimensions of the Ohaaki Rhyolite, fits well with the documented permeability structures described for lava domes (Buck et al., 1981; Wohletz and Heiken, 1992; Wooster et al., 2000; Watts et al., 2002; Gonnermann and Manga, 2003; Bluth and Rose, 2004; Sahetapy-Engel and Harris, 2009).

A typical lava dome consists of a magma body at some depth with a cylindrical-shaped zone or ‘conduit’ through which the magma rises to the surface (Fig. 3.11; Wohletz and Heiken, 1992; Watts et al., 2002; Bluth and Rose, 2004). Surface styles of eruptive lava domes are varied and typically complex, yet a common feature is an approximately cylindrical central lava plug partially encircled by an annular or concentric fracture zone of high permeability at the summit crater (Fig. 3.11;; Watts et al., 2002; Gonnermann and Manga, 2003; Bluth and Rose, 2004; Sahetapy-Engel and Harris, 2009). This concentric zone is the surface

expression of a deep-rooted fracture zone that forms in response to shear-induced fragmentation along the conduit walls of the ascending shallow magma body (Gonnermann and Manga, 2003; Bluth and Rose, 2004; Sahetapy-Engel and Harris, 2009). At the surface of the concentric fracture zone, multiple vent structures may form in response to ejection of pyroclastic material, generated at depth within the conduit shear-zone during repeat, and typically cyclical, explosive episodes (Costa et al., 2007; Sahetapy-Engel and Harris, 2009).

Critically, it is the concentric fracture zone with its vent structures that functions as the major conduit for heat and mass transfer to the surface from the shallow subsurface magma column (Gonnermann and Manga, 2003; Sahetapy-Engel and Harris, 2009). Concentric fracture zones are commonly disrupted by block and ash flows fed by the central lava plug, which spills out from the summit crater and deposits along the steep flanks of the dome. The latter imparts the characteristic horseshoe-like shape of the concentric fracture zones surrounding the apex (emergent lava plug) of many volcanic lava domes. The flanks of volcanic lava domes are typically characterized by a heavily brecciated carapace beneath which alternating layers of sphericular lava, brecciated lava, and obsidian may occur (Manley and Fink, 1987; Richnow, 1998).

We suggest that following cessation of eruptive activity, vent structures rooted to the Ohaaki Fault became preferred pathways for hydrothermal fluids, ascending from the underlying West Bank upflow (Fig. 3.11). Subsequently, localised silica deposition cemented the thin mantle of HFF above vent structures and along the OWTB, favoring hydro-fracturing (and/or hydrothermal eruptions) and giving rise to the concentric distribution of surface thermal activity about the apex of the dome. Conversely, the lack of evidence for thermal activity across the apex of the dome, where the HFF is very thin, is attributed to the presence of a massive and poorly permeable central lava plug. Although more subjective, the incomplete circle or horseshoe-like shape of the OWTB may reflect a low permeability flow lobe emplaced onto the NNW flank of the dome and the subsequent burial of a portion of the annular fracture zone, thereby sealing the area to hydrothermal fluid flow.

Support for the above structural model and a locally eruptive origin for the Ohaaki Rhyolite comes from a variety of sources including a detailed resistivity anisotropy survey of the OHW thermal area by Risk (1976). Risk (1976) found an approximately circular isotropic zone situated beneath the apex of the Ohaaki Rhyolite, about which strongly anisotropic lines radiated outwards into the surrounding country rock. This distinctive and symmetrical resistivity pattern indicates the presence of a massive and approximately circular body of coherent rock centred beneath the apex of the Ohaaki Rhyolite, about which linear fractures, filled with hydrothermal fluid, radiate out into the surrounding country rock. This structure fits well with that documented for volcanic lava domes where the intrusion of a pressurized cylindrical conduit (or shallow magma column) into surrounding country rock is accommodated by radial fracturing (Shelley, 1985;

Chadwick and Dieterich, 1995; Acocella and Neri, 2009). In this instance the coincidence of the approximately circular isotropic zone beneath the dome apex suggests that the Ohaaki Rhyolite is the surface expression of a circular magmatic conduit that intruded along the underlying Ohaaki Fault, a conclusion also reached by Risk (1976).

In accordance with the known permeability structures of volcanic lava domes, the existence of preferential flow paths developed along a fault is supported by reservoir isotherm data that depicts a spatially discrete and near vertical hydrothermal plume, ascending into the base of the Ohaaki Rhyolite, directly beneath the dome apex (Fig. 3.12). Here, the apex of the Ohaaki Rhyolite coincides with the lowest topographic relief on the base (or bottom) of the Ohaaki Rhyolite, which is also the location that the high temperature plume appears to enter the dome. The ascent of a hydrothermal plume through a zone of concentric fractures, developed about an approximately circular magmatic conduit, is consistent with the focusing of a surface mass and heat flow of ~90 kg $s^{-1}$ and 95 MW (Chapter 2), respectively, along the concentric fracture zone of the OWTB.

Evidence for a deep-rooted high permeability zone along the Ohaaki Fault, within the Ohaaki Rhyolite, is further supported by an iterative ray tracing model used to analyse seismic refraction data, which imaged a cone-shaped region at least 40 m wide at 200 m depth of anomalously low velocity beneath the Ohaaki Pool (Henrys, 1986). This distinctive velocity structure was explained in terms of a gaseous saturated fluid rising through a large cone-shaped explosion crater developed within the Ohaaki Rhyolite (Henrys, 1986). Although Henrys (1986) did not speculate as to the origins of the explosive force responsible for this structure, we argue that the location and shape of this structure, when taken in conjunction with the data presented above, fits well with the presence of an eruptive vent formed by the ejection of pyroclastic material along the Ohaaki Fault, within the Ohaaki Rhyolite dome.

Following burial of the extinct vent by the low permeability HFF, localised silicification appears to have favoured hydrothermal fracturing above the vent (or hydrothermal eruption) and formation of the deep Ohaaki Pool. Evidence for localised silica cementation of the HFF along the OWTC comes from drill core data (Simmons and Browne, 1990) and from the large sinter apron and silica stromatolites of the Ohaaki Pool. Here localise silica precipitation has sealed and strengthened the HFF favouring the development of open or gaping fractures above extinct vent structures formed within the Ohaaki Rhyolite. Self-structural permeability generation of this nature is well documented in hydrothermal systems with an often noted transition from diffuse to focused fluid flow in response to sealing and strengthening of low competency and high porosity reservoir rock (see Henneberger and Browne, 1988).

If the initial flow paths are sealed or choked by mineral deposition the pressure will build again until the fracture gradient is exceeded – either in the same locality or at another site along the OWTC. In order to

maintain relatively continuous flow of hot fluids at the ground surface this valving process must be relatively local. In other words, when some fractures are open others will be closed with valving happening at different times on individual fractures. Valving, causing the migration of the locus of alkali-Cl outflow along the OWTC is supported by shallow (100 m) alteration data that suggests an alkali-Cl outflow once occurred in the vicinity of well BR15 (Simmons and Browne, 1990). The occurrence of former high permeability flow paths along the OWTC are also supported by the large tract of intensely altered but 'cold' ground occurring between wells BR15 and BR22. This significant tract of altered but 'cold' ground was first noted in 1967 by Dickinson, some time prior to large scale extraction from the field.

A number of studies suggest that lava domes are mainly fed by dykes, with cylindrical conduits developing only at shallow levels (Mastin et al., 1988; Wohletz and Heiken, 1992; Nakada and Eichelberger, 2004). Although a feeder dyke, which may only be a few metres in width, has not been found during drilling, the inversely tapered shape of the hydrothermal plume that ascends up into the base of the Ohaaki Rhyolite may outline the remnant permeability of the dyke-conduit system associated with the dome (Fig. 3.12). Such a model is consistent with the lines of evidence outlined above and fits with the picture of a magmatically 'leaky' basement underlying the OHW thermal area. Evidence for a history of localised magma intrusion along the Ohaaki Fault comes from recent drilling within the OHW thermal area, and the intersection of andesite/dacite lavas within the deep Tahorakuri Formation that overlies the Ohaaki Fault scarp (Rae et al., 2007). Although the source of these lavas has not been drilled, the presence of a relatively shallow ($\geq$ 4.5 km), likely dacitic magma body, feeding the West Bank upflow has been postulated on the basis of gas geochemical data (Giggenbach, 1989; Christenson et al., 2002).

### 3.6.2 OHE thermal area fluid flow model

The distribution of permeability associated with the OHE thermal area is distinct from that of the OHW thermal area as there is no apparent correlation between structure contours on the top of the Broadlands Dacite, and the geometry of the high permeability zones. Rather, a sharp NNE-trending linear eastern boundary of the soil temperature and $CO_2$ flux anomaly (Figs. 3.8, 3.9 and 3.13) coincides with the projected location of the Broadlands Fault at the ground surface, and with a ~450 m long step in topography up to 2 m in height. This topographic scarp, which may have been eroded at its northern and southern ends, could represent the surface expression of the Broadlands Fault. If correct this interpretation would require that the fault displaces both the Broadlands Dacite reservoir and the HFF cap rock, and could locally influence the migration of geothermal fluids (Fig. 3.13). A similar conclusion (and inferred fault location) was reached by Grindley (1970) who mapped the trace of the Broadlands Fault from the alignment of surface thermal features within the OHE thermal area. Post 330 ka displacement by the Broadlands Fault cannot be unequivocally demonstrated using borehole data, suggesting that, if present, this displacement is likely to be <40 m (i.e. the lower size limit of resolvable fault displacement).

Displacement of the Broadlands Dacite by the Broadlands Fault is also supported by Rn/Th soil gas anomalies in the Ohaaki Field (Koga et al., 1982). Contour plots of the Rn/Th ratio reveal a number of elongate and NE-trending anomalies that display a strong correlation with the inferred traces of normal faults (Koga et al., 1982). In accord with the published literature these anomalies are interpreted to represent the expression of faults and/or fractures in the near-surface (Nishimura et al., 1990; Grainger et al., 1998; Ciotoli et al., 1999; Etiope and Martinelli, 2002). To the north and south of the OHE thermal area soil gas maps show a strong spatial correlation between Rn/Th anomalies and the inferred surface trace of the Broadlands Fault (Koga et al., 1982). The existence of these Rn/Th anomalies supports: (i) the occurrence of the Broadlands Fault at the surface of the OHE thermal area; (ii) its continuity across the greater Ohaaki Field, and; (iii) marked changes in the permeability of this fault in response to sharp spatial changes in the material properties of the Ohaaki Reservoir.

Our model for fluid flow in the OHE thermal area utilises the Broadlands Fault. We suggest that fracturing associated with the Broadlands Fault may produce high permeability zones in the Broadlands Dacite, and the locally hydrothermally cemented HFF, which provide near vertical pathways for fluid flow parallel to the fault surface (Fig. 3.13). When faulted, highly competent and low porosity rock is known to favour the development of permeable conduits for fluid flow due to the ability to sustain gaping fractures, and in response to cataclastic brecciation and misfit of opposing walls (Brown and Bruhn, 1996; Sibson, 2000). High permeability fractures may also develop in otherwise low competency and/or high porosity rock in response to localised sealing and cementation by hydrothermal minerals (Fournier and Seki, 1983; Henneberger and Browne, 1988; Fairley and Hinds, 2004). Evidence for the localised strengthening and sealing of the HFF above the apex of the Broadlands Dacite comes from the presence of locally intense precipitation of hydrothermal calcite (Hochstein and Henrys, 1989), and of quasi-circular $CO_2$ flux anomalies. These anomalies are consistent with the presence of high permeability conduits for fluid flow (Fig. 3.8).

Enhanced along-fault flow may be accompanied by reduced across-fault flow arising from the presence of low permeability (e.g., <0.01 mD) fault rock. Low permeability fault rock, which has also been referred to as fault core, is widely reported in the literature and may form by pore collapse, grain communition and hydrothermal mineral precipitation processes (Antonellini and Aydin, 1994; Caine et al., 1996; Rawling et al., 2001; Childs et al., 2009). The abrupt boundary along the eastern margin of the OHE thermal area is consistent with the presence of fault rock that produces a physical barrier, which blocks eastward migration of hydrothermal fluids. Similar abrupt transitions in shallow (0.2 m depth) surface temperatures were noted by Fairley and Hinds (2004) for the trace of the Borax Lake Fault, Alvord Basin of southeast Oregon, and have also been interpreted to indicate the presence of a low permeability fault core.

While the Broadlands Fault may have been important for enhancing the vertical flow of hydrothermal fluids from basement and restricting the eastward flow of these fluids, the OHE thermal area spreads up to 500 m from the fault and sits directly above the dacite dome apex. The spatial coincidence of the dome apex and the OHE thermal area suggests that hydrothermal fluids, which may be migrating up the Broadlands Fault at depths of hundreds to thousands of metres, are reaching, and possibly pooling, at the top of the dome. Locally the supply of hydrothermal fluids may be high due to the proximity of the fluid filled, fractured and faulted basement to the Broadlands Dacite reservoir (~300 m above), and to the ground surface (~ 900 m above) (Figs. 3.3b and 3.13). Migration of fluids through the low permeability HFF may be possible because locally the cap rock is fractured and at its thinnest (~110 m) across the dome apex (Fig. 3.3b and 3.13; Hochstein and Henrys, 1990). Fracturing of the seal, which is calcite cemented across the dome apex and likely to accommodate brittle rather than plastic deformation, could arise due to over-pressuring of the reservoir, or to earthquakes on nearby faults (e.g., Broadlands Fault).

### 3.6.3 Dome controlled fluid flow

In a recent diffuse-degassing survey of the nearby Rotorua hydrothermal field, Werner and Cardellini (2006) noted the localisation of major $CO_2$ degassing structures and upflows, with the occurrence of extinct rhyolite domes. In particular, $CO_2$ fluxes were elevated along the ridge crests at the top of both the north and south rhyolite domes of the Rotorua Field. From the location of emission structures along the crests of each dome Werner and Cardellini (2006) argued that old vent structures within the domes, rather than NE–SW faulting, governed fluid flow. Within the same field, faults cutting the base of these domes were also the sites of localised surface thermal activity (Werner and Cardellini, 2006). Although detailed flux or heat flow surveys have not been completed for others fields, the association of surface thermal areas with buried or partially emergent silicic lava domes is a notable feature of the majority of TVZ hydrothermal fields, including, but not limited to, the Ohaaki and Rotorua fields as mentioned above, as well as the Wairakei, Mokai, Waiotapu and Waimangu fields (McWilliams et al., 1957; Grindley, 1965; Bibby et al., 1984; Hunt et al., 1994).

As with Ohaaki, the hydrothermal systems hosted within active lava domes are short lived and it is the deep differentiated magma source that drives significant hydrothermal convection (Ishikawa, 1970; Wohletz and Heiken, 1992; Christenson et al., 2002; Werner and Cardellini, 2006; Chapter 2). The development of large convecting geothermal systems beneath silicic dome systems has been characterised for a number of volcanic hydrothermal fields globally (Ishikawa, 1970; Duffield et al., 1980; Wohletz and Heiken, 1992). The Coso field of California is one such example where a large convecting hydrothermal system is developed within a normal faulted Mesozoic basement below a system of young silicic domes (Duffield et al., 1980; Wohletz and Heiken, 1992). In Japan the majority of hydrothermal fields are developed around young volcanoes or near to shallow intrusives, with geothermal areas commonly developing close to silicic lava domes (Ishikawa,

1970). Therefore, globally silicic lava domes are regarded as a good indicator of a much larger thermal source at depth (Wohletz and Heiken, 1992).

Post-eruption, deeply derived hydrothermal fluid flow within a lava dome will be governed by dome stratigraphy and structure, as well as the structural setting of the region (Ishikawa, 1970; Duffield et al., 1980; Wohletz and Heiken, 1992; Werner and Cardellini, 2006; this paper). At Ohaaki the relative magnitude of mass flow through the domes of the area is also dependant upon the proximity to major upflow zones (Chapter 2). Some overlap between upflow zones and silicic domes is to be expected given the evidence for deep-seated fault control over the occurrence of both (Henrys and Hochstein, 1990; Wohletz and Heiken, 1992; Christenson et al., 2002; Werner and Cardellini, 2006; Rae et al., 2007).

The two Ohaaki Field examples presented in this paper include fluid flow through: (i) dome permeability structures rooted to an underlying source of heated fluids through a conduit and dyke system (hereafter referred to as 'cratered' domes) and; (ii) faulted domes. In both instances domes provide cross-stratal pathways for fluid flow by connecting the underlying hydrothermal system to the surface, and effectively bypassing low permeability cap rocks. The role of dome complexes as cross-stratal pathways for fluid flow is well illustrated by the location of all three surface thermal areas at Ohaaki above buried or partially emergent Quaternary lava domes. As well as cratered and faulted domes, Wohletz and Heiken (1992) define dome tephra aprons, dome complexes (one or more overlapping domes), caldera ring fault domes, and caldera resurgent domes, as possible sites of hydrothermal fluid circulation. Tephra aprons and tuff rings along with faulted domes play an important role in the fluid flow of the Coso Field (Duffield et al., 1980; Wohletz and Heiken, 1992). However, faults may also be sealed by the intrusion of feeder dykes (Wood et al., 2001), and some dome configurations (i.e., dome complexes) may mask the occurrence of high temperatures at depth due to sealing of more permeable units, or fracture zones by impermeable lavas (Wohletz and Heiken, 1992).

In addition to promoting cross-stratal fluid flow, lava domes of the TVZ provide islands of high competency ($\geq$10 MPa) and low porosity rock within the otherwise low competency (< 5 Mpa), and far more voluminous Quaternary cover sequence (Rowland and Sibson, 2004). The greater competency and lower bulk porosity of lava domes means they are more likely to favour high permeability flow paths when transected by normal faults, as demonstrated by this study, and that of Werner and Cardellini (2006) for the Rotorua Field. Therefore, silicic lava domes localise fluid flow through both their eruptive structure and stratigraphy and by the provision of locally competent and fractured rock.

Although the prevalence of dome controlled fluid flow within the TVZ has not been quantified by a detailed survey, examples from both Ohaaki and Rotorua provide a picture of hydrothermal reservoirs sealed by low competency cap rock, within which lava domes function as pathways of preferential vertical permeability,

focusing fluid flow and acting as pressure release valves for underlying hydrothermal reservoirs. From these observations the Quaternary dome complexes of the TVZ may constitute a major pathway of magmatic heat and mass release to the atmosphere long after eruption.

## 3.7 Conclusions

In this paper, we present fliud flow models of the permeability structures governing fluid flow within both major thermal areas of the Ohaaki hydrothermal field. From this and other published data we argue that hydrothermal fluid flow associated with the OHW thermal area exploits remnant permeability structures associated with the extrusion and eruption of the Ohaaki Rhyolite dome from vents beneath the area. We consider it likely that the Ohaaki Rhyolite extruded along structural permeability associated with the large Ohaaki Fault, which currently acts as a conduit for the ascent of the West Bank upflow into the overlying reservoir (Christenson et al., 2002; Rae et al., 2007). Localised intrusion of magma through the Ohaaki Fault is consistent with reservoir isotherm models (Fig. 3.12) and an established history of magma extrusion (andesite lavas within the deep Tahorakuri Formation that overlies the Ohaaki Fault scarp; Rae et al., 2007), and gas geochemical evidence for a shallow (≤ 4.5 km), possibly dacitic magma body beneath the area (Christenson et al., 2002).

In the smaller OHE thermal area permeability structures show no relationship to the known structure of volcanic dome complexes. Rather we argue that the fluid flow within this area is characterised by a ‘conduit-barrier’ fluid flow system (after Caine et al., 1996) associated with propagation of the Broadlands Fault, through a localised stratigraphic sequence of highly competent and low porosity rock. However, the spatial coincidence of the dome apex and the OHE thermal area suggests that hydrothermal fluids, which may be migrating up the Broadlands Fault at depths of hundreds to thousands of metres, are reaching, and possibly pooling, at the top of the dome.

The absence of any strong NE-trend to the pattern of surface thermal activity associated with the OHW thermal area likely reflects the masking of the Ohaaki Fault by the lavas of the Ohaaki Rhyolite. This interpretation is supported by anomalous Rn/Th ratios that depict a major NE-trending lineament coincident with the projected trace of the Ohaaki Fault, occurring both to the north and south of the Ohaaki Rhyolite dome (Koga et al., 1982). As noted above, such anomalies are strong evidence for the existence of major, albeit hidden, surface faults at Ohaaki, and the masking of the underlying high temperature reservoir by the poorly permeable and clay-rich HFF cap rock. Given the importance of the inferences that result from the preliminary work of Koga et al. (1982) additional Rn and Th soil gas measurements, modeled on the work of those investigators, but at a higher resolution, would lend more confidence to the interpretation of deep-seated fault control.

Apart from refined models of the permeability structures governing the surface discharge of hydrothermal fluids at Ohaaki, the results of this study are of broader significance, both regionally within the TVZ and globally, for understanding the role of material properties and structural elements in governing fluid flow. In particular we present evidence that volcanic dome complexes play a critical role in localising (focusing) fluid flow either through: (i) the presence of remnant permeability structures formed during the eruption of volcanic dome complexes, or; (ii) by favouring the development of high permeability fault-fracture networks when transected by normal faults. Further, the role of the clay-rich HFF in masking deep-seated fault control may be significant to: (i) the structural interpretations of the broader Taupo-Reporoa Basin, within which the HFF is very thick, and for which, the surface expression of normal faulting is conspicuously absent (Rowland and Sibson, 2004), and; (ii) studies of blind faults, and blind, fault-controlled hydrothermal systems globally (Grainger et al., 1998; Ciotoli et al., 1999; Guerra and Lombardi, 2001; Lewicki and Oldenburg, 2004).

## 3.8 Acknowledgements

We thank Mr. Hannu Sebeck and Mr. Mike Rosenberg for insightful comments and information that helped refine the direction of this work. Staff of the Contact Energy's geothermal group and those of GNS Wairakei are acknowledged for their logistical support and access to field data and equipment. Sheena Tarawera of GNS Science, Wairakei is acknowledged for her assistance in locating valuable historical reports and early aerial photographs of the Ohaaki Field. Funding for this study was provided by Contact Energy and the Mason Trust of the University of Canterbury.

## 3.9 References

Acocella, V. and Neri, M., 2009. Dike propagation in volcanic edifices; overview and possible developments. Tectonophysics, 471(1-2): 67-77.

Allis, R.G. and Webber, S., 1984. Shallow temperature measurements at Wairakei and Broadlands fields. Geophysics Division Report, 197: 27.

Allis, R.G. and Zhan, X., 2000. Predicting subsidence at Wairakei and Ohaaki geothermal fields, New Zealand. Geothermics, 29(4-5): 479-497.

Antonellini, M. and Aydin, A., 1994. Effect of faulting on fluid flow in porous sandstones: petrophysical properties American Association of Petroleum Geologists 78: 355-377.

Bibby, H.M., Dawson, G.B., Rayner, H.H., Stagpoole, V.M. and Graham, D.J., 1984. The structure of the Mokai geothermal field based on geophysical observations. Journal of Volcanology and Geothermal Research, 20(1-2): 1-20.

Bibby, H.M., Caldwell, T.G., Davey, F.J. and Webb, T.H., 1995. Geophysical evidence on the structure of the Taupo volcanic zone and its hydrothermal circulation. Journal of Volcanology and Geothermal Research, 68(1-3): 29-58.

Bluth, G.J.S. and Rose, W.I., 2004. Observations of eruptive activity at Santiaguito volcano, Guatemala. Journal of Volcanology and Geothermal Research, 136: 297-302.

Bromley, C.J. and Hochstein, M.P., 2005. Heat discharge of steaming ground at Karapiti (Wairakei), New Zealand, World Geothermal Congress 2005. In: Proceedings of the International Geothermal Association, Antalya, Turkey, pp. 1 - 7.

Brothers, R.N., 1957. The Volcanic Domes of Mayor Island, New Zealand. Transactions of the Royal Society of New Zealand. Vol. 84, Part 3, pp 549 – 560.

Brown, S.R. and Bruhn, R.L., 1996. Formation of voids and veins during faulting. Journal of Structural Geology, 18: 657 - 671.

Buck, M.D., Briggs, R.M., Nelson, C.S., 1981. Pyroclastic deposits and volcanic history of Mayor Island. New Zealand Journal of Geology and Geophysics, Vol. 24, pp. 449 – 467.

Burns, B.R., 1997. Vegetation change along a geothermal stress gradient at the Te Kopia Steamfield. Journal of the Royal Society of New Zealand, 27(2): 279-294.

Caine, J.S., Evans, J.P. and Forster, C.B., 1996. Fault zone architecture and permeability structure. Geology, 24: 1025 - 1028.

Camarda, M., De Gregorio, S., Favara, R. and Gurrieri, S., 2007. Evaluation of carbon isotope fractionation of soil $CO_2$ under an advective-diffusive regime: A tool for computing the isotopic composition of unfractionated deep source. Geochimica et Cosmochimica Acta, 71(12): 3016-3027.

Carapezza, M.L., Ricci, T., Ranaldi, M. and Tarchini, L., 2009. Active degassing structures of Stromboli and variations in diffuse $CO_2$ output related to the volcanic activity. Journal of Volcanology and Geothermal Research, 182(3-4): 231-245.

Chadwick, W.W., Jr. and Dieterich, J.H., 1995. Mechanical modeling of circumferential and radial dike intrusion on Galapagos volcanoes. Journal of Volcanology and Geothermal Research, 66(1-4): 37-52.

Childs, C., Manzocchi, T., Walsh, J.J., Bonson, C.G., Nicol, A. and Schopfer, M.P.J., 2009. A geometric model of fault zone and fault rock thickness variations. Journal of Structural Geology, 31(2): 117-127.

Chiodini, G., Granieri, D., Avino, R., Caliro, S., Costa, A. and Werner, C., 2005. Carbon dioxide diffuse degassing and estimation of heat release from volcanic and hydrothermal systems. Journal of Geophysical Research, 110: no.B8, 17.

Christenson, B.W., Mroczek, E.K., Kennedy, B.M., van Soest, M.C., Stewart, M.K. and Lyon, G., 2002. Ohaaki reservoir chemistry; characteristics of an arc-type hydrothermal system in the Taupo volcanic zone, New Zealand. Journal of Volcanology and Geothermal Research, 115(1-2): 53-82.

Ciotoli, G., Etiope, G., Guerra, M. and Lombardi, S., 1999. The detection of concealed faults in the Ofanto Basin using the correlation between soil-gas fracture surveys. Tectonophysics, 301(3-4): 321-332.

Cole, J.W., 1970. Structure and eruptive history of the Tarawera volcanic complex. New Zealand Journal of Geology and Geophysics, 13.

Cole, J.W., 1990. Structural control and origin of volcanism in the Taupo volcanic zone, New Zealand. Bulletin of Volcanology, 52(6): 445-459.

Contact Energy, 2006. Ohaaki well and feed zone stratigraphic database.

Costa, A., Melnik, O., Sparks, R.S.J. and Voight, B., 2007. Control of magma flow in dykes on cyclic lava dome extrusion. Geophysical Research Letters, 34(2).

Curewitz, D. and Karson, J.A., 1997. Structural settings of hydrothermal outflow; fracture permeability maintained by fault propagation and interaction. Journal of Volcanology and Geothermal Research, 79(3-4): 149-168.

Dawson, G.B. and Dickinson, D.J., 1970. Heat flow studies in thermal areas of the North Island of New Zealand. Geothermics, 2(Part 1): 466-473.

Dawson, G.B., 1988. Broadlands Geothermal Field Environmental Monitoring (Ground Temperature and Geothermal Feature Survey). Report No. 91, Department of Scientific and Industrial Research (D.S.I.R.), Wellington.

Dickinson, D.J., 1967. The natural heat output of the Broadlands geothermal area, 1967. Department of Scientific and Industrial Research - Geophysics Division, Wellington.

Duffield, W.A., Bacon, C.A. and Dalrymple, G.B., 1980. Late Cenozoic volcanism, geochronology, and structure of the Coso Range, Inyo County, California J. Geophys. Res., 85 2379–2380.

Etiope, G., Beneduce, P., Calcara, M., Favali, P., Frugoni, F., Schiattarella, M. and Smriglio, G., 1999. Structural pattern and $CO_2$-$CH_4$ degassing of Ustica Island, Southern Tyrrhenian basin. Journal of Volcanology and Geothermal Research, 88(4): 291-304.

Etiope, G. and Martinelli, G., 2002. Migration of carrier and trace gases in the geosphere; an overview. Physics of the Earth and Planetary Interiors, 129(3-4): 185-204.

Fairley, J.P. and Hinds, J.J., 2004. Field observation of fluid circulation patterns in a normal fault system. Geophysical Research Letters, 31.

Fournier, R.O. and Seki, Y., 1983. Self-sealing and brecciation resulting from quartz deposition within hydrothermal systems, Extended Abstracts - International Symposium on Water-Rock Interaction. pp. 137-140.

Fridriksson, T., Kristjansson, B.R., Armannsson, H., Margretardottir, E., Olafsdottir, S. and Chiodini, G., 2006. $CO_2$ emissions and heat flow through soil, fumaroles, and steam-heated mud pools at the Reykjanes geothermal area, SW Iceland. Applied Geochemistry, 21(9): 1551-1569.

Giammanco, S., Gurrieri, S. and Valenza, M., 1997. Soil $CO_2$ degassing along tectonic structures of Mount Etna (Sicily): the Pernicana fault. Applied Geochemistry, 12 (4.): 429-436.

Giggenbach, W.F., 1989. The chemical and isotopic position of the Ohaaki Field within the Taupo volcanic zone. In: P.R.L. Browne and K. Nicholson (Editors). 11th New Zealand Geothermal Workshop, University of Auckland Geothermal Institute, pp. 81-88.

Given, D.R., 1980. Vegetation on heated soils at Karapiti, central North Island, New Zealand, and its relation to ground temperature. New Zealand Journal of Botany, 18: 1–13.

Glover, R.B., Hunt, T.M. and Severne, C.M., 2000. Impacts of development on a natural thermal feature and their mitigation; Ohaaki Pool, New Zealand. Geothermics, 29(4-5): 509-523.

Gonnermann, H.M. and Manga, M., 2003. Explosive volcanism may not be an inevitable consequence of magma fragmentation. Nature, 426: 432 - 435.

Grainger, P., Duddridge, G.A. and Lombardi, S., 1998. Soil gases as fault tracers in clay basins; two case histories; the Bovey (UK) and Siena (I) basins, Joint NEA/EC workshop; Fluid flow through faults and fractures in argillaceous formations. Oecd, Paris.

Grindley, G.W., 1965. The geology, structure, and exploitation of the Wairakei geothermal field, Taupo, New Zealand. New Zealand Geological Survey Wellington New Zealand (NZL).

Grindley, G.W., 1970. Subsurface structures and relation to steam production in the Broadlands geothermal field, New Zealand. Geothermics, 2(Part 1): 248-261.

Guerra, M. and Lombardi, S., 2001. Soil-gas method for tracing neotectonic faults in clay basins: the Pisticci field (Southern Italy). Tectonophysics, 339(3-4): 511-522.

Hale, J.H. and Wadge, G, 2008. The transition from endogenous to exogenous growth of lava domes with the development of shear bands. Journal of Volcanology and Geothermal Research, vol. 171, no. 3-4, pp. 237 -257.

Healy, J., 1968. Geological report on the Broadlands Geothermal Field, Department of Scientific and Industrial Research, Rotorua, New Zealand.

Hedenquist, J.W., 1990. The thermal and geochemical structure of the Broadlands-Ohaaki geothermal system, New Zealand. Geothermics, 19(2): 151-185.

Heffner, J. and Fairley, J., 2006. Using surface characteristics to infer the permeability structure of an active fault zone. Sedimentary Geology, 184: 255-265.

Henneberger, R.C. and Browne, P.R.L., 1988. Hydrothermal alteration and evolution of the Ohakuri hydrothermal system, Taupo volcanic zone, New Zealand. Journal of Volcanology and Geothermal Research, 34(3-4): 211-231.

Henrys, S.A., 1986. Shallow structure of the Broadlands-Ohaaki geothermal field (NZ); analysis of seismic refracted arrivals by iterative ray tracing. Proceedings of the New Zealand Geothermal Workshop, University of Auckland Geothermal Institute, pp. 85-90.

Henrys, S.A. and Hochstein, M.P., 1990. Geophysical structure of the Broadlands-Ohaaki geothermal field (New Zealand). Geothermics, 19(2): 129-150.

Hochstein, M.P. and Henrys, S.A., 1989. Geophysical structure and densification of producing layers in the Broadlands-Ohaaki Field (New Zealand). 11th New Zealand Geothermal Workshop, University of Auckland Geothermal Institute, pp. 45-50.

Hunt, T.M., Glover, R.B. and Wood, C.P., 1994. Waimangu, Waiotapu, and Waikite geothermal systems, New Zealand: Background and history. Geothermics, 23(5-6): 379-400.

Hunt, T.M. and Graham, D.J., 1997. Shallow ground temperature and groundwater temperature monitoring at Ohaaki (Broadlands) Geothermal Field, IGNS, Taupo.

Hunt, T.M. and Bromley, C.J., 2000. Some environmental changes resulting from development of Ohaaki geothermal field, New Zealand. In: World Geothermal Conference, Kyushu, Japan, pp. 621 – 626.

IGNS, 1998. Ohaaki Geothermal Field - Geo-scientific Resource Information, Institute of Geological and Nuclear Sciences, New Zealand, Wairakei.

Ishikawa, T., 1970. Geothermal fields in Japan considered from the geological and petrological view point. Geothermics (Spec. Issue 2): 1205–1211.

Knapp, R.B. and Norton, D.L., 1978. The physical environment of hydrothermal systems; timing, location and orientation of fractures produced by thermal and magmatic processes, Eos, Transactions, American Geophysical Union. American Geophysical Union, Washington, pp. 1202.

Koga, A., Taguchi, S. and Mahon, W.A.J., 1982. The use of volatile constituents in geothermal fluids for assessing the type, potential and near surface permeability of a geothermal system; the Broadlands geothermal area, N.Z. Proceedings of Pacific Geothermal Conference, vol.4. University of Auckland Geothermal Institute, Auckland, pp. 135-138.

Koide, H. and Bhattacharji, S., 1975. Formation of fractures around magmatic intrusions and their role in ore localization. Economic Geology and the Bulletin of the Society of Economic Geologists, 70(4): 781-799

Lewicki, J.L. and Oldenburg, C.M., 2004. Strategies for Detecting Hidden Geothermal Systems by Near-Surface Gas Monitoring, Lawrence Berkeley National Laboratory

Lewis, J.F., 1968. Tauhara Volcano, Taupo Zone, Part 1 – Geology and Structure. New Zealand Journal of Geology and Geophysics, Vol. 11 pp. 212 – 224.

Lowell, R.P., Van Cappellen, P. and Germanovich, L.N., 1993. Silica precipitation in fractures and evolution of permeability in hydrothermal upflow zones. Science, 260(5105): 192-194.

MacDonald, W.J.P., 1975. The useful heat contained in the Broadlands geothermal field. Second United Nations symposium on the development and use of geothermal resources, San Francisco, Calif., United States.

Mahon, W.A.J. and Finlayson, J.B., 1972. The chemistry of the Broadlands geothermal area, New Zealand. American Journal of Science, 272(1): 48-68.

Manley, C.R. and Fink, J.H., 1987. Internal textures of rhyolite flows as revealed by research drilling. Geology, 15(6): 549-552.

Martin, R., Rodgers, K.A. and Browne, P.R.L., 2000. Aspects of the distribution and movement of aluminium in the surface of the Te Kopia geothermal field, Taupo volcanic zone, New Zealand. Applied Geochemistry, 15(8): 1121-1136.

Mastin, L.G., Pollard, D.D., 1988. Surface deformation and shallow dike intrusion processes at Inyo Craters, Long Valley, California. Journal of Geophysical Research, 93(B11): 13,221-13,235.

McWilliams, J.A., Dick, I.D., Studt, F.E., Grindley, G.W., Steiner, A., Benseman, R.F., Thompson, G.E.K., Banwell, C.J., McWilliams, J.A., Lloyd, E.F., Wilson, S.H. and Healy, J., 1957. The geothermal structure of the Waiotapu thermal area. DSIR Geothermal Report, 4: 66-77.

Nakada, S. and Eichelberger, J., 2004. Looking into a volcano; drilling Unzen. Geotimes, 49(3): 14-17.

Natale, G., Hernandez, P., Mori, T. and Notsu, K., 2000. Pressure gradient measurements in volcanic diffuse gas emanations. Geophysical Research Letters, 27(24): 3985-3987.

Nicol, A., Mazengarb, C., Chanier, F., Rait, G., Uruski, C. and Wallace, L., 2007. Tectonic evolution of the active Hikurangi subduction margin, New Zealand, since the Oligocene. Tectonics 26.

Nishimura, S., Katsura, I., Durrance, E.M., Galimov, E.M., Hinkle, M.E., Reimer, G.M., Sugisaki, R. and Augustithis, S.S., 1990. Radon in soil gas; applications in exploration and earthquake prediction. Theophrastus Publ., Athens.

Norton, D. and Knapp, R., 1977. Transport phenomena in hydrothermal systems; the nature of porosity. American Journal of Science, 277(8): 913-936.

Rae, A.J., Rosenberg, M.D., Bignall, G., Kilgour, G.N. and Milicich, S.D., 2007. Geological results of production well drilling in the western steamfield, Ohaaki geothermal system: 2005-2007. 29th New Zealand Geothermal Workshop, University of Auckland Geothermal Institute, pp. 7.

Rawling, G.C., Goodwin, L.B. and Wilson, J.L., 2001. Internal architecture, permeability structure, and hydrologic significance of contrasting fault-zone types. Geology, 29(1): 43-46.

Read, S.A.L., Pender, M.J., Barker, P.R. and Ellis, S.M., 2003. Consolidation testing of Huka Falls Formation; properties related to subsidence at Ohaaki and Wairakei. In: S.A. Crawford, P. Baunton and S. Hargraves (Editors), Proceedings of Technical Groups, Institution of Professional Engineers New Zealand, vol. 30(1GM), pp. 291-300.

Richnow, J., 1998. Dome growth model of the Ngongotaha Dome, Rotorua, North Island. In: K.N. Bassett and D.C. Nobes (Editors), Geological Society of New Zealand Miscellaneous Publication, vol. 101A. Geological Society of New Zealand, Lower Hutt, pp. 196.

Risk, 1976. Detection of buried zones of fissured rock in geothermal fields using resistivity anisotropy measurements. 2nd United Nations symposium on the Development and use of geothermal resources, Berkeley, CA, United States.

Rosenberg, M.D., Hunt, T.M., Simmons, S.F., Morgan, O.E. and Dunstall, M.G., 1999. Ohaaki geothermal field; some properties of Huka Falls Formation mudstones. 21st New Zealand Geothermal Workshop. University of Auckland Geothermal Institute. pp. 89-94.

Rowland, J.V. and Sibson, R.H., 2004. Structural controls on hydrothermal flow in a segmented rift system, Taupo volcanic zone, New Zealand. Geofluids, 4(4): 259-283.

Sahetapy-Engel, S.T. and Harris, A.J.L., 2009. Thermal structure and heat loss at the summit crater of an active lava dome. Bulletin of Volcanology, 71(1): 15-28.

Shelley, D., 1985. Determining paleo-flow directions from groundmass fabrics in the Lyttelton radial dykes, New Zealand. Journal of Volcanology and Geothermal Research, 25(1-2): 69-79.

Sibson, R.H., 2000. Fluid involvement in normal faulting. Journal of Geodynamics, 29(3-5): 469-499.

Stratford, W.R. and Stern, T.A., 2006. Crust and upper mantle structure of a continental backarc, central North Island, New Zealand. Geophysics Journal International 166: 469-484

Tanaka, H.K.M., Nakano, T., Takahashi, H., Yoshida, J., Ohshima, H., Maekawa, T., Watanabe, H. and Niwa, K., 2007. Imaging the conduit size of the dome with cosmic-ray muons: The structure beneath Showa-Shinzan Lava Dome, Japan. Geophysical Research Letters, 34: 1 - 5.

Thompson, G.E.K., 1967. Ground temperatures at a depth of one metre. Report, Department of Scientific and Industrial Research - Geophysics Division, Wellington, New Zealand.

Watts, R.B., Herd, R.A., Sparks, R.S.J. and Young, S.R., 2002. Growth patterns and emplacement of the andesitic lava dome at Soufriere Hills Volcano, Montserrat. Memoirs of the Geological Society of London, 21: 115-152.

Werner, C. and Cardellini, C., 2006. Comparison of carbon dioxide emissions with fluid upflow, chemistry, and geologic structures at the Rotorua geothermal system, New Zealand. Geothermics, 35(3): 221-238.

Wilson, C.J.N., Houghton, B.F., McWilliams, M.O., Lanphere, M.A., Weaver, S.D. and Briggs, R.M., 1995. Volcanic and structural evolution of Taupo volcanic zone, New Zealand; a review. Journal of Volcanology and Geothermal Research, 68(1-3): 1-28.

Wohletz, K. and Heiken, G., 1992. Volcanology and Geothermal Energy. University of California Press, Berkeley, 435 pp.

Wood, C.P., 1994. The Waiora Formation geothermal aquifer, Taupo volcanic zone, New Zealand. 16th New Zealand Geothermal Workshop, University of Auckland Geothermal Institute, pp. 121-126.

Wood, C.P., 1996. Basement geology and structure of TVZ geothermal fields. 18th New Zealand Geothermal Workshop, University of Auckland Geothermal Institute, pp. 157-162.

Wood, C.P., Brathwaite, R.L. and Rosenberg, M.D., 2001. Basement structure, lithology and permeability at Kawerau and Ohaaki geothermal fields, New Zealand. Geothermics, 30(4): 461-481.

Wooster, M.J., Kaneko, T., Nakada, S. and Shimizu, H., 2000. Discrimination of lava dome activity styles using satellite-derived thermal structures. Journal of Volcanology and Geothermal Research, 102(1-2): 97-118.

## 1.7 Figures

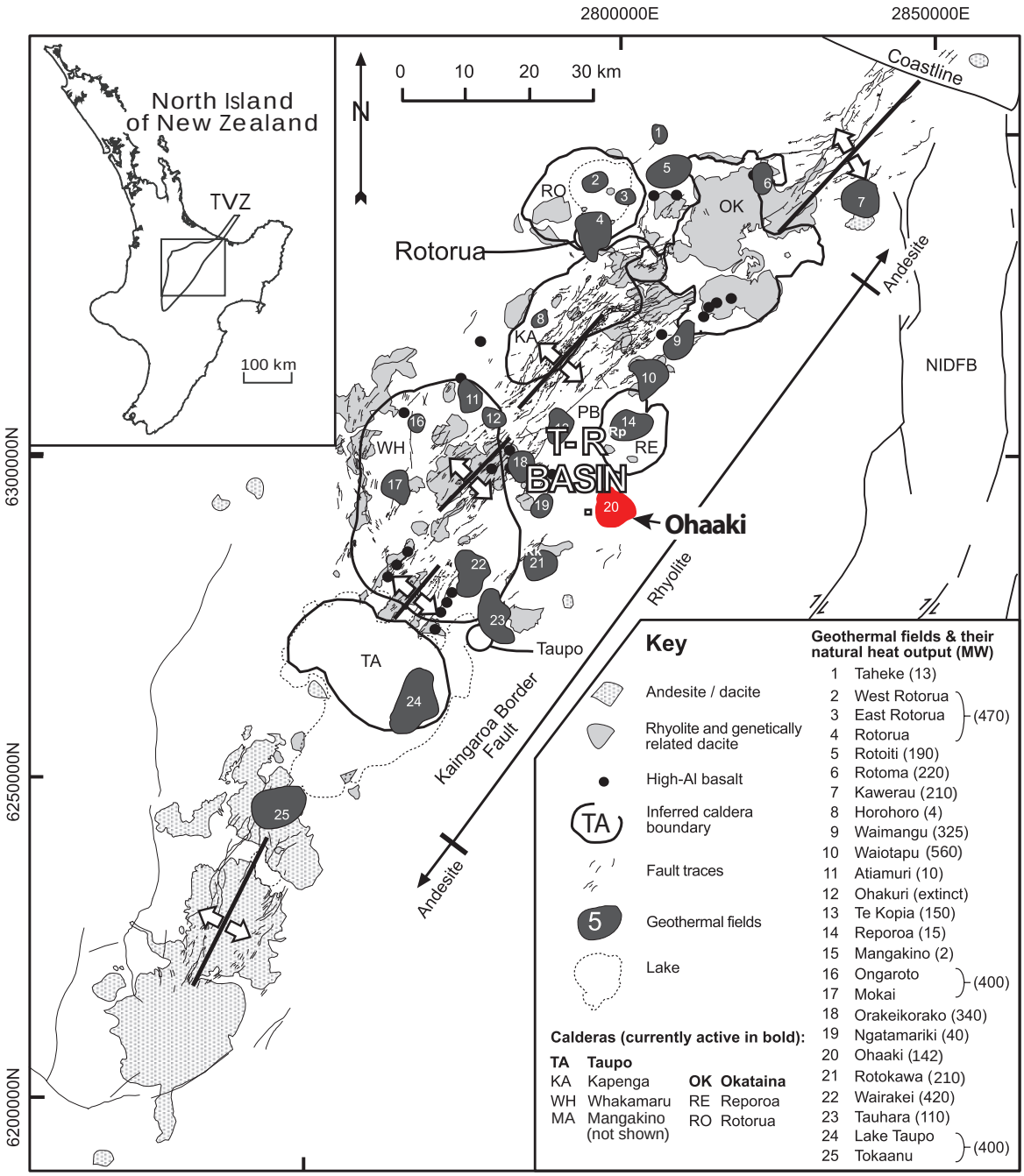


Figure 3.1. Map of the Taupo Volcanic Zone showing the distribution of geothermal systems, defined by the presence of low-resistivity zones (<30 Ωm) in relation to rift architecture, major volcanic rock types and caldera boundaries (modified from Rowland & Sibson 2004). Where T-R basin denotes the location of the Taupo Reporoa Basin and the Ohaaki hydrothermal field is in red. NIDFB, North Island Dextral Fault Belt. Major towns, Taupo and Rotorua, are labelled.

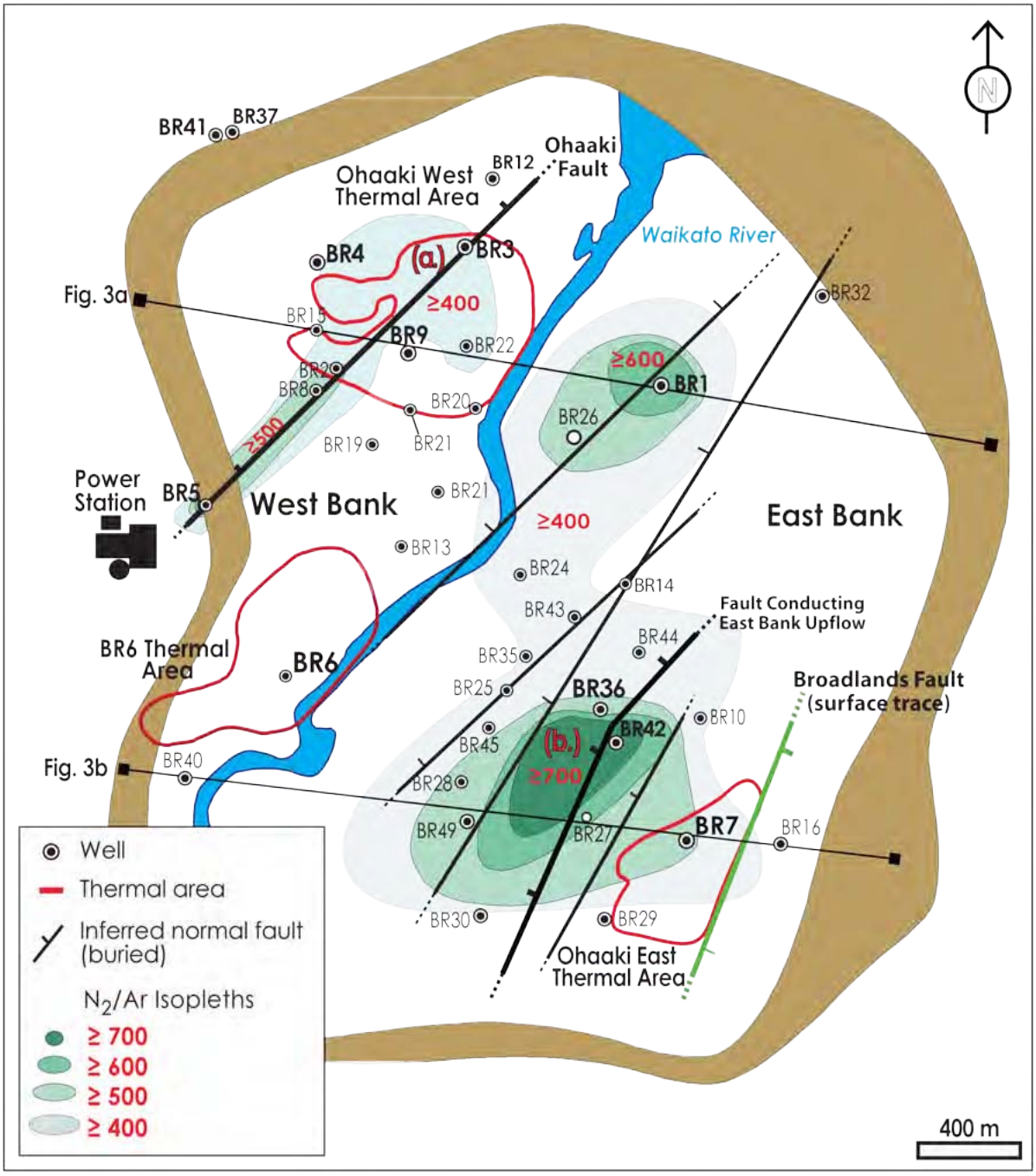


Figure 3.2. Plan view of the Ohaaki Field including resistivity boundary, inferred deep-seated normal faults, $N_2$/Ar isopleths and location of major thermal areas (from Christenson et al., 2002; Wood et al., 2001). $N_2$/Ar isopleths denote the major hydrothermal upflows of the field. The Ohaaki Fault occurs in the upper left of the field and conducts the West Bank upflow. The East Bank upflow occurs through another major normal fault in the SE. The surface trace of the Broadlands Fault is shown in green (this study). The location of both major thermal areas, Ohaaki West (OHW) and Ohaaki East (OHE), as well as the low temperature BR6 thermal area are shown. Thermal areas are delineated by 1.0 m depth temperatures ≥ 25ºC after Allis and Webber, (1983) and this study. The line of cross-section for Figures 3a and 3b are also displayed.

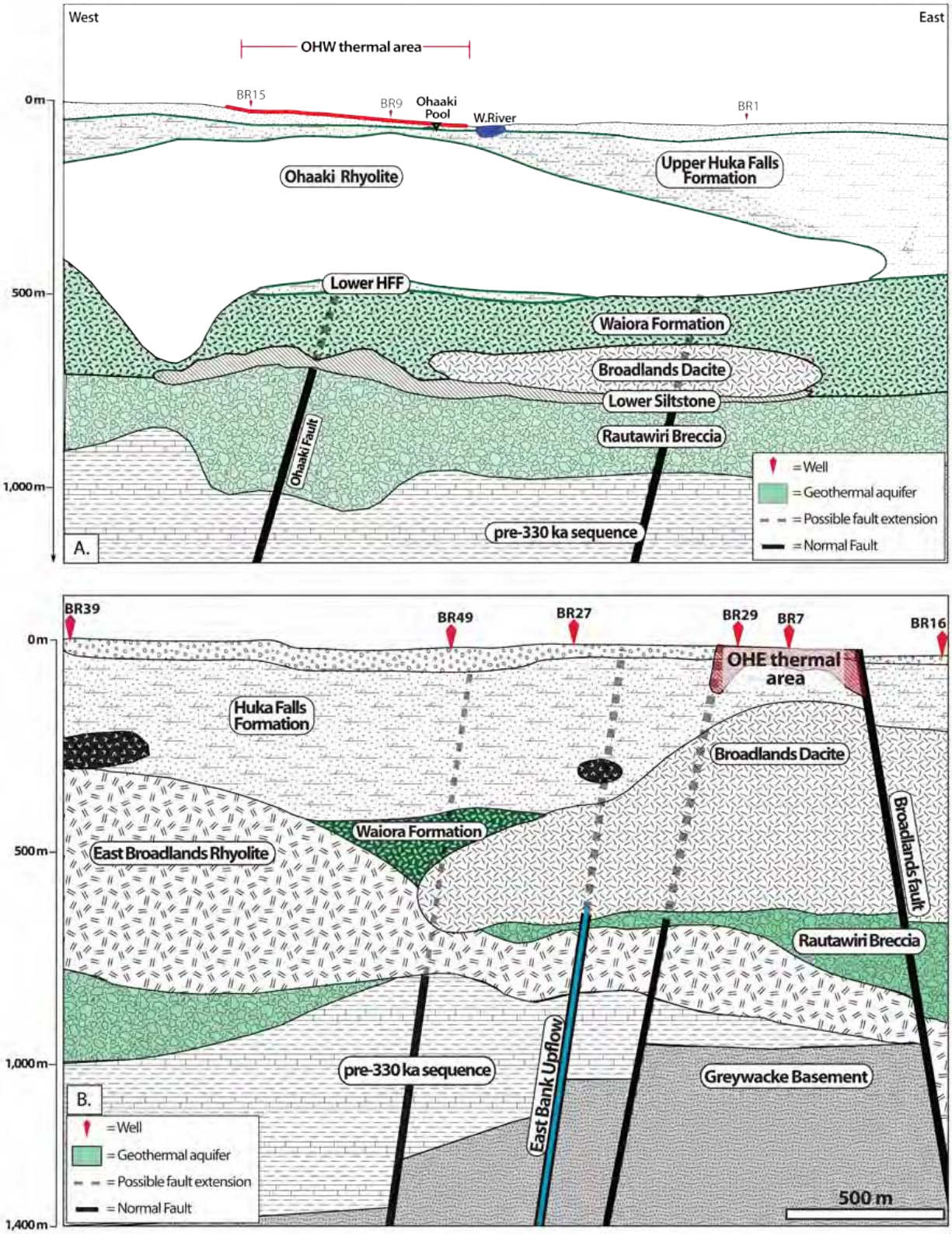


Figure 3.3. East – west cross sections through the Ohaaki reservoir (modified from Milicich, 2010). (a) Cross section through the NW sector of the field and the OHW thermal area. (b) Cross section through the SE sector of the field and the OHE thermal area. Fault locations are idealised and not to scale. The black blobs occurring within the HFF, (b), are distal flow lobes of the Ohaaki Rhyolite.

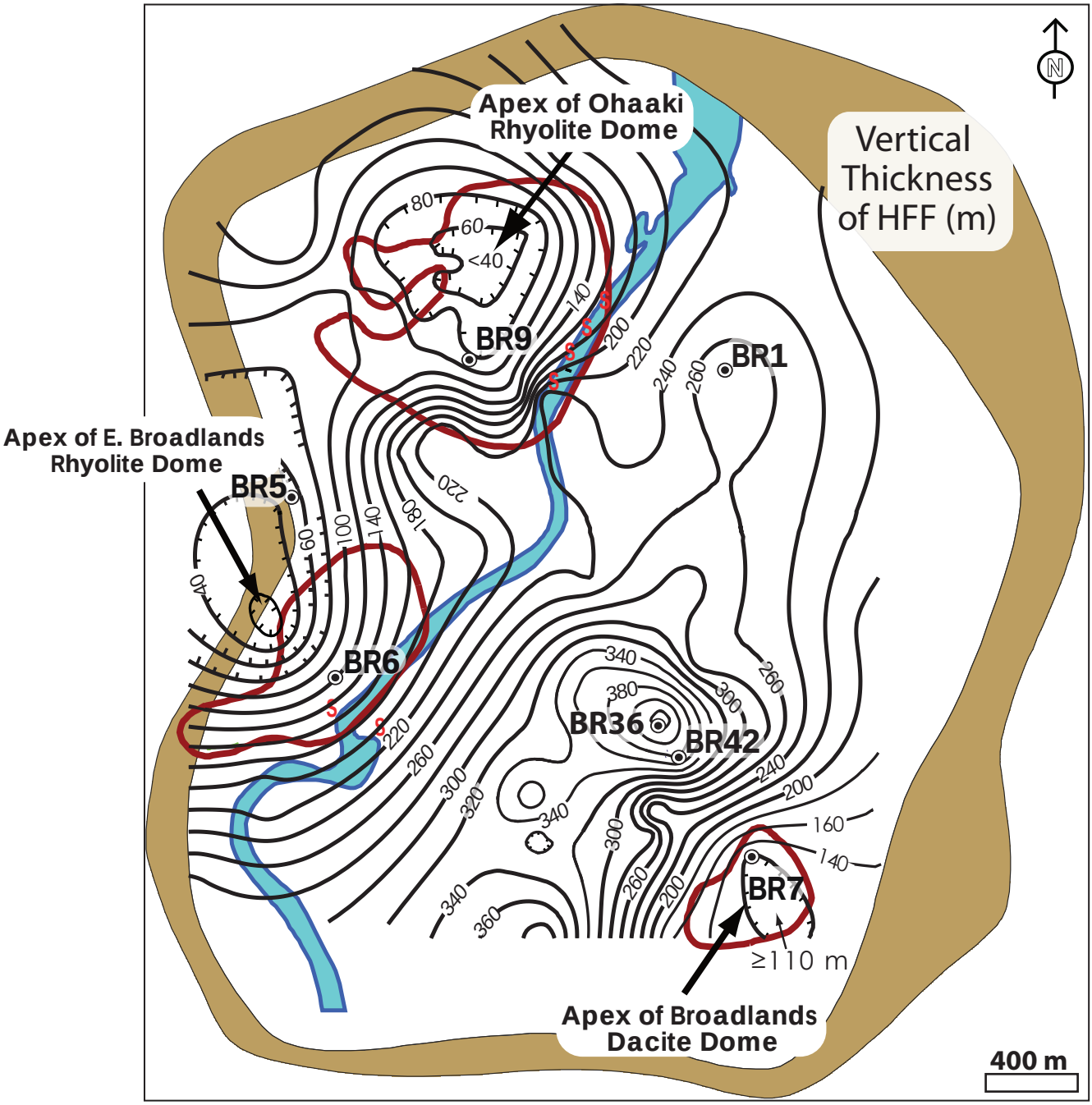


Figure 3.4. Contour plot of the combined vertical thickness of the HFF; shown in m. Note the thinning of the HFF and the occurrence of thermal areas (red outlines) above the apices of the Ohaaki Rhyolite dome in the NW, the Broadlands Dacite dome in the SE and the East Broadlands Rhyolite in the SW.

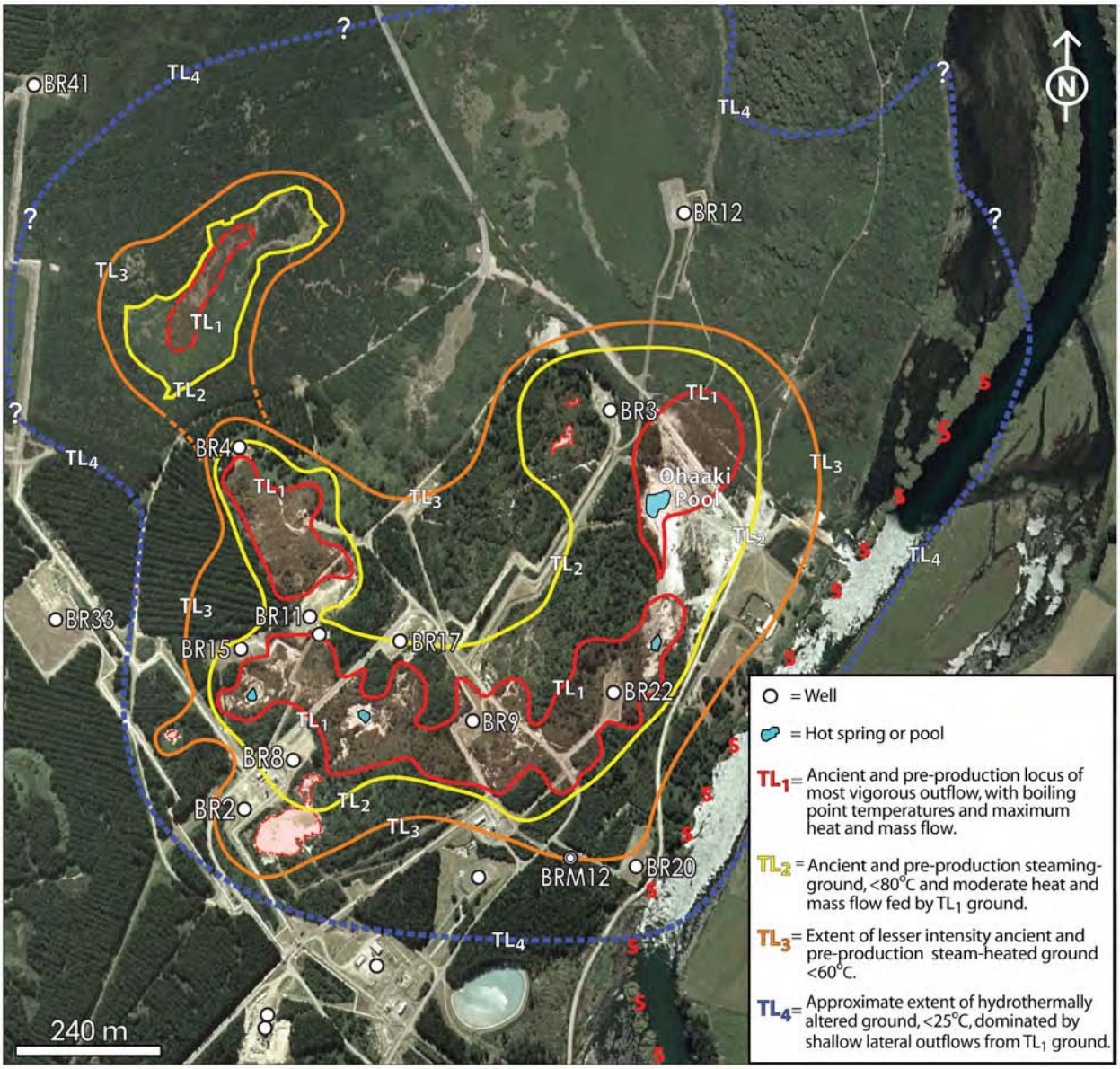


Figure 3.5. Composite map of the extent of pre-production and ancient (i.e., extinct) thermal activity associated with the OHW thermal area. Thermal intensity levels for pre-production activity were assigned according to surveys of soil temperature, thermal features, surface heat-flow and soil volatile concentrations (Thompson, 1967; Dawson, 1967; Koga et al., 1982; Allis and Webber, 1984; Dawson, 1988). The extent and thermal intensity of extinct (ancient) thermal ground was assigned from mapping of vegetative composition and plant stature, soil alteration intensity, and proximity to extinct or active pre-production outflow sites. Pre-production refers to thermal activity mapped prior to 1988 after which the field was developed for geothermal power generation. The “S” symbols denote sites of pre-production seepage of dilute alkali-Cl hot water to the Waikato River form the OHW thermal area.

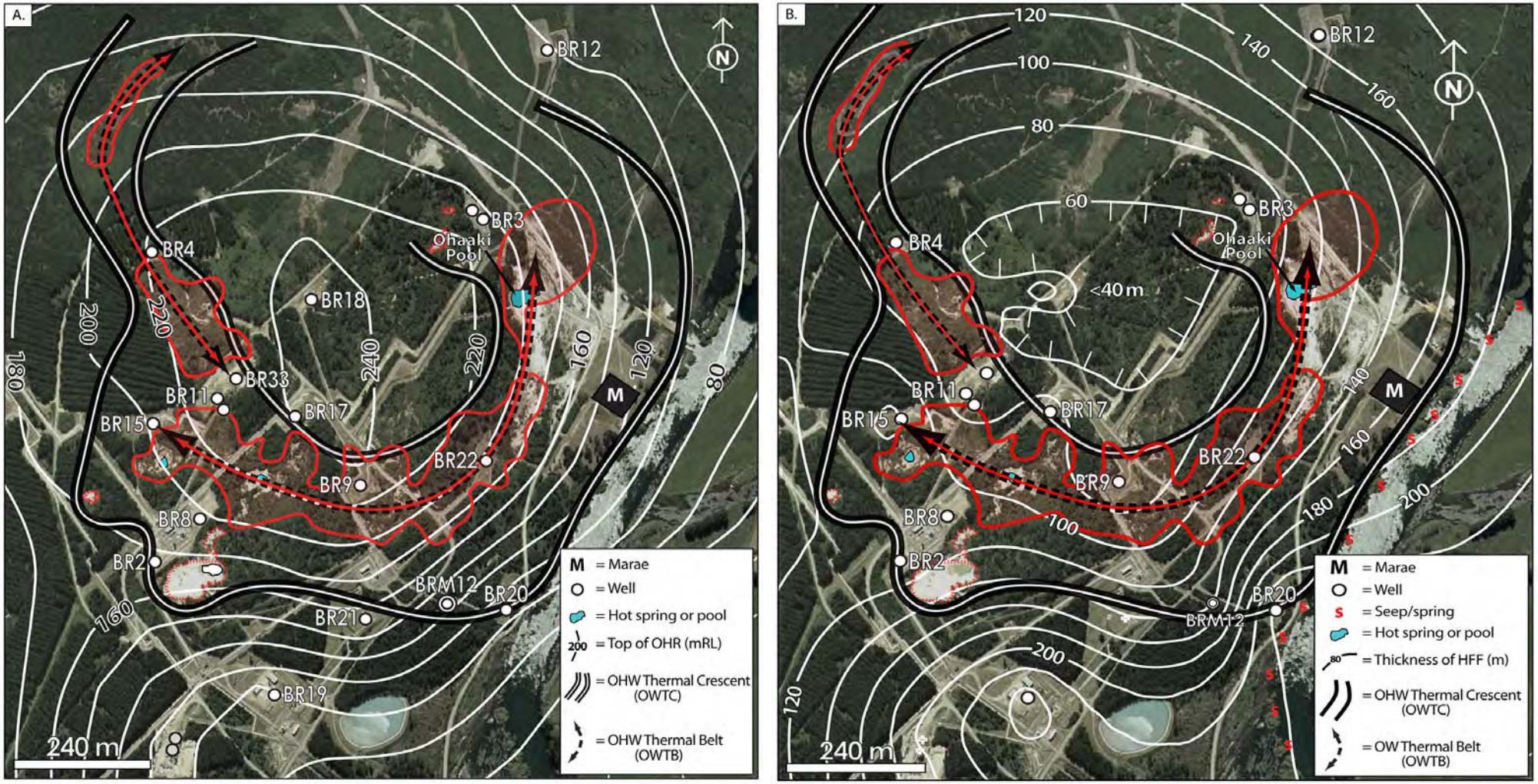


Figure 3.6. (a) Superposition of surface thermal activity (red outlines) associated with the OHW thermal area onto contours of the upper surface of the OHR dome. (b) Superposition of surface thermal activity associated with the OHW thermal area onto contours of the combined vertical thickness of the HFF overlying the OHR dome. Note the partial encircling of the apex of the dome by the locus of most vigorous thermal activity (i.e., the Ohaaki West Thermal Belt) and the conspicuous absence of thermal activity, both pre-production and ancient, across the apex of the dome where the HFF is thinnest. Features outlined by red dashed lines were extinct or minor steam-heated features prior to production.

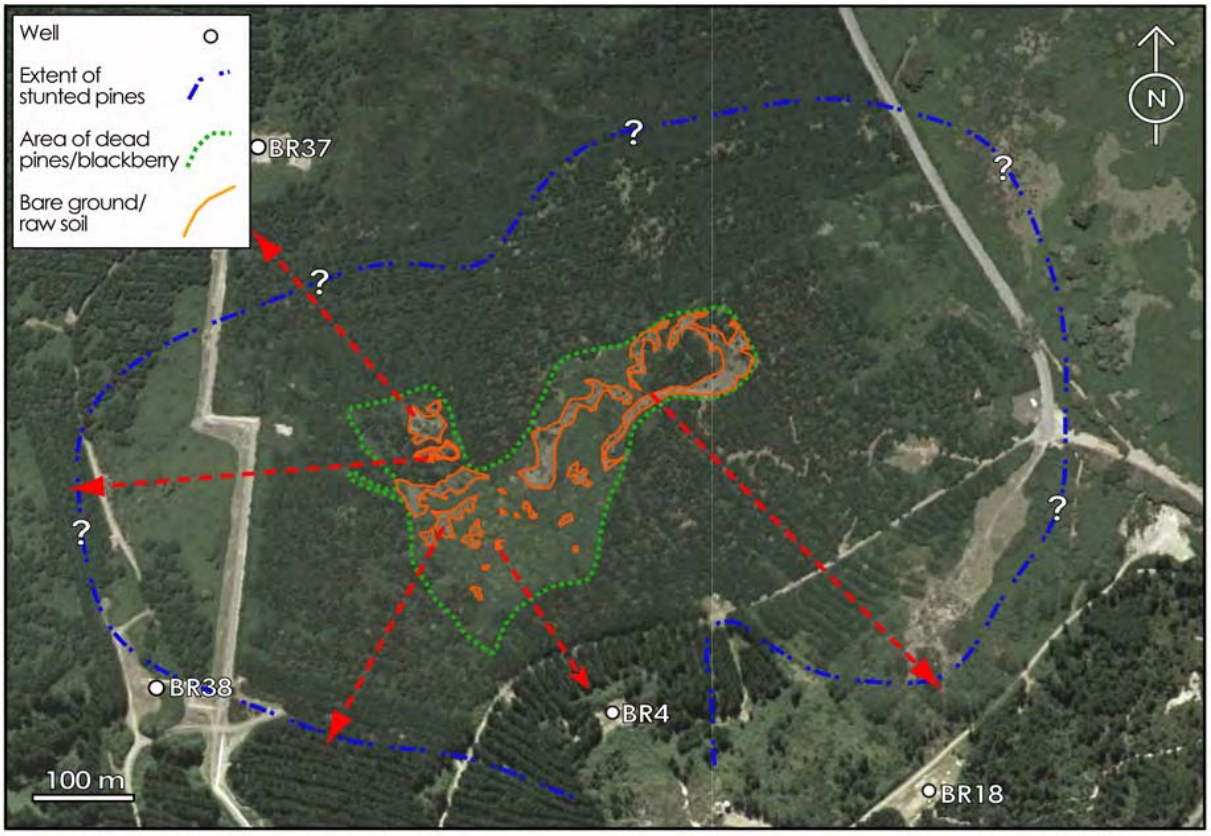


Figure 3.7. Annotated aerial photograph of the vegetative composition and ground cover over an extinct outflow site NNW of well BR4. Within the centre of the outflow, highly altered soils have resulted in the death of planted pine saplings. Here, the vegetative composition is dominated by wild blackberry with rare patches of bare ground. Arrows extending from the tree kill zone indicate the extent of sickly and stunted pines as well as the general increase in plant stature and health with distance from the former outflow site.

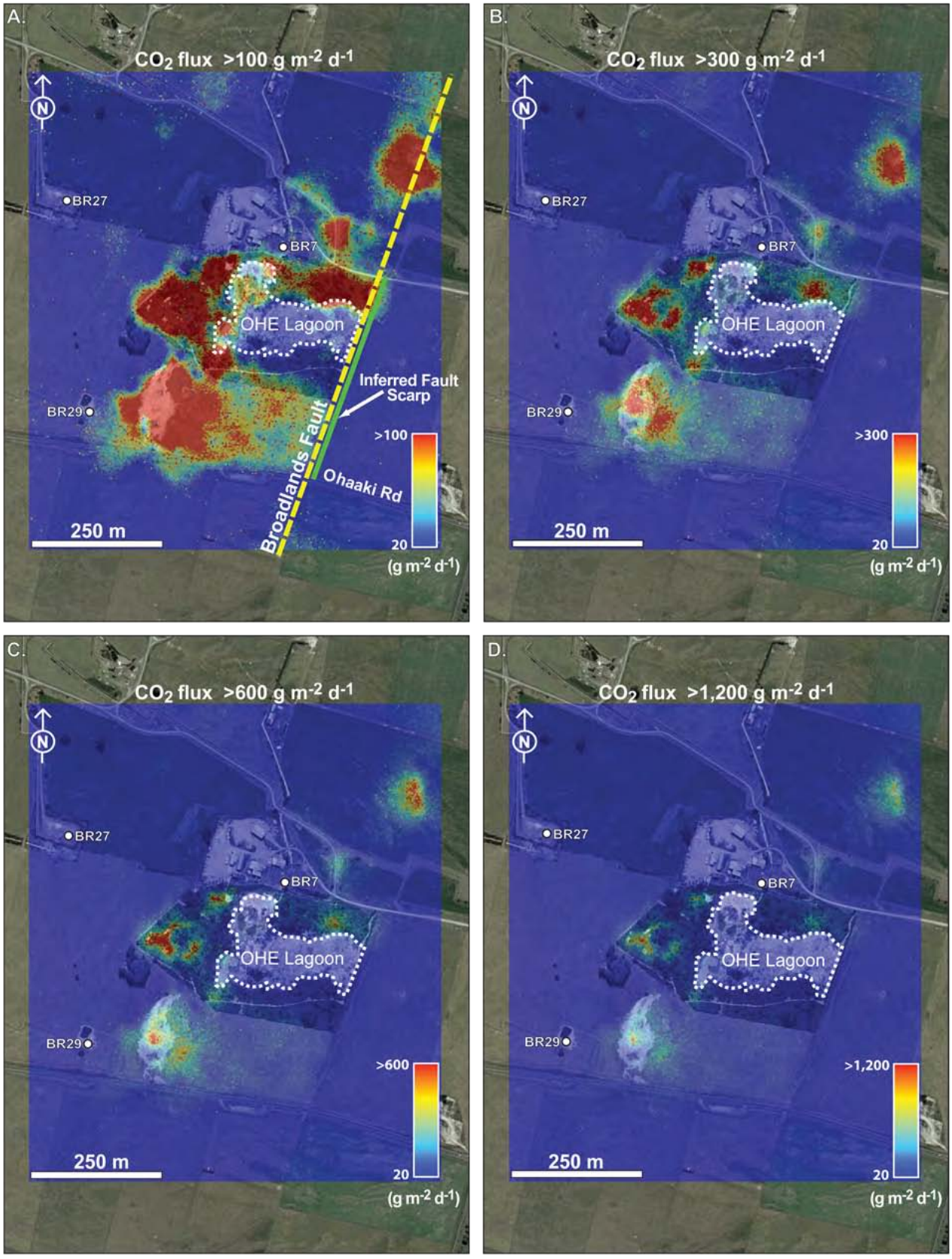


Figure 3.8. (a) – (d) Simulated pixel plots of $CO_2$ flux progression from 100 g m$^{-2}$ d$^{-1}$ to 1,200 g m$^{-2}$ d$^{-1}$ occurring across the surface of the OHE thermal area and inferred location of Broadlands Fault trace. Note: (i) coincidence of sharp northern boundary of flux anomaly with inferred fault scarp; (ii) strong NE-trend to eastern boundary; (iii) occurrence of quasi-circular flux anomalies or 'blebs' with increasing magnitude of flux, and; (iv) the low $CO_2$ flux across the lagoon area, within which the $CO_2$ flux from several steam-heated pools and numerous small boiling mud pots was not assessed.

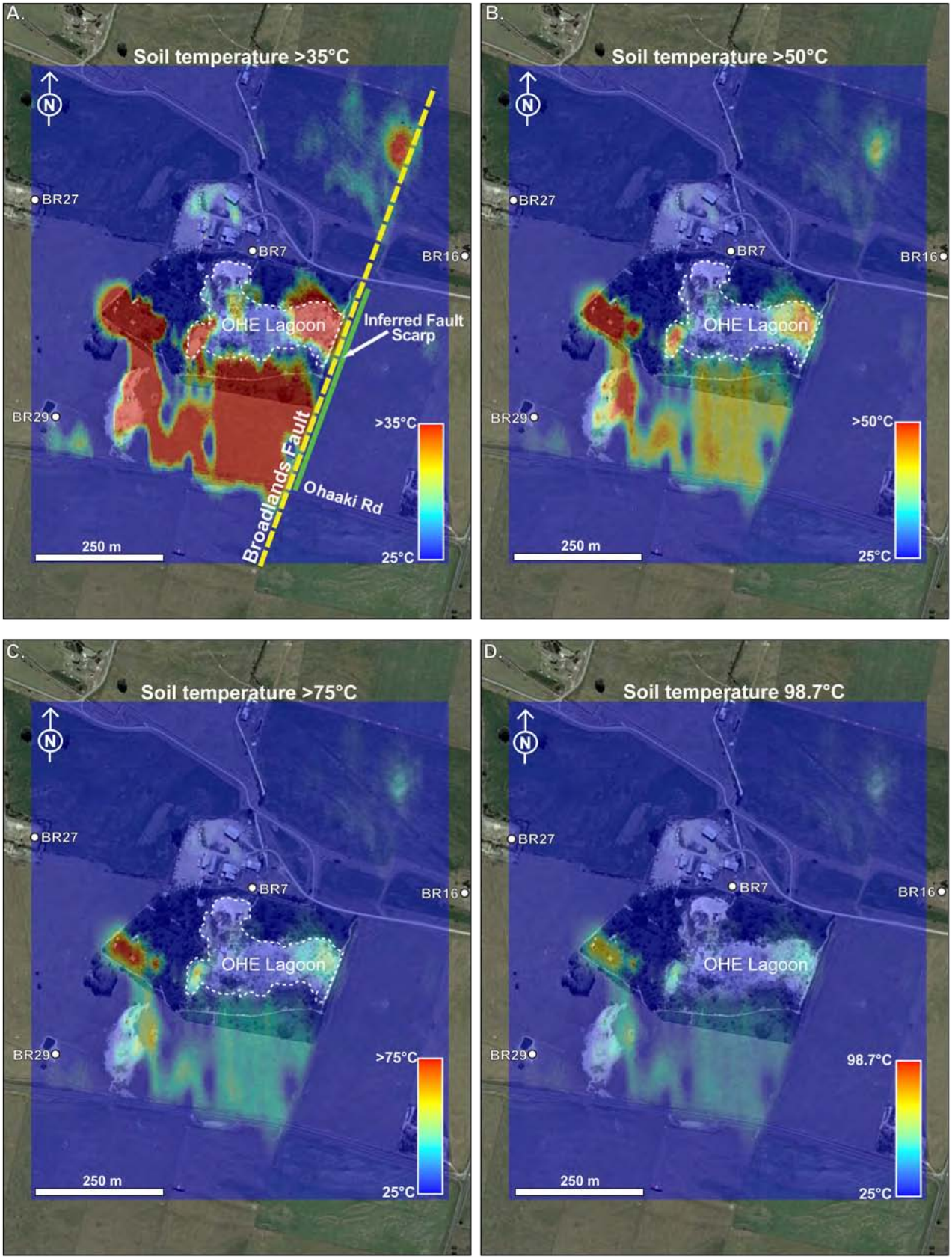


Figure 3.9. (a) – (d) Simulated pixel plots of shallow (0.15 m) soil temperature progression from 35ºC to boiling point (98.7ºC) occurring across the surface of the OHE thermal area and the inferred trace of the Broadlands Fault. Note: (i) the coincidence of the sharp northern boundary of the soil temperature anomaly with inferred fault scarp; (ii) the strong NE-trend to eastern boundary, and; (iii) the low temperatures across much of the OHE lagoon. The temperature of the large steam-heated pools and numerous small boiling mud pots that occur within the OHE lagoon were not included in this model.

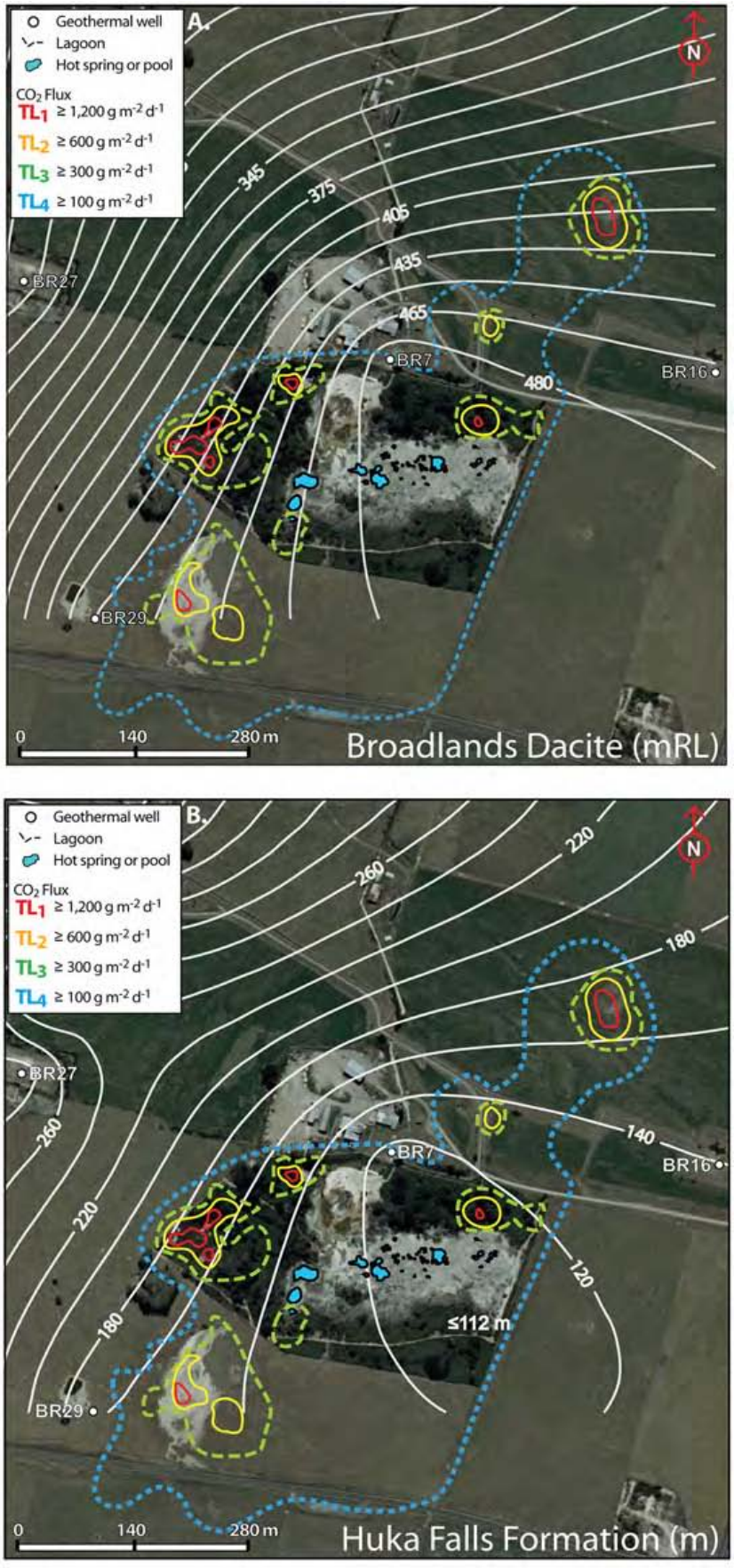


Figure 3.10. (a) Contours of the upper surface of the Broadlands Dacite dome and surface thermal intensity levels (TL1 - TL4) defined according to $CO_2$ flux and surface heat flow measurements made across this area (Chapter 2). (b) Contours of the combined vertical thickness of the HFF, which overlies the Broadlands Dacite, and thermal intensity levels. Aside from the gross controls of the dome apex over thinning of the HFF, there appears to be no apparent correlation between high permeability zones (defined by intensity levels) and

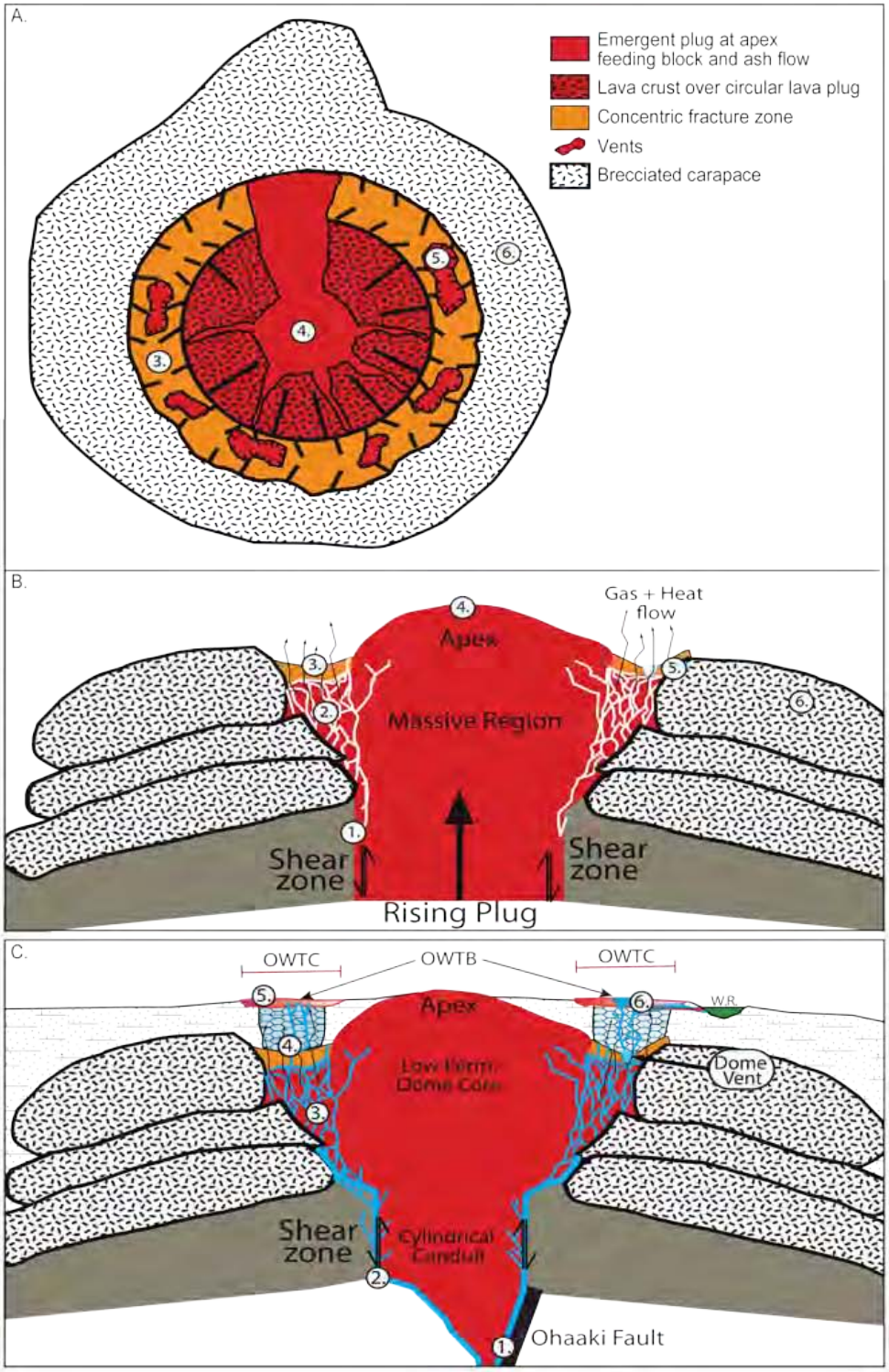


Figure 3.11. (a - b) Cross-section and plan view of idealized lava dome structure modified from Sahetapy-Engel and Harris (2009). Where; (1.) denotes the presence of a high permeability shear zone developed between the ascending magma body and surrounding country rock (i.e., conduit shear zone); (2) a permeable fracture zone developed by intermittent and typically cyclical evacuation of heat, gases, and solids from the deep shear zone; (3) the surface expression of the annular fracture zone developed about an approximately circular lava plug; (4) the apex of an approximately circular lava plug (dome core) of low permeability; (5) a surface vent structure formed by ejection of pyroclastic material within the deep conduit shear zone, and; (6) an outer brecciated carapace associated with the emplacement of block and ash flows sourced from the ascending lava plug. (c) Idealised model of dome control fluid flow for the OHW thermal area: (1) eruption of dyke feeding conduit system up Ohaaki Fault; (1 - 2) ascent of West Bank upflow through the remnant permeability associated with the conduit shear zone of the Ohaaki Rhyolite dome; (3) fluid flow through eruption related fracture zone; (4) locally intense silicification and hydro-fracturing of the HFF overlying the concentric fracture zone of the Ohaaki Rhyolite and development of preferential flow paths (see Hochstein and Henrys, 1990); (5) development of the concentric pattern of surface thermal activity characteristic of the OHW thermal area and best defined by the OWTB, and; (6) development of the deep Ohaaki Pool above an extinct volcanic vent (Henrys, 1986).

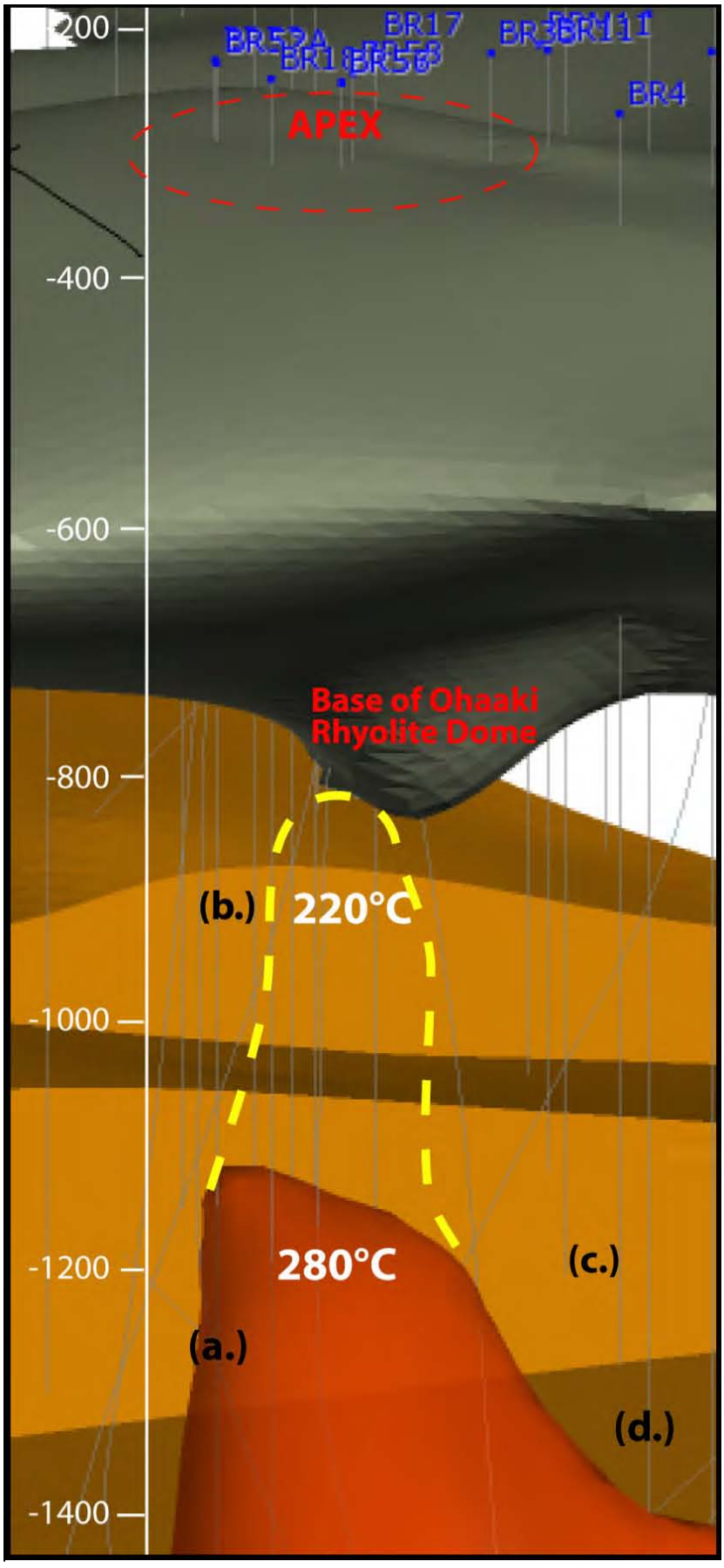


Figure 3.12. Ascent of hydrothermal plume up into the base of the Ohaaki Rhyolite (modified from Milicich, 2010). Where: (a) is the outline of the 280°C plume, and; (b) that of the 220°C plume. The background depicts the: (c and d) faulted (Ohaaki Fault) greywacke basement. Scale is in meters of relative relief (mRL).


86

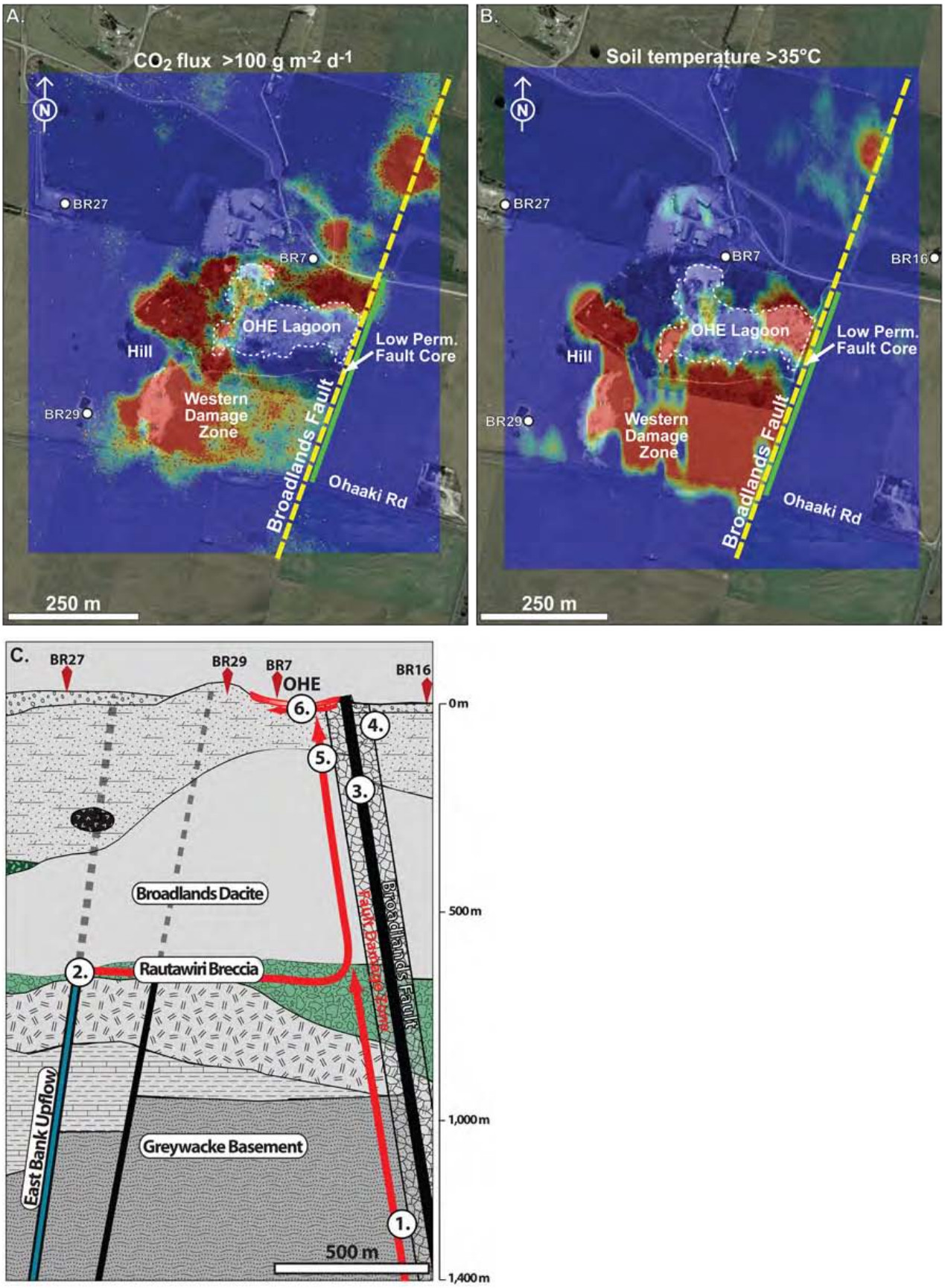


Figure 3.13. (a and b) Plan view of conceptual "conduit-barrier" fluid flow system (after Caine et al., 1996) associated with the propagation of the Broadlands Fault. (c) Cross-section model of conduit-barrier fluid flow system associated with the Broadlands Fault and the OHE thermal area, where location; (1.) denotes the migration of hydrothermal fluids from Greywacke Basement up along the Broadlands Fault. (2) location of a major feed zone within the Rautawiri Breccia and lateral fluid flow pathways from the East Bank upflow (Contact Energy, 2006); (3 and 4) permeable Western Damage Zone and low permeability of the Broadlands Fault core, which acts as a barrier to cross fault flow to the east; (5) pooling of hydrothermal fluids above the dome apex the dome, and; (6) locally hydrothermally cemented HFF within which vertical conduits act as preferential fluid pathways for the surface activity of the OHE thermal area.

Table 3.1– Relationship between thermal intensity levels and ground conditions (vegetative composition), soil temperature and heat flow for the Ohaaki West thermal area

| Thermal Level | Ground conditions /vegetation | Soil Temp (ºC) | Depth (cm) | Heat flow (W $m^{-2}$ ) |
|---|---|---|---|---|
| TL 1 | Bare ground, small audible steam vents, sulphur encrusted steam vents | 97.5 | 0 – 1.5 | ≥ 3,000 |
| | Bare ground, visible steam | 97.5 | 1.5 – 3.0 | 1,500 - 2,600 |
| | Bare ground, thermal clay crust | 97.5 | 3.0 – 7.0 | 1,000 – 1,500 |
| | Dead wood, algae, soft thermal clay | 97.5 | 7.0 - 13.0 | 1,500 - 800 |
| | Moss | 97.5 | 13.0 – 24.0 | 800 - 400 |
| TL 2 | Moss, lichens | 80 - 85 | 15 | 250 |
| | Low stunted leptosperms (Kanuka, Manuka) | 60 - 80 | 15 | 125 |
| TL 3 | Taller leptosperms, broom | 40 - 60 | 15 | 40 |
| | Small pines (radiata), leptosperms, broom | 25 - 40 | 15 | 4 |
| TL 4 | Large pines, indigenous broadleaf forest | 25 - ambient | 15 | <0.2 |

Thermal intensity levels are defined according to established relationships between soil temperature, heat flow, and ground cover/vegetation composition (Dawson and Dickinson, 1970; Burns, 1997; Bromley and Hochstein, 2005). Mean ambient air temperature at Ohaaki is 12ºC and boiling point occurs at 98.7ºC (~300 mRSL).

# Chapter 4

# A model to explain the spatial variation in the magnitude of pressure-induced ground subsidence – Ohaaki hydrothermal field, New Zealand

**Clinton Rissmann[a], Jerry Fairley[b], Jim Cole[a], Sarah Milicich[c], Bruce Christenson[d], David Bell[a]**

*[a]Department of Geological Sciences, University of Canterbury, Private Bag 4800, Christchurch, New Zealand*

*[b]Department of Geological Sciences, University of Idaho, Moscow, Idaho, USA*

*[c]GNS Science, Wairakei Research Centre, Taupo, New Zealand*

*[d]GNS Science, P.O. Box 30368, Lower Hutt, New Zealand*

*To be submitted to:* **Geothermics**

## Contributions

Mr. Rissmann developed this study after casually observing a strong spatial relationship between the permeability structures mapped in Chapter 3 and maps of ground subsidence published for the Ohaaki Field. The strength of the spatial relationships justified further investigation of the literature and modelling of up-to-date levelling data. Mr. Rissmann wrote the manuscript whilst Sarah Milicich of GNS Science, Wairakei, provided computer-generated cross-section models for the Ohaaki Field. Suggestions made under technical and editorial review by Prof. Cole (hazards and volcanology) and Drs. Fairley (hydrological modelling), Leybourne (fluid geochemistry) and White (geology and geothermal) and Mr. Bell (engineering geology) were incorporated into the manuscript.

## 4.1 Abstract

Within the exploited hydrothermal fields of the Taupo Volcanic Zone (TVZ), ground subsidence occurs in response to host rock consolidation (e.g., pore collapse) due to the propagation of deep pressure decline into the shallow, poorly permeable (0.05 – 0.3 mD) and highly compressible (10 – 30 $kbar^{-1}$) mudstones of the

Huka Falls Formation (HFF). In order to address the commonly noted but seldom quantified spatial relationship between areas of major ground subsidence and sites of surface alkali-Cl outflow occurring within New Zealand hydrothermal fields (i.e., Wairakei and Ohaaki fields), a detailed analysis of the spatial relationships between an up-to-date model (ca. 1988 – 2006) of pressure-induced ground subsidence and recent maps of surface structural permeability (i.e., permeable faults and fractures) was undertaken for the Ohaaki Field. These maps indicate a strong spatial relationship between the distribution of permeable structures governing the fluid outflow of the Ohaaki West (OHW) thermal area and the location and shape of the main Ohaaki subsidence bowl (MOSB). On the basis of this strong spatial correlation, we argue that the permeability structures of the OHW thermal area, that once conducted alkali-Cl hot waters, function as conduits for the propagation of pressure decline from the underlying reservoir to the near-surface compressible formations, resulting in the localisation of zones of preferential pore fluid drainage and development of major subsidence features. Field wide, an analysis of the spatial relationship between the magnitude of ground subsidence and the shallow hydrogeology of the Ohaaki Reservoir indicates a strong spatial correlation between the type and extent of rock units (i.e., alkali-Cl bearing aquifer or aquitard) directly underlying the HFF cap rock, and the magnitude of low amplitude subsidence (i.e., basal consolidation of the HFF) occurring at the surface of the field. The influence of the lithology underlying the HFF is shown by the spatial correlation between the extent of the shallow Waiora Formation geothermal aquifer and ground subsidence currently $\geq$ 50 cm at the surface of the field. The waning of low amplitude ground subsidence towards the margins of the hot water reservoir is attributed to a general transition from aquifer to aquitard towards the boundaries of the field, and also a systematic decline in the magnitude of the pressure drop occurring at the base of the HFF. Collectively, these observations indicate that the spatial variability in the magnitude of ground subsidence occurring at the surface of the Ohaaki Field is best explained by: (i) the spatial variance of rock properties (i.e., aquifers and aquitards) underlying the HFF; (ii) the distribution of subvertical permeability as faults and fractures within the poroelastic HFF and the connection of this permeability to a liquid pressure domain (i.e., the alkali-Cl reservoir), and; (iii) a systematic decline in the pressure drop occurring at the base of the HFF towards the margins of the hot water reservoir. This model can be used to assess the risk and likely spatial distribution of ground subsidence for undeveloped and underdeveloped hydrothermal fields for which a poroelastic rock unit, similar to the HFF, occurs at or near the surface of the field by: (i) identifying areas of liquid versus steam dominated thermal activity; (ii) recognising the extent of the hydrothermal reservoir, and; (iii) understanding the spatial nature of the hydrogeological and structural relationships governing fluid flow.

## 4.2 Introduction

### 4.2.1 Background

Within the exploited hydrothermal fields of the Taupo Volcanic Zone (TVZ; Fig. 4.1), large scale ground subsidence occurs in response to host rock consolidation (e.g., pore collapse) where a deep pressure decline has propagated into the shallow, poorly permeable (0.05 – 0.3 mD) and highly compressible (10 – 30 $kbar^{-1}$) Huka Falls Formation (HFF) (Hatton, 1970; Narasimhan and Goyal, 1984; Allis 1983a; Allis, 1990; Allis et al., 1997; Allis and Zhan, 2000; Allis, 2000; Grant, 2000; Bloomer and Currie, 2001; White et al., 2005). A lag between deep pressure decline and consolidation is attributed to the low permeability of the HFF and the slow drainage of clay layers (i.e., 'aquitard drainage') subjected to basal pressure decline (Allis et al., 1997).

Consolidation of the HFF due to pressure decline is manifest at the surface as a decrease in surface ground elevation. However, the latter is seldom uniform (i.e., differential ground subsidence), with distinct spatial trends in the amount of ground subsidence occurring across the surface of the Ohaaki and Wairakei fields. These spatial trends are characterized by: (i) one or more small areas ($\leq$ 1.5 $km^2$) of high magnitude (4 – 15 m) ground subsidence that occur as simple or complex troughs or quasi-spherical shaped surface depressions (commonly referred to as subsidence 'bowls'), superimposed upon; (ii) a broader pattern of lower amplitude background subsidence that extends across the majority of the field ($\geq$95%) and which declines in magnitude with distance from major subsidence features, before petering out at, or near, the margins of the underlying hot water reservoir (Allis, 1983; Allis et al., 1997; Allis, 2000; Allis and Zhan, 2000; Bloomer and Currie, 2001; Hole et al., 2005; White et al., 2005).

A number of studies have noted a strong spatial correlation between sites of former or active liquid outflow (i.e., alkali-Cl surface thermal activity) and major subsidence features (i.e., 'bowls') for both the Ohaaki and Wairakei fields (Allis, 1983; Allis et al., 1997). The observed spatial overlap between major subsidence 'bowls' and sites of liquid dominated outflows at both Ohaaki and Wairakei led Allis (1983) to suggest these features develop where pressure decline has propagated up into the HFF, exploiting the same sub-vertical permeable pathways (i.e., faults and/or fractures), that once acted as conduits for the ascent of alkali-Cl hot waters.

Conversely, White et al. (2005) attributed the location and crescent-like shape of the main Ohaaki subsidence bowl (MOSB) to preferential pore fluid drainage from a steep stratigraphic contact between the HFF and underlying southern and eastern flanks of the Ohaaki Rhyolite dome. Enhanced lateral permeability enables pore fluids to drain more rapidly from the consolidating layer resulting in local increases in the rate of consolidation, and the magnitude of subsidence occurring within a given period. However, White et al. (2005) did not consider the control of former alkali-Cl fluid pathways (faults or fractures) over the propagation of pressure decline.

Away from the major subsidence bowls, the broad areas of low amplitude background subsidence that extend out to the margins of each field were attributed to the restriction of pressure propagation to the basal layers of the HFF (Allis, 1983). However, no model has previously been proposed to explain the spatial variability of low amplitude ground subsidence, including: (i) the observed spatial correlation between the extent of low amplitude ground subsidence and that of the hot water reservoirs; (ii) the general tendency of low amplitude ground subsidence to decline in magnitude towards, and then peter out at, the margins of a hot water reservoir; (iii) the occurrence of distinct zones of lesser or greater low amplitude subsidence, and (iv) the occurrence of sharp boundaries between zones of low amplitude subsidence.

Recognition of the existence of some form of hydro-structural control over the distribution of ground subsidence within TVZ hydrothermal fields is important as the magnitude of ground subsidence is seldom correlated with the spatial pattern of mass withdrawal (Hatton, 1970; Allis, 1990; Allis, 2000; Grant, 2000; Bloomer and Currie, 2001).

Therefore, in this paper we seek to demonstrate that ground subsidence is a function of the near-surface permeability structure, which is in turn controlled by the underlying geology and structure of the Ohaaki Field. We accomplish this by comparing recent maps of cumulative ground subsidence with detailed maps of the shallow permeability structure. The model we propose has considerable potential to: (i) predict the location, magnitude and type of subsidence for undeveloped and underdeveloped hydrothermal fields, across which a low permeability poroelastic rock unit occurs at or near the surface of the reservoir, and; (ii) improve the predictive qualities of subsidence models (see Grant, 2000).

### 4.2.2 Ohaaki Reservoir Geology

The Ohaaki reservoir is a liquid-dominated hydrothermal field, containing high non-condensable gas concentrations, which cause boiling to occur at depths > 1,500 m (Grant, 1977; Hedenquist, 1990; Christenson et al., 2002). Deep reservoir temperatures reach a maximum of 310ºC with the hot water reservoir, as defined by the area of low resistivity, extending across an area of 12.7 $km^2$ (Figs. 4.2) (Hedenquist, 1990; Christenson et al., 2002). Several large normal faults transect the greywacke basement, which is down-faulted to the west (Wood et al., 2001). These faults act as conduits for high temperature fluids to enter the Ohaaki reservoir, feeding two major upflow zones in the NW (West Bank upflow) and SE (East Bank upflow) of the field (Figs. 4.2 and 4.3) (Hedenquist, 1990; Christenson et al., 2002; Rae et al., 2007).

The reservoir overlying the greywacke basement is a complex assemblage of pre-330 ka volcaniclastic rocks and post-330 ka volcanic domes intercalated with pyroclastic deposits from large caldera-forming eruptions to the west (Fig. 4.3). With the exception of the fractured and brecciated apex of each dome, lavas are thought

to act as aquitards to vertical fluid movement (Henrys and Hochstein, 1990; Hedenquist, 1990). Conversely, pyroclastic flow deposits and porous volcaniclastic units (i.e., the Rangitaiki Ignimbrite, Rautawiri Breccia and the shallow Waiora Formation) act as aquifers hosting high temperature alkali-Cl waters and enabling ascending alkali-Cl hot waters to spread laterally (Wood, 1994). The reservoir is capped by the poorly permeable mudstones of the HFF, which at Ohaaki are especially thick (up to 430 m) (Contact Energy, 2006). The Waiora Formation forms the most important shallow alkali-Cl hosting aquifer and in places directly underlies the HFF (Fig. 4.3).

The HFF thins (locally to nothing) above the apex of each shallow dome, and this enables hydrothermal fluids to rise to the surface (Chapter 2 and 3). Elsewhere the HFF is especially thick (mean = 220 m and up to 430 m; Contact Energy, 2007) and forms a very effective barrier to fluid ascent (MacDonald, 1975; Koga et al., 1982; Chapter 2; Chapter 3). Of the three thermal areas at Ohaaki, only Ohaaki West (OHW) was directly fed by a large liquid outflow of alkali-Cl hot water. Conversely, the much smaller Ohaaki East (OHE) and BR6 thermal areas are purely steam-heated with no evidence of alkali-Cl outflows (Mahon and Finlayson, 1970; Chapter 2).

### 4.2.3 Shallow structure of the Ohaaki Field

In Chapter 3 a model of lava dome controlled fluid flow was presented for the Ohaaki West (OHW) thermal area within which the MOSB occurs. Maps of soil temperature (at 0.15 m and 1.0 m depth) (Thompson, 1967; Allis and Webber, 1984), surface thermal features (Dawson, 1988), soil volatile concentrations (Koga et al., 1982), along with aerial photography, soil alteration intensity and vegetative composition (i.e., species richness and stature) were combined to map the distribution and relative intensity of surface thermal activity (Fig. 4.4). The findings of this study indicated the localisation of significant vertical permeability within the locally cemented HFF through which hydrothermal fluids (vapour and liquid phase) ascend to the surface from the underlying West Bank upflow (Fig. 4.4).

This permeability occurs as a concentric fracture belt developed about the apex of the extinct Ohaaki Rhyolite dome and is referred to as the Ohaaki West Thermal Belt (OWTB) (Fig. 4.4; Chapter 3). The OWTB is the surface expression of a deep-rooted concentric fracture zone that extends through the base of the Ohaaki Rhyolite and which has functioned as the historical locus of heat and mass flow for the OHW thermal area (Chapter 3). Evolution of this fracture zone occurred in response to the intrusion of the Ohaaki Rhyolite, resulting in the development of a conduit shear zone about the ascending shallow magma plug. Post-eruption, the conduit shear zone functioned as a preferential flow path for the ascent of hydrothermal fluids from the underlying West Bank upflow to the surface.

The eastern end of the OWTB coincides with the large alkali-Cl outflow of the Ohaaki Pool (Fig. 4.4). This feature dried up soon after production began at the field (Glover et al., 2000). With distance from the OWTB, the intensity of surface thermal activity (i.e., heat and mass flow) wanes rapidly in response to decreasing permeability within the HFF (Chapter 3). The extent of surface thermal activity surrounding the OWTB is defined by the Ohaaki West thermal crescent (OWTC), which delineates the bounds of all documented and extinct thermal activity associated with the OHW thermal area (Chapter 3).

The structural permeability necessary for fluid flow is restricted to the OWTC, with no evidence for surface thermal activity across the massive and poorly permeable rhyolitic plug (i.e., apex) of the Ohaaki Rhyolite dome (Fig. 4.4; Chapter 3). The low permeability of the dome apex extends to the NNW along the long axis of the dome, across an area inferred to be the outflow of a low permeability flow lobe (Chapter 3). Outside of the OHW thermal area, significant structural permeability is limited to the vicinity of the steam-heated Ohaaki East (OHE) and BR6 thermal areas (Fig. 4.2). Within the larger OHE thermal area surface thermal activity is governed by the development of a high permeability fault damage zone (Broadlands Fault) within the competent and low porosity lavas of the Broadlands Dacite (Chapter 3).

Elsewhere across the field, faults developed within the HFF are of low permeability, blocking the ascent of hydrothermal fluids and masking the dominant signature (i.e., elevated soil temperatures and $CO_2$ flux) of the underlying high temperature reservoir (Chapter 3). The low permeability of faults developed in the HFF is supported by the tendency of this weak and highly porous unit to deform plastically in response to applied stress (Nairn, 1982; Read et al., 2003) and for low permeability fault core to develop in response to pore collapse and grain communition (Antonellini and Aydin, 1994).

### 4.2.4 Development and Subsidence History

Subsidence across the northwestern bore field was first noted soon after intensive production testing of Ohaaki Field began in 1969 (Allis et al., 1997). During the test period extraction averaged 25,000 tonnes per day (tpd) and without re-injection resulted in a deep pressure decline of 1.5 MPa (15 bar) within 4 years, but only by 0.8 MPa (8 bar) in shallow wells (Fig. 4.5; Hunt and Bromley, 2000; White et al., 2005; Contact Energy, 2007). During the test discharge period subsidence rates of up to 150 mm/y were determined from repeat leveling surveys of benchmarks, with a total cumulative subsidence value of almost 200 mm over the 3 years of testing (Allis et al., 1997).

Following the end of the testing period, subsidence slowed and then ceased in response to a rebound in reservoir pressures, largely due to recharge from shallow aquifers (Fig. 4.5; Allis et al., 1997; Hunt and Bromley, 2000; Bloomer and Currie, 2001). However, there was no rebound at ground level. In 1988, the Ohaaki Power station was commissioned and mass withdrawal increased to 45,000 tpd, with approximately

28,000 tpd reinjected at the margins of the reservoir (White et al., 2005). Following commissioning, deep reservoir pressure declined rapidly, resulting in a total deep pressure decline of 2.5 MPa (25 bar) by the year 2000.

Following commissioning of the field, and ensuing pressure decline, the liquid-fed thermal activity of the OHW thermal area also declined, with the drying up of all steam-heated pools and the large (9 – 23 l/s) alkali-Cl outflow of the Ohaaki Pool (Glover et al., 2000). Despite a deep-seated pressure decline of 8 – 24 bar (up to ca. 2001; Contact Energy, 2007) beneath the steam-heated OHE thermal area, no obvious decline in surface thermal activity has occurred there (Hunt and Bromley, 2000; Chapter 2).

In response to ongoing mass withdrawal, subsidence rates accelerated to 500 mm/yr by the late 1990's across the northwestern bore field, with the development of a distinctive crescent shaped subsidence 'bowl' within the liquid dominated outflow zone of the OHW thermal area (Allis et al., 1997). By 1997 this feature occupied an area of ~1.5 $km^2$, as defined by the 100 mm/yr subsidence rate contour, and was ~ 3 m deep. Broad, lower amplitude subsidence extended across the remainder of the field with the magnitude of ground subsidence declining towards the margins of the hot water reservoir.

## 4.3 Methods

Topographic levelling data for the Ohaaki field came from 680 survey points for which precise levels were available for dates prior to and up to 1988, and that were correlated with the latest 2006 survey (Fig. 4.6; Contact Energy, 2007). Exhaustive checking of the data set revealed some anomalous data, particularly for the surveys conducted in 1993, and this data was excluded along with any other benchmarks that lacked complete time series data for 1988 to 2006. The cumulative or total subsidence, in cm, was then calculated by subtracting the levelling height of the 2006 survey from the earliest levelling measurement (ca. 1988). This approach was justified on the basis that relatively minor subsidence occurred prior to full-scale development of the field (Allis et al., 1997; Allis, 2000).

Using the total calculated subsidence and the coordinates of each benchmark, a map of total subsidence for the entire Ohaaki Field was generated using the kriging function in Golden Software's Surface Mapping System (version 8.01). Single point anomalies generated by kriging were checked and rechecked against the data set to verify the accuracy of the model and also compared with earlier maps of subsidence rate (Allis et al., 1997; Allis, 2000; White et al., 2005). A map of total subsidence was thought to better define the total pattern and spatial extent of ground subsidence than traditional maps of subsidence rate (mm $yr^{-1}$).

Accurate subsidence modelling was favoured by the good benchmark coverage within key areas of the field including the Ohaaki West (OHW) thermal area, the East Bank upwelling (in vicinity of wells BR36 and

BR42), the southeastern sector of the field (including the OHE thermal area) and along the western, eastern and southern margins of the field (Fig. 4.6). However, a lack of recent levelling data to the SE and NE of the OHW thermal area means that the eastern margin of the MOSB is poorly defined, as is subsidence occurring from this area towards the NE boundary of the field. Sparse benchmark coverage between wells BR3/BR12 and BR32, BR20 and BR47 and BR6 and BRM5 is also noted.

Image maps (DEM) of total subsidence were generated using 1 cm increments onto which contours of total cumulative ground subsidence, with an interval of 50 cm, were overlaid. Levels from benchmarks beyond the margins of the field indicate that a value of 1 cm was sufficient to discriminate between pressure-induced ground subsidence and minor regional background subsidence (~2.6 mm $yr^{-1}$; Geonet, 2009). All major subsidence features (i.e., subsidence bowls or troughs) were also denoted, along with the location of areas of surface thermal activity.

Detailed 2D cross-sections of the Ohaaki reservoir are provided from a computer-based 3D model of the Ohaaki reservoir (Milicich, 2010). Overlaid on each cross-section are inferred fault zones as defined by previous workers, including recent maps of the shallow structures governing fluid flow within both major thermal areas (Wood, 1996; Wood et al., 2001; Rae et al., 2007; Chapter 3). However, it should also be noted that faults and fault paths shown in cross-section are not to scale and are idealised to provide a general understanding of fluid movement within the Ohaaki Reservoir.

So as to interpret the nature of the spatial relationship between ground subsidence and shallow structural permeability, maps of shallow structural permeability, developed during an earlier study (Chapter 3), were superimposed, onto the subsidence model of the OHW thermal area. Similarly, the spatial relationship between the shallow hydrogeology of the Ohaaki Field and ground subsidence was assessed by overlaying total cumulative subsidence onto the 2D cross-sections of the Ohaaki Reservoir.

## 4.4 Results

### 4.4.1 Subsidence across the Ohaaki field

Total cumulative subsidence for pre-1988 to 2006 is displayed in Fig. 4.7 for the Ohaaki Field. Using a value of 10 cm as a threshold, it is apparent that the majority of the field (> 95%; or ~ 12 $km^2$) has been affected by pressure-induced ground subsidence. Further, the lateral extent of subsidence appears to closely match the extent of the hot water reservoir as defined by the resistivity boundary. The MOSB is immediately obvious in the upper, centre-left sector of the field, as a crescent-shaped depression, and as noted in previous studies shows some spatial correlation with a general outline of the OHW thermal area. Despite a general increase in the magnitude of subsidence, the above spatial relationships are consistent with previous assessments of subsidence at Ohaaki (Allis et al., 1997; Allis, 2000; White et al., 2005).

Further aspects of the pattern of ground subsidence are evident, including the observation that the area between the 50 cm and 60 cm contour appears to constitute a major transition in low amplitude ground subsidence between the moderate to high total subsidence of the field interior, and the minor total subsidence that extends to the field margins (Fig. 4.7). The latter is qualified by noting that the lateral change in the magnitude of subsidence, per unit distance, decreases markedly beyond the 50 cm or 60 cm contour towards the margins of the field.

Overall, ground subsidence ≥ 50 cm is most extensive across the northern half of the field (Fig. 4.7). Here, sharp spatial transitions, or 'steps,' in the magnitude of ground subsidence are evident between the MOSB and the western, southwestern, northwestern and northern margins of the field. Conversely, the eastern boundary of the MOSB is less sharp, with broad contour intervals radiating outwards from the MOSB. Levels taken from benchmarks that extend in a thin line from well BR22 through BR1, and towards the margins of the field, suggest that the rate of change in the magnitude of subsidence between the MOSB and wells BR26 and BR1 is much sharper than displayed by the model (Figs. 4.6 and 4.7). In general, the pattern of subsidence across the northern half of the Ohaaki Field is distinctly radial, decreasing in magnitude in a step-like fashion from the MOSB towards the margins of the field.

Across the central and southern sectors of the field the amount (current maximum = 110 cm) and extent of subsidence, ≥ 50 cm contour, is much lower than across the northern half of the field (Fig. 4.7). Here, the area of subsidence, ≥ 50 cm, is characterized by a wedge or 'horn' shape, the apex of which peters out in the vicinity of well BR30. Radiating outwards from this wedge is a broad zone of low amplitude background subsidence, which gradually declines in magnitude (from 40 cm to nil) towards the margins of the field. As with the northern extent of the field, the 50 cm contour of the southern half of the field denotes a sharp transition in the magnitude of subsidence from the moderate low amplitude subsidence of the interior (50 cm – 110 cm), to the minor and low amplitude subsidence of the outer margins (0 cm - 40 cm). In particular, the southeastern path of the 50 cm contour describes a sharp but irregular boundary that passes close to wells BR44, BR36, BR28, BR49 and BR30, and separates the OHE thermal area from the main body of subsidence (≥ 50 cm) that occurs to the west. From well BR30 the 50 cm contour turns northwest in a broad arc that passes through well BR6, bisecting the BR6 thermal area and passing through wells BR34 and BR50.

### 4.4.2 The main Ohaaki subsidence 'bowl'

The MOSB, as defined by the dashed 300 cm contour interval, is comprised of four major subsidence features, or 'intense surface depressions' (ISD), that coalesce to form a distinctive crescent-shaped depression (Fig. 4.8). About their centres ISD 1 and 3 are roughly spherical, whereas ISD 2 and 4 are elliptical. Total subsidence is greatest within ISD 1 where the ground level has subsided by more than 480 cm. Total

subsidence within ISD 2 and 4 currently exceeds 400 cm whereas subsidence currently exceeds 380 cm at the center of ISD 3.

To the NW is the small ISD 5, which has subsided by ≥ 210 cm. This comparatively isolated ISD is of a composite shape, somewhere between an ellipse and a sphere, and in Fig. 4.8 is connected to the MOSB by the 150 cm contour. Notably, a thin embayment of relatively minor subsidence (100 cm - 150 cm), oriented approximately NNW, occurs between ISD 5 and well BR3. This thin embayment of relatively low subsidence trends NNW from well BR9 through well BR18.

Taken as a whole, the pattern of major subsidence associated with the OHW thermal area is characterised by the 4 major ISD that are quasi-circular or elliptical in shape about their centres, and which coalesce to form the distinctive crescent-shaped depression of the MOSB. Also evident is that the magnitude of total subsidence declines rapidly with increasing distance from the centre of each major ISD.

### 4.4.3 Spatial Relationship between the MOSB and the OHW thermal area

Figure 4.9 defines the extent and shape of the MOSB in relationship to the pattern of thermal ground associated with the OHW thermal area. It is apparent that the distinctive crescent shape of the MOSB coincides closely with the shape of the OWTC. Indeed, the match is so good that the 200 cm subsidence contour could conceivably be used to delineate the extent of ancient and historical thermal activity. Also evident is a strong spatial correlation between the 4 major ISD (1 – 4), which comprise the centre of the MOSB, and the liquid fed OWTB.

Further evidence for a good fit between surface permeable structures and the MOSB comes from the precise spatial correlation between the nucleus of ISD 4 and the alkali-Cl outflow of the Ohaaki Pool, which occurs along the OWTB (Fig. 4.9). Although ISD 1 to 3 occur along the OWTB they do not appear to be correlated with any surface features indicative of historically active alkali-Cl hot springs. However, there is sufficient data to suggest that each major ISD coincides spatially with a discrete high permeability flow path developed within the OWTB, and connected to the underlying West Bank upflow (see discussion).

Another notable aspect of the spatial relationship between subsidence and thermal activity is the sharp decrease in the magnitude of ground subsidence with distance from the fracture permeability of the OWTB (Fig. 4.9). The latter coincides with the waning of surface heat and mass flow away from the main fracture permeability of the OWTB (Chapter 3). To the north, the narrow NNW trending embayment of relatively low subsidence coincides with the low permeability core (dome apex) of the Ohaaki Rhyolite dome. The embayment of relatively low ground subsidence extends to the NNW across an area theorized to be the location of a low permeability flow lobe emplaced during the eruption of the Ohaaki Rhyolite (Chapter 3).

In summary, the overall crescent shape of the MOSB coincides well with the documented permeable structures around the Ohaaki Rhyolite dome and the OHW thermal area, as defined in Chapter 3. Approximately 13 years ago, Allis et al. (1997) also noted that the crescent shape of the MOSB appeared to reflect its distribution about the circular crest (apex) of the Ohaaki Rhyolite dome and noted that the major subsidence features coincided with the locus of historical alkali-Cl outflows.

### 4.4.4 Spatial relationship between ground subsidence and hydrogeology

Comparison of the extent of ground subsidence with the hydrogeology of the Ohaaki Reservoir indicates that a strong spatial relationship exists between the extent of aquifer-like units containing alkali-Cl hot waters. In particular, a strong correlation is evident between the Waiora Formation geothermal aquifer and current ground subsidence in excess of 50 cm (Figs. 4.10 – 4.13). The latter is particularly well illustrated by the cross-section through the southern portion of the Ohaaki Reservoir (Fig. 4.10). Here the extent of ground subsidence, ≥ 50 cm, is restricted to the area across which the HFF directly overlies the Waiora Formation aquifer. East and west of this area the Waiora Formation aquifer pinches out against the low permeability lavas of the Broadlands Dacite and East Broadlands Rhyolite, respectively. Significantly, as the Waiora Formation aquifer pinches out, subsidence declines sharply and diminishes in magnitude towards the margins of the field. The pinching out of the Waiora Formation aquifer against the flanks of the Broadlands Dacite dome coincides with the distinctive horn shape of the 50 cm contour across the southern portion of the Ohaaki Field, and the sharp but irregular transition in the magnitude of ground subsidence east of the Broadlands Fault (Figs. 4.7 and 4.10).

Across the northern and central sectors of the field the HFF is divided by the Ohaaki Rhyolite into upper and lower units (Figs. 4.11, 4.12 and 4.13). Across these areas, ground subsidence ≥ 50 cm is spatially correlated with the extent of the lower HFF wherever it overlies the Waiora Formation geothermal aquifer. Where the lower HFF is absent (i.e., the HFF occurs as a single unit) and the HFF directly overlies aquitard lavas (East Broadlands Rhyolite, Broadlands Rhyolite and Ohaaki Rhyolite), ground subsidence is < 50 cm.

Adjacent to the MOSB, an area of ground subsidence currently ≥ 100 cm extends towards the east (Fig. 4.7). Here, the upper HFF overlies the steep and intensely brecciated flanks of the Ohaaki Rhyolite dome, which is known to host alkali-Cl hot waters (Fig. 4.12; Healy, 1968; Grindley, 1970; Hochstein and Henrys, 1990). Although the true extent of the dome breccia aquifer is difficult to constrain, drill hole stratigraphic data indicates that the brecciated carapace thins from ~ 90 m in the vicinity of well BR3, to just 30 m in well BR1 (Healy, 1968). Beneath the lavas of the Ohaaki Rhyolite, the lower HFF overlies the Waiora Formation hydrothermal aquifer but pinches out somewhere between well BR26 and well BR1 (Fig. 4.12). Although the exact extent of the lower HFF and the upper dome breccia aquifer are difficult to constrain, it is notable that a

general spatial correlation exists between the extent of these two units and subsidence ≥ 100 cm. This relationship likely extends to the north and (BR12) and NW (BR4).

Finally, the small OHE thermal area shows only minor (< 20 cm) ground subsidence and no correlation with the pattern of surface permeability associated with the Broadlands Fault Damage Zone (Figs. 4.7 and 4.10; Chapter 3). A lack of correlation between the extent of surface thermal activity and the pattern of ground subsidence is also evident for the minor BR6 thermal area (Fig. 4.7).

## 4.5 Discussion

### 4.5.1 MOSB and the OHW thermal area

From the detailed comparison between the nature of the MOSB and the permeability distribution of the OHW thermal area it is evident that a strong spatial correlation exists between the two. Therefore, on the basis of earlier conceptual models (Allis, 1990; Allis et al., 1997; Allis, 2000; Grant, 2000; White et al., 2005), we argue that the observed spatial overlap between the OWTB and the MOSB reflects the role of the concentric fracture zone of the OWTB as a high permeability conduit for: (i) the ascent of alkali-Cl hot waters from the underlying reservoir to the surface; (ii) the propagation of pressure decline from the reservoir to the surface or near surface, and; (iii) the development and localisation of zones of preferential pore fluid drainage.

Our interpretation differs from that of White et al. (2005) who attributed the crescent shape of the MOSB to lateral fluid drainage associated with the steep slope between the HFF and the flanks of the Ohaaki Rhyolite dome. Steep stratigraphic contacts resulting in enhanced lateral fluid drainage from the consolidating layer were also used by these authors to explain the location of the main Wairakei subsidence bowl. White et al. (2005) argued that since its inception in the 1970's the lateral migration of the MOSB by ~ 500 m to the east strongly supported the concept of lateral drainage. However, Allis et al. (1997) noted that the trend in horizontal movement was to the centre of the MOSB, which as demonstrated in this study occurs directly above the concentric fracture zone of the OWTB. Lateral migration was therefore a feature of the incipient MOSB and we attribute this migration to the drainage of pore fluids towards the site of greatest permeability (i.e., the OWTB).

Support for the development of major ISD above high permeability flow paths within the HFF comes from the direct spatial overlap between the nucleus of ISD 4 and the alkali-Cl outflow of the Ohaaki Pool (Fig. 4.9). Here, the Ohaaki Pool is connected to the West Bank upflow by several large vents (up to 5 m in diameter) developed within the HFF that widen into a large (40 m wide at 200 m deep) cone-shaped explosion crater within the Ohaaki Rhyolite (Henrys, 1986; Glover et al., 2000; Chapter 2; Chapter 3). The connection of the Ohaaki Pool to the underlying reservoir and the rapid propagation of deep pressure decline to the surface are indicated by the fluctuations of water level within the pool, in response to pressure changes

associated with early discharge testing (Glover et al., 2000). Upon production of the field in 1989 the Ohaaki Pool dried up completely in response to a sharp decrease in reservoir pressure (Allis et al., 1997; Glover et al., 2000).

The existence of ISD 1 and 3 above similar high permeability flow paths is supported by the localisation of anomalously $CO_2$ flux rates (>32,000 g $m^{-2}$ $d^{-1}$) to the bounds of ISD 3 (Chapter 2), and the presence of locally intense silicification of the HFF in the vicinity of ISD 1 (Hochstein and Henrys, 1989). Hochstein and Henrys (1989) attributed the localised nature of the silicification occurring in the vicinity of ISD 1 to the shallow boiling of alkali-Cl hot waters in this area. Whereas the anomalous $CO_2$ flux rates of ISD 3 are indicative of a direct link between the West Bank upflow (the $CO_2$ source) and the surface in this location (Giggenbach, 1984; Werner and Cardellini, 2006; Chapter 2; Chapter 3). In both instances, a deep-seated connection to the underlying liquid dominated reservoir is indicated.

The occurrence of a large cone-shaped explosion crater developed within the Ohaaki Rhyolite directly beneath the Ohaaki Pool raises the possibility that each individual ISD, occurring along the OWTB, is developed above a deep-rooted volcanic vent (Chapter 3). The existence of multiple vents formed within a concentric fracture zone fits with the known structure of lava domes (Watts et al., 2002; Sahetapy-Engel and Harris, 2009), a local eruptive origin for the Ohaaki Rhyolite (Risk, 1976; Healy, 1968; Chapter 3), and a heat and mass flow of 90 MW and 90 kg $s^{-1}$, respectively, focused along the OWTB (Chapter 2 and 3).

The moderate to low subsidence occurring across the apex of the Ohaaki Rhyolite is explained in terms of the thinning of the HFF and also the presence of the massive and poorly permeable core of the Ohaaki Rhyolite dome (Risk, 1976; Chapter 3). Our preferred interpretation is that the low permeability of the dome core limits the propagation of pressure decline up into the HFF. The restriction of vertical permeability for pressure propagation to the vicinity of the OWTB is supported by the rapid decline in the intensity (i.e. magnitude of heat and mass flow) of thermal activity with distance from the OWTB (Figs. 4.4 and 4.9). This decline in the vertical permeability of the HFF, with distance from the OWTB, coincides with a rapid decline in subsidence with distance from the centre of the MOSB.

### 4.5.2 General model for the ground subsidence of the Ohaaki Field

Away from the major subsidence bowls, Allis and others (1983, 1997 and 2000) have argued that broad areas of low amplitude background subsidence surrounding local ISD relate to the restriction of pressure propagation to the basal layers of the HFF. The relative magnitude of basal consolidation however, will depend on whether an alkali-Cl bearing aquifer or an aquitard underlies the HFF. In general, a pressure decline will propagate more readily from an alkali-Cl bearing aquifer up into the base of the HFF than from an aquitard.

The influence of the spatial transition from aquifer to aquitard over the magnitude of ground subsidence is best demonstrated across the southern extent of the reservoir (Figs. 4.8 and 4.11). Here the transition from aquifer (Waiora Formation) to aquitard (Broadlands Dacite) is correlated spatially with the sharp but irregular transition in the magnitude of ground subsidence east of the line between wells BR36 and BR30. Similarly, the western extent of the ≥ 50 cm contour coincides spatially with the pinching out of the Waiora Formation against the flanks of the East Broadlands Rhyolite, and the transition from aquifer to aquitard. Therefore, the horn shape of the ≥50 cm contour across the southern half of the field, coincides with the lateral extent of the Waiora Formation that overlies the lower HFF across this half of the field. A similar, albeit slightly more complicated, spatial relationship is recognised for the northern half of the field.

Although the low amplitude fringe of ground subsidence, < 50 cm, radiating out towards the margins of the field coincides with a prevalence of aquitard lavas (Figs. 4.10 – 4.13), the general decline in the amount of subsidence towards the field margins is explained in terms of a lateral decline in the pressure drop occurring within the deep reservoir. Pressure point data for production and monitoring wells at Ohaaki indicates a general decrease in the magnitude of both shallow and deep pressure decline, with proximity to the margins of the field (Contact Energy, 2007). This gradual decline coincides with the extent of the hot water reservoir. Therefore, the often noted correlation between both the extent of the hot water reservoir and ground subsidence is a factor of the coupled relationship between the hot water reservoir and reservoir pressure. As the pressure drop wanes towards the boundary so to does the propagation of this pressure decline up into the base of the HFF.

Finally, despite a deep pressure decline of between 8 – 24 bar, and evidence for integrated sub-vertical permeability (i.e., the Broadlands Fault Damage Zone), the magnitude of subsidence in the vicinity of the OHE thermal area is minor (≤ 20 cm) and shows no spatial correlation with the distribution of the shallow structural permeability mapped for this area (Chapter 3). Here the shallow reservoir beneath the OHE thermal area is structurally isolated from shallow lateral outflows of alkali-Cl hot waters by the Broadlands Dacite dome (Fig. 4.10). The absence of significant ground subsidence in this locality likely reflects the buffering of vertical pressure propagation by a thick vapour phase zone that underlies this area (Grindley, 1970; Browne and Ellis, 1970; Chapter 2). Well BR7, within the OHE thermal area, was the only well at Ohaaki to discharge dry steam (Browne and Ellis, 1970). Key here is that unlike aquifers containing alkali-Cl hot waters, localised vapour phase zones tend to buffer pressure changes propagating vertically (Sorey et al., 1980; Grant, 1988), thereby limiting the extent of the pressure drop acting on the base of the HFF and ensuing consolidation of this formation.

## 4.6 Conclusion

In this paper we argue that the spatial patterns in the magnitude of ground subsidence occurring across the surface of the Ohaaki Field can best be explained by the spatial distribution of structural and hydrogeological controls over the propagation of pressure decline from the underlying liquid dominated reservoir up into the HFF. These controls include: (i) the spatial distribution of sub-vertical permeability within the HFF and the connection of this permeability to liquid pressure domains (alkali-Cl bearing aquifers); (ii) the spatial distribution of aquifers and aquitards beneath the HFF; (iii) the existence of thick vapour phase zones, which buffer the vertical propagation of deep pressure decline towards the surface and; (iv) the extent of the hot water reservoir.

In particular, we note that where anomalous vertical permeability, linked to a liquid pressure domain, occurs within the HFF that localised surface depressions of high magnitude develop (i.e., ISD). The latter is best defined by the very strong spatial correlation between the permeability distribution of the OHW thermal area and the location and shape of the MOSB. Here, deep-seated permeability governs: (i) the ascent of alkali-Cl hot waters from the underlying reservoir to the surface (or in the event of a large pressure decline, drainage in the other direction); (ii) the propagation of pressure decline from the reservoir to the surface or near surface; (iii) the development and localisation of zones of preferential pore fluid drainage, and; (iv) the development of localised ISD.

In the absence of subvertical permeability within the HFF, pressure decline within the HFF is restricted to the basal layers, and is greatest in those regions where the HFF directly overlies an aquifer containing alkali-Cl hot waters. In these instances, consolidation is sub-horizontally (laterally) distributed and the resultant ground subsidence is of low amplitude. Basal consolidation is responsible for the broad area of moderate ground subsidence (currently, $\geq$ 50 cm) that extends outwards from the MOSB and across ~ 80% of the field (Fig. 4.7).

Conversely, wherever the HFF directly overlies an aquitard, vertical pressure propagation from the deep reservoir and the corresponding consolidation of the basal layers of the HFF, is restricted. This restriction is manifest at the surface of the field as a change in the magnitude of ground subsidence, and in the southern half of the Ohaaki Field is well correlated with the pinching out of the Waiora Formation against the aquitard lavas of the East Broadlands Rhyolite and the Broadlands Dacite. In addition, the gradual decline in ground subsidence towards the margins of the field reflects a general decline in the deep pressure drop acting on the base of the HFF towards the margins of the hot water reservoir. Therefore, the often noted correlation between both the extent of the hot water reservoir and ground subsidence is a factor of the coupled relationship between the hot water reservoir and reservoir pressure.

Despite a deep pressure decline of between 8 and 24 bar beneath the OHE thermal area, the minor ground subsidence and absence of any spatial correlation between ground subsidence and the structural permeability is due to the buffering of shallow pressures by a thick (~ 600 m) vapour dominated zone. Accordingly, only in thermal areas with a good connection to an underlying alkali-Cl aquifer is deep reservoir pressure decline expected to propagate rapidly to the surface (Sorey et al., 1980; Grant, 1988; Glover et al., 2000). The latter is well illustrated by the rapid decline in the water level of the Ohaaki Pool during discharge testing (Glover et al., 2000).

In this model, the total cumulative subsidence occurring at any one location across the surface of the Ohaaki Field may be defined according to the sum of one or more consolidation domains. For example, the total cumulative subsidence of the MOSB is considered the sum of three major subsidence domains acting at different depths beneath the surface (Fig. 4.12). The first domain corresponds to the sub-vertical permeability of the OWTB developed within the HFF, the second to basal consolidation of the upper HFF above the brecciated carapace aquifer of the Ohaaki Rhyolite dome, and thirdly, basal consolidation occurring within the lower HFF where it directly overlies the Waiora Formation. Elsewhere, the net or total ground subsidence at the surface of the field may correspond to just one consolidation domain, with the magnitude of ground subsidence depending on whether or not this domain occurs above an alkali-Cl bearing aquifer or an aquitard, as well as its proximity to the margins of the field (Figs. 4.10 to 4.13). Therefore, by identifying individual consolidation domains the spatial distribution in the magnitude of ground subsidence at the surface of the Ohaaki Field may be explained.

This study considers the spatial variation in the magnitude of ground subsidence occurring across the entire Ohaaki Field. In doing so we have produced a general spatio-structural model through which key hydrothermal characteristics may be used to delineate areas according to categories of relative subsidence risk. These key elements include: (i) identifying areas of liquid versus steam dominated thermal activity; (ii) mapping shallow structural permeability; (iii) defining the extent of aquifers and aquitards beneath the consolidating layer and; (iv) knowing the extent of the hot water reservoir. Much of the data required for predictive assessment of subsidence risk in undeveloped, underdeveloped and producing hydrothermal fields of the TVZ is available from: (i) aerial and field reconnaissance; (ii) regional geological models and bore hole stratigraphy, and; (iii) early literature on the structure and hydrothermal activity of individual fields. However, application of this model to other hydrothermal fields, throughout the TVZ, is required in order to further test its validity. If this model proves to be successful at other fields (i.e., the Wairakei Field), it may warrant application to other fields throughout the TVZ, or to hydrothermal fields globally where a poroelastic unit similar to the HFF occurs in close proximity to the surface.

Finally, as the spatial structure and hydrogeology of the Ohaaki Field govern the pattern of ground subsidence, the latter may be used to refine our understanding of the extent of subsurface aquifers and aquitards, and better resolve the shallow 3D structure of a hydrothermal reservoir.

## 4.7 Acknowledgements

The authors would like to thank the Geothermal Group of Contact Energy Ltd, New Zealand, for access to stratigraphic, pressure, and levelling databases for the Ohaaki Field, as well as for logistical and funding support. Thanks also to an anonymous reviewer whose experience in the topic of production-induced ground subsidence greatly improved the quality of this manuscript.

## 4.8 References

Allis, R., 1990. Subsidence at Wairakei field. Geothermal Resources Council Transactions, 14(11): 1081-1087.

Allis, R.G., 1983. Comparison of subsidence at Wairakei, Broadlands and Kawerau Fields, New Zealand. 8th workshop on Geothermal reservoir engineering, Stanford University, Stanford Geothermal Program, pp. 181-183.

Allis, R.G. and Webber, S., 1984. Shallow temperature measurements at Wairakei and Broadlands fields. Geophysics Division Report, 197: 27.

Allis, R.G., 2000. Review of subsidence at Wairakei Field, New Zealand. Geothermics, 29(4-5): 455-478.

Allis, R.G. and Zhan, X., 2000. Predicting subsidence at Wairakei and Ohaaki geothermal fields, New Zealand. Geothermics, 29(4-5): 479-497.

Antonellini, M. and Aydin, A., 1994. Effect of faulting on fluid flow in porous sandstones: petrophysical properties American Association of Petroleum Geologists, 78: 355-377.

Bloomer, A. and Currie, S., 2001. Effects of geothermal induced subsidence. 23rd New Zealand Geothermal Workshop, University of Auckland Geothermal Institute, pp. 3-8.

Browne, P.R.L. and Ellis, A.J., 1970. The Ohaki-Broadlands hydrothermal area, New Zealand; mineralogy and related geochemistry. American Journal of Science, vol. 269, no.2, pp. 97-131.

Christenson, B.W., Mroczek, E.K., Kennedy, B.M., van Soest, M.C., Stewart, M.K. and Lyon, G., 2002. Ohaaki reservoir chemistry; characteristics of an arc-type hydrothermal system in the Taupo volcanic zone, New Zealand. Journal of Volcanology and Geothermal Research, 115(1-2): 53-82.

Contact Energy, 2007. Ohaaki Reservoir Pressures, Contact Energy.

GeoNet, 2009. Hazard monitoring network, New Zealand. GPS time series index, accessed August, 2009. http://www.geonet.org.nz/resources/gps/timeseries/index.html.

Giggenbach, W.F., 1984. Mass transfer in hydrothermal alteration systems; a conceptual approach. Geochimica et Cosmochimica Acta, 48(12): 2693-2711.

Glover, R.B., Hunt, T.M. and Severne, C.M., 2000. Impacts of development on a natural thermal feature and their mitigation; Ohaaki Pool, New Zealand. Geothermics, 29(4-5): 509-523.

Grant, M.A., 1977. Broadlands; a gas-dominated geothermal field. Geothermics, 6(1-2): 9-29.

Grant, M.A., 2000. Projected subsidence at Tauhara. 22nd New Zealand Geothermal Workshop, University of Auckland Geothermal Institute, pp. 247-250.

Grindley, G.W., 1970. Subsurface structures and relation to steam production in the Broadlands geothermal field, New Zealand. Geothermics, 2(Part 1): 248-261.

Hatton, J.W., 1970. Ground subsidence of a geothermal field during exploitation. Geothermics, 2(Part 2): 1294-1296.

Healy, J., 1968. Geological report on the Broadlands Geothermal Field, Department of Scientific and Industrial Research Rotorua.

Hedenquist, J.W., 1990. The thermal and geochemical structure of the Broadlands-Ohaaki geothermal system, New Zealand. Geothermics, 19(2): 151-185.

Henrys, S.A., 1986. Shallow structure of the Broadlands-Ohaaki geothermal field (NZ); analysis of seismic refracted arrivals by iterative ray tracing. 8th New Zealand Geothermal Workshop, University of Auckland, Geothermal Institute, pp.85-90.

Henrys, S.A., and Hochstein, M.P., 1990. Geophysical structure of the Broadlands-Ohaaki geothermal field (New Zealand). Geothermics, 19(2): 129-150.

Hochstein, M.P. and Henrys, S.A., 1989. Geophysical structure and densification of producing layers in the Broadlands-Ohaaki Field (New Zealand). 11th New Zealand Geothermal Workshop, University of Auckland Geothermal Institute, pp. 45-50.

Hole, J.K., Bromley, C.J., Stevens, N.F., Wadge, G. Subsidence at the Wairakei-Tauhara geothermal field, New Zealand from 1996-2005 measured by ERS interferometry. Journal of Volcanology and Geothermal Research, vol. 166, no. 3-4, pp.125-146.

Hunt, T.M. and Bromley, C.J., 2000. Some environmental changes resulting from development of Ohaaki geothermal field, New Zealand. World Geothermal Conference, Kyushu, Japan, pp. 621-626.

MacDonald, W.J.P., 1975. The useful heat contained in the Broadlands geothermal field. Second United Nations symposium on the development and use of geothermal resources, San Francisco, Calif., United States, pp. 1113-1119.

Mahon, W.A.J. and Finlayson, J.B., 1972. The chemistry of the Broadlands geothermal area, New Zealand. American Journal of Science, 272(1): 48-68.

Milicich, S.D., 2010. A 3D computer model of the Ohaaki Reservoir. GNS Science, Wairakei.

Nairn, I., 1982. Geology of Kawerau geothermal field (MK11): results of drilling. 1977 - 1982. Geothermal circular IN/1:1v.

Narasimhan, T.N. and Goyal, K.P., 1984. Subsidence due to geothermal fluid withdrawal. In: T.L. Holzer (Editor), Reviews in Engineering Geology, vol.6. Geological Society of America (GSA), Boulder, pp. 35-66.

Rae, A.J., Rosenberg, M.D., Bignall, G., Kilgour, G.N. and Milicich, S.D., 2007. Geological results of production well drilling in the western steamfield, Ohaaki geothermal system: 2005-2007. 29th New Zealand Geothermal Workshop, University of Auckland Geothermal Institute, pp. 7.

Read, S.A.L., Pender, M.J., Barker, P.R. and Ellis, S.M., 2003. Consolidation testing of Huka Falls Formation; properties related to subsidence at Ohaaki and Wairakei. In: S.A. Crawford, P. Baunton and S. Hargraves (Editors), Proceedings of Technical Groups - Institution of Professional Engineers New Zealand, vol. 30(1GM). Institution of Professional Engineers New Zealand, Wellington, pp. 291-300.

Risk, G.F., 1976. Detection of buried zones of fissured rock in geothermal fields using resistivity anisotropy measurements. Department of Scientific and Industrial Research, New Zealand, Geophysics Division Report, Report: 102, pp.78-100.

Sahetapy-Engel, S.T. and Harris, A.J.L., 2009. Thermal structure and heat loss at the summit crater of an active lava dome. Bulletin of Volcanology, 71(1): 15-28.

Thompson, G.E.K., 1967. Ground temperatures at a depth of one metre. Department of Scientific and Industrial Research - Geophysics Division, Wellington.

Watts, R.B., Herd, R.A., Sparks, R.S.J. and Young, S.R., 2002. Growth patterns and emplacement of the andesitic lava dome at Soufriere Hills Volcano, Montserrat. Memoirs of the Geological Society of London, 21: 115-152.

Werner, C. and Cardellini, C., 2006. Comparison of carbon dioxide emissions with fluid upflow, chemistry, and geologic structures at the Rotorua geothermal system, New Zealand. Geothermics, 35(3): 221-238.

White, P.J., Lawless, J.V., Terzaghi, S., Okada, W., 2005. Advances in subsidence modelling of exploited geothermal fields. In: Proceedings of the 2005 World Geothermal Congress, April, Antalya, Turkey, Paper 222, 10 pp.

Wood, C.P., 1994. Aspects of the geology of Waimangu, Waiotapu, Waikite and Reporoa geothermal systems, Taupo volcanic zone, New Zealand. Geothermics, 23(5-6): 401-421.

Wood, C.P., 1996. Basement geology and structure of TVZ geothermal fields, New Zealand. 18th New Zealand Geothermal Workshop, University of Auckland Geothermal Institute, pp. 157-162.

Wood, C.P., Brathwaite, R.L. and Rosenberg, M.D., 2001. Basement structure, lithology and permeability at Kawerau and Ohaaki geothermal fields, New Zealand. Geothermics, 30(4): 461-481.

## 1.7 Figures

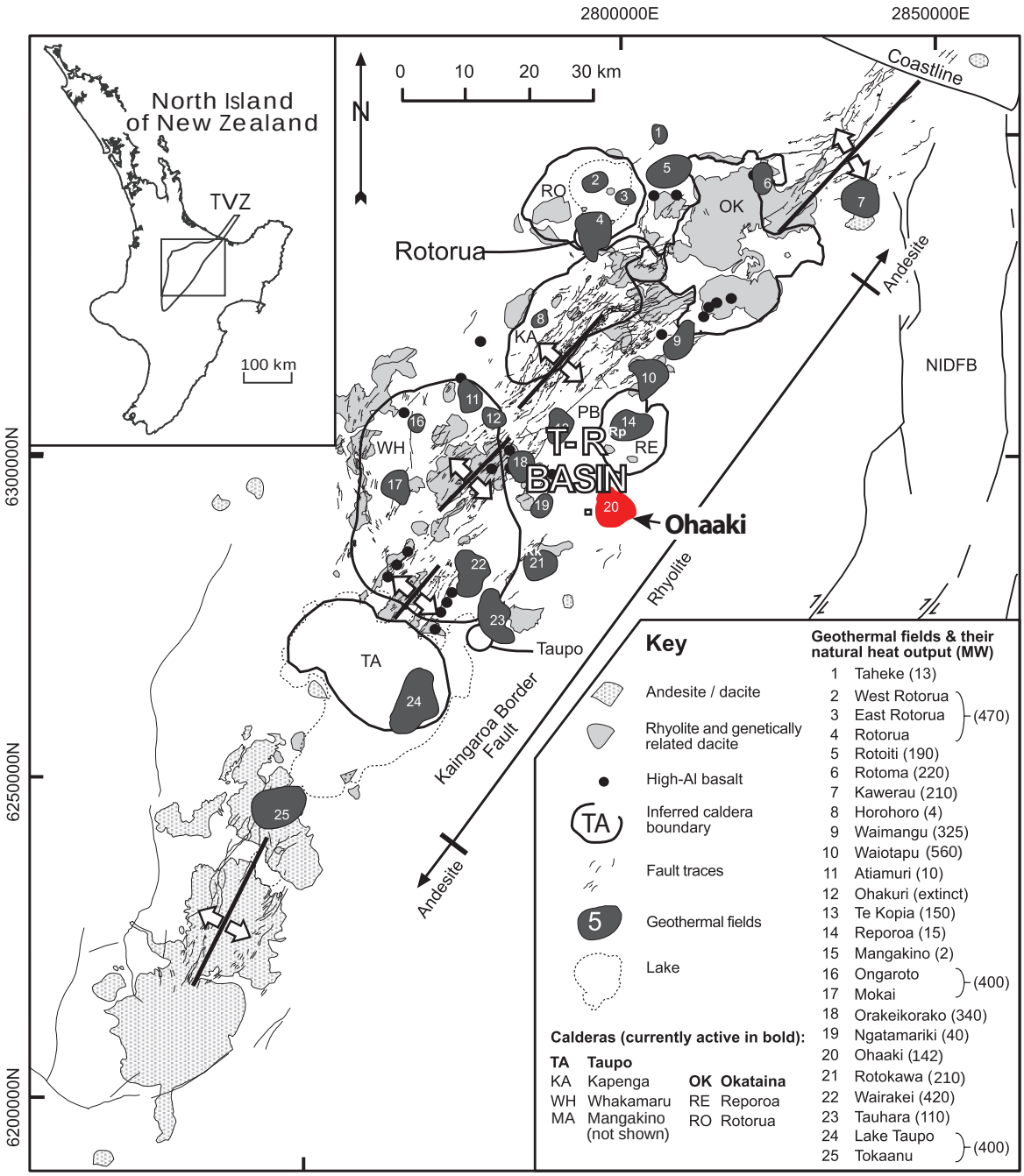


Figure 4.1. Map of the Taupo Volcanic Zone showing the distribution of geothermal systems, defined by the presence of low-resistivity zones (<30 Ωm) in relation to rift architecture, major volcanic rock types and caldera boundaries (modified from Rowland & Sibson 2004). Where T-R basin denotes the location of the Taupo Reporoa Basin and the Ohaaki hydrothermal field is in red. NIDFB, North Island Dextral Fault Belt. Major towns, Taupo and Rotorua, are labelled.

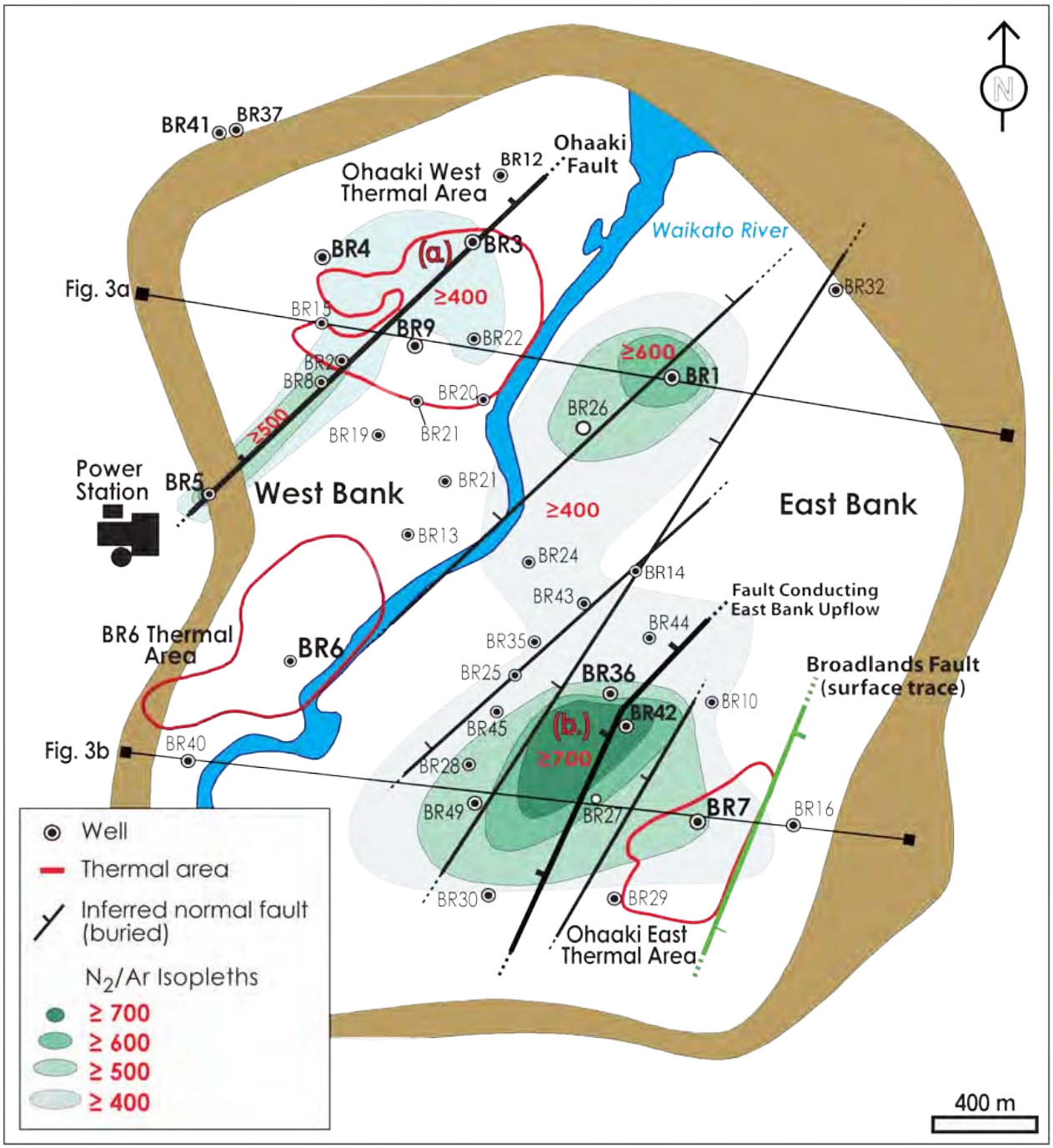


Figure 4.2. Plan view of the Ohaaki Field including resistivity boundary, inferred deep-seated normal faults, $N_2$/Ar isopleths and location of major thermal areas (from Christenson et al., 2002; Wood et al., 2001). $N_2$/Ar isopleths denote the major hydrothermal upflows of the field. The Ohaaki Fault occurs in the upper left of the field and conducts the West Bank upflow. The East Bank upflow occurs through another major normal fault in the SE. The surface trace of the Broadlands Fault is shown in green (this study). The location of major thermal areas, Ohaaki West (OHW) and Ohaaki East (OHE), and low temperature BR6 thermal area are shown. Thermal areas are delineated by 1.0 m depth temperatures ≥ 25ºC after Allis and Webber, (1984) and this study. The line of cross-section for Figures 3a and 3b are also displayed.

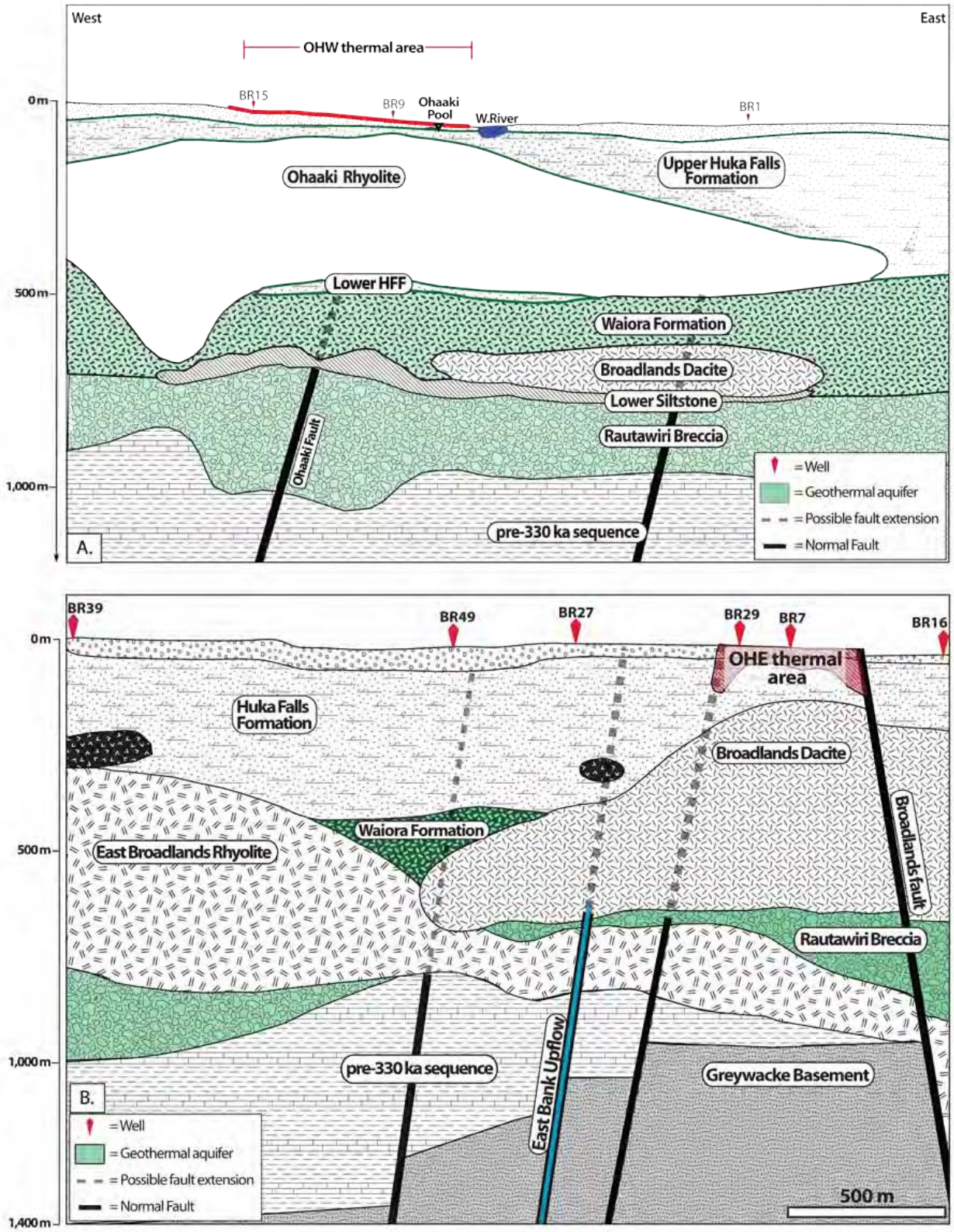


Figure 4.3. East – west cross sections through the Ohaaki reservoir (modified from Milicich, 2010). (a) Cross section through the NW sector of the field and the OHW thermal area. (b) Cross section through the SE sector of the field and the OHE thermal area. Fault locations are idealised and not to scale.

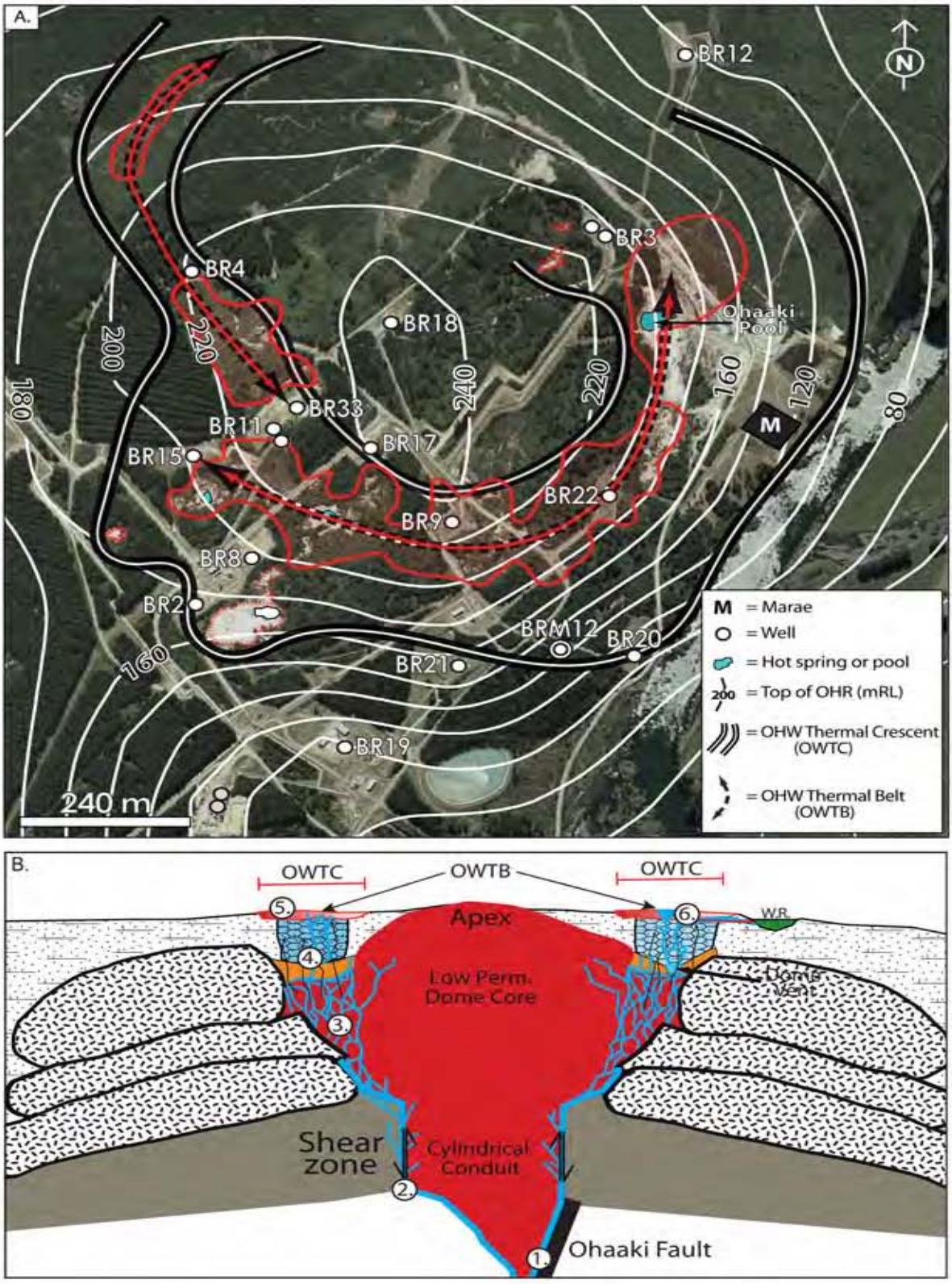


Figure 4.4. (a) Superposition of surface thermal activity associated with the OHW thermal area onto contours of the Ohaaki Rhyolite dome (Chapter 2). Note the partial encircling of the apex of the dome by the locus of most vigorous thermal activity (i.e., the Ohaaki West Thermal Belt) and the conspicuous absence of thermal activity, both pre-production and ancient, across the apex of the dome where the HFF is thinnest. (b) Idealised model of dome control fluid flow for the OHW thermal area (Chapter 2): (1) location of erupted feeder dyke along Ohaaki Fault; (1 - 2) ascent of West Bank upflow through the remnant permeability associated with the conduit shear zone of the Ohaaki Rhyolite dome; (3) fluid flow through eruption related fracture zone; (4) locally intense silicification and hydro-fracturing of the HFF overlying the concentric fracture zone of the Ohaaki Rhyolite and development of preferential flow paths; (5) development of the concentric pattern of surface thermal activity characteristic of the OHW thermal area and best defined by the OWTB, and; (6) development of the deep Ohaaki Pool above an extinct volcanic vent.

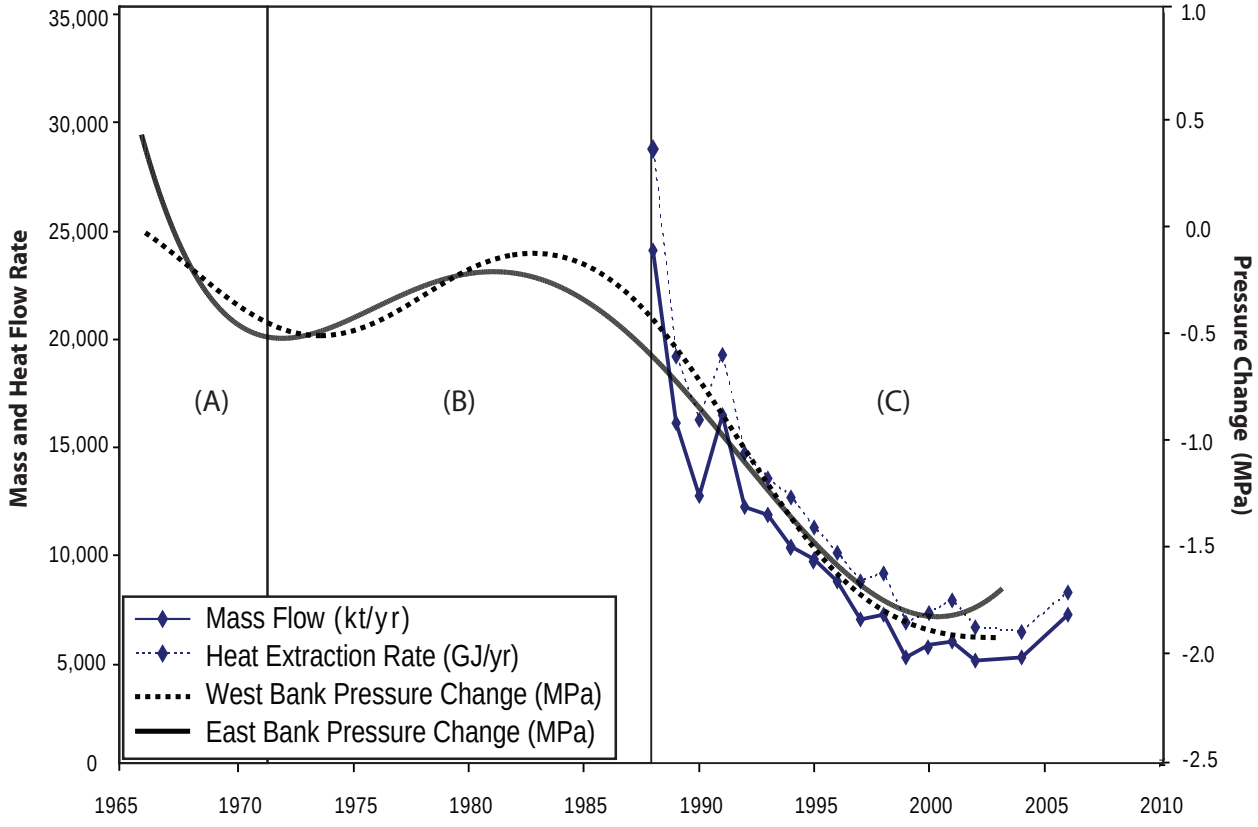


Figure 4.5. Characteristic trends at Ohaaki due to development (updated from Hunt and Bromley, 2000). This figure shows the total mass and heat flow from production wells, and the trend in pressure changes for the West- and East Bank reservoirs. Pressure changes are based on production well data for the deep reservoir (≥ -161 mRL) (data from Contact Energy, 2007). (A) Is the Test Discharge Period, (B) the Recovery Period, and (C) the Production Period.

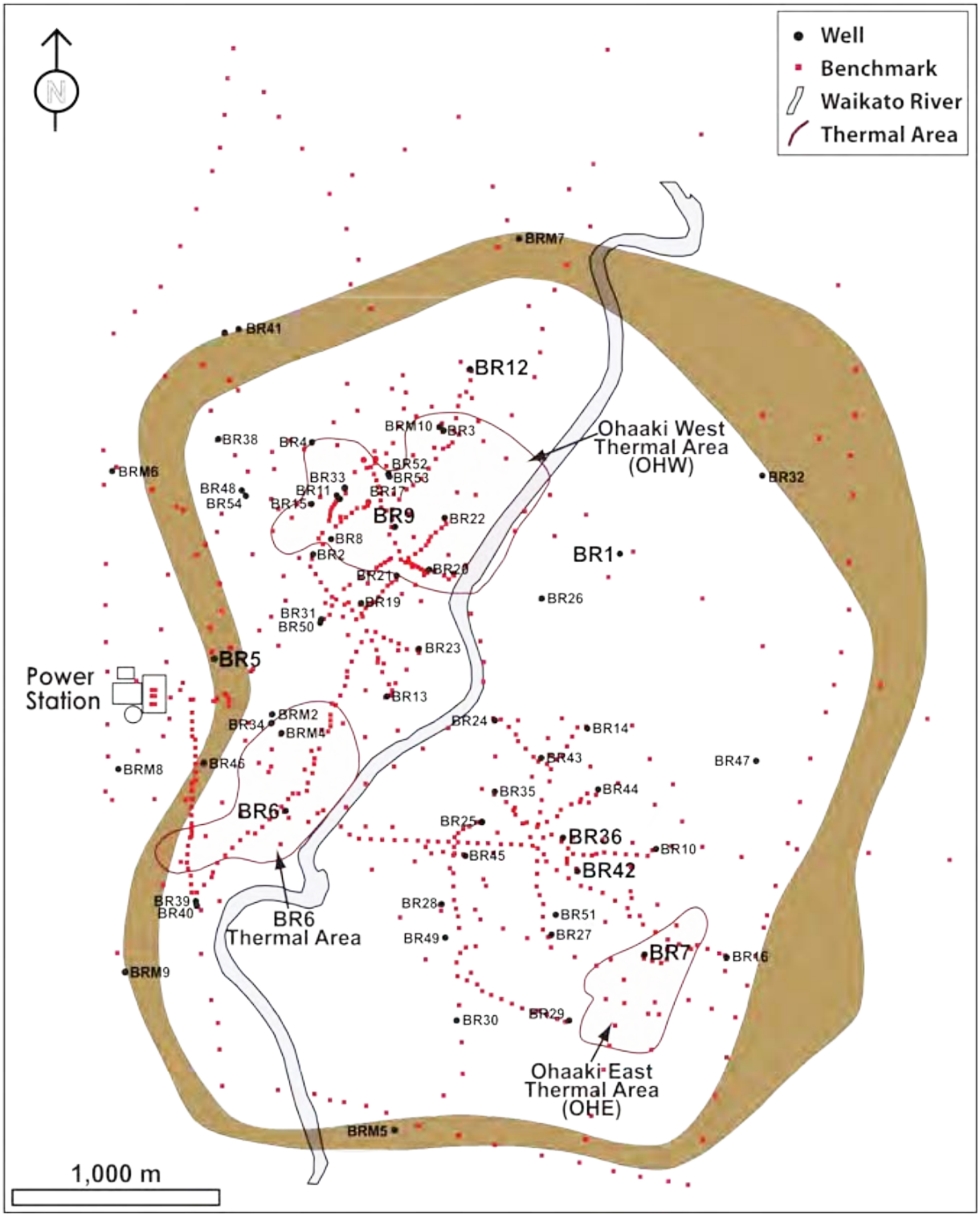


Figure 4.6. Plan view of Ohaaki Field and benchmark (levelling sites) locations used for subsidence model. A total of 23 benchmarks extend beyond the SE margin (OHE thermal area) of the field and are not shown in this figure.

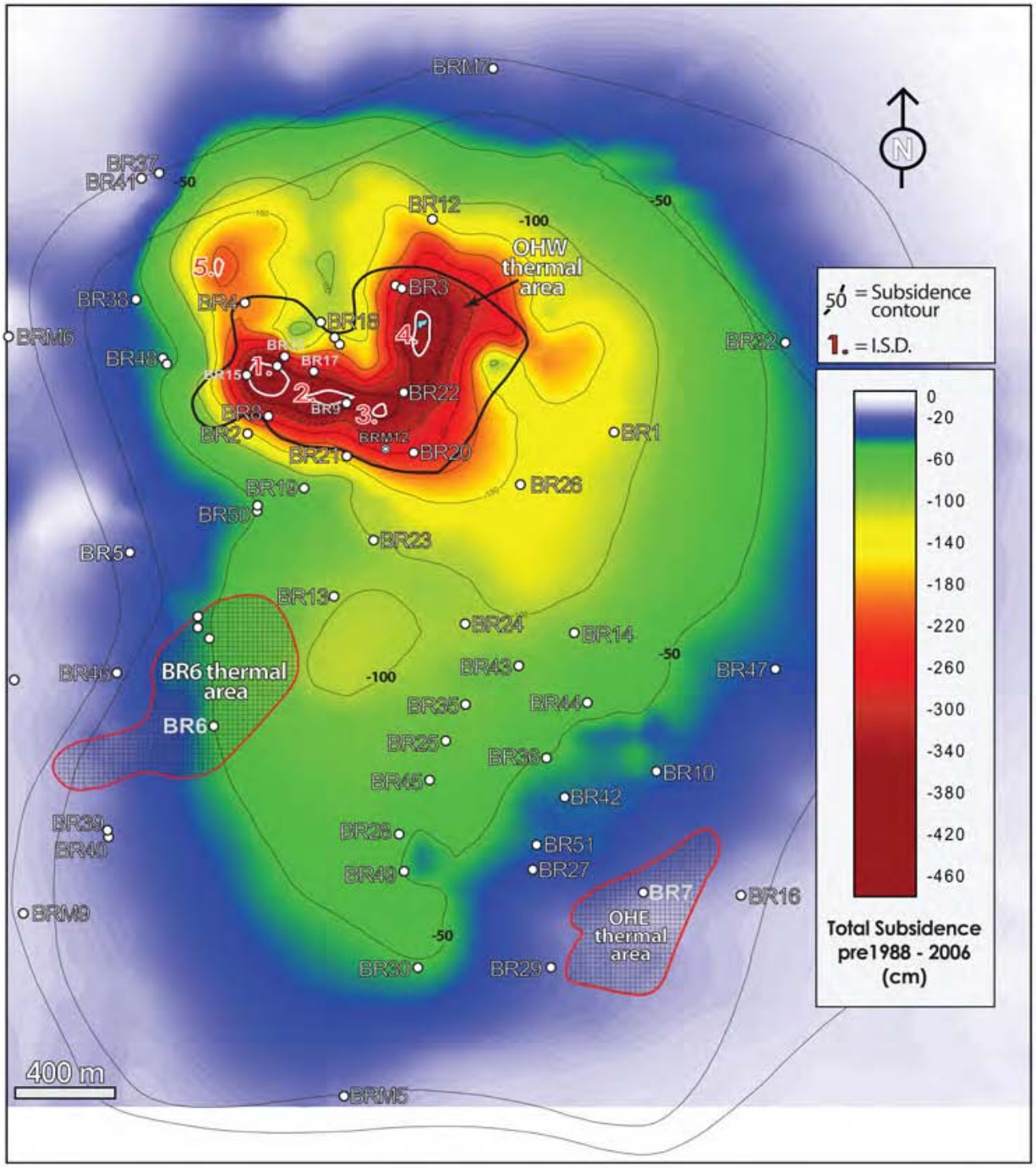


Figure 4.7. Cumulative total ground subsidence model (cm) for the Ohaaki Field. Where numbers 1 – 5 denote the location of intense surface depressions (ISD); OHW = Ohaaki West thermal area; OHE = Ohaaki East thermal area and; BR6 = BR6 thermal area. Ground subsidence > 10 cm occurs across the majority of the field. Note: (i) the crescent shape of the Main Ohaaki Subsidence Bowl (MOSB) in the NW; (ii) the general spatial overlap between the OHW thermal area and the MOSB; (iii) pronounced steps in the magnitude of ground subsidence with distance from the MOSB and towards the margins of the field; (iv) the general decline and petering our of low amplitude ground subsidence towards the margins of the field and; (v) the lack of correlation between the steam heated OHE and BR6 thermal areas and magnitude of ground subsidence.

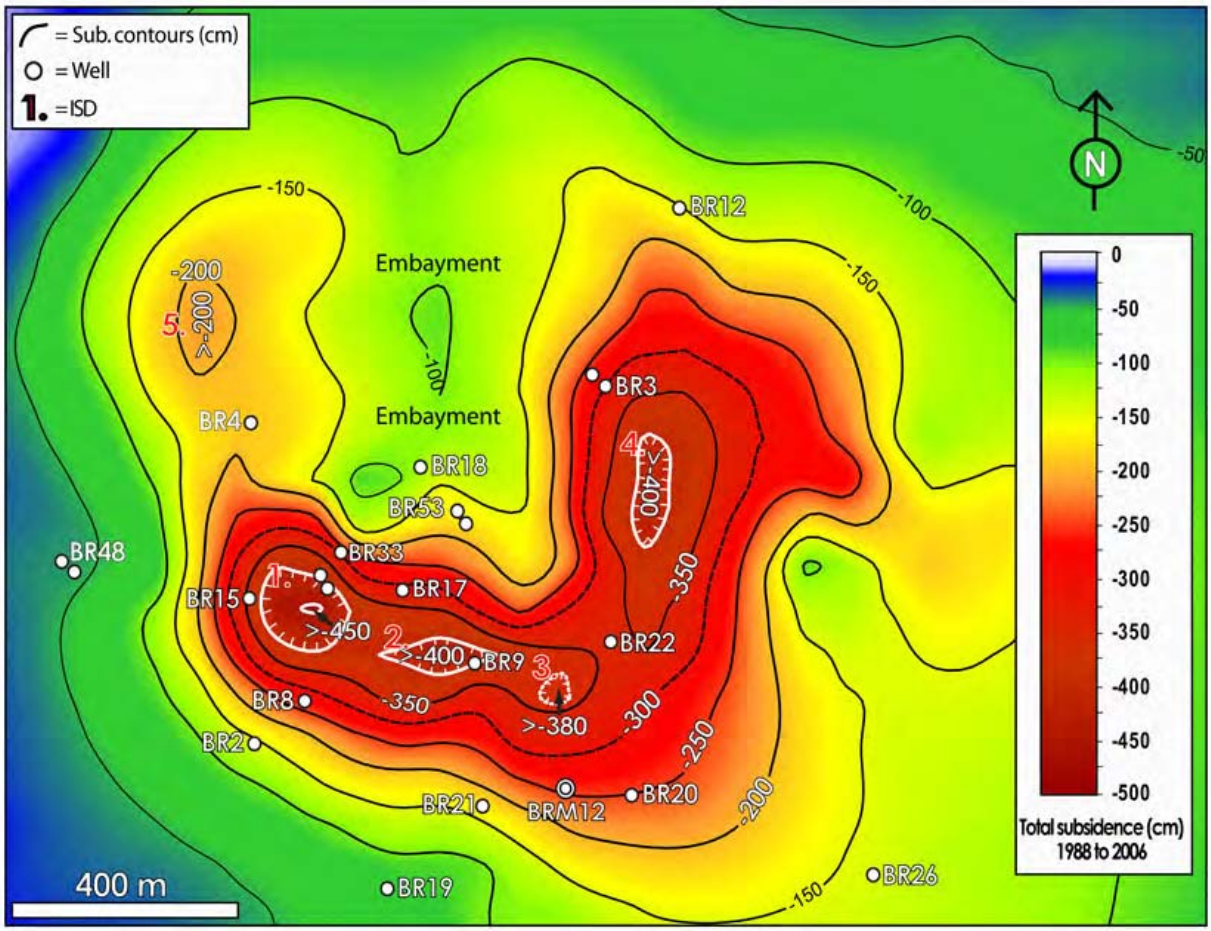


Figure 4.8. Total cumulative subsidence of the Main Ohaaki Subsidence Bowl (MOSB). Note: (i) the coalescence of the 4 major ISD to form the distinctive crescent shape of the MOSB; (ii) the location of ISD 5 outside of the MOSB, and; (iii) the narrow NNW trending embayment of relatively low ground subsidence.

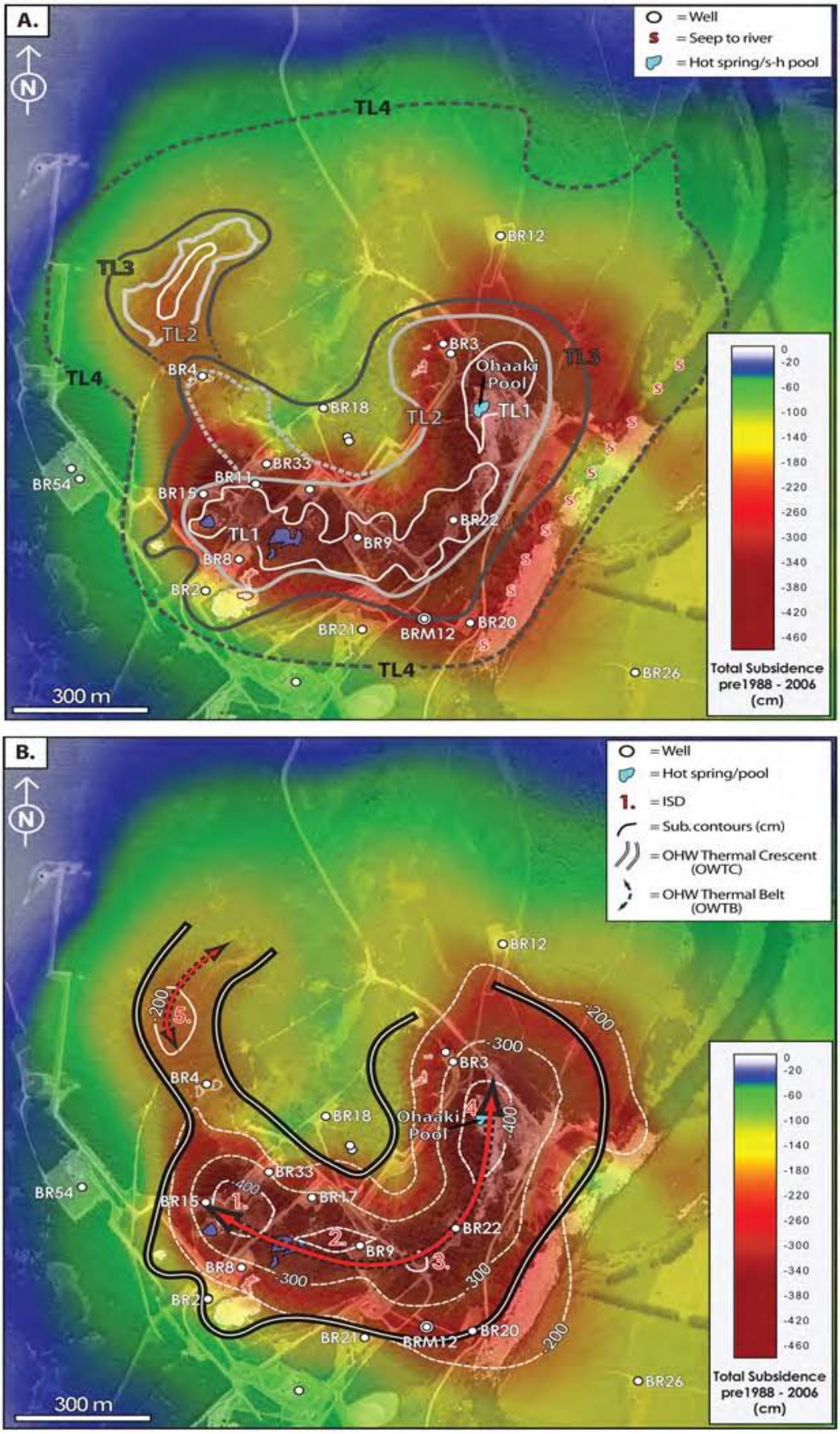


Figure 4.9. (a-b) Spatial relationship between the extent and intensity of surface thermal activity and ground subsidence for the Ohaaki West thermal area. Note the strong spatial correlations between: (i) ISD 1 – 4 and the concentric fracture zone of the Ohaaki West Thermal Belt (OWTB); (ii) the alkali-Cl Ohaaki Pool and the nucleus of ISD 4; (ii) embayment of relatively low magnitude subsidence and the long axis of the Ohaaki Rhyolite dome. Also evident is the general decline in subsidence with distance from the liquid fed OWTB.

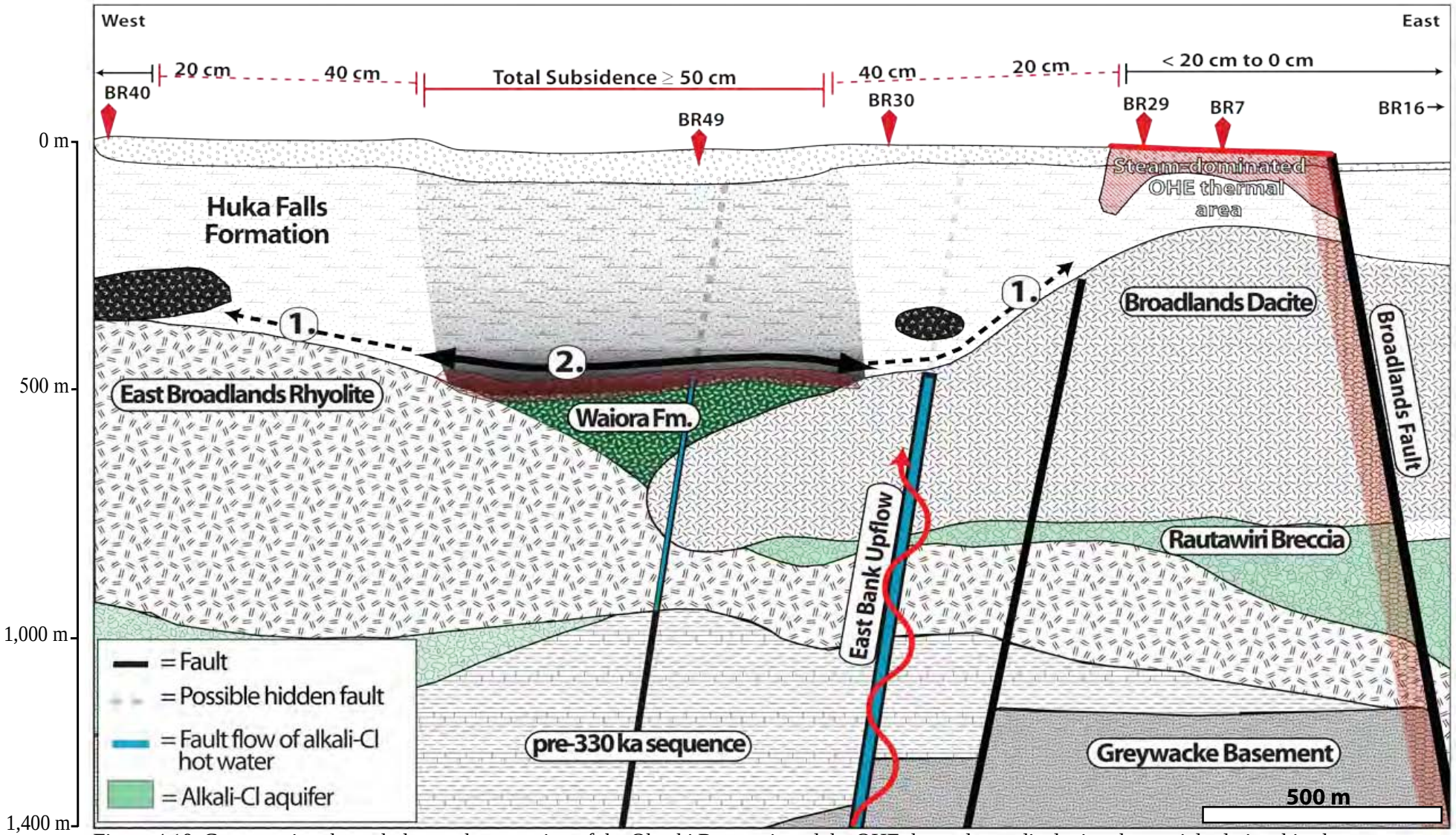


Figure 4.10. Cross section through the southern portion of the Ohaaki Reservoir and the OHE thermal area displaying the spatial relationships between reservoir hydrogeology and sub-vertical permeability. Numbers 1 - 2 correspond to the Waiora and Aquitard consolidation domains (basal consolidation), respectively. Note: (i) the spatial correlation between the extent of the shallow Waiora Formation alkali-Cl aquifer and ground subsidence ≥ 50 cm; (ii) the spatial correlation between the aquitard lavas of the East Broadlands Rhyolite and the Broadlands Dacite and a transition in ground subsidence to values < 50 cm; (iii) the general decline in the magnitude of ground subsidence towards the margins of the field and; (iv) the minor ground subsidence of the OHE thermal area.

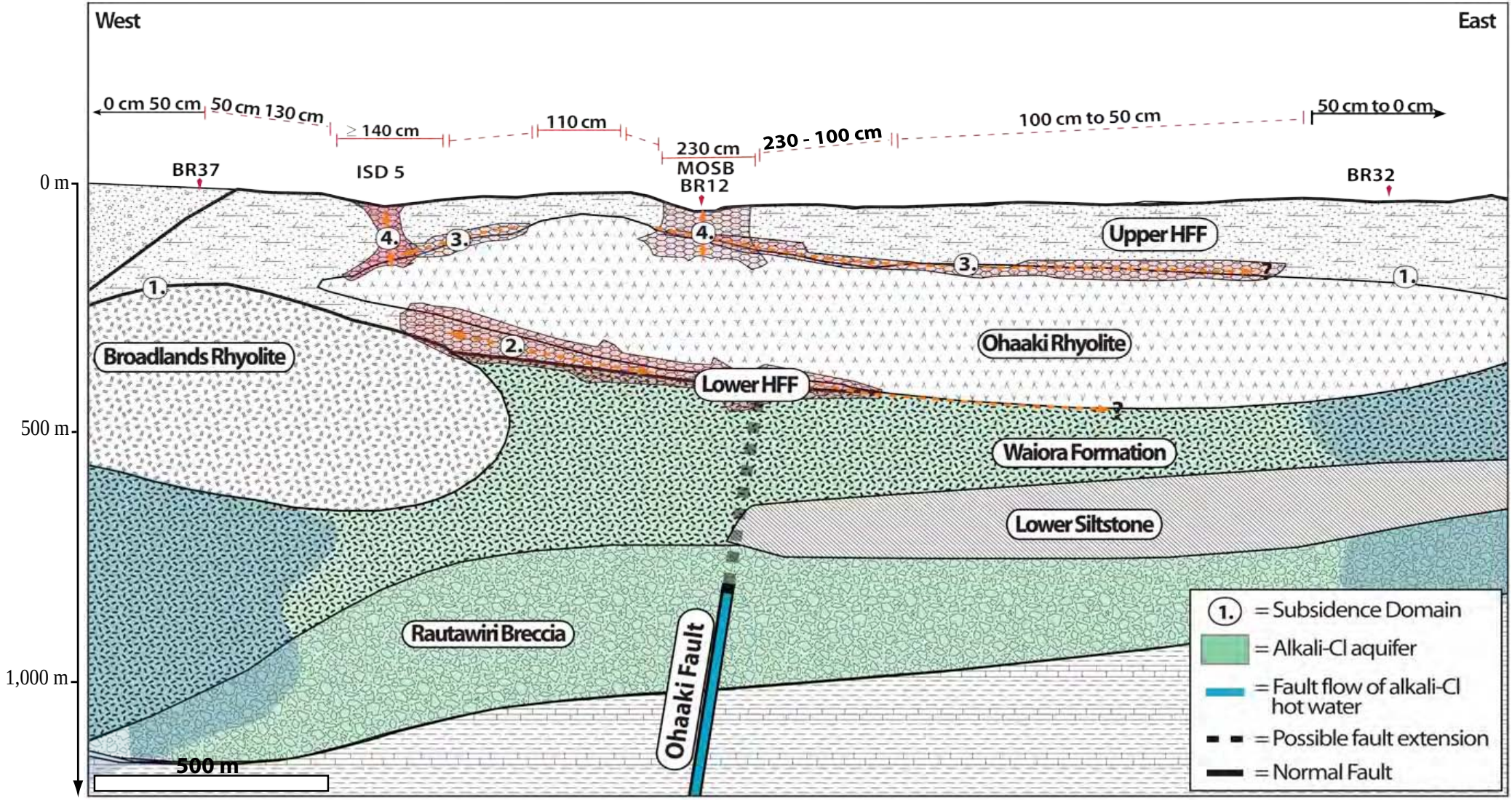


Figure 4.11. Cross section through the northern sector of the Ohaaki displaying the spatial relationships between reservoir hydrogeology and sub-vertical permeability. Ground subsidence >100 cm is correlated with the extent of the Lower HFF and the dome breccia aquifer of the Ohaaki Rhyolite (i.e., domains 2 and 3, respectively) both of which are poorly constrained. Domain 4 denotes the northern most extent of ISD 4 and sub-vertical consolidation of the HFF. Domain 1 corresponds to aquitard consolidation and/or the waning of lateral pressure decline at the base of the HFF towards the margins of the hot water reservoir.

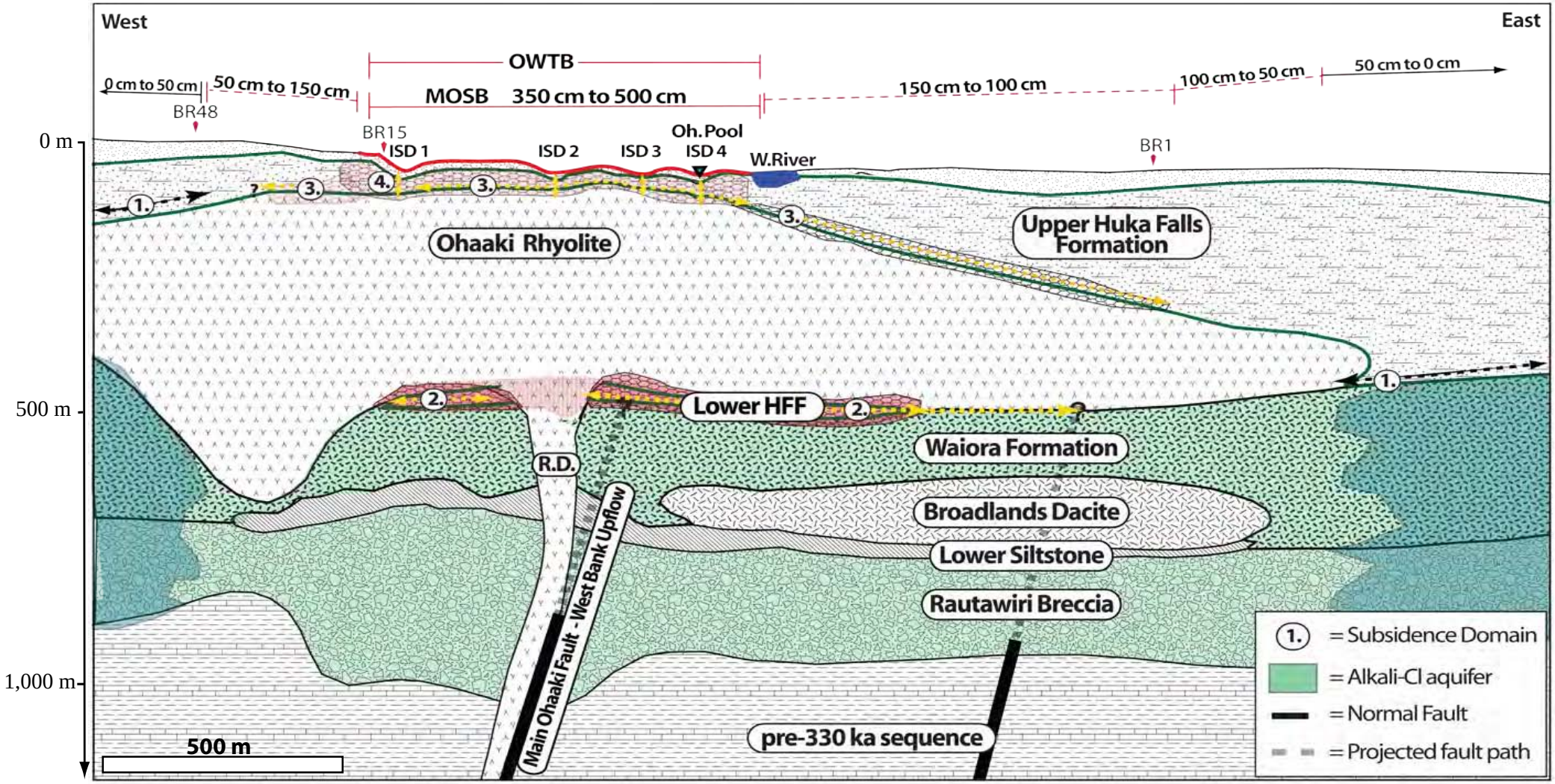


Figure 4.12. Cross section through the Ohaaki Reservoir and OHW thermal area displaying the spatial relationships between reservoir hydrogeology and sub-vertical permeability. Extent of MOSB coincides with basal consolidation domains 2 and 3 and subvertical consolidation domain 4. Ground subsidence >100 cm shows a general correlation with the extent of the Lower HFF and the dome breccia aquifer of the Ohaaki Rhyolite (i.e., domains 2 and 3, respectively) both of which are poorly constrained. Vertical arrows denote the sub-vertical consolidation of the HFF associated with each major ISD. Domain 1 corresponds to aquitard consolidation and/or the waning of lateral pressure decline at the base of the HFF towards the margins of the hot water reservoir.

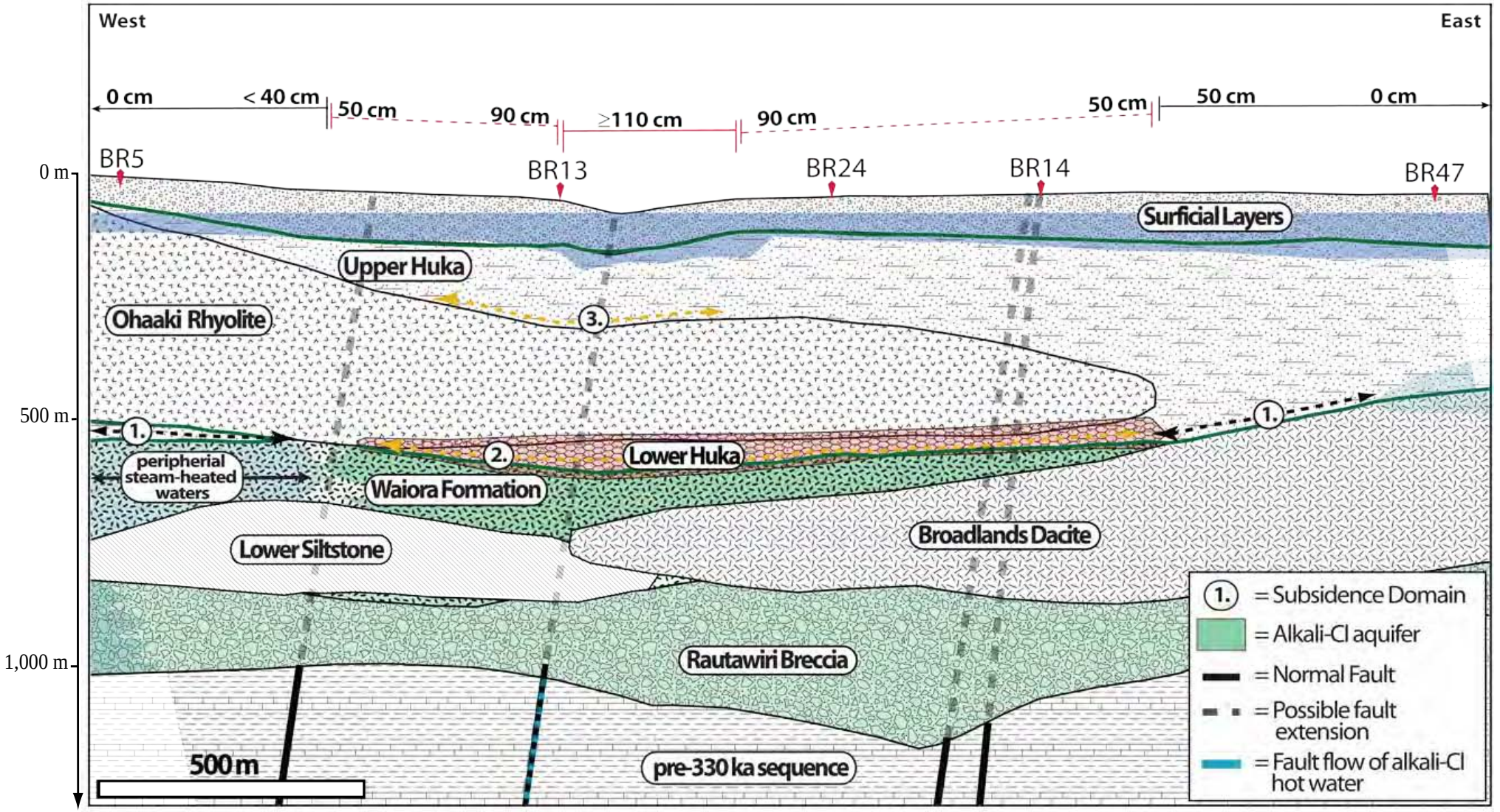


Figure 4.13. Cross section through the central portion of the Ohaaki Reservoir displaying the spatial relationships between reservoir hydrogeology and sub-vertical permeability. Ground subsidence >50 cm is correlated with the extent of the Lower Huka Falls Formation where it directly overlies the Waiora Formation hydrothermal aquifer. Domain 3 denotes possible basal consolidation of the Upper HFF where it overlies the Ohaaki Rhyolite breccia aquifer. Domain 1 corresponds to aquitard consolidation and/or the waning of lateral pressure decline at the base of the HFF towards the margins of hot water reservoir.

# Chapter 5

# Conclusions and Future Research

The objectives of this thesis were to provide a better understanding of the chemical and structural controls of the magnitude, nature, and location of surface fluid flow within the Ohaaki hydrothermal field. In particular I sought to address: (i) the heat and mass flow (emissions) from hydrothermal reservoirs, quantify the changes in surface heat and mass flow following ~20 years of production of the reservoir; (ii) define and better understand the spatial distribution of permeability structures governing fluid flow; (iii) develop source to surface models of fluid flow for both major thermal areas, and; (iv) provide a spatio-structural context to the pattern of pressure-induced ground subsidence. These objectives were achieved through:

1. Quantifying the total surface heat and mass flow for the Ohaaki Field, both prior to production of the field for electrical energy generation and following ~ 20 years of generation.
2. Comparison of the surface heat and mass flow with the chemistry and structure of the Ohaaki Field.
3. Placing the heat and mass flow of the Ohaaki Field within a regional and global context.
4. The generation of detailed maps of surface heat and mass flow from which permeability structures were determined, and integrated structural models of fluid flow from source to surface developed.
5. Placement of the structural controls over fluid flow within the Ohaaki Field into a regional and global perspective.
6. Generation of a model that accounts for the observed spatial variance in the magnitude of pressure-induced ground subsidence across the Ohaaki Field. This new model resulted in predictive models of subsidence risk that can be applied to undeveloped and underdeveloped fields, for which a poro-elastic cap rock occurs within the near surface.

In the following sections I have reviewed the major findings of this thesis and expanded on the global significance of this work. I then conclude with a perspective on future research directions.

## 5.1 Heat and mass flow assessment

The primary outcomes of the initial heat and mass flow assessment of the Ohaaki Field indicate a current $CO_2$ emission rate of 111 ± 6.7 t $d^{-1}$ (40,515 ± 2,445 t $yr^{-1}$), with an associated observed heat flow (i.e., derived from soil temperature measurements) of 70 ± 6.4 MW. These figures contrast with a pre-production emission rate and surface heat flow of 97 t $d^{-1}$ (or ~35,400 t $yr^{-1}$) and 122 MW, calculated from pre-1980 heat flow surveys. These results indicate only minor changes in the net $CO_2$ emission rates for the Ohaaki Field, despite 20 years of production. However, the similarity of $CO_2$ emission rates masks

a 40% increase in $CO_2$ emissions from new areas of intense steaming ground, which is offset by $CO_2$ emission losses associated with the drying up of all steam heated pools and alkali-Cl outflows from the Ohaaki West (OHW) thermal area in response to production-induced pressure decline.

Although soil diffuse degassing has increased by 40% a net decrease of ~ 50 MW (42%) in surface heat flow, following 20 years of production of the field, reflects the drying up of alkali-Cl outflows due to production (Figs. 5.1 and 5.2). The increase in soil diffuse degassing reflects permeability enhancement due to ground subsidence and a possible production-induced increase in the vapour pressure of the steam envelope supplying the OHW thermal area. By comparison, no significant changes are inferred for the surface heat and mass flow associated with the steam-heated Ohaaki East (OHE) thermal area, despite 20 years of production and a deep pressure decline of 7 – 24 bar (ca. 2000). The absence of significant changes at OHE is attributed to the structural isolation of this area from shallow lateral outflows of alkali-Cl hot waters and the presence of a thick vapour phase zone that has buffered the vertical propagation of deep seated pressure decline to the surface (Figs. 5.1 and 5.2).

Of the net $CO_2$ released from the Ohaaki Reservoir, >95% discharges to the atmosphere through the soil zone. Similarly, the majority (>95%) of the current surface heat flow is associated with areas of thermal ground (Fig. 5.1). However, prior to production, the natural heat flow associated with the alkali-Cl hot springs (Ohaaki Pool) and seepage to the Waikato River accounted for ~50% of the natural surface heat flow (Fig. 5.1). Although alkali-Cl outflows were significant in the overall heat budget of the Ohaaki Reservoir, geochemical evidence indicates that >95% of the original dissolved $CO_2$ concentration of these waters was lost prior to discharging at the surface. Therefore, at the surface, alkali-Cl hot waters did not contribute significantly to the pre-production $CO_2$ emissions of the Ohaaki Field.

The thermal ground area normalised $CO_2$ emission rate for the Ohaaki Field equates to 24,500 t $yr^{-1}$ $km^{-2}$. This figure is comparable to normalised $CO_2$ emission rates calculated for the Rotorua hydrothermal field (25,500 t $yr^{-1}$ $km^{-2}$), is four times higher than that calculated for the Karapiti (Wairakei-Tauhara geothermal system) thermal area, and falls within the upper middle range of $CO_2$ emissions calculated for volcanic degassing areas globally. Subsoil $\delta^{13}CO_2$ signatures collected from both thermal areas suggest a two-stage fractionation process for low-flux sites, characterized by boiling during fluid ascent within the underlying reservoir, and subsequent isotopic enrichment as $CO_2$ diffuses through the porous media of the soil zone. For high-flux sites the $\delta^{13}CO_2$ signature is unaffected by near surface (soil zone) fractionation processes, and reflects the composition of the boiled magmatic $CO_2$ source.

From the magnitude of $CO_2$ flux and the total emission rate for a given area it was possible to identify and differentiate between major upflow zones and peripheral thermal areas supplied by steam-heated groundwaters.

## 5.2 Structural and geological controls over fluid flow

Normalising $CO_2$ emissions and heat flow by the area of the high temperature reservoir supports earlier observations that the surface heat flow at Ohaaki is small relative to the size of the high-temperature reservoir. However, when normalised by the area of thermal ground it is apparent that surface fluid discharge at Ohaaki is highly focused (high volume per unit area) relative to other Taupo Volcanic Zone (TVZ) hydrothermal systems. This discovery is consistent with the role of buried or emergent dome complexes at Ohaaki as cross-stratal pathways of high permeability connecting the underlying reservoir to the surface, and bypassing several hundred metres of the poorly permeable Huka Falls Formation (HFF) cap rock.

At OHW, I conclude that after eruption of the Ohaaki Rhyolite dome, extinct vent structures, rooted to the Ohaaki Fault, became preferred pathways for hydrothermal fluids ascending from the underlying West Bank upflow. Subsequently, localised silica deposition cemented the thin mantle of HFF above vent structures and along the Ohaaki west thermal belt (OWTB), favouring hydro-fracturing (hydrothermal eruptions) and giving rise to the concentric distribution of surface thermal activity about the apex of the dome. Conversely, the lack of evidence for thermal activity across the apex of the dome, where the HFF is absent (or very thin), is attributed to the presence of a massive and poorly permeable central lava plug. Therefore, the pattern of high heat and mass flow at OHW is inferred to arise from concentric fractures in the dome, which are charged by vertical fluid flow up along the Ohaaki Fault. These findings confirm earlier interpretations of an eruptive origin for the Ohaaki Rhyolite, and its extrusion along the Ohaaki Fault.

At OHE, fluid flow is governed by a “conduit-barrier” system formed by the propagation of the deep-seated Broadlands Fault to the surface. Although the Broadlands Fault is responsible for enhancing the vertical flow of hydrothermal fluids from the basement and restricting the eastward flow of these fluids, the spatial coincidence of the dome apex and the OHE thermal area suggests that hydrothermal fluids, migrating up the Broadlands Fault at depths of hundreds to thousands of metres, ascend to, and pool, at the top of the dome. Locally the supply of hydrothermal fluids to the dome apex is attributed to the proximity of the Broadlands Dacite reservoir to the surface and the underlying fluid-filled, fractured and faulted basement. The formation of high permeability pathways within the HFF, that mantles the dome, is ascribed to brittle, rather than plastic, deformation of the cap rock due to localised hydrothermal cementation.

To the north and south of the OHE thermal area, soil gas maps show a strong spatial correlation between Rn/Th anomalies and the inferred surface trace of the Broadlands Fault (Koga et al., 1982). The existence of these Rn/Th anomalies supports: (i) the occurrence of the Broadlands Fault at the surface of the OHE thermal area; (ii) its continuity across the greater Ohaaki Field, and; (iii) marked changes in the permeability of this fault in response to sharp spatial changes in the material properties of the Ohaaki Reservoir. Elsewhere across the broader Ohaaki Field, contour plots of the Rn/Th ratio reveal a number of

elongate and NE-trending anomalies that display a strong correlation with the inferred traces of normal faults (Koga et al., 1982). The implications of these findings are that deep-seated normal faults do propagate to the surface, but that the rock properties of the reservoir (especially the HFF) restrict the permeability of these faults, and therefore, mask the dominant physicochemical (heat and mass flow) signature of fault control and the underlying hot water reservoir.

## 5.3 Ground subsidence

Using the models of fluid flow and surface permeability developed in Chapters 2 and 3, I made an assessment of the spatial relationship between permeability and pressure-induced ground subsidence. In this study I demonstrate that the spatial variance in the magnitude of ground subsidence at Ohaaki is readily explained by the structural, hydrogeological and hydrothermal elements of the Ohaaki Reservoir. These elements include: (i) the distribution of subvertical permeability as faults and fractures within the poro-elastic HFF and the connection of this permeability to a liquid pressure domain (i.e., the alkali-Cl reservoir); (ii) the location of vapour versus liquid dominated outflows; (iii) the relative extent and spatial variance of aquifers and aquitards that underlie the HFF, and; (iv) a systematic decline in the pressure drop occurring at the base of the HFF towards the margins of the hot water reservoir.

At OHW I argue that the location and shape of the main Ohaaki subsidence bowl (MOSB) is controlled by the distribution of subvertical permeability, as extinct volcanic vents, which extend as hydrothermal eruption craters up into the HFF. These vents govern: (i) the ascent of alkali-Cl hot waters from the underlying reservoir to the surface (or in the event of a large pressure decline, drainage in the other direction); (ii) the propagation of pressure decline from the reservoir to the surface or near surface; (iii) development and localization of zones of preferential pore fluid drainage, and; (iv) development of localised intense surface depressions (ISD). These findings validate the assertions of a number of workers who advocated for structural control over major subsidence features.

In the absence of subvertical permeability within the HFF, pressure decline is restricted to the basal layers, and is greatest in those regions where the HFF directly overlies an aquifer containing alkali-Cl hot waters. In these instances, consolidation is sub-horizontally (laterally) distributed and the resultant ground subsidence is of low amplitude. Conversely, wherever the HFF directly overlies an aquitard, vertical pressure propagation from the deep reservoir and the corresponding consolidation of the basal layers of the HFF is restricted. This restriction is manifest at the surface of the field as a change in the magnitude of ground subsidence, and in the southern half of the Ohaaki Field is well correlated with the pinching out of the Waiora Formation against the aquitard lavas of the East Broadlands Rhyolite and the Broadlands Dacite.

Although the low amplitude fringe of ground subsidence, < 50 cm, radiating out towards the margins of the field coincides with a prevalence of aquitard lavas, the general decline in the amount of subsidence towards the field margins is explained in terms of a lateral decline in the pressure drop occurring within the deep reservoir. This gradual decline coincides with the extent of the hot water reservoir, which is the

dominant pressure domain. The often noted correlation between both the extent of the hot water reservoir and ground subsidence is therefore a result of the coupled relationship between the hot water reservoir and reservoir pressure.

I conclude this study by noting that the total cumulative subsidence, occurring at any one location across the surface of the Ohaaki Field, may be defined according to the sum of one or more consolidation domains. For example, the total cumulative subsidence of the MOSB is considered the sum of three major subsidence domains acting at different depths beneath the surface. The first domain corresponds to the subvertical permeability developed within the HFF, the second to basal consolidation of the upper HFF above the brecciated carapace aquifer of the Ohaaki Rhyolite dome, and the third, to basal consolidation occurring within the lower HFF where it directly overlies the Waiora Formation. Therefore, by identifying individual consolidation domains the spatial variance in the magnitude of ground subsidence across the surface of the Ohaaki Field is explained.

This model enables areas of potential risk of ground subsidence to be identified for undeveloped or underdeveloped hydrothermal fields.

## 5.4 Contributions to regional and global research endeavors

### 5.4.1 Heat and mass flow assessment

The comparison of the mass flow rates calculated from $CO_2$ flux and observed surface heat flow indicate that a significant portion ($\geq$ 40%) of the ascending steam phase is lost before reaching the soil zone. This observation supports recent findings that $CO_2$ flux provides a more accurate measure of the heat and mass released from volcanic and volcanic-hydrothermal reservoirs than traditional temperature-based measurement of heat flow (Chiodini et al., 2005; Fridriksson et al., 2006). More importantly, these findings raise the possibility that traditional temperature-based measurements of surface heat flow systematically underestimate the heat and mass released from geothermal reservoirs. On the basis of this study, and that of Fridriksson et al. (2006) for the Reykjanes geothermal area, the underestimate of heat and mass release where calculations are based solely on observed heat flow may range as high as 40 – 90% for individual systems. Evidence for such large underestimates has wide-reaching implications for regional (TVZ) and global models of heat and mass flow in volcanic settings (Diez-Gil et al., 1987; Hochstein, 1995; Hurwitz et al., 2003; Chiodini et al., 2005).

Data from this study also contributes to global endeavors to better characterize the source, composition, pathways, and magnitude of magmatic carbon emissions from volcanic environments (Kerrick et al., 1995; Seward and Kerrick, 1996; Chiodini et al., 1999; Mörner and Etiope, 2000; Werner et al., 2000; Bergfeld et al., 2001; Mörner and Etiope, 2002). Furthermore, the statistically guided sampling and simulated modeling of $CO_2$ flux at Ohaaki meets global directives for more studies, providing both a direct measure of greenhouse gas emissions and a measure of the uncertainty of the estimate (IPCC, 1996; GCP, 2003; GHGIS, 2009). This study also demonstrates the utility of $CO_2$ flux surveys for geothermal prospecting. In particular, the finding that the magnitude of $CO_2$ flux, along with the emission rate, can

identify and differentiate between major upflow zones and peripheral steam-heated groundwaters, is of significant value to global exploration endeavours (Klusman et al., 2000; Lewicki and Oldenburg, 2004).

### 5.4.2 Structural and geological controls over fluid flow

One of the more significant outcomes of this study has been the identification of strongly contrasting permeability distributions associated with extinct silicic lava domes. The two examples presented in this study include fluid flow through: (i) remnant dome permeability structures rooted to an underlying source of heated fluids through a conduit and dyke system (hereafter referred to as 'cratered' domes), and; (ii) faulted domes. In both instances domes provide cross-stratal pathways for fluid flow, connecting the underlying reservoir to the surface, by bypassing several hundred metres of poorly permeable cap rock. Therefore, silicic lava domes localise fluid flow through both their eruptive structure and stratigraphy, and by the provision of locally competent and low porosity rock.

The recognition that domes favour fluid flow by acting as cross-stratal pathways has not often been noted (both regionally and globally) with little effort to quantify the role of these structures as geological elements governing the discharge of fluids from large convective systems. However, from a literature survey of the geology and incidence of surface thermal activity within the TVZ hydrothermal field, it is apparent that the Quaternary dome complexes of the TVZ constitute a major pathway of magmatic heat and mass release to the atmosphere long after eruption. This observation departs from, and modifies the view that, faults and associated fracturing dominate the release of fluids at the surface of hydrothermal systems (Curewitz and Karson, 1997). Further, this finding has significant implications for regional and global models of crustal heat and mass transfer, and geothermal prospecting, wherever silicic dome systems overlie large convective hydrothermal systems (Wohletz and Heiken, 1992; Rowland and Sibson, 2004).

In addition to the role of lava domes in focusing fluid flow, this study presents strong evidence for the propagation of deep-seated normal faults to the surface of the Ohaaki Field. Detection of these faults has formerly eluded geological, geophysical and borehole methods, likely as the result of low displacement within the post-330 ka cover sequence, masking by recent alluvium, and most significantly the influence of the material properties of the HFF cap rock over the permeability of these structures. Direct geochemical evidence for the propagation of normal faults to the surface of the Ohaaki Field may have significant implications for the broader Reporoa area, where surficial evidence for faulting is conspicuously absent (Rowland and Sibson, 2004).

The detection of these 'hidden' faults highlights the greater resolution of soil gas surveys, relative to other techniques, in delineating low displacement faults or those masked by the material properties of the reservoir (Ciotoli et al., 1999; Guerra and Lombardi, 2001). The demonstration of sharp permeability contrasts and a conceptual understanding of the role of material properties in fluid flow is critical for a wide range of endeavours globally, including but not limited to: (i) earthquake and volcanic hazard

prediction (Nishimura et al., 1990; Chiodini et al., 1998); (ii) exploration and extraction of geothermal, mineral, and hydrocarbon resources (Hinkle et al., 1986; Bertrami et al., 1990; Klusman et al., 2000; Lewicki and Oldenburg, 2004; Leybourne et al., 2008); (iii) identification and understanding of local and regional tectonic structures (Koga et al., 1982; Baubron et al., 2002; Finizola et al., 2002; Aiuppa et al., 2004); (iv) the sealing effectiveness of geological formations for radioactive waste disposal and carbon sequestration (Gascoyne and Wuschke, 1997; Beaubien et al., 2002; Voltattorni et al., 2008); (v) patterns of exploitation-induced land subsidence (Burbey, 2002; Anderssohn et al., 2008), and; (vi) testing of conceptual models of fluid flow by comparing predicted behaviours against observations of active systems (Heffner and Fairley, 2006).

### 5.4.3 Ground subsidence

Production-induced ground subsidence due to mass withdrawal is a global phenomenon (Gabrysch, 1979; Sun et al., 1999; Li and Gao, 2004; Tomas et al., 2005; Giuseppe et al., 2006; Phien-wej et al., 2006; Hole et al., 2007; Anderssohn et al., 2008; Wang et al., 2009). The majority of studies on ground subsidence due to mass withdrawal have focused on the mechanical and hydrogeological processes responsible, with an impressive number of high quality modeling studies aimed at predicting the future behavior of already subsiding ground (Bau et al., 1999; Allis and Zhan, 2000; White et al., 2005). However, few studies have been able to provide predictive models for undeveloped or underdeveloped hydrothermal reservoirs, for which key stratigraphic units and exploitation characteristics suggest a predisposition to production-induced ground subsidence. Such a model has been absent from the scientific endeavour addressing ground subsidence within the exploited fields of the TVZ.

To my knowledge this thesis provides the first study that demonstrates the structural, hydrogeological and hydrothermal controls governing the spatial variation in the magnitude of ground subsidence at the surface of a TVZ hydrothermal reservoir. The value of this model is its potential to identify areas susceptible to ground subsidence prior to the development of a field, which has significant implications for infrastructure protection and development. Furthermore, a better understanding of the spatial controls over ground subsidence may be used to better guide management strategies aimed at minimising or preventing ground subsidence in prospective or recently developed reservoirs.

## 5.5 Future research directives

At the culmination of this PhD study a number of future research directions are apparent. These include both regional and global endeavors, as well as possible research directions for Mr. Rissmann, such as:

- Additional direct surveys of $CO_2$ flux and heat flow within the TVZ to address the paucity of $CO_2$ emission data for this region (a regional magmatic carbon inventory for the TVZ), and to revise the heat and mass flow release from geothermal reservoirs.
- Application of soil gas surveys to resolve/delineate the hidden or buried faults within the Reporoa Basin and elsewhere throughout New Zealand.

- A quantitative assessment of the influence of Quaternary dome complexes on fluid flow within the TVZ.
- Application of the Ohaaki subsidence model developed in this study to the Wairakei Field, the outcomes of which will guide subsidence risk mapping of undeveloped or underdeveloped hydrothermal reservoirs within the TVZ.
- Additional high resolution surveys of hydrothermal fluid flow about established structural elements (faults and lava domes).
- Further calibration and then deployment of the water-based calorimeter developed in this study to determine the empirical relationship between surface heat flow and boiling point depth for the Ohaaki Field (see Appendix 1).
- Development of a method to determine the uncondensed molar $H_2O/CO_2$ ratio of the vapour phase supplying steam-heated soils. Such a technique is necessary where high mass flow fumarolic vents (focused discharges) are absent. Determination of the molar $H_2O/CO_2$ ratio enables the heat and mass flow, associated with water vapour, to be calculated from $CO_2$ flux data (see Appendix 2).
- Comparison of soil gas compositional analyses (major, trace, and hydrocarbon species) collected during this study, with deep reservoir fluids, so as to better understand changes in hydrothermal fluid composition during ascent. This study would seek to establish the exploration potential of detailed soil gas sampling in reconstructing deep reservoir temperatures, fluid composition and source magmas.
- Application of soil gas techniques for hydrocarbon, mineral and geothermal exploration.

As outlined in the above sections these research directives have both regional and global significance. Of the above directions, I am particularly interested in further $CO_2$ and heat flow work with the intention of providing a regional emissions and heat flow inventory for the TVZ. Such work would also seek to address regional spatial trends in carbon emissions and source signatures, as well as carbon-loading within regional aquifers. It is hoped that the methodologies and instrumentation I have developed during this thesis will equip me to achieve this goal. Another area of particular interest is the application of soil gas and hydrochemical surveys to better understand the role of faults and fractures in the migration of fluids.

## 5.6 References

Aiuppa, A., Caleca, A., Federico, C., Gurrieri, S. and Valenza, M., 2004. Diffuse degassing of carbon dioxide at Somma-Vesuvius volcanic complex (Southern Italy) and its relation with regional tectonics. Journal of Volcanology and Geothermal Research, 133(1-4): 55-79.

Allis, R.G. and Zhan, X., 2000. Predicting subsidence at Wairakei and Ohaaki geothermal fields, New Zealand. Geothermics, 29(4-5): 479-497.

Anderssohn, J., Wetzel, H.-U., Walter, T.R., Motagh, M., Djamour, Y. and Kaufmann, H., 2008. Land subsidence pattern controlled by old alpine basement faults in the Kashmar Valley, northeast Iran; results from InSAR and levelling. Geophysical Journal International, 174(1): 287-294.

Bau, D., Gambolati, G. and Teatini, P., 1999. Residual land subsidence over depleted gas fields in the northern Adriatic Basin. Environmental & Engineering Geoscience, 5(4): 389-405.

Baubron, J.-C., Rigo, A. and Toutain, J.-P., 2002. Soil gas profiles as a tool to characterise active tectonic areas: the Jaut Pass example (Pyrenees, France). Earth and Planetary Science Letters, 196(1-2): 69-81.

Beaubien, S.E., Lombardi, S. and Voltattorni, N., 2002. Radon studies for investigation of nuclear waste deposits and natural emissions. In: J. Klerkx and B. Imanackunov (Editors), NATO Science Series. Series IV, Earth and Environmental Sciences, vol. 13. Kluwer Academic Publishers, Dordrecht, pp. 245-260.

Bergfeld, D., Goff, F. and Allard, P., 2001. High $CO_2$ flux measurements in volcanic and geothermal areas, methodologies and results. Chemical Geology, 177(1-2): 1-1.

Bertrami, R., Buonasorte, G., Ceccarelli, A., Lombardi, S., Pieri, S. and Scandiffio, G., 1990. Soil gases in geothermal prospecting; two case histories (Sabatini Volcanoes and Alban Hills, Latium, central Italy). Journal of Geophysical Research, 95(B13): 21,475-21,481.

Burbey, T.J., 2002 The influence of faults in basin-fill deposits on land subsidence, Las Vegas Valley, Nevada. Hydrogeology Journal, 10(525-538).

Chiodini, G., Frondini, F., Kerrick, D.M., Rogie, J., Parello, F., Peruzzi, L. and Zanzari, A.R., 1999. Quantification of deep $CO_2$ fluxes from central Italy; examples of carbon balance for regional aquifers and of soil diffuse degassing. In: J.-L. Probst, H. Faure and J. Veizer (Editors), Chemical Geology. Elsevier, Amsterdam, pp. 205-222.

Chiodini, G., Granieri, D., Avino, R., Caliro, S., Costa, A. and Werner, C., 2005. Carbon dioxide diffuse degassing and estimation of heat release from volcanic and hydrothermal systems. Journal of Geophysical Research, 110: no.B8, 17.

Ciotoli, G., Etiope, G., Guerra, M. and Lombardi, S., 1999. The detection of concealed faults in the Ofanto Basin using the correlation between soil-gas fracture surveys. Tectonophysics, 301(3-4): 321-332.

Contact Energy, 2006. Production well geochemical data – Ohaaki Reservoir, Contact Energy Ltd, New Zealand.

Contact Energy, 2007. Pressure Point Data - Ohaaki Reservoir, Contact Energy Ltd, New Zealand.

Curewitz, D. and Karson, J.A., 1997. Structural settings of hydrothermal outflow; fracture permeability maintained by fault propagation and interaction. Journal of Volcanology and Geothermal Research, 79(3-4): 149-168.

Diez-Gil, J.L., Arana, V., Ortiz, R. and Yuguero, J., 1987. Stationary convection model for heat transfer by means of geothermal fluids in post eruptive systems. Geothermics, 16(1): 77-89.

Finizola, A., Sortino, F., Lénat, J.-F. and Valenza, M., 2002. Fluid circulation at Stromboli volcano (Aeolian Islands, Italy) from self-potential and $CO_2$ surveys. Journal of Volcanology and Geothermal Research, 116(1-2): 1-18.

Gabrysch, R.K., 1979. Land-surface subsidence in Houston-Galveston region, Texas, AAPG Bulletin. American Association of Petroleum Geologists, Tulsa, pp. 455-456.

Gascoyne, M. and Wuschke, D.M., 1997. Gas migration through water-saturated, fractured rock; results of a gas injection test. Journal of Hydrology, 196(1-4): 76-98.

GCP, 2003. Global Carbon Project Report No. 1: Science Framework and Implementation. Report No. 1, Earth System Science Partnership (IGBP, IHDP, WCRP, DIVERSITAS), Canberra, Australia.

GHGIS, 2009. Global Greenhouse Gas Information System Interagency Workshop on Needs and Capabilities. In: Riley Duren et al. (Editors), Global Greenhouse Gas Information System Interagency Workshop on Needs and Capabilities, Albuquerque, New Mexico.

Giuseppe, G., Pietro, T. and Massimiliano, F., 2006. Anthropogenic land subsidence. Dixue Qianyuan = Earth Science Frontiers, 13(1): 160-178.

Guerra, M. and Lombardi, S., 2001. Soil-gas method for tracing neotectonic faults in clay basins: the Pisticci field (Southern Italy). Tectonophysics, 339(3-4): 511-522.

Heffner, J. and Fairley, J., 2006. Using surface characteristics to infer the permeability structure of an active fault zone. Sedimentary Geology, 184: 255-265.

Hinkle, M.E., Sato, M., Matsuo, S. and King, C.-Y., 1986. Using volatile constituents of soils and soil gases to determine the presence of copper-zinc ore bodies at Johnson Camp, Arizona, Journal of Geophysical Research. American Geophysical Union, Washington, pp. 12,359-12,365.

Hochstein, M.P., 1995. Crustal heat transfer in the Taupo volcanic zone (New Zealand): comparison with other volcanic arcs and explanatory heat source models. Journal of Volcanology and Geothermal Research, 68(1-3): 117-151.

Hole, J.K., Bromley, C.J., Stevens, N.F. and Wadge, G., 2007. Subsidence in the geothermal fields of the Taupo volcanic zone, New Zealand from 1996 to 2005 measured by InSAR. Journal of Volcanology and Geothermal Research, 166(3-4): 125-146.

Hurwitz, S., Kipp, K.L., Ingebritsen, S.E. and Reid, M.E., 2003. Groundwater flow, heat transport, and water table position within volcanic edifices; implications for volcanic processes in the Cascade Range. Journal of Geophysical Research, 108: no.B12, 19.

IPCC, 1996. IPCC Guidelines for national greenhouse gas inventories. Accessed May 2008, http://www.ipcc.ch.

Kerrick, D.M., McKibben, M.A., Seward, T.M. and Caldeira, K., 1995. Convective hydrothermal $CO_2$ emission from high heat flow regions. Chemical Geology, 121(1-4): 285-293.

Klusman, R.W., Moore, J.N. and LeRoy, M.P., 2000. Potential for surface gas flux measurements in exploration and surface evaluation of geothermal resources. Geothermics, 29(6): 637-670.

Koga, A., Taguchi, S. and Mahon, W.A.J., 1982. The use of volatile constituents in geothermal fluids for assessing the type, potential and near surface permeability of a geothermal system; the Broadlands geothermal area, N.Z, Proceedings of Pacific Geothermal Conference, vol.4. University of Auckland Geothermal Institute, Auckland, pp. 135-138.

Lewicki, J.L. and Oldenburg, C.M., 2004. Strategies for Detecting Hidden Geothermal Systems by Near-Surface Gas Monitoring, Lawrence Berkeley National Laboratory

Leybourne, M.I., Cameron, E.M., Rissmann, C.F.W. and Miller, N.R., 2008. Understanding water sources, age and flow paths in hydrochemical exploration; constraints from stable and radiogenic isotopes in the hyper-arid Atacama Desert, Chile, Geochimica et Cosmochimica Acta. Elsevier, New York, pp. A539.

Li, Y. and Gao, G., 2004. Ground subsidence in areas of loose porous aquifers. Acta Geologica Sinica, 78(3): 829-837.

Mörner, N.-A. and Etiope, G., 2002. Carbon degassing from the lithosphere. Global and Planetary Change, 33(1-2): 185-203.

Phien-wej, N., Giao, P.H. and Nutalaya, P., 2006. Land subsidence in Bangkok, Thailand. Engineering Geology, 82(4): 187-201.

Rowland, J.V. and Sibson, R.H., 2004. Structural controls on hydrothermal flow in a segmented rift system, Taupo volcanic zone, New Zealand. Geofluids, 4(4): 259-283.

Seward, T.M. and Kerrick, D.M., 1996. Hydrothermal $CO_2$ emission from the Taupo Volcanic Zone, New Zealand. Earth and Planetary Science Letters, 139(1-2): 105-113.

Sun, H., Grandstaff, D. and Shagam, R., 1999. Land subsidence due to groundwater withdrawal; potential damage of subsidence and sea level rise in southern New Jersey, USA. Environmental Geology, 37(4): 290-296.

Tomas, R., Marquez, Y., Loepez-Sanchez, J.M., Delgado, J., Blanco, P., Mallorqui, J.J., Martinez, M., Herrera, G. and Mulas, J., 2005. Mapping ground subsidence induced by aquifer overexploitation using advanced differential SAR interferometry; Vega Media of the Segura River (SE Spain) case study. Remote Sensing of Environment, 98(2-3): 269-283.

Voltattorni, N., Cinti, D., Pizzino, L., Quattrocchi, F. and Sciarra, A., 2008. Study of natural gas leakages for the risk assessment of $CO_2$ geological storage.

Wang, G.Y., You, G., Shi, B., Yu, J. and Tuck, M., 2009. Long-term land subsidence and strata compression in Changzhou, China. Engineering Geology, 104(1-2): 109-118.

Werner, C., Brantley, S.L. and Boomer, K., 2000. $CO_2$ emissions related to the Yellowstone volcanic system; 2, Statistical sampling, total degassing, and transport mechanisms. Journal of Geophysical Research, 105(B5): 10831-10846.

White, P.J., Lawless, J.V., Terzaghi, S., Okada, W., 2005. Advances in subsidence modelling of exploited geothermal fields. In: Proceedings of the 2005 World Geothermal Congress, April, Antalya, Turkey, Paper 222, 10 pp.

Wohletz, K. and Heiken, G., 1992. Volcanology and Geothermal Energy. University of California Press, Berkeley.

## 5.7 Figures

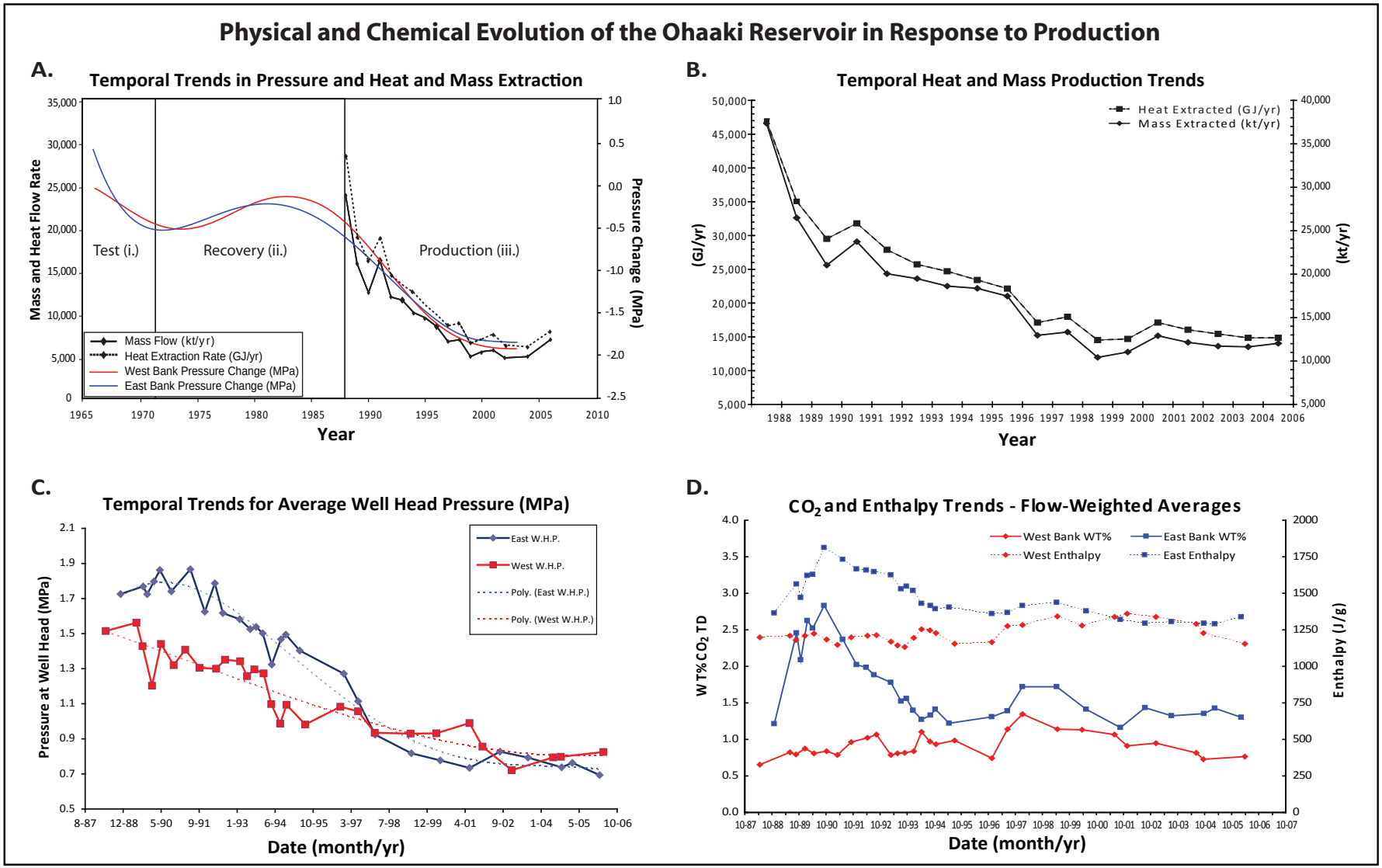


Figure 5.1. Conceptual diagrams displaying the temporal evolution of physical and chemical characteristics of the Ohaaki Reservoir in response to production. A. Characteristic trends at Ohaaki due to development. Pressure changes are based on production well data for the deep reservoir (≥ -161 m RmL), where: (i.) Test Discharge Period, (ii.) Recovery Period, and (iii.) Production Period. B. Enlargement of the temporal trend in heat and mass production from the Ohaaki Reservoir. An initial steep decline in heat and mass extraction in the first two years of production is followed by a more gradual decline and the eventual flattening of the curve as the system appears to approach a steady state. C. Temporal trend of average well head pressure (W.H.P.). Here a sharp decline in W.H.P. over the first 10 years of production is followed by a more gradual decline and eventual flattening for both East- and West Bank reservoirs and appears to approach a steady state. D. Trends in weight % $CO_2$ and enthalpy of production fluids from West and East Bank reservoirs. Flow weighted averages for the East Bank reservoir display an initial spike in WT% $CO_2$ and enthalpy in response to production of the reservoir and then decline sharply before flattening out. West Bank production fluids do not show any spike in WT% $CO_2$ or enthalpy and vary little over the time period displayed. All data from Contact Energy (2006, 2007).

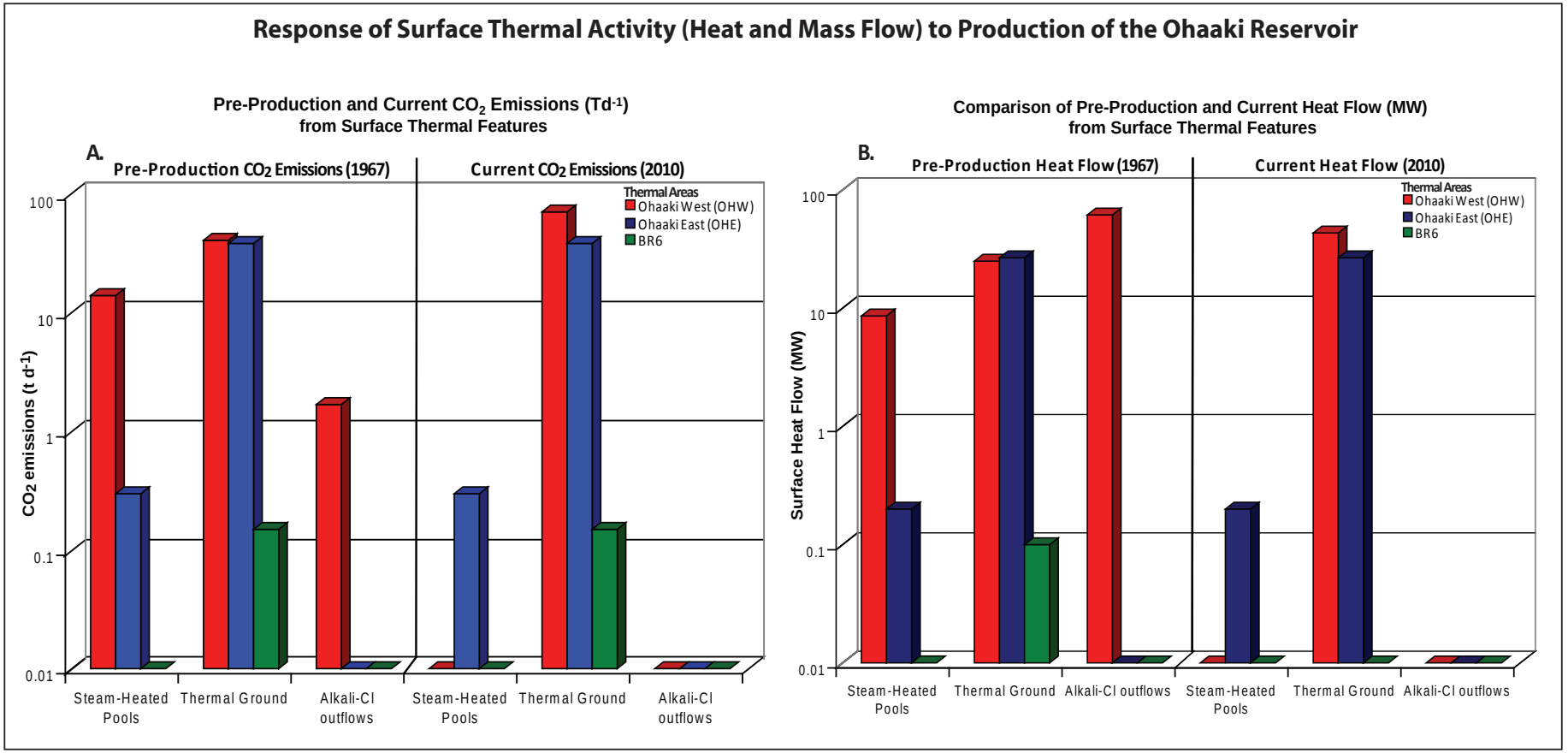


Figure 5.2. Response of surface thermal features to 20 years of production of the Ohaaki Reservoir. A. Inventory of pre-production (1967) and current (2010) $CO_2$ emission signatures from various surface thermal features occurring within the Ohaaki West (OHW), Ohaaki East (OHE) and BR6 thermal areas. The main changes have been: (i) the decline in $CO_2$ emissions from steam-heated pools and alkali-Cl outflows, within the OHW thermal area, in response to the drying up of these features due to production-induced pressure decline of the Ohaaki Reservoir (see Fig. 5.1), and; (ii) an increase in the extent and consequently the contribution of thermal ground $CO_2$ emissions due to fracturing of the HFF in response to production-induced ground subsidence within the OHW thermal area (see Chapter 2 and 4 and Fig. 2.8). B. Inventory of pre-production (1967) and current (2010) surface heat flow from various surface thermal features within the Ohaaki West (OHW), Ohaaki East (OHE) and BR6 thermal areas. The main changes have been: (i) the loss of a large heat flow signature associated with the alklai-Cl outflows (~61.5 MW) and steam-heated pools (~9 MW) from the OHW thermal area in response to the drying up of these features due to production-induced pressure decline of the Ohaaki Reservoir (see Fig. 5.1), and; (ii) an increase in the extent of thermal ground and consequently surface heat flow by ~16 MW due to fracturing of the HFF in response to production-induced ground subsidence within the OHW thermal area (see Chapter 2 and 4 and Fig. 2.8). A and B. The lack of a significant change in surface heat flow and $CO_2$ emissions associated with the OHE thermal area despite 20 years of production is attributed to the buffering of deep-seated pressure decline by a thick vapour-phase zone that exists beneath this thermal area (Chapter 2 & 3).

# Appendix 1.

# Development of a water-based calorimeter for surface heat flux assessment

**Clinton Rissmann[a] and Stefan Lendnal[b]**

[a]*Department of Geological Sciences, University of Canterbury, Private Bag 4800, Christchurch, New Zealand*

[b]*Syft Technologies, P.O. Box 28149, New Zealand*

## Contributions

The original design of the calorimeter is based on that of Hochstein and Bromley (2002, 2005). Important design modifications were made through discussion between Mr. Rissmann and Mr. Lendnal. Mr. Lendnal constructed the calorimeter and designed the electronics. Several improvements were made to the instrument after initial field testing by Mr. Rissmann. The calibration rig was designed and constructed by Mr. Rissmann. The electronic configuration for monitoring power input to the calibration rig was designed and implemented by Mr. Lendnal. All field testing was carried out by Mr. Rissmann. Laboratory trials were a joint effort between Mr. Rissmann and Mr. Lendnal.

## A1.1 Introduction

A number of studies, both within the Taupo Volcanic Zone (TVZ) and globally, have utilised empirical power law functions, developed for the Wairakei hydrothermal field, to assess the total heat flux of volcanic and volcanic hydrothermal fields (Dickinson, 1967; Sorey and Colvard, 1994; Allis et al., 1999; Mongillo and Graham, 1999; Fridriksson et al., 2006). Empirical functions were first developed by Banwell et al. (1957), refined by Thompson et al. (1964) and then recast by Dawson (1964). These functions were based on the observed relationship between total surface heat flux, $Q_{tot}$ in W/m$^2$, and soil temperature, at a given reference depth (Tz, most commonly 0.15 m) or boiling point depth ($z_{BP}$).

A criticism of applying the Wairakei empirical functions to other hydrothermal areas is the possibility that variances in the soil physical properties, and/or differing $CO_2/H_2O$ molar ratios of the vapour phase supplying these areas, may govern a unique relationship between surface heat flux and soil temperature. In such instances the Wairakei empirical functions may not correctly represent the surface heat flux. Furthermore, the large uncertainty (scatter), poor reproducibility, and small number of observations on which the Wairakei

empirical functions were based, result in large uncertainty and low predictive power (Banwell et al., 1957; Dawson, 1964; Robertson and Dawson, 1964; Thompson et al., 1964). In particular, the empirical functions developed for reference depths of 0.15 and 0.35 m show significant scatter (Banwell et al., 1957; Dawson, 1964; Robertson and Dawson, 1964; Thompson et al., 1964).

Recently, Hochstein and Bromley (2002) designed a new water-filled calorimeter so as to readdress the relationship between surface heat flux and soil temperature within the Wairakei Field (Karapiti thermal area). Through calorimeter design improvements, laboratory testing, and calibration, these authors made repeat measurements of the total surface heat flux (the combined convective and conductive heat flux) and soil temperature gradients at 24 sites. Repeat measurements at all 24 sites, made during the summer months over successive years, display a range between 0.03 and 2.0 $kW/m^2$ for total surface heat flux. At four sites repeat heat flux measurements over the course of several days and weeks were shown to differ from the mean by <7%. This high reproducibility is a first in calorimeter studies.

Repeat measurement of the soil temperature gradient, before and after placement of the calorimeter, reveal small irregular changes, typically <1ºC, in the temperature records from shallow depths (about 0.05 m) beneath the calorimeter (Hochstein and Bromley, 2002). Hochstein and Bromley (2002) describe a decrease of between 1ºC and 3°C at 0.01 m depth, at 8 out of 12 sites where spatial temperature measurements were taken before and after the calorimeter survey. These small temperature changes were responsible for an increase in near-surface temperature gradients of between 3 and 10%, which increased the conductive flux component. These results indicate that deployment of the calorimeter for periods of 5 minutes did not greatly perturb the vapour stream (Hochstein and Bromley, 2002). From the successful campaign of Hochstein and Bromley (2005) a new empirical power law function was defined for the relationship between total surface heat flux and boiling point depth.

Despite the contribution of Hochstein and Bromley (2005) to the improved accuracy and reproducibility of heat flux measurements, the question surrounding the applicability of the Wairakei empirical heat flux soil temperature function to other fields is still untested. Therefore, in this Appendix we describe the design and calibration of our own water-filled calorimeter, which is to be deployed to define the empirical relationship between total surface heat flux, and boiling point depth at Ohaaki, as part of a future study.

## A1.2 Heat transfer in steaming ground

Thermal activity develops at the surface of a hydrothermal reservoir wherever sufficient vertical permeability exists for fluids to ascend from the underlying reservoir to the surface. Whether the thermal area is fed purely by an ascending vapour phase, or by a liquid hot water component, will depend on the nature of the hydrothermal reservoir (vapour- or liquid-dominated), the prevalence of two-phase conditions (i.e., non-

condensable gas concentrations), proximity to a major upflow zone, and whether vertical permeability is sufficiently evolved for the passage of alkali-Cl hot waters.

Heat and mass transfer from an underlying two-phase reservoir, to an area of surface thermal activity, occurs as an advective plume of hot water vapour (steam), and $CO_2$ ascends through the reservoir to the surface. The water vapour within the ascending plume condenses near the surface of the soil, forming a liquid condensate layer. Droplets of liquid condensate then migrate downwards under gravity, developing a counter-flux to the ascending vapour phase. Conversely, the $CO_2$ component of the ascending vapour phase does not condense within the soil profile, and in most instances ascends through the condensate layer to the surface (Corey and Brooks, 1997; Dane et al., 1997; Chiodini et al., 2005; Hochstein and Bromley, 2005). However, if the soil becomes saturated by aqueous condensate or soil water, the flux of $CO_2$ may be impeded (Evans et al., 2001; Granieri et al., 2003; Hochstein and Bromley, 2005; Fridriksson et al., 2006).

Although $CO_2$ forms an important component of the advective plume, it contributes little to the overall heat flux at the surface (Todesco et al., 2003; Chiodini et al., 2005). However, the ratio of water vapor to non-condensable gas (primarily $CO_2$) does influence the heat transfer capacity of the plume, by facilitating higher advective heat transfers, at lower temperatures, for low ratios of $H_2O$ to $CO_2$ (Chiodini et al., 2005). Conversely, at high ratios of water vapour to $CO_2$ (low $CO_2$ concentrations within the ascending plume) the contribution of the heat transported by water vapour to the total heat flux quickly decreases with declining temperatures (McKibbin and Pruess, 1989; Chiodini et al., 2005).

Above the zone of aqueous condensation the mass flux of water vapour is typically minor, and heat transfer is dominated by conduction, resulting in top-down linear soil temperature profiles (Chiodini et al., 2005; Hochstein and Bromley, 2005). The tendency for water vapour to condense within the upper portion of the soil profile gives rise to the observation that almost all of the energy conveyed by advection at depth is transferred primarily by conduction in the upper part of the soil (Bromley and Hochstein, 2005; Chiodini et al., 2005; Hochstein and Bromley, 2005). However, in some instances convective heat transfer may constitute a significant (>15 - 50%) portion of the total ($Q_{tot}$) heat flux (Chiodini et al., 2005; Hochstein and Bromley, 2005). The convective heat transfer component is especially important when the mass flux of steam through the soil is very large, or where the molar ratio of water vapour to noncondensable gases is small (i.e., $x_{H_2O}/x_{GAS} = < 1.0$, due to high noncondensable gas content in the ascending plume) (Chiodini et al., 2005; Hochstein and Bromley, 2005).

In summary, the dominant component processes responsible for the transfer of heat and mass to the surface of hydrothermal reservoirs includes: (i) advective transport of water vapour (heat) and $CO_2$ at depth; (ii) condensation of water vapour and ensuing conductive heat transfer within the near surface, and; (iii)

combined advective-diffusive gas transport of $CO_2$ within the near surface. Other mechanisms involved in lesser transfer of heat and mass within the near surface include diffusion, evaporation, and capillary draw (Bromley and Hochstein, 2005; Chiodini et al., 2005; Hochstein and Bromley, 2005).

## A1.3 Measuring heat flux

Total heat flux ($Q_{tot}$) from the surface of an area of thermal ground is the sum of the conductive ($Q_{cond}$) and convective ($Q_{conv}$) flux given in W/m$^2$. The convective component relates to the transfer of heat by a mobile vapour phase (water vapour), whereas the conductive component accounts for the transfer of thermal energy along a temperature gradient. Total heat flux may therefore be computed from:

$$Q_{tot} = Q_{conv} + (Q_{cond} + \Delta Q_{dy}) \quad (1)$$

where $\Delta Q_{dy}$ is a seasonal component, which in colder seasons causes a decline of ground temperatures and boiling point depth. During the summer months, and assuming dry weather (≥ 5 days without rain), $\Delta Q_{dy}$ is sufficiently small as to be negligible (Hochstein and Bromley, 2005).

The proportions of the conductive and convective heat flux components at any one site vary with the soil temperature gradient and the physical properties of the soil (Bromley and Hochstein, 2001; Hochstein and Bromley, 2002). The conductive heat transfer for a given depth may be calculated by Fourier's Law:

$$Q_{cond} = -\lambda_{soil}(dT/dz) \quad (2)$$

where $Q_{cond}$ is the conductive heat flux in Wm$^{-2}$, $\lambda_{soil}$ is the bulk thermal conductivity of the soil (W m$^{-1}$ ºC$^{-1}$) at depth z, and $d$T/$d$z is the temperature gradient in (ºC m$^{-1}$). However, the convective heat flux component, the mobile vapour phase ascending through the soil to the atmosphere, cannot be measured directly (Bromley and Hochstein, 2001; Newson et al., 2001; Hochstein and Bromley, 2002). An indirect assessment of the convective component can be obtained by measuring the total heat flux ($Q_{tot}$) at the surface since:

$$Q_{conv} = (Q_{tot} - Q_{cond}) \quad (3)$$

## A1.4 Construction of a water calorimeter for thermal ground

The total surface heat flux, $Q_{tot}$, can be measured by a water-filled ground calorimeter (Banwell et al., 1957; Hochstein and Bromley, 2002; Hochstein and Bromley, 2005). A closed calorimeter, containing a water cell, was preferred due to the poor reproducibility of measurements by open calorimeters (air calorimeter or

differential psychometer) (Banwell et al., 1957). Our closed calorimeter uses water, with its high heat capacity as the transfer medium. The calorimeter design is shown in Figs. A1.1 and A1.2.

To minimise losses from the ground to the water cell we used a thin (1.0 mm) aluminium plate that was mounted to a mantle (20 mm thickness) of polytetrafluoroethylene (PTFE). PTFE was preferred due to its stability at high temperatures, resistance to acidic conditions, low thermal conductivity (0.25 W/mK at 25ºC), and low thermal diffusivity (0.093 – 0.097 $mm^2/s$). The lid (15 mm thickness) was also constructed from PTFE. To minimise conductive losses or gains the PFTE lid was fixed to a circular section of medium density fibreboard (MDF of 0.12 - 0.15 W/mK at 25ºC), which houses an insulating layer, 50 mm thick, of expanded polystyrene foam (0.03 W/mK at 25ºC). The polystyrene foam was adhered and sealed by silicon adhesive to the MDF sheet, and the foam reservoir was capped by a MDF lid of 20 mm thickness. The PTFE mantle was insulated by 25 mm of Armaflex® foam (0.038 W/mK at 25ºC). The MDF top of the calorimeter was then painted with white enamel and finished with highly reflective aluminium tape.

Five mini-thermistors of low output impedance and small thermal capacity were used as temperature sensors, two deployed within the water cell, two countersunk (5 mm and 10 mm, respectively) into the PTFE lid beneath the insulating double layer of MDF and polystyrene, with the fifth monitoring ambient air temperature outside of the calorimeter. The water cell was mixed by a stirrer fixed to a reduction gear box and driven by a small DC motor, which turned the stirrer at c. 0.5 revolution per second (Fig A1.2). The heat generated by the mechanical work of the stirrer is small (< 0.3 W) and can be ignored. The electronics were housed above the polystyrene layer within the MDF top and consist of a microprocessor that interfaces to: (i) an array of thermistors; (ii) on/off switch (independent control of stirrer and logging); (iii) stirrer control circuit, and; (iv) an SD card for logging the temperature-time data (Fig. A1.2). The thermistors have a small amount of signal conditioning to ensure that there is a high level of accuracy of measurement. The temperature output of each thermistor is logged to the SD memory card each second for the measurement duration.

## A1.5 Laboratory testing

### A1.5.1 Efficiency testing

The calorimeter was calibrated within an electronics laboratory under constant air temperature (20.0ºC ± 2.0ºC). The calorimeter was placed on a testing rig constructed from a block of Formathane® (polyisocyanurate) of dimensions 100 mm x 400 mm x 400 mm (Fig. A1.3). Formathane was selected for its low thermal conductivity (0.02 W/mK), and stability at temperatures of up to 140ºC. A circular area slightly (0.5 mm) larger than the base of the calorimeter (0.023 $m^2$) was recessed by 5 mm into the formathane block, into which tightly coiled heating cable (O.D. of 1.0 mm), insulated with silicone rubber, (O.D. 2.9 ± 0.1 mm)

was placed. Heating cable was preferred over a heating plate or block due its low thermal mass and hence negligible heat storage capacity (<0.01 kJ). The resistance (2 ohm/m) and length (10 m) of the cable was chosen so as to comfortably accommodate the maximum heat flux of 4.0 kW/m$^2$ reported in the literature. The power to the heating cable was supplied by a regulated DC source. Two calibrated multi-meters were used to accurately measure input power; one measuring current (amps) and the other voltage (V). The heating cable was terminated in a four-wire configuration so that the voltage, in parallel, was monitored at the input of the heating cable, providing a more accurate measure of power input. The temperature of the coiled heating cable (heating pad) was also monitored by a K-type thermocouple and a digital meter.

From the known material constants it was estimated that the aluminium bottom plate (0.07 kg) and the PTFE mantle (0.80 kg) can store *c.* 1.0 kJ when their temperature is raised by 1ºC (neglecting transients). The PTFE lid (0.6 kg) can also store up to 0.7 kJ when its temperature is raised by 1ºC. This heat is most likely associated with the latent heat of minor vapour ascending from the water cell to the lid, within the tightly sealed calorimeter, when the temperature of the water in the calorimeter exceeds the lid temperature. To account for the anomalous heat, AQ, transferred to the water cell within the calorimeter we followed the protocol of Hochstein and Bromley (2002):

$$AQ = mc(T_2 - T_1) + L(b + m) + L(l) \quad (4)$$

where *m* and *c* denote the mass and specific heat of water within the calorimeter and $T_1$ and $T_2$ are the mean temperatures of liquid water at the start time (time $T_1$) and the end time of the monitoring period ($T_2$). The terms L(b+m) and L(l) describe the minor heat storage components for the bottom and mantle and the lid of the calorimeter, respectively (Hochstein and Bromley, 2002).

Due to a malfunction of the calorimeter thermistors the calibration phase was limited to two measurement cycles, with an imposed heat flux of 9.26 W (or ~408 W/m$^2$). Each measurement consisted of two five minute heating cycles (on the heating plate), separated by two five minute cooling cycles (calorimetry was removed from the heating plate and placed on a foam block) (Figs. A1.3). The resultant values of AQ were then compared with the known heat input (W) into the base of the calorimeter, which indicated an error of the order +1 to +5 % (for ($T_2 - T_1$) <5ºC) (Fig. A1.4 and Table A1.1). Further calibration is planned for the future, once technical issues with the calorimeter thermistors are resolved.

### A1.5.2 Heat transfer testing

Any temperature difference between the water and the lid of the calorimeter may induce minor heating or cooling that can cause a small drift in water temperature (Hochstein and Bromley, 2002, 2005).

Consequently, we sought to quantify the influence of water temperature on lid drift, and that of lid temperature on the drift within the water cell, and hence any influence on $Q_{tot}$. During both different trials the calorimeter was seated on the formathane calibration rig so as to minimise losses or gains through the thin aluminum base of the calorimeter.

The role of lid temperature on the water drift was assessed by heating the lid separately, and then placing the lid on the water cell. After each trial the water cell was emptied and left to equilibrate with ambient air temperature before refilling. The imposed temperature differences between the heated lid and the water cell were 5ºC, 11.65ºC and 26ºC, respectively. Despite constant cooling over the duration of the trial the lid temperature was never lower than that of the water in the cell. This was important to ensure heat flux was occurring only in one direction (i.e., from the lid to the water cell). The recorded heat flux from the lid to the water cell was calculated by:

$$Q_{lid} = \frac{mc(\Delta T_{cell} / \Delta t)}{A} \quad (5)$$

where $m$ is the water mass, $c$ its specific heat of water (4187 J/g/ºC), $T_{cell}$ is the average temperature of the water cell, and A is the area of the calorimeter lid. The uncertainty in computing the mean ($\Delta T_{cell}/\Delta t$) values of the water cell was reduced by using a least squares linear fit applied to successive segments of the record. The heat flux from the lid ($Q_{lid}$) into the air space above the water cell was calculated by Fourier's Law ($W/m^2$); given the known thermal conductivity of PTFE and the respective depths of both thermistors (5 mm and 10 mm) within the PTFE lid (Eq. 2).

Although the calculation of heating rate was complicated by the cooling of the lid, the conductive heat flux within the PTFE lid was always much larger (3 - 10 times) than the heat transfer to the water cell. This is to be expected as the thermal conductivity of the air space (both dry and saturated air) between the warm lid and the cooler surface of the water within the cell is small (i.e., between 0.025 to 0.027 W/mK over the temperature range of these trials and from 0% - 100% humidity) (Tsilingiris, 2008). Nonetheless, a mean heat flux to the water cell of 1.1 W, 1.85 W and 3.8 W was calculated for imposed temperature differences of 5ºC, 11.65ºC and 26ºC in the three trials. These results demonstrate a potentially significant heat gain from the lid in situations where the lid temperature is allowed to exceed the water temperature within the cell. This situation can be avoided in the field either by moving from cooler to warmer sites (lower to higher heat flux), or quenching the lid with cold water and then allowing the lid to equilibrate with ambient air temperature.

At this stage there is insufficient data on the influence of lid temperature drift on the heating rate within the water cell. In addition to failure of the thermistors, the calibration rig also malfunctioned during later trials.

Therefore, further testing is required, at both lower and higher imposed heat flux values, to assess the role of lid temperature drift on the flux of heat through the base of the calorimeter.

## A1.6 Future work

Surface heat flow data was measured from a number of sites at Ohaaki (15 in total) and from a few sites at Karapiti and Ngatamariki. However, repeat failure of the calibration rig and calorimeter thermistors during the laboratory testing has hampered the interpretation of this data. Currently, a generation II calorimeter is being built with a conformably coated circuit board, and refined PT1000 thermistors of greater sensitivity and reliability. These sensors will be self-calibrating. Furthermore, the calibration rig is being redeveloped with involvement from the Chemical Engineering Faculty at the University of Canterbury. The aims of this future collaboration are to: (i) calibrate the machine over a wide range of imposed heat flow values; (ii) better understand the role of temperature drift within the lid on the heating response of the water cell, and; (iii) make any necessary modifications to the instrumentation to improve efficiency.

From these aims we hope to: (i) apply the lid drift correction factors to data collected from Ohaaki; (ii) make additional measurements of surface heat flow and boiling point depth at Ohaaki during the summer months of 2011 (i.e., January and February); (iii) develop an empirical power-law function for surface heat flow and boiling point depth for the Ohaaki Field, and; (iv) contrast the nature of this new power-law function with that of Dawson (1964), and Hochstein and Bromley (2005). From these outcomes we can address the technical concerns raised in the review in Chapter 2, and address concerns over the application of empirical heat flow equations to thermal areas other than Wairakei.

## A1.7 References


Allis, R.G., Nash, G.D., Johnson, S.D., Johnson, S.D., Allis, R.G., Thomasson, R.L., Hanson, J., Capuano, L.E., Jr., Schochet, D., Livesay, B., Page, T., Lovekin, J.W. and Johnson, S.E., 1999. Conversion of thermal infrared surveys to heat flow; comparison from Dixie Valley, Nevada, and Wairakei, New Zealand, Transactions - Geothermal Resources Council, vol. 23. GRC - Geothermal Resources Council, Davis, pp. 499-504.

Banwell, C.J., Cooper, E.R., Thompson, G.E.K. and McCree, K.J., 1957. Physics of the New Zealand thermal area. Report 123, Department of Scientific and Industrial Research (DSIR), Wellington.

Bromley, C.J. and Hochstein, M.P., 2001. Thermal properties of steaming ground (Wairakei Field, NZ). 23rd New Zealand Geothermal Workshop, University of Auckland Geothermal Institute, pp. 69-74.

Chiodini, G., Granieri, D., Avino, R., Caliro, S., Costa, A. and Werner, C., 2005. Carbon dioxide diffuse degassing and estimation of heat release from volcanic and hydrothermal systems. Journal of Geophysical Research, 110: no.B8, 17.

Corey, A.T. and Brooks, R.H., 1997. The Brooks-Corey relationships. In: M.T. van Genuchten, F.J. Leij and L. Wu (Editors), Proceedings of the international workshop on Characterization and measurement of the hydraulic properties of unsaturated porous media University of California at Riverside, pp. 13-18.

Dane, J.H., Hofstee, C., Oostrom, M., Liu, H.H. and Corey, A.T., 1997. Determination of capillary pressure-saturation-permeability relations for non-wetting fluids in water wet porous media. In: M.T. van Genuchten, F.J. Leij and L. Wu (Editors), Proceedings of the international workshop on Characterization

and measurement of the hydraulic properties of unsaturated porous media. University of California at Riverside, Riverside, pp. 207-216.
Dawson, G.B., 1964. The nature and assessment of heat flow from hydrothermal areas. New Zealand Journal of Geology and Geophysics, 7(1): 155-171.
Dickinson, D.J., 1967. The natural heat output of the Broadlands geothermal area, 1967. Report, Department of Scientific and Industrial Research - Geophysics Division, Wellington.
Evans, W.C., Sorey, M.L., Kennedy, B.M., Stonestrom, D.A., Rogie, J.D. and Shuster, D.L., 2001. High $CO_2$ emissions through porous media; transport mechanisms and implications for flux measurement and fractionation. Chemical Geology, 177: 15-29.
Fridriksson, T., Kristjansson, B.R., Armannsson, H., Margretardottir, E., Olafsdottir, S. and Chiodini, G., 2006. $CO_2$ emissions and heat flow through soil, fumaroles, and steam-heated mud pools at the Reykjanes geothermal area, SW Iceland. Applied Geochemistry, 21(9): 1551-1569.
Granieri, D., Chiodini, G., Marzocchi, W. and Avino, R., 2003. Continuous monitoring of $CO_2$ soil diffuse degassing at Phlegraean Fields (Italy); influence of environmental and volcanic parameters. Earth and Planetary Science Letters, 212(1-2): 167-179.
Hochstein, M.P. and Bromley, C.J., 2002. Assessment of heat losses of steaming ground by calorimetry. In: S. Soengkono and P.R.L. Browne (Editors), 24th New Zealand Geothermal Workshop. University of Auckland Geothermal Institute, pp. 261-266.
Hochstein, M.P. and Bromley, C.J., 2005. Measurement of heat flux from steaming ground. Geothermics, 34(2): 131-158.
McKibbin, R. and Pruess, K., 1989. Some effects of non-condensible gas in geothermal reservoirs with steam-water counterflow. Geothermics, 18(3): 367-375.
Mongillo, M.A. and Graham, D.J., 1999. Quantitative evaluation of airborne video TIR survey imagery, 21st NZ Geothermal Workshop. University of Auckland Geothermal Institute, pp. 151-156.
Newson, J.A., O'Sullivan, M.J., Bromley, C.J. and Hochstein, M.P., 2001. Modelling shallow heat transfer at Karapiti. 23rd New Zealand Geothermal Workshop, University of Auckland Geothermal Institute, pp. 219-224.
Robertson, E.I. and Dawson, G.B., 1964. Geothermal heat flow through the soil at Wairakei. New Zealand Journal of Geology and Geophysics, 7(1): 134-143.
Sorey, M.L. and Colvard, E.M., 1994. Measurements of heat and mass flow from thermal areas in Lassen Volcanic National Park, California, 1984–93. US Geological Survey, Water Resources Investigations Report 94-4180-A: 35 p.
Thompson, G.E.K., Banwell, C.J., Dawson, G.B. and Dickinson, D.J., 1962. Prospecting of hydrothermal areas by surface thermal surveys. New sources of energy, United Nations Conference, Rome, vol. 2.
Todesco, M., Chiodini, G. and Macedonio, G., 2003. Monitoring and modelling hydrothermal fluid emission at La Solfatara (Phlegrean Fields, Italy); an interdisciplinary approach to the study of diffuse degassing. Journal of Volcanology and Geothermal Research, 125(1-2): 57-79.

## A1.8 Figures and Tables

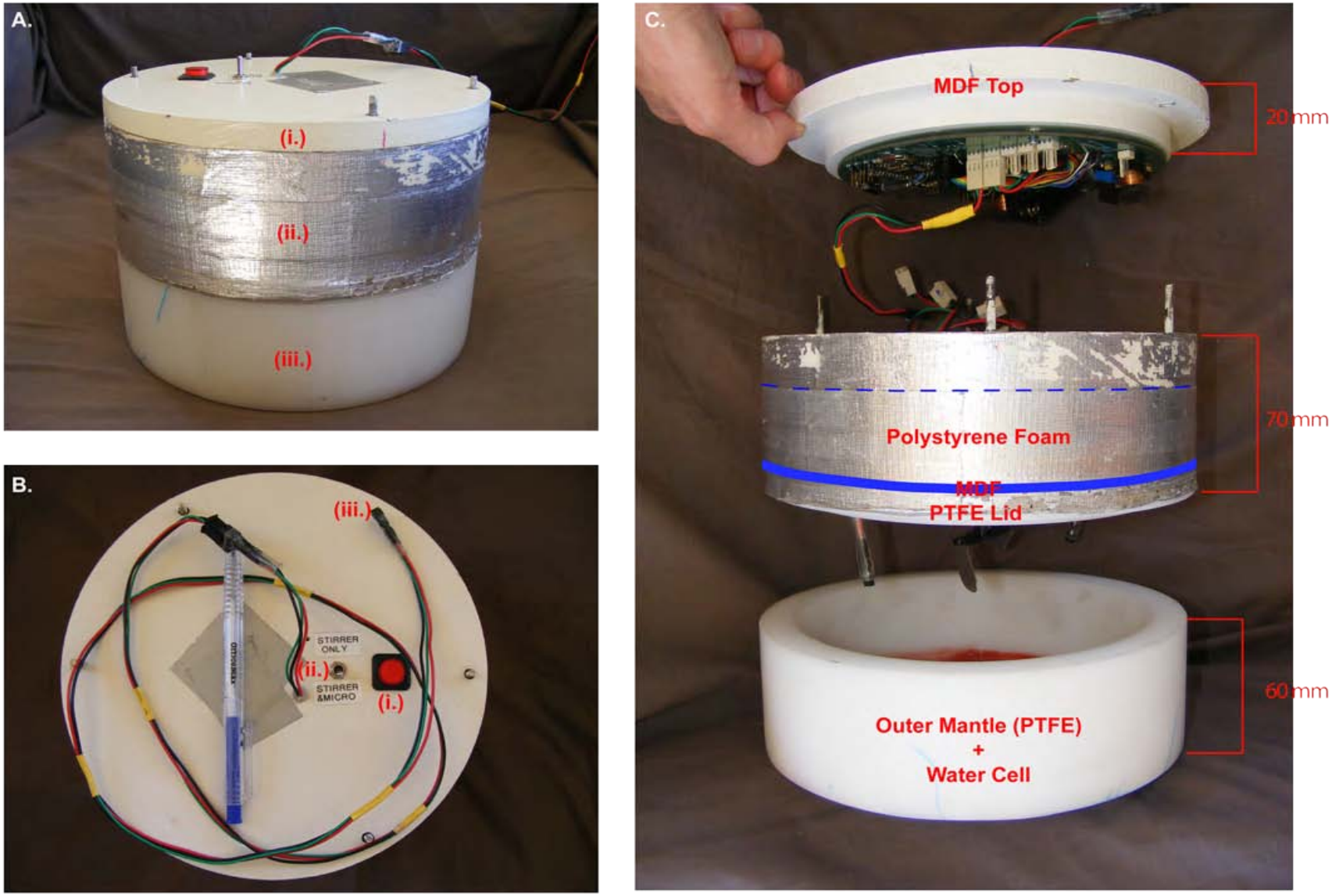


Figure A1.1. Water calorimeter design. (A) Calorimeter, where (i) is the top of the calorimeter; (ii) is the insulated body, and; (iii) the water cell. (B) Calorimeter top where: (i) is the on/off button for the data logger; (ii) is the stirrer and micro logger toggle, and; (iii) is the air temperature thermistor. In the field the air temperature thermistor is mounted ~ 1.15 m off the ground. (C) Component pieces of the calorimeter.

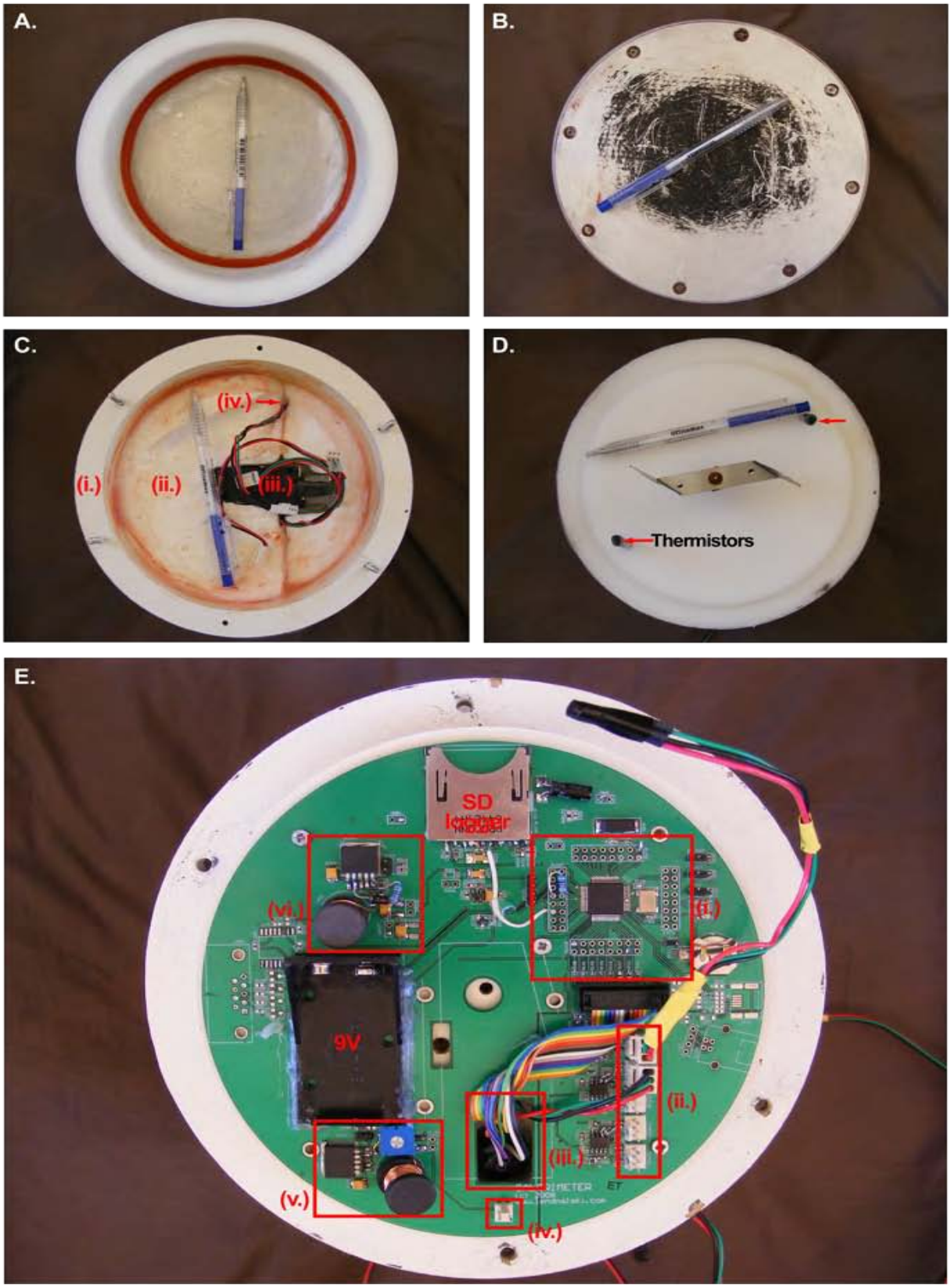


Figure A1.2. Internal components of calorimeter. (A) Water cell. (B) Thin aluminium base of water cell. (C) Internal view of insulated body of calorimeter where; (i) is the MDF mantle that overlies the PTFE lid; (ii) polystyrene foam; (iii) reduction gear box and electric motor for stirrer, and; (iv) one of two thermistors embedded within the PTFE lid. (D) Underside of PTFE lid showing water cell thermistors and stirrer. (E) Internal electronics of calorimeter on underside of top where; (i) ARM7 Microprocessor; (ii) thermistor input array; (iii) connections to external buttons/switches; (iv) stirrer power connector; (v) motor control and switch mode power supply; (vi) switch mode power supply for microprocessor.

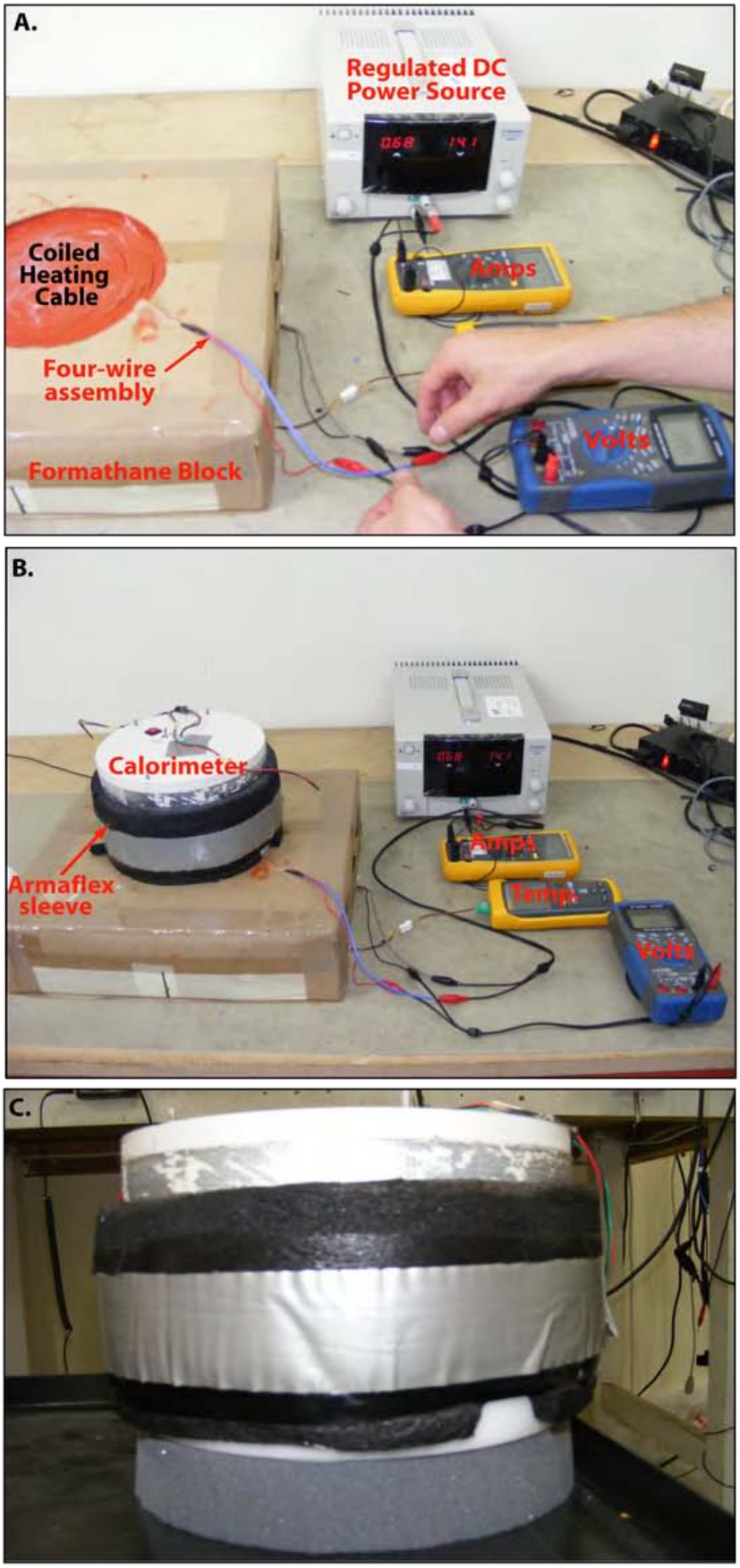


Figure A1.3. Calibration and laboratory setup. (A) Calibration rig including formathane block and coiled heating cable. Power is supplied to the heating cable through a monitored four wire assembly to ensure high accuracy. (B) Heating cycle, calorimeter is placed on heating pad for 5 minutes. (C) Cooling cycle, calorimeter is removed from heating pad and placed on foam insulation for 5 minutes.

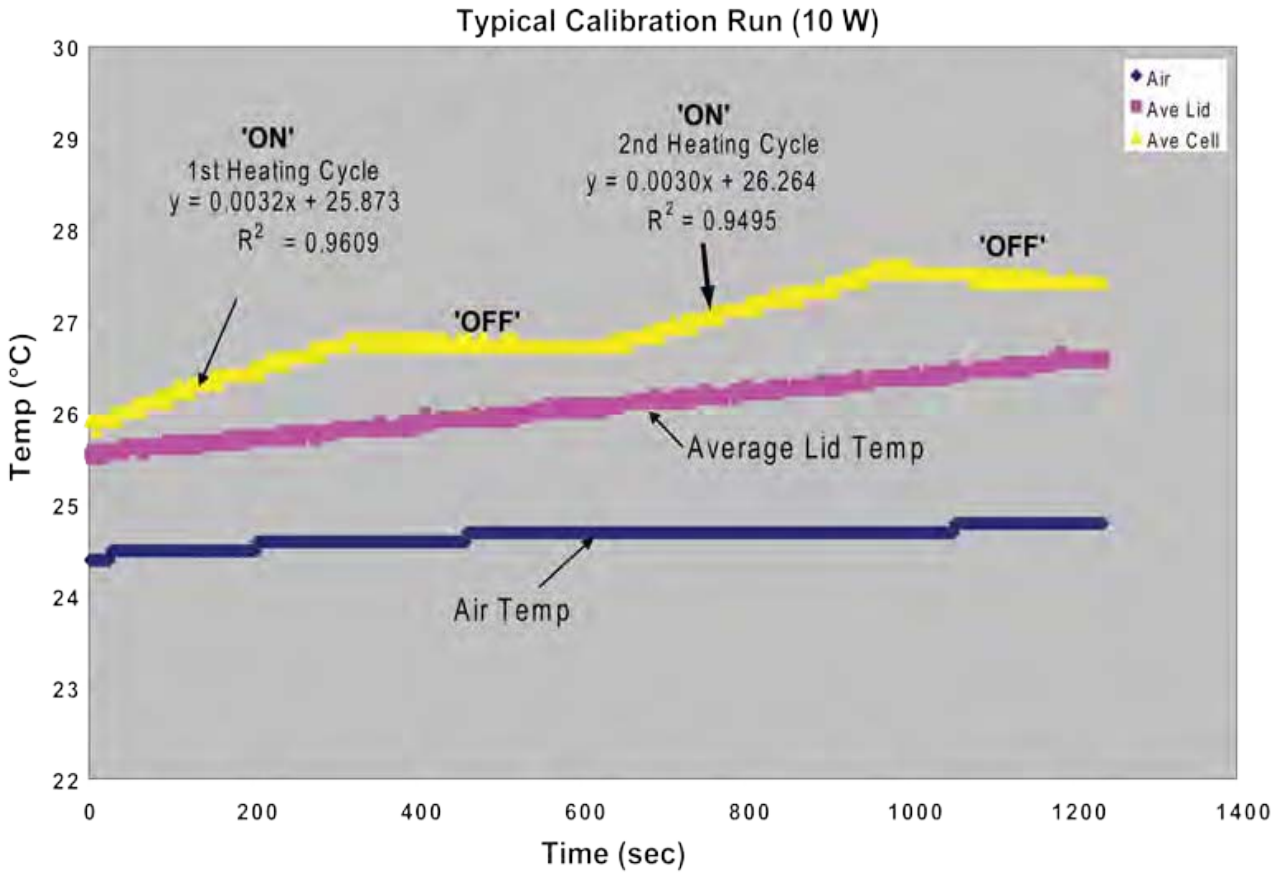


Figure A1.4. Typical calibration run. Gradients of heating curves (ºC/s) for each heating cycle were assessed by a least-squares linear fit applied to each heating segment of the record. The gradient for each heating cycle was used to calculate the calorimeter heat flux.

| Calibration Trials | 1st Run | | 2nd Run | |
|---|---|---|---|---|
| | 1st Cycle | 2nd Cycle | 1st Cycle | 2nd Cycle |
| Voltage (V) | 13.81 | 13.81 | 13.81 | 13.81 |
| Current (A) | 0.671 | 0.671 | 0.671 | 0.671 |
| Power In (W) | 9.26 | 9.26 | 9.26 | 9.26 |
| $\Delta T/\Delta t$ (°C/s) | 0.0033 | 0.0032 | 0.003 | 0.003 |
| Heat flow Imposed ($W/m^2$) | 408.5 | 408.5 | 408.5 | 408.5 |
| Heat flow Calmeter ($W/m^2$) | 426.2 | 413.3 | 387.5 | 387.5 |
| Difference | 4% | 1% | 5% | 5% |

Table A1.1 Results of calorimeter laboratory calibration trail. Parameters used in calorimeter heat flux calculation: (i) mass of water 0.7 kg; (ii) area of calorimeter base 0.0223 $m^2$; specific heat capacity of water, 4186 kJ/kg/°C. Where $\Delta T/\Delta t$ (°C/s) is the heating rate of the water cell for each heating cycle. A mean relative error of +4% was calculated for the two runs.

# Appendix 2.

# Construction of a heated sampling device to characterise the molar $H_2O/CO_2$ ratio of the vapour phase supplying surface thermal areas

**Clinton Rissmann[a], Bruce Christenson[b], Stefan Lendnal[c]**

*[a]Department of Geological Sciences, University of Canterbury, Private Bag 4800, Christchurch, New Zealand*

*[b]GNS Science, P.O. Box 30368, Lower Hutt, New Zealand*

*[c]Syft Technologies, P.O. Box 28149, New Zealand*

## Contributions

Mr. Rissmann designed and built the $H_2O/CO_2$ sampling rig after guidance from Dr. Bruce Christenson. Mr. Lendnal connected and tested the PID controller and wiring for both the thermocouple and the power supply. Field sampling was conducted by Mr. Rissmann after initial guidance from Dr. Christenson. Sample analysis by gas chromatography was undertaken by Dr. Christenson.

## A2.1 Introduction

Increasingly, $CO_2$ flux surveys are being used to estimate the heat and mass released from hydrothermal reservoirs (Brombach et al., 2001; Chiodini et al., 2005; Fridriksson et al., 2006). In order for estimates of water vapour heat and mass flow to be made from $CO_2$ flux data, an accurate and representative measure of the molar $H_2O/CO_2$ ratio of the vapour phase supplying areas of surface thermal activity is required. Two difficulties surround $H_2O/CO_2$ sampling: (i) condensation of water vapour within the sampling device, which alters the $H_2O/CO_2$ ratio of the vapour phase artificially, and; (ii) acquisition of $H_2O/CO_2$ ratios that are representative of the uncondensed vapour phase supplying a thermal area.

In this Appendix we describe the construction and deployment of a heated vapour sampler to assess the molar $H_2O/CO_2$ ratio of the vapour phase supplying surface thermal activity at Ohaaki, and present our preliminary results. This study was motivated by the uncertainty surrounding values of $CO_2$ concentration (i.e., 0.6 mol) reported by Mahon and Finlayson (1972) for the vapour phase supplying the Ohaaki West (OHW) thermal area. It was hoped that a robust measure of the $H_2O/CO_2$ ratio would address technical issues raised in the review of Chapter 2.

## A2.2 Deriving a representative $CO_2$ concentration

An estimate of the steam mass flow accompanying $CO_2$ flux was derived by assuming that $CO_2$ is transported toward the surface by steam, with a $CO_2$ concentration equal to that of the deep Ohaaki reservoir (Fridriksson et al., 2006). The dissolved $CO_2$ concentration of deep parental fluids at Ohaaki is well established with values of 0.60 – 0.75 molal reported by Simmons and Christenson (1994) from fluid inclusion analysis. The steam fraction produced by adiabatic boiling of the 0.60 – 0.75 molal parent fluid from 310ºC to 98.7ºC is equal to 0.437. By assuming that the dissolved $CO_2$ within the parent fluid will partition more or less quantitatively into the steam phase, the composition of geothermal steam at the surface at Ohaaki, $CO_2$, should range between to 1.37 - 1.72 molal or 60.3 g – 75.5 g of $CO_2$ per kg of steam.

## A2.3 Construction of a heated vapour phase sampling rig

To minimise condensation losses a heated vapour phase sampling rig was built (Fig A2.1). The rig is built around an inverted stainless (grade 316) funnel and pipe. The pipe through which the sample is drawn is wound with 4 m of 300 $\Omega$ $m^{-1}$ heating cable. The heating cable was attached to the pipe by blobs of red silicon (rated to 260ºC) and left to dry. A K-type thermocouple was secured directly to the metal surface of the sampling pipe by means of a radiator hose clamp. Once the cable had dried in place and the thermocouple was attached, both the heating cable and the thermocouple were coated with a thick layer of red silicon. The pipe was then lagged with glass cloth, and heat resistant Armaflex® rubber foam, all of which was sealed with an outer layer of aluminum foil tape (Fig. A2.1)

The heating cable and K-type thermocouple were interfaced to an Omron® Proportional, Integral and Derivative (PID) controller. A PID or 'auto tune' controller was preferred as it provides the most accurate and stable temperature control, by automatically compensating for changes in current loading and energy changes within the system of interest. The latter are important when using a portable field generator for a power supply. The desired operating temperature is input via the PID interface (Fig. A2.1). Once the pipe reaches the desired sampling temperature it is thermostatically maintained by the PID controller.

## A2.4 Field sampling for the $H_2O/CO_2$ ratio

In the field, a hole approximately 0.8 m deep was dug, into which a stainless steel (grade 316) funnel was placed inverted and buried (Fig A2.2). The piping neck of the funnel was left to protrude slightly above ground level so that the insulated heating pipe could be attached. The funnel and attached sampling tube were left to equilibrate overnight (≥18 hours). The following day the sampling tube was plugged into a portable generator and heated to a temperature of ≥110ºC ± 2.5ºC prior to sampling. Vapour phase samples were drawn into evacuated Giggenbach flasks with a flow-through setup. The concentration of $CO_2$ was analyzed

by gas chromatography, whereas the mass of condensed water vapour was determined by repeat weighing of the sample flasks.

Only two different sites were able to be sampled before a heavy rainfall curtailed the sampling program. The first location, at Ohaaki West (OHW), was disappointing due to cooler than expected ground temperatures. The cooler ground temperatures likely reflect both a seasonal component (sampling was undertaken in early November of 2009) and localised rainfall over the week prior to sampling. At Ohaaki East however, a better site of high temperature was located, from which significant volumes of condensate were sampled.

For the OHE sample site the first two sample runs returned $CO_2$ concentrations of 5.2 and 5.7 mmol or 0.23 and 0.25 g $kg^{-1}$. These values are ~300 times lower than predicted by steam fractionation calculations and ~100 times slower than measured by Mahon and Finlayson (1972) for the OHW thermal area. These results are surprising and require further investigation before they can be considered representative of the $CO_2$ concentration of the vapour phase supplying the thermal areas of the Ohaaki Field. Further sampling is planned for late summer of 2011.

## A2.5 References


Brombach, T., Hunziker, J.C., Chiodini, G., Cardellini, C. and Marini, L., 2001. Soil diffuse degassing and thermal energy fluxes from the southern Lakki Plain, Nisyros (Greece). Geophysical Research Letters, 28(1): 69-72.

Chiodini, G., Granieri, D., Avino, R., Caliro, S., Costa, A. and Werner, C., 2005. Carbon dioxide diffuse degassing and estimation of heat release from volcanic and hydrothermal systems. Journal of Geophysical Research, 110: no.B8, 17.

Fridriksson, T., Kristjansson, B.R., Armannsson, H., Margretardottir, E., Olafsdottir, S. and Chiodini, G., 2006. $CO_2$ emissions and heat flow through soil, fumaroles, and steam-heated mud pools at the Reykjanes geothermal area, SW Iceland. Applied Geochemistry, 21(9): 1551-1569.

Mahon, W.A.J. and Finlayson, J.B., 1972. The chemistry of the Broadlands geothermal area, New Zealand. American Journal of Science, 272(1): 48-68.

Simmons, S.F. and Christenson, B.W., 1994. Origins of calcite in a boiling geothermal system. American Journal of Science, 294(3): 361-400.

## A2.6 Figures


Figure A2.1. Components of heated vapour sampler. (A) Stainless (316 grade) sampling pipe before addition of heating cable, K-type thermocouple, and external lagging. (B) Neck of sampling pipe which is attached to inverted funnel. (C) Lagged sampling pipe where: (i) outer aluminium foil tape; (ii) Armaflex temperature resistant foam; (iii) glass cloth; (iv) red silicon adhesive. (D) Lagged sampling pipe with: (i) neck; (ii) thermocouple cable; (iii) silicon tubing outlet. (E) PID controller showing temperature output and input interface.

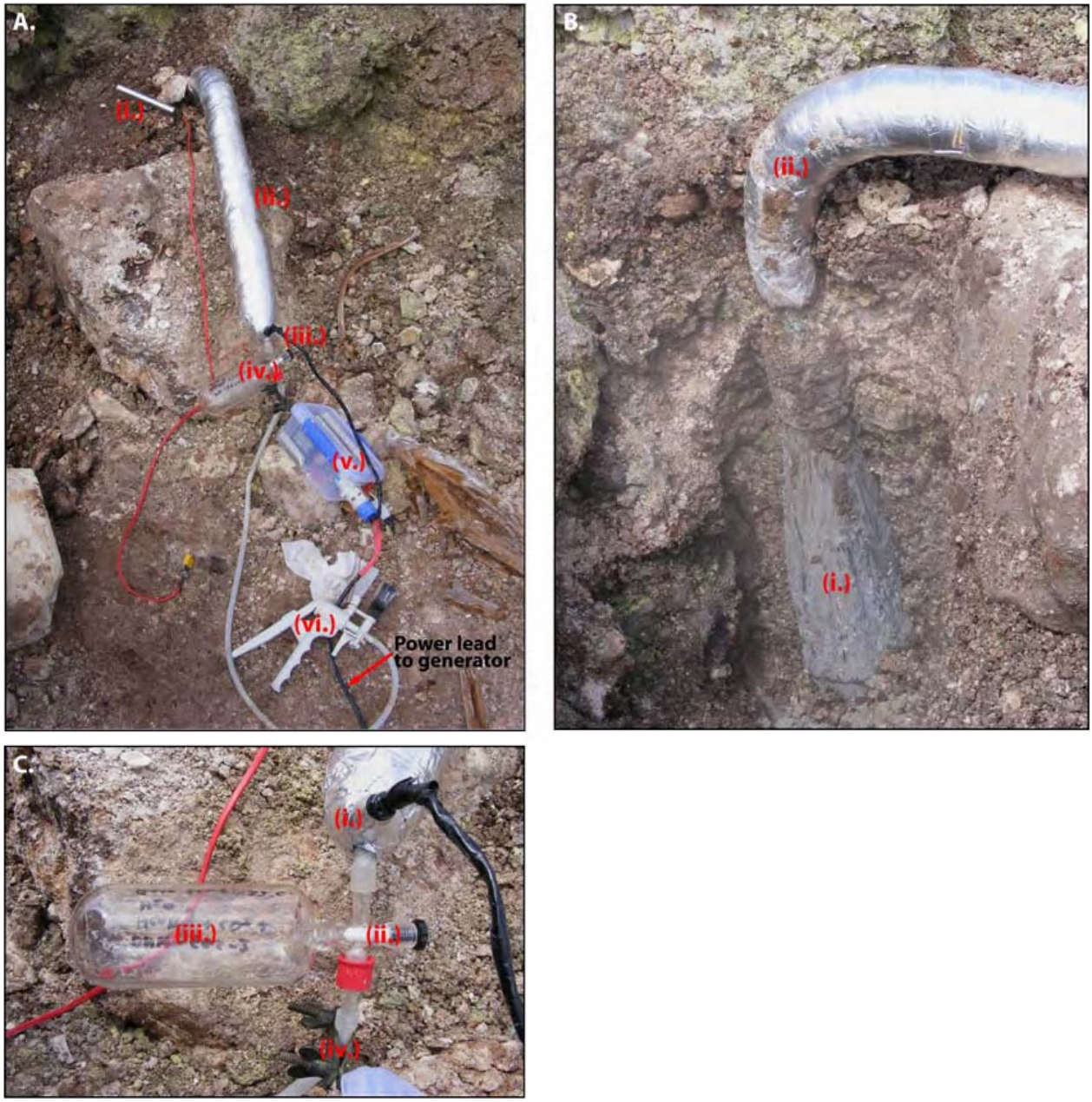


Figure A2.2. Field deployment of heated vapour sampler. (A) Sampling set up: (i) temperature probe monitoring temperature at 0.5 m depth; (ii) heated sampling pipe; (iii) thermocouple cable to PID controller; (iv) evacuated sample bottle; (v) PID controller; (vi) vacuum pump and waste line. (B) Excavation and exposure of: (i) inverted funnel, and; (ii) sampling pipe. (C) Close up of sampling collection system, where (i): outlet of heated sampling pipe; (ii) Teflon valve of flow through flask; (iii) evacuated Giggenbach flask, and; (iv) clamp on silicon waste tube.